ВЕСТНИК ТРАНСПЛАНТОЛОГИИ И ИСКУССТВЕННЫХ ОРГАНОВ

VESTNIK TRANSPLANTOLOGII I ISKUSSTVENNYKH ORGANOV

RUSSIAN JOURNAL OF TRANSPLANTOLOGY AND ARTIFICIAL ORGANS

УЧРЕДИТЕЛЬ: ОБЩЕРОССИЙСКАЯ ОБЩЕСТВЕННАЯ ОРГАНИЗАЦИЯ ТРАНСПЛАНТОЛОГОВ «РОССИЙСКОЕ ТРАНСПЛАНТОЛОГИЧЕСКОЕ ОБЩЕСТВО»

THE OFFICIAL JOURNAL OF ALL-RUSSIAN PUBLIC ORGANIZATION OF TRANSPLANTOLOGISTS "RUSSIAN TRANSPLANT SOCIETY"

2025. Том XXVII. № 1

2025. Vol. XXVII. № 1

Научно-практический журнал основан в 1999 г.
Регистр. № 018616

Scientific and Practical Journal was founded in 1999
Reg. № 018616

Журнал «Вестник трансплантологии и искусственных органов» включен ВАК РФ в перечень российских рецензируемых научных изданий, в которых должны быть опубликованы результаты диссертационных работ

Журнал «Вестник трансплантологии и искусственных органов» включен ФГБУ «НМИЦ ТИО им. ак. В.И. Шумакова» Минздрава России в перечень российских рецензируемых научных изданий, в которых должны быть опубликованы основные результаты исследований в рамках диссертаций, представляемых к защите в диссертационный совет ФГБУ «НМИЦ ТИО им. ак. В.И. Шумакова» Минздрава России

Журнал «Вестник трансплантологии и искусственных органов» индексируется в Scopus и размещен на платформе Web of Science Core Collection: Emerging Science Citation Index

"Russian Journal of Transplantology and Artificial Organs" is included in the list of leading peer-reviewed scientific publication editions, produced in the Russian Federation and is recommended for publication of primary results of dissertation research

"Russian Journal of transplantology and artificial organs" is included by the Federal State Budgetary Institution "Shumakov National Medical Research Center of Transplantology and Artificial Organs" of the Ministry of Health of Russia in the list of Russian peer-reviewed scientific publications in which the main results of research should be published within the framework of dissertations submitted for defense to the dissertation council of Shumakov National Medical Research Center of Transplantology and Artificial Organs

"Russian Journal of Transplantology and Artificial Organs" is indexed in Scopus and in the Emerging Science Citation Index of the Web of Science Core Collection

ISSN 1995-1191

Адрес для корреспонденции:

Россия, 123182, Москва, ул. Щукинская, 1
Тел./факс +7 (499) 193 87 62
E-mail: vestniktranspl@gmail.com
Интернет-сайт журнала: http://journal.transpl.ru
Научная электронная библиотека: http://elibrary.ru

Address for correspondence:

1, Shchukinskaya st., Moscow 123182, Russia
Tel./Fax +7 (499) 193 87 62
E-mail: vestniktranspl@gmail.com
Journal's web site: http://journal.transpl.ru
Scientific eLibrary: http://elibrary.ru

Подписной индекс в каталоге почты России – ПН380

СОДЕРЖАНИЕ

СТРАНИЦА ГЛАВНОГО РЕДАКТОРА

КЛИНИЧЕСКАЯ ТРАНСПЛАНТОЛОГИЯ

CONTENTS

EDITORIAL

CLINICAL TRANSPLANTOLOGY

ПРИОРИТЕТНЫЕ НАПРАВЛЕНИЯ НАУЧНЫХ ИССЛЕДОВАНИЙ В ОБЛАСТИ ТРАНСПЛАНТОЛОГИИ И ИСКУССТВЕННЫХ ОРГАНОВ

Актуальной и насущной потребностью сегодняшнего дня является повышение результативности научных исследований для укрепления национальной безопасности нашей страны и обеспечения научного мирового лидерства. Для формирования эффективной системы управления фундаментальными, поисковыми, прикладными научными исследованиями разработаны программы, в которые включены перспективные научные направления в соответствующих областях науки.

В Программе фундаментальных научных исследований в Российской Федерации на долгосрочный период (2021–2030 годы, утверждена распоряжением Правительства Российской Федерации от 31.12.2020 № 3684-р) сформулированы следующие направления в области трансплантологии и искусственных органов:

- *персонифицированные способы диагностики и лечения критических состояний, до и после трансплантации солидных органов;*
- *молекулярно-генетические механизмы регуляции функционирования аллотрансплантата солидных органов;*
- *перфузионные технологии и молекулярные механизмы сохранения и ревитализации донорских органов;*
- *компьютерное, математическое моделирование функции сердечно-сосудистой системы взрослых и детей в условиях вспомогательного кровообращения;*
- *технологии получения длительно пролиферирующих печеночных прогениторных клеток путем репрограммирования гепатоцитов человека для трансплантации при печеночной недостаточности;*

PRIORITY AREAS OF SCIENTIFIC RESEARCH IN THE FIELD OF TRANSPLANTOLOGY AND ARTIFICIAL ORGANS

Today, improving the effectiveness of scientific research is crucial to strengthening our nation's national security and maintaining global leadership in science and innovation. Programs that cover promising scientific areas in the pertinent scientific fields have been designed to provide an efficient management structure for fundamental, exploratory, and applied scientific research.

The Program of Basic Scientific Research in the Russian Federation for the Long Term (2021–2030), approved on December 31, 2020 (Order No. 3684-r) by the Government of the Russian Federation, formulated the following areas in the field of transplantology and artificial organs:

- *individualized approaches to diagnosis and treatment of critical conditions, both before and after solid organ transplantation;*
- *molecular and genetic mechanisms of regulation of solid organ allograft functioning;*
- *perfusion technologies and molecular mechanisms for organ preservation and revitalization;*
- *computer, mathematical modeling of the functioning of adult and pediatric cardiovascular systems under assisted circulation;*
- *techniques for obtaining long-term proliferating hepatic progenitor cells by reprogramming human hepatocytes for transplantation in liver failure;*
- *technologies for growing bioequivalents in a bioreactor or in a living organism for temporary or permanent replacement of damaged or lost organs and tissues.*

– *технологии выращивания в биореакторе или в живом организме биоэквивалентов для временной или постоянной замены поврежденных или утраченных органов и тканей.*

Кроме того, сформулированы перспективные направления поиска в области клинических и медико-биологических исследований трансплантации солидных органов, которые касаются эпигенетических аберраций в технологиях здоровьесбережения реципиентов, анализа микроРНК, значимых для формирования иммунной толерантности и/или снижения риска развития отторжения, технологии коррекции иммуносупрессии, вспомогательного кровообращения, перфузии донорских органов.

Координационным советом Минздрава России по исследованиям и разработкам в области медицинской науки утверждены (28.12.2023 г.) следующие приоритеты исследований и разработок в интересах медицины и здравоохранения:

– *диагностические тест-системы и методы неинвазивной и малоинвазивной диагностики острой и хронической дисфункции трансплантированных органов;*
– *лекарственные препараты для предотвращения и лечения острого и хронического отторжений трансплантированных органов;*
– *медицинские изделия и лекарственные препараты для ex vivo перфузии и реабилитации донорских органов для трансплантации;*
– *устройства для кратковременной и длительной вспомогательной поддержки кровообращения у детей и взрослых;*
– *программы физической реабилитации прижизненных доноров органов и фрагментов органов и средства для их осуществления;*
– *технологии физической и психологической реабилитации реципиентов донорских органов, включая репродуктивную функцию, включая детей-реципиентов различного возраста.*

Решение поставленных задач обеспечит улучшение качества оказания медицинской помощи в области трансплантации органов, доступ граждан к самым современным технологическим решениям, воплощенным в конкретной медицинской продукции.

С уважением,
академик РАН С.В. Готье

In addition, promising areas of search in the field of clinical and biomedical research of solid organ transplantation have been formulated. They include epigenetic aberrations in recipient health-preserving technologies, analysis of miRNAs, which are crucial for formation of immune tolerance and/or reduction of organ rejection risk, immunosuppression correction techniques, assisted circulation, and organ perfusion.

On December 28, 2023, the Russian Ministry of Health Coordinating Council for Medical Science Research and Development adopted the following priorities for medical and healthcare-related research and development:

– *diagnostic test systems and methods for non-invasive and minimally invasive diagnostics for acute and chronic transplant dysfunction;*
– *pharmaceuticals for prevention and treatment of acute and chronic transplant rejection;*
– *medical devices and pharmaceuticals for ex vivo organ perfusion and rehabilitation;*
– *devices for short-term and long-term assisted circulation in children and adults;*
– *physical rehabilitation programs for living organ donors and means for their implementation;*
– *technologies for physical and psychological rehabilitation of organ recipients, including their reproductive function, as well as pediatric recipients of various ages.*

Addressing the above tasks would enhance the standard of medical care in the field of organ transplantation, grant access for citizens to cutting-edge tech solutions embodied in specific medical products.

Sincerely,

Sergey Gautier,
Fellow, Russian Academy of Sciences
Editor-in-chief, Russian Journal
of Transplantology and Artificial Organs

DOI: 10.15825/1995-1191-2025-1-8-16

CURRENT CONCEPTS OF VASCULAR COMPLICATIONS FOLLOWING KIDNEY TRANSPLANTATION (A LITERATURE REVIEW)

A.A. Zharikov[1], *D.A. Saydulaev*[1], *S.V. Gautier*[1, 2]

[1] Shumakov National Medical Research Center of Transplantology and Artificial Organs, Moscow, Russian Federation

[2] Sechenov University, Moscow, Russian Federation

Even with advancements in surgical techniques, vascular complications remain life-threatening conditions and can lead to graft loss and sometimes recipient death. This paper examines the causes of vascular complications following a kidney transplant (KT), as well as international experience in the application of methods for early diagnosis, treatment and prevention of these complications.

Keywords: kidney transplantation; vascular complications; prevention of vascular complications.

INTRODUCTION

Vascular complications are a significant concern in kidney transplantation (KT), occurring in 3–15% of recipients, with graft loss rates ranging from 12.6% to 66.7% in affected patients [1–3].

Early vascular complications include arterial and venous thrombosis, arterial dissection, vascular damage during the retrieval procedure (cuts and lacerations), arteriovenous fistulas, pseudoaneurysms, and hematomas. Later came stenosis or kinking of the renal artery and less often of the renal vein, as well as external compression due to the presence of fluid accumulations around the graft [1, 3]. The most common complications are arterial stenoses of the graft (3–12.5 %), followed by arterial and venous thromboses (0.1–8.2%) and vascular wall dissection (0.1 %). Arteriovenous fistulas or pseudoaneurysms occur less frequently [3].

RENAL ARTERY THROMBOSIS

Renal artery thrombosis (RAT) is the leading cause of kidney transplant loss in the early post-transplant period. It is a rare complication with a reported incidence ranging from 0.2% to 3.5% [4, 5].

RAT most often develops within minutes to hours post-transplant and can occur as a result of hyperacute rejection, anastomosis occlusion, renal artery stenosis (RAS), renal artery kinking, and blood hypercoagulable state [6, 7]. In the first hours after surgery, RAT often presents subtly, with sudden oliguria or anuria and a rapid rise in plasma creatinine being the earliest signs [5]. Other clinical signs of RAT include worsening hypertension, pain at the graft site, which may occur as a result of tissue edema [7].

Additional diagnostic methods are necessary for early detection, such as color flow mapping, which helps differentiate thrombosis from acute rejection or acute tubular necrosis [8]. Catheter angiography and magnetic resonance angiography are the primary techniques for confirming the diagnosis by revealing reduced or absent blood flow to the graft. However, in emergency situations, angiography may not always be feasible [7, 9]. Screening ultrasound with duplex scanning is considered the standard method for assessing graft perfusion [10].

In cases of complete arterial occlusion due to thrombosis, graft loss can occur. However, if thrombosis is limited to small distal branches and does not affect the main renal artery, the outcome may still be favorable [11, 12]. If the inferior pole branch is involved, it may lead to ischemia and subsequent necrosis of the ureter [13].

In cases of RAT, emergency surgery is the only viable option to salvage the transplanted kidney [5, 7]. The standard procedure typically involves thrombectomy with anastomotic repair. While the role of interventional treatment for graft artery thrombosis remains unclear, there have been reports of successful cases using catheter-directed thrombolysis, with or without percutaneous angioplasty and/or stent placement [4, 14–16].

Ayvazoglu et al. reported that among 8 RAT cases, 5 patients underwent thrombectomy with arterial anastomotic reformation, and 3 patients underwent percutaneous transluminal angioplasty, thrombolysis and stent placement [16].

Harraz et al. analyzed cases of vascular accidents – renal artery thrombosis (19) and renal vein thrombosis (4), which accounted for 23 (1%) vascular accidents among 2208 cases of live donor kidney transplant (KT) between 1976 and 2011. In 12 RAT patients (63%), the

Corresponding author: Andrey Zharikov. Address: 1, Shchukinskaya str., Moscow, 123182, Russian Federation. Phone: (962) 983-68-70. E-mail: zharikof94@mail.ru

graft was salvaged by open revascularization. The most important stages of their surgical strategy were ensuring vascular control, revision of arterial anastomosis, thrombus extraction and perfusion of the graft with preserving solution, heparinized saline and vasodilators with removal of perfusate through venotomy followed by reanastomosis [15].

Aktas et al. reported 3 cases of salvage of renal grafts with RAT by thrombectomy and formation of a new anastomosis. Two other RAT patients underwent percutaneous transluminal angioplasty, thrombolysis and stent placement [4].

RENAL VEIN THROMBOSIS

Renal vein thrombosis (RVT) is one of the major vascular complications after KT and one of the major causes of immediate graft loss [27]. According to various reports, the incidence of early post-transplant RVT ranges from 0.1% to 5.5% [17], 0.3% to 4.2% [27], and 0.14% [5]. RVT usually develops within the first 5 days after surgery, with peak incidence within the first 48 hours, although there are cases of delayed RVT occurring after the first postoperative week [7].

Common causes of RVT are anatomical anomalies or technical problems during surgery [27], including graft vein kinking, vascular endothelial injury during surgical manipulation or during graft pretreatment [18, 19]. External compression caused by hematoma or lymphatic fluid accumulation is also referred to as a direct cause of RVT [6].

The short and thin-walled nature of the right renal vein (RRV) often presents technical challenges during right KT [17, 18]. However, Natour et al. reported that the side of KT is not directly associated with RVT risk [20]. To overcome these technical difficulties, lengthening the RRV by incorporating a segment of the inferior vena cava or gonadal vein in deceased donor right KT has proven effective. This approach facilitates venous anastomosis and is likely a key factor in the currently low incidence of RVT [21].

Higher doses of cyclosporine are also associated with a higher incidence of venous thrombosis. Another important reason is hypercoagulable states such as antithrombin III, protein C or protein S deficiency [22].

Clinically, RVT usually presents with a significant increase in the size and density of the graft, pain or discomfort in the graft area, increasing hematuria with rapidly decreasing urine output, proteinuria, graft dysfunction, oliguria, and/or complete anuria [23]. Indirect signs include ipsilateral lower extremity edema, subfebrile temperature, and, in severe cases, massive retroperitoneal hemorrhage.

Doppler ultrasound with color flow mapping is the primary and first-line diagnostic method for detecting RVT. They can detect absence of blood flow in the renal vein, swollen graft, and abnormal arterial signal with a plateau-like reverse diastolic flow [7, 8, 17]. Loss of corticomedullary differentiation and paranephral fluid can also be detected [7]. Magnetic resonance or computed tomography venography is a more accurate but less frequently used procedure as a routine assessment method [17].

Surgical intervention is almost always required when RVT is detected in a kidney transplant. According to Cambou et al., venous thrombosis was the cause of graft loss in 86.4% of cases, with only intraoperative thrombosis being associated with better graft survival (63.5%), which is probably due to the possibility of immediate intervention. In the case of surgical intervention, the graft is subjected to new ischemia-reperfusion injury with consequences in the form of delayed recovery of function or eventually graft function may not recover at all [17].

In a study by Fathi et al., three out of seven grafts with RVT were salvaged after open thrombectomy [24]. A study conducted by Haberal et al. reported that two out of four grafts were salvaged after emergency revision venous thrombectomy with restoration of blood flow. In two patients, treatment was unsuccessful and graftectomy was performed [25], which was necessary to prevent progressive congestive edema and graft rupture, which can lead to life-threatening bleeding and patient death [26]. According to Harraz et al., two RVT cases were resolved by percutaneous catheter-directed thrombolytic therapy and one case by thrombectomy and revascularization [15].

According to Lerman et al., immediate intervention within 1 hour of the onset of thrombosis can salvage the graft. Lerman et al. report a case in which the graft was salvaged after open thrombectomy and reimplantation of the kidney [27].

Early RVT has a poor prognosis. Evidence suggests that intraoperative monitoring for vascular complications is critical to the success of transplantation if intraoperative RVT occurs. In addition, screening for prothrombotic conditions in potential kidney recipients with risk factors for thrombosis and the justified use of perioperative anticoagulant therapy are important strategies to prevent thrombus formation [28].

RENAL ARTERY STENOSIS

The incidence of transplant RAS is reported to range between 1% and 23% [33]. RAS is the most common vascular complication following a KT [4, 6, 16]. The wide range of incidence has been attributed to the lack of uniformity in the definition of the condition and the different imaging techniques used to make the diagnosis [29]. Other reports suggest that RAS affects about 3% of all renal transplants [7].

RAS is a potentially reversible cause of refractory post-transplant hypertension, where narrowing of the renal artery of the graft obstructs blood flow and leads to renal hypoperfusion [30]. RAS is typically diagnosed

between 3 months and 2 years after transplantation, though earlier or later manifestations can occur [31]. This complication should be suspected in patients with treatment-refractory arterial hypertension, worsening condition, elevated creatinine levels, decreased graft function, reduced urine output, or unexplained fluid retention [7]. Occasionally, clinically asymptomatic stenoses are incidentally detected during routine ultrasound surveillance of the recipient and graft [31].

Most RAS cases are prone to progression leading to graft loss. Therefore, early and accurate diagnosis of this condition is important [31]. Digital subtraction angiography is widely considered the gold standard for imaging RAS, but it is an invasive technique requiring the use of nephrotoxic contrast agents. Computed tomographic angiography and magnetic resonance angiography with contrast are also commonly used imaging techniques to diagnose RAS [31]. However, Doppler ultrasound angiography is preferred as the initial imaging choice because of its accessibility and non-invasiveness [9]. Signs of RAS are seen at the narrowing site and include an elevated peak systolic velocity (PSV), an abnormal ratio of PSV in the main renal artery compared to the superior iliac artery, and an aliasing effect due to turbulence. A PSV of 340–400 cm/s at the anastomosis site is considered a reliable criterion for RAS, which, however, should be considered in the context of other parameters [7].

Once the diagnosis is established, various surgical interventions are performed for hemodynamically significant stenosis [32]. Endovascular techniques, including percutaneous transluminal angioplasty and stent placement, are the first-line therapy. In refractory cases or with complex anatomical features, open surgical intervention follows [7].

Earlier studies have shown that following an endovascular procedure, a significant majority of patients experienced improvement in their kidney function (85–93%) and blood pressure (63–83%) to a more normal level. The risk of recurrence ranged from 10% to 33%, but was lower when angioplasty was combined with stenting [33].

This is supported by a meta-analysis by Ngo et al., which noted higher patency rates with stent placement for RAS compared to angioplasty alone (90.4% *vs.* 73%) [34]. Drug-eluting balloons and stents have also been successfully used to treat RAS [35]. A recent systematic review further demonstrated that endovascular treatment of RAS preserves graft function and hemodynamic parameters [35].

RISK FACTORS FOR THROMBOTIC COMPLICATIONS

Risk factors for thrombotic complications can be broadly categorized into three groups: donor-related, recipient-related and those caused by to the peculiarities of the surgical intervention itself. Thrombosis may also develop as a result of a technical error during anastomosis, intima damage, decreased blood flow due to constriction or twisting of vessels, stasis, hypercoagulation, or exceeding the target levels of immunosuppressive drugs in the blood [3]. Other causes include acute rejection and external compression by hematoma or lymphocele [5].

Donor risk factors for thrombotic complications

Donor risk factors for thrombotic complications include advanced donor age, vascular anomalies in the graft (such as multiple vessels), use of the right kidney as a graft, deceased donor kidneys versus living related donor kidneys, and prolonged warm and cold ischemia times. A donor age older than 60 years [36], or in some reports older than 50 years [6], is considered a significant risk factor for renal graft thrombosis.

As the demand for kidney transplants surpasses donor organ availability, medical professionals are increasingly utilizing kidneys with multiple renal arteries (MRAs) to expand the donor pool. While MRAs often require vascular reconstruction during transplantation, which was historically associated with a higher risk of early post-transplant complications such as graft thrombosis [37], recent studies suggest that this is no longer a significant concern. Modern surgical techniques and improved perioperative management have contributed to comparable outcomes between grafts with MRAs and those with single renal arteries, with no significant increase in postoperative complications or adverse events [37–42].

Only one retrospective study from Iran reported significantly higher surgical complication rates after transplantation of renal allografts with multiple arteries compared to cases that did not require vascular reconstruction. The authors found vascular complications in 25.4% of patients with multiple arteries, compared to 8.2% in recipients of single-artery grafts [43]. The presence of multiple arteries has previously been identified as an independent risk factor for bleeding [44], with a nephrectomy rate of 22% in severe cases. This may explain the findings of Salehipour et al. [43], where the reported bleeding rate was 6.1%, compared to 1.9% in the study by Osman et al.

There is no consensus on whether right renal grafts increase the risk of thrombosis compared to left renal grafts. One report suggests that the use of a right donor kidney increases the risk of thrombosis [36]. The main explanation proposed is that right KT may present technical difficulties because of the short and more ‘fragile’ right renal vein [18, 19].

These difficulties were partially addressed by Fallani et al., who utilized cryopreserved vascular grafts to lengthen renal vessels. Their study analyzed KT outcomes between 2012 and 2020, focusing on right kidney

grafts, including those with abnormal vascularization and cases requiring vessel lengthening. For grafts with multiple vessels, vein lengthening resulted in shorter warm ischemia and overall surgery times, making them comparable to standard grafts. For right kidney grafts using vessel lengthening, surgical times were similar to those of left kidney grafts. The authors concluded that the functional outcomes of these surgical approaches were comparable [46].

In another study, researchers from Spain found no significant difference in the use of right or left donor kidneys with respect to early posttransplant thrombosis. To control for donor-related factors, they compared the outcomes of contralateral kidney transplants from the same donor (24 pairs of transplants). However, they observed a striking discrepancy in the thrombosis rates based on the side of transplantation: 21 thrombosed grafts on the right (87.5%) compared to only three on the left [46].

An increased risk of thrombosis in deceased donor kidneys compared with grafts from living related donors has not been consistently observed in either earlier studies [43, 47] or more recent research. A recent study analyzing a cohort of 446 patients who received grafts from both living and deceased donors found no significant difference in renal artery thrombosis rates between the two groups [48].

While early studies did not identify warm ischemia time as a risk factor for thrombosis [44], a more recent study from Tunisia highlighted prolonged warm ischemia as a potential risk factor for vascular thrombosis [49]. An increased incidence of thrombosis has been reported in cases where cold ischemia time exceeded 24 hours [36].

Recipient-related risk factors for thrombotic complications

Recipient-related factors are considered more critical for KT outcomes than donor-related factors [50]. Recipient-related risk factors include age, the underlying disease leading to end-stage renal disease (ESRD), comorbidities, and the choice, order, and duration of renal replacement therapy (RRT).

It is well established that recipients younger than 5 years and older than 50 years are more susceptible to graft thrombosis [35]. However, KT is increasingly being performed in older patients [51–54]. In the United States, the proportion of patients aged 65–74 years on the transplant waiting list has risen from 2% in the 1990s to over 10% in 2012. Similarly, in Europe, the average recipient age has increased by 10 years over the past two decades. For example, in the Netherlands, the proportion of kidney transplant recipients over 65 years of age grew from 22.8% in 2005 to 39.8% in 2017 [53, 55].

The underlying disease that led to ESRD significantly influences transplant outcomes. Individuals with diabetes mellitus and diabetic nephropathy are at a significantly increased risk of thrombosis due to hyperactive platelets, elevated prothrombotic clotting factors, and impaired fibrinolysis [56]. Diabetes accelerates the development of atherosclerosis, further increasing the risk of thrombotic complications. Cardiovascular disease and angiopathy associated with atherosclerosis also contribute to a higher likelihood of thrombosis in these patients [6].

Obesity (BMI >30 kg/m) has been associated with an increased risk of thrombosis, as well as a paradoxical protective effect against postoperative bleeding [41, 64]. Given the global rise in obesity, more high-BMI patients are undergoing KT [57]. While BMI likely interacts with other patient-specific factors, it remains an important consideration for transplant candidacy and post-transplant outcomes [58].

The choice, order, and duration of RRT can influence transplant outcomes significantly. A systematic review analyzing 76 studies (1968–2019) found that preemptive transplantation offers better long-term survival and a lower risk of graft loss [59].

Preemptive transplantation – where a kidney transplant is performed before the initiation of dialysis – has been shown to significantly improve long-term survival and reduce the risk of graft loss. A systematic review that analyzed 76 studies from 1968 to 2019 confirmed these benefits, highlighting the importance of early transplantation in optimizing patient outcomes [59].

The selection, sequence, and duration of RRT play a crucial role in transplant outcomes. A systematic review of 76 studies (1968–2019) found that preemptive transplantation significantly improves long-term survival and reduces the risk of graft loss [59].

Several large-cohort studies have reported a significantly higher incidence of thrombotic graft loss in patients who underwent peritoneal dialysis (PD) before transplantation compared to those on hemodialysis (HD) [60]. This increased risk is attributed to elevated levels of procoagulant factors, such as apolipoprotein A and coagulation factors II, VII, VIII, IX, X, XI, and XII, in PD patients, likely due to a moderate nonspecific inflammatory response of the peritoneum to dialysate exposure. However, other studies suggest that the type of dialysis does not significantly influence the risk of graft thrombosis [61].

PATHOPHYSIOLOGY OF HEMOSTATIC CHANGES IN RENAL TRANSPLANT RECIPIENTS

In KT, all three components of Virchow's triad – endothelial damage, circulatory stasis, and a hypercoagulable state – are present [62, 63]. These factors can contribute to thrombosis due to issues arising during vascular anastomosis and reconstruction, vascular intima damage, reduced blood flow from vessel constriction, compression, or twisting, as well as graft congestion. Additionally, the hypercoagulable state may result from

the pathophysiology of chronic kidney disease (CKD) itself or associated comorbidities [3].

Historically, patients with end-stage CKD were considered to be in a "hypocoagulant" state, meaning they had an increased tendency to bleed rather than clot. In the early 1980s, studies demonstrated that patients with uremia often suffer from anemia, and their bleeding time is strongly dependent on anemia. Correcting anemia to a hematocrit level above 30% was found to significantly reduce bleeding time and the severity of hemorrhagic manifestations [64].

Recent studies have identified CKD as a risk factor for thromboembolic complications. CKD is associated with a prothrombotic state, marked by elevated tissue factor activity, increased fibrinogen, and higher D-dimer levels [65]. The disease also involves systemic inflammation, oxidative stress, activation of the renin-angiotensin-aldosterone system, anemia, microalbuminuria, hyperhomocysteinemia, hyperparathyroidism, and bone and mineral metabolism disorders. Specific apolipoprotein isoforms and platelet hyperreactivity contribute to a hypercoagulable state, increasing the risk of arterial and venous thromboembolic events and accelerating the progression of kidney failure [63, 66].

Paradoxically, while ESRD patients are at increased risk for thrombosis, they also have a higher propensity for bleeding, with a 4% incidence of postoperative bleeding after transplantation compared to 1% in general surgery [67]. This may be attributed to profound imbalances between procoagulant and anticoagulant mechanisms in CKD patients.

PREVENTION OF THROMBOTIC COMPLICATIONS IN KIDNEY TRANSPLANTATION

Rapid identification of thrombotic complications is crucial for successful prophylaxis in KT, as treatment options are largely limited to emergency surgery and thrombectomy. While perioperative prophylactic antithrombotic therapy appears justified, no standardized protocols currently exist [68]. Existing thrombosis prevention guidelines primarily focus on venous thromboembolism and do not specifically address thrombosis at surgical sites [69]. Additionally, the European Association of Urology guidelines do not recommend routine postoperative prophylaxis with unfractionated or low-molecular-weight heparin for low-risk living-donor transplant recipients [70].

Patients with advanced CKD face a delicate balance between thromboembolic risk and bleeding complications, making anticoagulant therapy particularly challenging. Due to hemostatic alterations and multiple comorbidities, CKD and ESRD patients are often excluded from clinical trials evaluating anticoagulation therapy [71, 72]. Consequently, there is limited evidence on the efficacy and safety of anticoagulants in this population, and no standardized risk assessment scale exists to accurately determine individual thromboembolic and hemorrhagic risk. Additionally, pharmacokinetic and pharmacodynamic alterations related to impaired renal function further complicate anticoagulation management [63].

As a result, reliable data for establishing evidence-based guidelines on perioperative antithrombotic therapy remain limited [73]. Consequently, different medical centers implement their own protocols for perioperative anticoagulation and postoperative thromboprophylaxis [68].

CONCLUSION

Advancements in surgical techniques, perioperative management, and immunosuppressive therapy have significantly improved KT outcomes and patient survival. However, vascular complications remain a major challenge, posing risks to both the graft and the recipient. A thorough analysis of these complications highlights three key areas requiring special attention: the intrinsic characteristics of the donor organ, recipient-associated risk factors, and the complexity of the surgical procedure – all of which underscore the importance of preventive strategies.

The authors declare no conflict of interest.

REFERENCES

1. *Gómez Dos Santos V, Hevia Palacios V, Galeano Álvarez C, Olavarría Delgado A, Díez Nicolás V, Jiménez Álvaro S et al.* Renal allograft transplant vascular complications. Diagnostic and treatment. *Arch Esp Urol*. 2021; 74 (10): 1013–1028.
2. *Mayhew M, Solomon R, LaGuardia H, Shaw K, Arenas J, Hranjec T*. Vascular Complications in Renal Transplantation: Surgical Salvage of Renal Artery Dissection. *Transplant Direct*. 2022; 8 (6): e1340.
3. *Verloh N, Doppler M, Hagar MT, Kulka C, von Krüchten R, Neubauer J et al*. Interventional Management of Vascular Complications after Renal Transplantation. *Rofo*. 2023; 195 (6): 495–504.
4. *Aktas S, Boyvat F, Sevmis S, Moray G, Karakayali H, Haberal M*. Analysis of vascular complications after renal transplantation. *Transplant Proc*. 2011; 43 (2): 557–561.
5. *Tavakkoli M, Zafarghandi RM, Taghavi R, Ghoreifi A, Zafarghandi MM*. Immediate Vascular Complications After Kidney Transplant: Experience from 2100 Recipients. *Exp Clin Transplant*. 2017; 15 (5): 504–508.
6. *Zhang J, Xue W, Tian P, Zheng J, Ding C, Li Y et al*. Diagnostic and therapeutic strategies for vascular complications after renal transplantation: a single-center experience in 2,304 renal transplantations. *Front Transplant*. 2023; 2: 1150331.
7. *Sugi MD, Joshi G, Maddu KK, Dahiya N, Menias CO*. Menias. Imaging of Renal Transplant Complications throughout the Life of the Allograft: Comprehensive

Multimodality Review. *Radiographics*. 2019; 39 (5): 1327–1355.
8. *Srivastava A, Kumar J, Sharma S, Abhishek, Ansari MS, Kapoor R*. Vascular complication in live related renal transplant: An experience of 1945 cases. *Indian J Urol*. 2013; 29 (1): 42–47.
9. *Dimitroulis D, Bokos J, Zavos G, Nikiteas N, Karidis NP, Katsaronis P, Kostakis A*. Vascular complications in renal transplantation: a single-center experience in 1367 renal transplantations and review of the literature. *Transplant Proc*. 2009; 41 (5): 1609–1614.
10. *Granata A, Clementi S, Londrino F, Romano G, Veroux M, Fiorini F, Fatuzzo P.* Renal transplant vascular complications: the role of Doppler ultrasound. *J Ultrasound*. 2014; 18 (2): 101–107.
11. *Nuriakhmetov RR, Zagitov AR, Panteleev VS, Musin IR, Biganyakov II, Mukhametova RR et al*. Vascular complications of the early postoperative period in patients after kidney transplantation. *Bashkortostan Medical Journal*. 2022; 17 (2): 54–60. (In Russ.).
12. *Rajan DK, Stavropoulos SW, Shlansky-Goldberg RD*. Management of transplant renal artery stenosis. *Semin Intervent Radiol*. 2004; 21 (4): 259–269.
13. *Antonopoulos IM, Yamaçake KG, Oliveira LM, Piovesan AC, Kanashiro H, Nahas WC*. Revascularization of living-donor kidney transplant with multiple arteries: long-term outcomes using the inferior epigastric artery. *Urology*. 2014; 84 (4): 955–959.
14. *Klepanec A, Balazs T, Bazik R, Madaric J, Zilinska Z, Vulev I.* Pharmacomechanical thrombectomy for treatment of acute transplant renal artery thrombosis. *Ann Vasc Surg*. 2014; 28 (5): 1314e11-4.
15. *Harraz AM, Shokeir AA, Soliman SA, Osman Y, El-Hefnawy AS, Zahran MH et al*. Salvage of grafts with vascular thrombosis during live donor renal allotransplantation: a critical analysis of successful outcome. *Int J Urol*. 2014; 21 (10): 999–1004.
16. *Ayvazoglu Soy EH, Akdur A, Kirnap M, Boyvat F, Moray G, Haberal M*. Vascular Complications After Renal Transplant: A Single-Center Experience. *Exp Clin Transplant*. 2017; 15 (Suppl 1): 79–83.
17. *Cambou L, Millet C, Terrier N, Malvezzi P, Timsit MO, Anglicheau D et al*. Management and Outcome After Early Renal Transplant Vein Thrombosis: A French Multicentre Observational Study of Real-Life Practice Over 24 Years. *Transpl Int*. 2023; 36: 10556.
18. *Carolan C, Tingle SJ, Thompson ER, Sen G, Wilson CH*. Comparing outcomes in right versus left kidney transplantation: A systematic review and meta-analysis. *Clin Transplant*. 2021; 35 (11): e14475.
19. *Kulkarni S, Wei G, Jiang W, Lopez LA, Parikh CR, Hall IE*. Outcomes From Right Versus Left Deceased-Donor Kidney Transplants: A US National Cohort Study. *Am J Kidney Dis*. 2020; 75 (5): 725–735.
20. *Natour AK, Ahmed S, Kim DY, Malinzak L, Rteil A, Kabbani L*. Risk of Ipsilateral Deep Vein Thrombosis After Kidney Transplantation: A Retrospective Study. *Cureus*. 2022; 14 (4): e24482.
21. *Di Cocco P, Kandilis A, Rajagopal P, Herbert P, Hassen Y, Hakim N*. Surgical Stapler for Right Renal Vein Elongation Using the Inferior Vena Cava in Kidney Transplant. *Exp Clin Transplant*. 2016; 14 (5): 564–566.
22. *Tekin S, Erok B, Win NN, Agolli E, Uçak A, Akyol H et al*. A successful kidney transplantation in case of completely occluded inferior vena cava and iliac veins: a case of inherited antithrombin deficiency. *Revista de Nefrologia, Dialisis y Trasplante*. 2021; 41 (4): 304–310.
23. *Santos JE, Gaspar A, Querido S, Jorge C, Weigert A, Gabriel HM et al*. Unexpected success in early post-transplantation renal vein thrombosis: A case report and literature review. *Clin Nephrol Case Stud*. 2021; 9: 19–25.
24. *Fathi T, Samhan M, Gawish A, Donia F, Al-Mousawi M*. Renal allograft venous thrombosis is salvageable. *Transplant Proc*. 2007; 39 (4): 1120–1121.
25. *Haberal M, Boyvat F, Akdur A, Kırnap M, Özçelik Ü, Yarbuğ Karakayalı F*. Surgical Complications After Kidney Transplantation. *Exp Clin Transplant*. 2016; 14 (6): 587–595.
26. *Humar A, Matas AJ.* Surgical complications after kidney transplantation. *Semin Dial*. 2005; 18 (6): 505–510.
27. *Lerman M, Mulloy M, Gooden C, Khan S, Khalil A, Patel L, Zhou XJ*. Post transplant renal vein thrombosis, with successful thrombectomy and review of the literature. *Int J Surg Case Rep*. 2019; 61: 291–293.
28. *Ponticelli C, Moia M, Montagnino G.* Renal allograft thrombosis. *Nephrol Dial Transplant*. 2009; 24 (5): 1388–1393.
29. *Kadoya Y, Zen K, Matoba S*. Endovascular treatment of transplant renal artery stenosis based on hemodynamic assessment using a pressure wire: a case report. *BMC Cardiovasc Disord*. 2018; 18 (1): 172.
30. *Baird DP, Williams J, Petrie MC, Smith JR*. Transplant Renal Artery Stenosis. *Kidney Int Rep*. 2020; 5 (12): 2399–2402.
31. *Li H, Shao G, Zhao Y, Zhong H*. The value of inflow inversion recovery MRI for the diagnosis of transplant renal artery stenosis: comparison with digital subtraction angiography. *Egypt J Radiol Nucl Med*. 2022; 53 (7).
32. *Qi R, Qi G, Zhu D, Wang J*. Diagnosis and Treatment of Early Transplant Renal Artery Stenosis: Experience From a Center in Eastern China. *Transplant Proc*. 2020; 52 (1): 179–185.
33. *Bruno S, Remuzzi G, Ruggenenti P*. Transplant renal artery stenosis. *J Am Soc Nephrol*. 2004; 15 (1): 134–141.
34. *Ngo AT, Markar SR, De Lijster MS, Duncan N, Taube D, Hamady MS*. A Systematic Review of Outcomes Following Percutaneous Transluminal Angioplasty and Stenting in the Treatment of Transplant Renal Artery Stenosis. *Cardiovasc Intervent Radiol*. 2015; 38 (6): 1573–1588.
35. *Hinojosa-Gonzalez DE, Salgado-Garza G, Torres-Martinez M, Villegas-De Leon SU, Bueno-Gutierrez LC, Herrera-Carrillo FE et al*. Endovascular Treatment of Transplant Renal Artery Stenosis: A Systematic Review and Meta-analysis. *J Endovasc Ther*. 2022; 29 (2): 294–306.
36. *Van den Berg TAJ, Minnee RC, Lisman T, Nieuwenhuijs-Moeke GJ, van de Wetering J, Bakker SJL, Pol RA*. Perioperative antithrombotic therapy does not increase the incidence of early postoperative thromboembolic

complications and bleeding in kidney transplantation – a retrospective study. *Transpl Int*. 2019; 32 (4): 418–430.
37. *Panwar P, Bansal D, Maheshwari R, Chaturvedi S, Desai P, Kumar A*. Management of donor kidneys with double renal arteries with significant luminal discrepancy: A retrospective cohort study. *Indian J Urol*. 2020; 36 (3): 200–204.
38. *Scheuermann U, Rademacher S, Wagner T, Lederer A, Hau HM, Seehofer D, Sucher R*. Influence of Multiple Donor Renal Arteries on the Outcome and Graft Survival in Deceased Donor Kidney Transplantation. *J Clin Med*. 2021; 10 (19): 4395.
39. *Yamanaga S, Rosario A, Fernandez D, Kobayashi T, Tavakol M, Stock PG, Kang SM*. Inferior long-term graft survival after end-to-side reconstruction for two renal arteries in living donor renal transplantation. *PLoS One*. 2018; 13 (7): e0199629.
40. *Popov Z, Stankov O, Stavridis S, Saidi S, Ivanovski O, Spasovski G et al*. Management of Multiple Renal Arteries and Unusual Venous Anatomy During Kidney Transplant: From a Simple Technical Problem to a Graft-Saving Procedure. *Exp Clin Transplant*. 2020; 18 (7): 763–770.
41. *Garcia LE, Parra N, Gaynor JJ, Baker L, Guerra G, Ciancio G*. Clinical Outcomes Following Single *vs.* Multiple Vessel Living-Donor Kidney Transplantation: A Retrospective Comparison of 210 Patients. *Front Surg*. 2021; 8: 693021.
42. *Mahajan AD, Patel ND, Singh Pal L, Bathe S, Darakh PP, Patil M*. Retrospective Analysis of the Comparison Between Single Renal Artery Versus Multiple Renal Arteries in Living Donor Kidney Transplant: Does It Affect the Outcome? *Exp Clin Transplant*. 2021; 19 (1): 38–43.
43. *Salehipour M, Salahi H, Jalaeian H, Bahador A, Nikeghbalian S, Barzideh E et al*. Vascular complications following 1500 consecutive living and cadaveric donor renal transplantations: a single center study. *Saudi J Kidney Dis Transpl*. 2009; 20 (4): 570–572.
44. *Osman Y, Shokeir A, Ali-el-Dein B, Tantawy M, Wafa EW, el-Dein AB, Ghoneim MA*. Vascular complications after live donor renal transplantation: study of risk factors and effects on graft and patient survival. *J Urol*. 2003; 169 (3): 859–862.
45. *Fallani G, Maroni L, Bonatti C, Comai G, Buzzi M, Cuna V et al*. Renal Vessel Extension With Cryopreserved Vascular Grafts: Overcoming Surgical Pitfalls in Living Donor Kidney Transplant. *Transpl Int*. 2023; 36: 11060.
46. *Amézquita Y, Méndez C, Fernández A, Caldes S, Pascual J, Muriel A et al*. Risk factors for early renal graft thrombosis: a case-controlled study in grafts from the same donor. *Transplant Proc*. 2008; 40 (9): 2891–2893.
47. *McDonald RA, Smith JM, Stablein D, Harmon WE*. Pretransplant peritoneal dialysis and graft thrombosis following pediatric kidney transplantation: a NAPRTCS report. *Pediatr Transplant*. 2003; 7 (3): 204–208.
48. *Fakhr Yasseri AM, Namdari F, Gooran S, Ahmadi A, Dehghani S, Asadi M et al*. Living versus deceased kidney transplantation: Comparison of complications. *Urologia*. 2021; 88 (3): 185–189.
49. *Zaghbib S, Chakroun M, Saadi A, Boussaffa H, Bouzouita A, Derouiche A et al*. Vascular Complications of Renal Transplantation: Risk Factors and Impact on Graft Survival. *Nephrology Dialysis Transplantation*. 2022; 37 (Issue Suppl 3): gfac087.026.
50. *Schaapherder AF, Kaisar M, Mumford L, Robb M, Johnson R, de Kok MJC et al*. Donor characteristics and their impact on kidney transplantation outcomes: Results from two nationwide instrumental variable analyses based on outcomes of donor kidney pairs accepted for transplantation. *EClinicalMedicine*. 2022; 50: 101516.
51. *Hammad E, Broering D, Shah Y, Nazmi A, Al Abassi A, Brockmann JG et al*. Outcomes of Kidney Transplantation in Older Recipients. *Ann Transplant*. 2023; 28: e938692.
52. *Yemini R, Rahamimov R, Ghinea R, Mor E*. Long-Term Results of Kidney Transplantation in the Elderly: Comparison between Different Donor Settings. *J Clin Med*. 2021; 10 (22): 5308.
53. *Tegzess E, Gomes Neto AW, Pol RA, de Boer SE, Peters-Sengers H, Sanders JF, Berger SP*. Comparative survival of elderly renal transplant recipients with a living donor versus a deceased donor: A retrospective single center observational study. *Transpl Int*. 2021; 34 (12): 2746–2754.
54. *Mehta J, Ndubueze O, Tatum D, Jeon H, Paramesh A, Killackey M, Vijay A*. Kidney Transplant Outcomes in Recipients Over the Age of 70. *Cureus*. 2023; 15 (1): e34021.
55. *Artiles A, Domínguez A, Subiela JD, Boissier R, Campi R, Prudhomme T et al*. Kidney Transplant Outcomes in Elderly Population: A Systematic Review and Meta-analysis. *Eur Urol Open Sci*. 2023; 51: 13–25.
56. *Alsharidah AS.* Diabetes mellitus and diabetic nephropathy: a review of the literature on hemostatic changes in coagulation and thrombosis. *Blood Res*. 2022; 57 (2): 101–105.
57. *Reggiani F, Moroni G, Ponticelli C*. Cardiovascular Risk after Kidney Transplantation: Causes and Current Approaches to a Relevant Burden. *J Pers Med*. 2022; 12 (8): 1200.
58. *Schold JD, Augustine JJ, Huml AM, Fatica R, Nurko S, Wee A, Poggio ED*. Effects of body mass index on kidney transplant outcomes are significantly modified by patient characteristics. *Am J Transplant*. 2021; 21 (2): 751–765.
59. *Azegami T, Kounoue N, Sofue T, Yazawa M, Tsujita M, Masutani K et al*. Efficacy of pre-emptive kidney transplantation for adults with end-stage kidney disease: a systematic review and meta-analysis. *Ren Fail*. 2023; 45 (1): 2169618.
60. *Che X, Yang X, Yan J, Yuan Y, Ma Q, Ying L et al*. Effects of pretransplant peritoneal *vs.* hemodialysis modality on outcome of first kidney transplantation from donors after cardiac death. *BMC Nephrol*. 2018; 19 (1): 235.
61. *Lin HT, Liu FC, Lin JR, Pang ST, Yu HP*. Impact of the pretransplant dialysis modality on kidney transplantation outcomes: a nationwide cohort study. *BMJ Open*. 2018; 8 (6): e020558.

62. *Thiessen L, MacDonell S, Wall C, Jacob P, Shoker A, Moser MAJ*. Transplant renal vein thrombosis in a recipient with aberrant venous anatomy. *CEN Case Rep*. 2018; 7 (2): 264–267.
63. *Aursulesei V, Costache II*. Anticoagulation in chronic kidney disease: from guidelines to clinical practice. *Clin Cardiol*. 2019; 42 (8): 774–782.
64. *Livio M, Gotti E, Marchesi D, Mecca G, Remuzzi G, de Gaetano G*. Uraemic bleeding: role of anaemia and beneficial effect of red cell transfusions. *Lancet*. 1982; 2 (8306): 1013–1015.
65. *Oe Y, Sato E, Sato H, Miyazaki M, Ito S, Takahashi N*. Uremic toxins alter coagulation and fibrinolysis-related genes expression in human endothelial cells. *Thromb Res*. 2020; 186: 75–77.
66. *Lau YC, Proietti M, Guiducci E, Blann AD, Lip GYH*. Atrial Fibrillation and Thromboembolism in Patients With Chronic Kidney Disease. *J Am Coll Cardiol*. 2016; 68 (13): 1452–1464.
67. *Chahal R, Alexander M, Yee K, Jun CMK, Dagher JG, Ismail H et al*. Impact of a risk-stratified thromboprophylaxis protocol on the incidence of postoperative venous thromboembolism and bleeding. *Anaesthesia*. 2020; 75 (8): 1028–1038.
68. *Van den Berg TAJ, Nieuwenhuijs-Moeke GJ, Lisman T, Moers C, Bakker SJL, Pol RA*. Pathophysiological Changes in the Hemostatic System and Antithrombotic Management in Kidney Transplant Recipients. *Transplantation*. 2023; 107 (6): 1248–1257.
69. *Anderson DR, Morgano GP, Bennett C, Dentali F, Francis CW, Garcia DA et al*. American Society of Hematology 2019 guidelines for management of venous thromboembolism: prevention of venous thromboembolism in surgical hospitalized patients. *Blood Adv*. 2019; 3 (23): 3898–3944.
70. *Breda A, Budde K, Figueiredo A, Lledó García E, Olsburgh J, Regele H et al*. EAU Guidelines on Renal Transplantation (European Association of Urology). 2022. 56 s.
71. *D'Apolito M, Du X, Pisanelli D, Pettoello-Mantovani M, Campanozzi A, Giacco F et al*. Urea-induced ROS cause endothelial dysfunction in chronic renal failure. *Atherosclerosis*. 2015; 239 (2): 393–400.
72. *Baaten CCFMJ, Schröer JR, Floege J, Marx N, Jankowski J, Berger M, Noels H*. Platelet Abnormalities in CKD and Their Implications for Antiplatelet Therapy. *Clin J Am Soc Nephrol*. 2022; 17 (1): 155–170.
73. *Surianarayanan V, Hoather TJ, Tingle SJ, Thompson ER, Hanley J, Wilson CH*. Interventions for preventing thrombosis in solid organ transplant recipients. *Cochrane Database Syst Rev*. 2021; 3 (3): CD011557.

The article was submitted to the journal on 13.08.2024

DOI: 10.15825/1995-1191-2025-1-17-22

APPLICATION OF COMBINED ENDOSCOPIC TREATMENT OF PATIENTS WITH BRONCHIAL STENOSIS AFTER LUNG TRANSPLANTATION USING THULIUM LASER, BALLOON DILATION, CRYOABLATION, AND AIRWAY STENTING

M.T. Bekov[1], I.V. Pashkov[1], K.S. Smirnov[1], Ya.S. Yakunin[1], E.F. Shigaev[1], A.Z. Guluev[1], T.S. Kryukova[1], O.M. Tsirulnikova[1, 2], S.V. Gautier[1, 2]

[1] Shumakov National Medical Research Center of Transplantology and Artificial Organs, Moscow, Russian Federation

[2] Sechenov University, Moscow, Russian Federation

Bronchial stenosis (BS) is a persistent, breathing-independent narrowing of the bronchial lumen, primarily brought on by scar and/or granulation tissue. BS occurring after lung transplantation tend to be recurrent, resulting in a higher frequency of hospitalizations compared to the group of patients without this complication. Minimally invasive endoscopic repair of the bronchial lumen is a generally recognized treatment for BS. This article demonstrates the experience of using a combined technique for restoring the lumen and preventing recurrent stenosis using thulium laser, balloon dilation, cryoablation, and stenting (hereinafter referred to as the combined technique).

Keywords: lung transplantation, airway complications, bronchial stenosis, thulium laser, endoscopic balloon dilation, cryoablation, airway stenting.

INTRODUCTION

Bronchial stenosis (BS) is one of the most common airway complications that occur after a lung transplant (LT) [1–3]. According to medical literature, it typically occurs between 3–6 months after an LT [4]. Balloon dilation, bronchial bougienage, argon plasma coagulation (APC), laser use, cryoablation, and stenting are all endoscopic techniques used to restore bronchial lumen and prevent a recurrence [5–6]. Among these, balloon dilation, bougienage, APC, and laser therapy provide immediate effects, while cryoablation has a delayed therapeutic impact [7–8]. Airway stenting is a method used to prevent recurrent bronchial stenosis. Despite the availability of various endoscopic techniques for bronchial lumen restoration and the use of stenting to maintain bronchial patency, BS remains a frequently recurring complication. This, in turn, leads to increased hospitalizations and a reduced quality of life for lung transplant recipients. This article presents the experience of using a combined approach – incorporating thulium laser, balloon dilation, cryoablation, and stenting – to restore bronchial lumen and prevent recurrent stenosis in lung transplant recipients at the Shumakov National Medical Research Center of Transplantology and Artificial Organs ("Shumakov Transplant Center").

Table 1

ISHLT classification of bronchial stenoses

Stenoses	Location	a – anastomotic site
		b – anastomotic and lobar/segmental site
		c – lobar/segmental site only
	Extent	1 – 0% to 25% reduction in cross-sectional area
		2 – >25% to 50% reduction in cross-sectional area
		3 – >50% but <100% reduction in cross-sectional area
		4 – 100% obstruction

MATERIALS AND METHODS

Between September 2014 and November 2024, a total of 119 lung transplants were performed at the Shumakov Transplant Center. The primary diagnostic methods for detecting BS post-transplant included bronchoscopy and chest computed tomography, while spirometry was used at later stages to identify suspected cases. To classify and assess the severity of BS, we applied the bronchial complication classification proposed by the International Society for Heart and Lung Transplantation (ISHLT) (Table 1) [9].

The primary treatment methods for BS in lung transplant recipients at the Shumakov Transplant Center include mechanical bougienage, balloon dilation, APC, and stenting. However, in most cases, these approaches provided only short-term relief, necessitating repeated interventions.

Corresponding author: Maksat Bekov. Address: 1, Shchukinskaya str., Moscow, 123182, Russian Federation. Phone: (926) 399-49-75. E-mail: doctorbekov@gmail.com

Since 2020, cryoablation has been introduced as an independent treatment for BS. This technique has proven effective, particularly in managing BS caused by granulation tissue overgrowth [8].

Since 2021, the thulium laser has been used for scar tissue dissection. When used for recanalizing scar stenoses, it demonstrated a reduced carbonization effect and greater precision compared to APC.

The primary criterion for selecting patients for endoscopic bronchial lumen restoration using a combined approach was the presence of grade 2–4 BS, as well as recurrent BS despite previous airway recanalization attempts.

Endoscopic procedures employing the combined technique were performed in an operating room under general anesthesia, with a preference for rigid intubation and high-frequency mechanical ventilation. Following tracheal intubation, the tracheobronchial tree was thoroughly examined.

The first stage of the procedure involved the dissection of scar tissue using a thulium laser. The pulse energy was initially set at a minimum of 0.025 J with a frequency of 240 Hz. When an increased intensity was required, priority was given to adjusting the radiation frequency rather than the energy level. To minimize tissue carbonization, continuous irrigation and aspiration of a 0.9% sodium chloride solution were performed using a catheter (Fig. 1).

Following scar dissection, the next stage involved balloon dilatation using three-step balloons with incremental diameter increases of 1 mm (6–7–8 mm, 8–9–10 mm, 10–11–12 mm, 12–13.5–15 mm). The required pressure inside the balloon was generated using a specialized blower (Fig. 2).

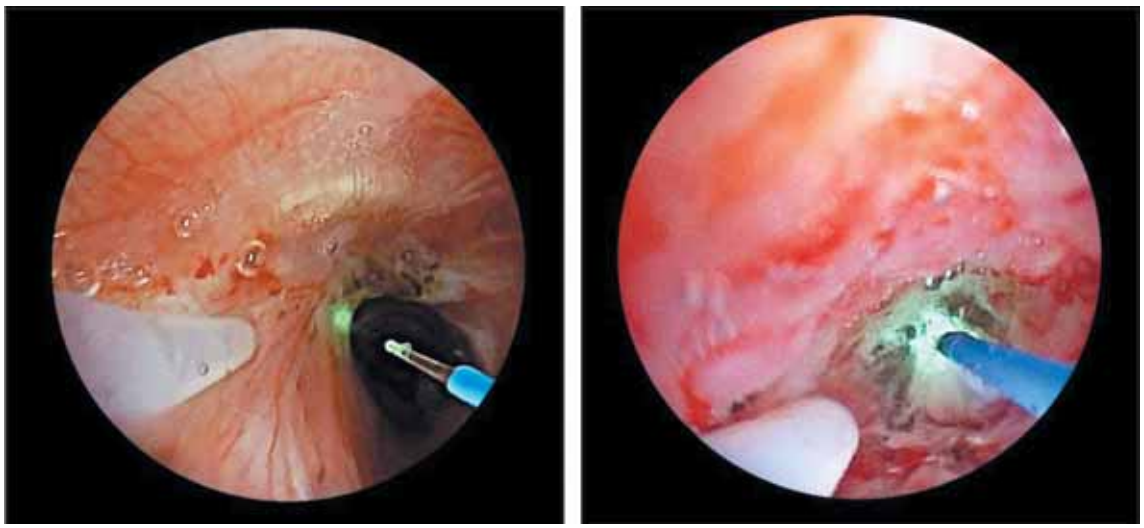

Fig. 1. Stage of vaporization with irrigation with sodium chloride 0.9%

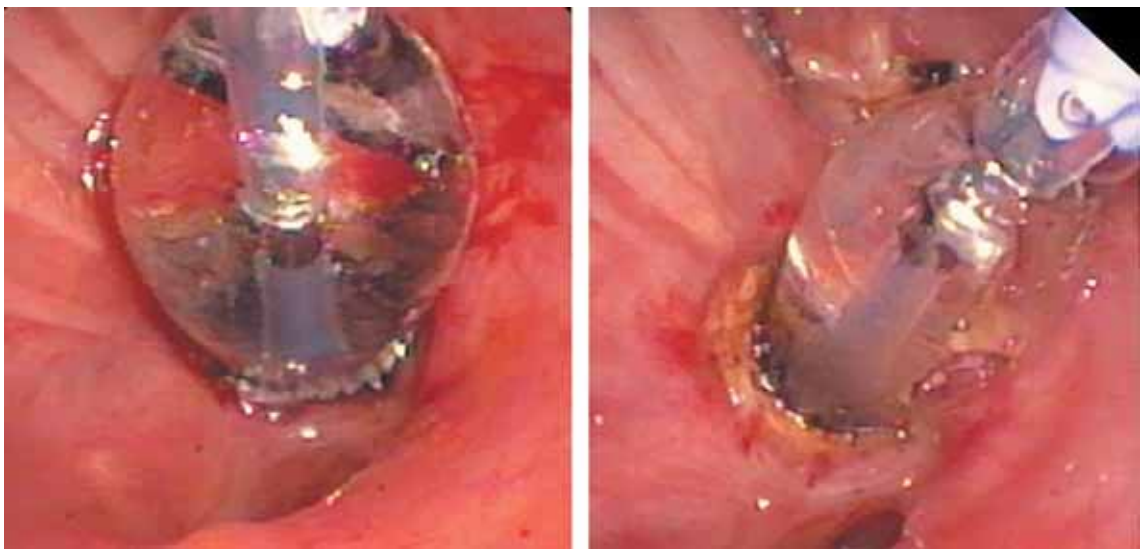

Fig. 2. Balloon bronchoplasty stage

To prevent recurrence, cryotherapy was applied to the stenotic area. The cryoprobe was placed in direct contact with the bronchial mucosa at the site of stenosis, followed by freeze-thaw cycles lasting 30–45 seconds each. Tissue thawing was allowed to complete before the cryoprobe was detached from the mucosa. A total of three freeze-thaw cycles were performed in each treatment zone. The cryoprobe was then repositioned 5–6 mm from the previous site, and the cryotherapy sessions were repeated until the entire stenotic area was treated (Fig. 3).

In cases of impaired bronchial framework function, stenting was performed using a self-expanding nitinol stent (Fig. 4).

RESULTS

The combined technique for bronchial lumen restoration was applied to seven lung transplant recipients with BS. Among them, two patients (28.58%) were diagnosed with intermediate BS, while five (71.42%) had multifocal stenosis. Prior to undergoing the combined technique, the patients had an average of 5.8 ± 1.5 endoscopic recanalization attempts.

A total of 19 surgical interventions were performed using the combined technique for 34 cases of stenosis, averaging 2.71 procedures per patient. The key characteristics of BS in this patient group are summarized in Table 2 and illustrated in Figs. 5–7.

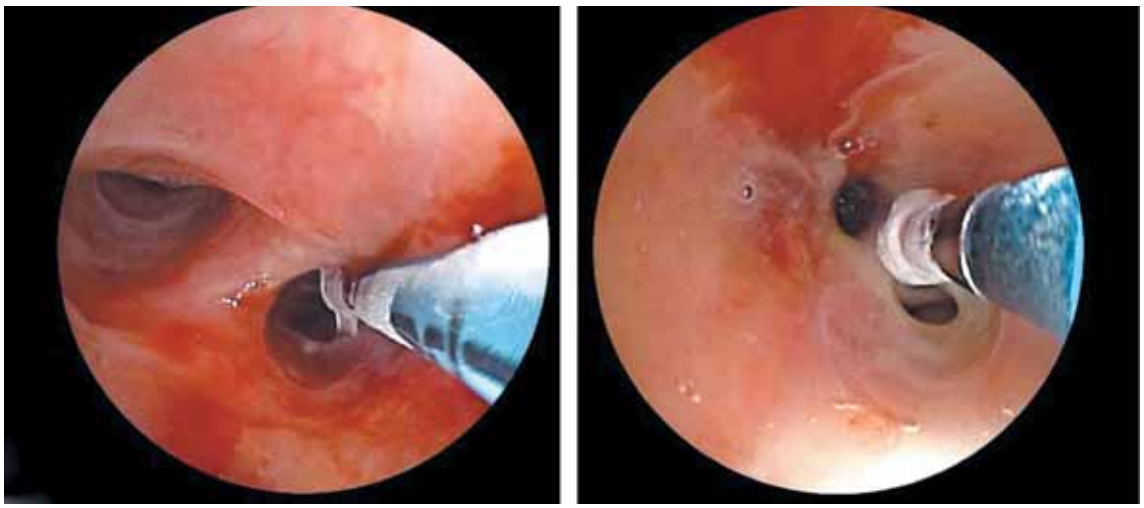

Fig. 3. Cryotherapy stage

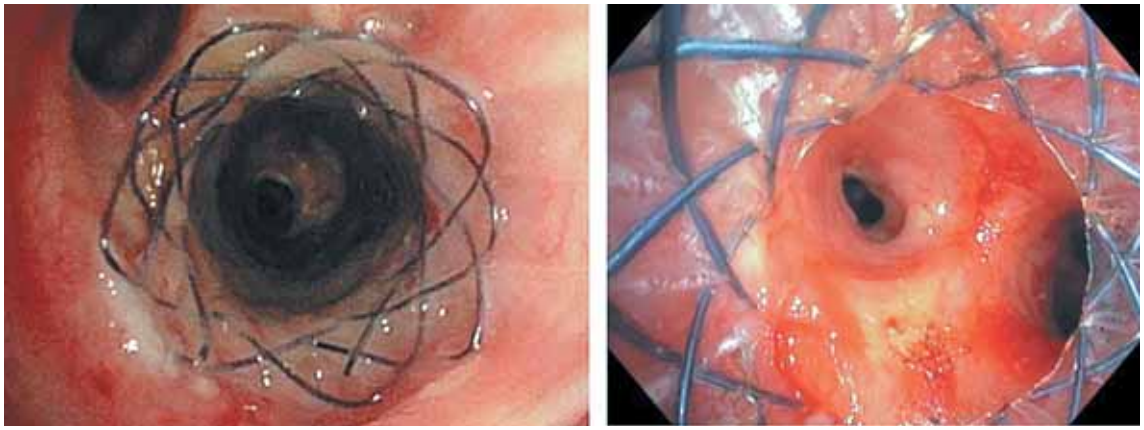

Fig. 4. Bronchial stenting stage

Table 2

Number of surgical interventions according to ISHLT stenosis classification

Types of stenosis	Number of operations
Central airway stenosis	7
Distal airway stenosis	11
Combined airway stenosis	1

Repeated surgical interventions in lung transplant recipients with BS who underwent endoscopic recanalization using the combined technique were associated with the following complications: recurrent narrowing of the lumen at the proximal or distal edge of the nitinol stent (5 cases, 14.7%) and stent migration during diagnostic

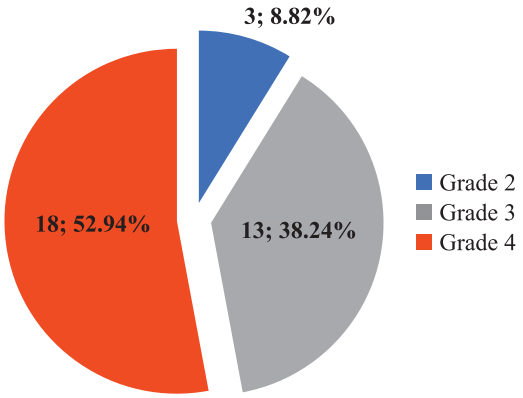

Fig. 5. Extent of bronchial stenosis according to ISHLT classification

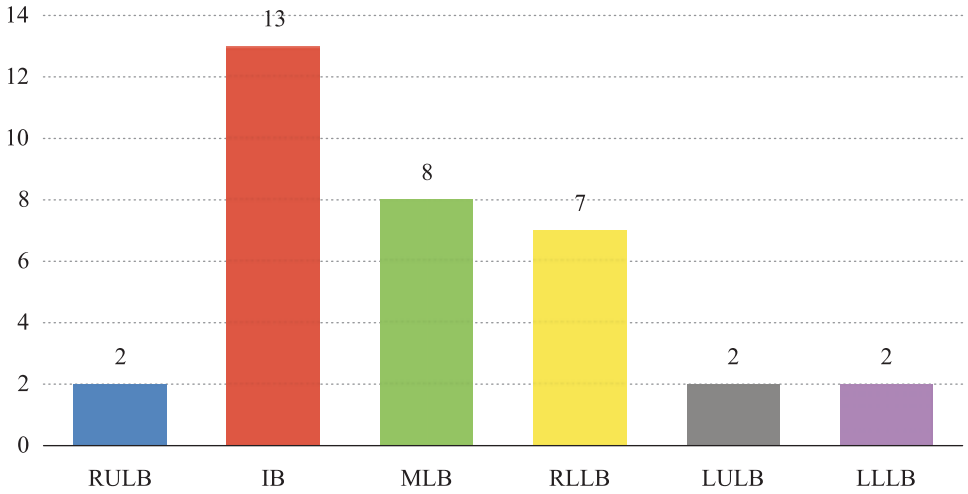

Fig. 6. Location of bronchial stenosis for which recanalization was performed using a combined technique. RULB, right upper lobe bronchus; IB, intermediate bronchus; MLB, middle lobe bronchus; RLLB, right lower lobe bronchus; LULB, left upper lobe bronchus; LLLB, left lower lobe bronchus)

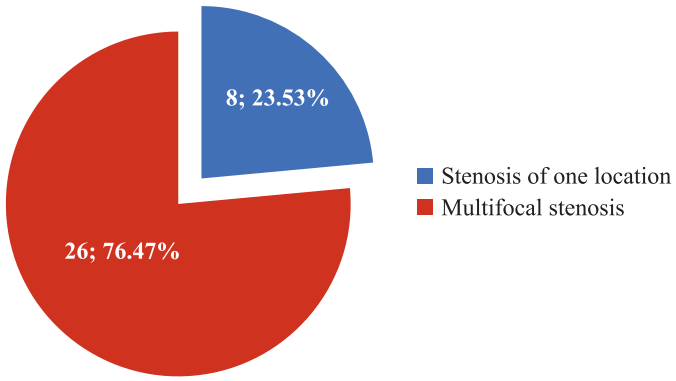

Fig. 7. Prevalence of bronchial stenosis

bronchoscopy (1 patient, 2.9%). There were no cases of bleeding and bronchial wall rupture in the study group.

The stent was removed in cases where no recurrent BS was detected for at least one year post-stenting. A persistent remission, with a recurrence-free period exceeding one year, was achieved in six lung recipients (85.71%).

CONCLUSION

Despite advancements in surgical techniques for lung transplantation, improved postoperative management, and minimally invasive endoscopic interventions, the incidence of recurrent BS in lung recipients remains high. This highlights the need for developing new approaches to endoscopic treatment for this patient cohort.

The use of a combined technique – incorporating thulium laser, balloon dilation, cryoablation, and stenting – for bronchial lumen restoration and recurrent stenosis prevention in lung recipients has proved to be effective in lung transplant recipients. Notably, no significant complications, such as bleeding or bronchial wall rupture, were observed, further supporting the safety and efficacy of this approach.

Recurrent BS when using the combined technique was primarily attributed to lumen narrowing at the proximal and distal edges of the nitinol stent. In cases of recurrence, repeat surgical intervention involving thulium laser, balloon dilation, and cryoablation was performed.

According to several studies, the recurrence rate during stenting may be reduced by using Dumont silicone stents [10–12]. However, the structural characteristics of silicone stents – such as an average wall thickness of 1 mm and the presence of outer protrusions that prevent migration – can narrow the bronchial lumen, making them unsuitable for stenting in lobar and segmental bronchi.

The development of alternative stent materials, including biodegradable options, integration of 3D printing technology, and the use of drug-eluting stents, may offer promising solutions for reducing recurrence rates in BS treatment [13–15].

The authors declare no conflict of interest.

REFERENCES

1. *Santacruz JF, Mehta AC.* Airway complications and management after lung transplantation: ischemia, dehiscence, and stenosis. *Proc Am Thorac Soc.* 2009; 6 (1): 79–93. doi: 10.1513/pats.200808-094GO.
2. *Machuzak M, Santacruz JF, Gildea T, Murthy SC.* Airway complications after lung transplantation. *Thorac Surg Clin*. 2015; 25 (1): 55–75. doi: 10.1016/j.thorsurg.2014.09.008.
3. *Faccioli E, Dell'Amore A, Ferrigno P, Schiavon M, Mammana M, Terzi S, Rea F.* Surgical management of post-transplant bronchial stenoses: a single-center experience. *Surg Today*. 2022 Mar; 52 (3): 449–457. doi: 10.1007/s00595-021-02360-z.
4. *Mahajan AK, Folch E, Khandhar SJ, Channick CL, Santacruz JF, Mehta AC, Nathan SD.* The diagnosis and management of airway complications following lung transplantation. *Chest*. 2017; 152 (3): 627–638. doi: 10.1016/j.chest.2017.02.021.
5. *Pashkov IV, Bekov MT, Gautier SV.* Bronchial complications after lung transplantation. *Russian Journal of Transplantology and Artificial Organs*. 2021; 23 (1): 140–149. doi: 10.15825/1995-1191-2021-1-140-149.
6. *Simonova MS, Rusakov MA, Parshin VD.* Airway complications after lung transplantation. *Pirogov Russian Journal of Surgery Khirurgiya. Zurnal im. N.I. Pirogova*. 2021; 7: 77–83. doi: 10.17116/hirurgia202107177.
7. *Bekov MT, Pashkov IV, Latypov RA, Oleshkevich DO, Smirnov KS, Yakunin YaS et al.* Thulium fiber laser use in interventional bronchoscopy in lung recipients. *Russian Journal of Transplantology and Artificial Organs*. 2023; 25 (4): 41–45. doi: 10.15825/1995-1191-2023-4-41-45.
8. *Bekov MT, Pashkov IV, Mozheiko NP, Latypov RA, Oleshkevich DO, Smirnov KS et al.* Cryotechnology in lung and heart-lung transplantation. *Russian Journal of Transplantology and Artificial Organs*. 2023; 25 (3): 31–37. doi: 10.15825/1995-1191-2023-3-31-37.
9. *Crespo MM, McCarthy DP, Hopkins PM, Clark SC, Budev M, Bermudez CA et al.* ISHLT Consensus Statement on adult and pediatric airway complications after lung transplantation: Definitions, grading system, and therapeutics. *J Heart Lung Transplant.* 2018; 37 (5): 548–563. doi: 10.1016/j.healun.2018.01.1309.
10. *Gasanov AM*. Diagnosticheskaya i operativnaya endoskopya pri transplantacii legkih. [Dissertation]. M., 2023; 35.
11. *Sundset A, Lund MB, Hansen G, Bjørtuft Ø, Kongerud J, Geiran OR*. Airway complications after lung transplantation: long-term outcome of silicone stenting. *Respiration*. 2012; 83 (3): 245–252. doi: 10.1159/000334905.
12. *Guibert N, Saka H, Dutau H.* Airway stenting: Technological advancements and its role in interventional pulmonology. *Respirology*. 2020; 25 (9): 953–962. doi: 10.1111/resp.13801.
13. *Van Pel R, Gan T, Klooster K, Daniels JM, Ruigrok D, Hellemons M, Slebos D.* Lung Transplant Airway Complications Treated with Biodegradable Stents; A Multi-Center Experience. *J Heart Lung Transplant.* 2023; 42 (4): S531. doi: 10.1016/j.healun.2023.02.1453.
14. *Bekov MT, Pashkov IV, Smirnov KS, Yakunin YaS, Shilkin DN, Chashchin IS et al.* Fabrication of a 3D printed everolimus-eluting stent made of thermoplastic polyurethane and polylactide. *Russian Journal of Transplantology and Artificial Organs*. 2024; 26 (1): 47–54. doi: 10.15825/1995-1191-2024-1-47-54.
15. *Zhu GH, Ng AH, Venkatraman SS, Boey FY, Wee AL, Trasti SL, Yee Lim LH.* A novel bioabsorbable drug-eluting tracheal stent. *Laryngoscope*. 2011; 121 (10): 2234–2239. doi: 10.1002/lary.22175.

The article was submitted to the journal on 08.11.2024

DOI: 10.15825/1995-1191-2025-1-23-31

ADVERSE EFFECTS OF IMMUNOSUPPRESSIVE THERAPY AFTER KIDNEY TRANSPLANT

S.V. Popov[1, 2, 6], R.G. Guseinov[1–3], K.V. Sivak[1, 4], V.V. Perepelitsa[1, 2], I.O. Schmidt[1], N.S. Bunenkov[1, 5], T.A. Lelyavina[1, 7]

[1] St. Luke's Clinical Hospital, St. Petersburg, St. Petersburg, Russian Federation
[2] St. Petersburg Medico-Social Institute, St. Petersburg, Russian Federation
[3] St. Petersburg State University, St. Petersburg, Russian Federation
[4] Smorodintsev Research Institute of Influenza, St. Petersburg, Russian Federation
[5] Pavlov University, St. Petersburg, Russian Federation
[6] Kirov Military Medical Academy, St. Petersburg, Russian Federation
[7] Almazov National Medical Research Centre, St. Petersburg, Russian Federation

This paper reviews the sources and generality of knowledge regarding the adverse effects of immunosuppressive therapy, which play an important role in the full functioning of a transplant. The article regarding the importance of the dynamic impact of immunosuppressant medications on transplant function and the need for reasonable regimen and dosage selection of individual drugs or their combination to minimize adverse effects.

Keywords: immunosuppression, immunosuppressive agents, kidney transplantation, nephrotoxic side effects.

Kidney disease has affected humans since time immemorial, but it is only in the last four decades that the actual incidence has been documented and identified as a global health problem [1]. Chronic kidney disease is an important public health problem that places a significant burden on patients, their families and health care systems [2]. Kidney transplantation (KT) is the preferred treatment for end-stage renal disease. Improvements in surgical techniques and immunotherapy have changed the field of KT. The 1-year and 5-year survival rates of KT patients are 95% and 90%, respectively [3]. KT provides better survival compared to dialysis but does not fully improve quality of life. The overall risk of death in transplant recipients is at least three times higher than in the general population, and transplant recipients have a significantly reduced quality of life even compared to patients with other chronic diseases. Strategies such as optimization of selection, cross-matching and surgical techniques, improved perioperative care, effective antiviral, antifungal and antibacterial therapy and chronic immunosuppression have led to improved patient outcomes and increased allograft survival over the past decades.

The first successful human kidney transplant was performed in 1954 by Dr. Joseph Murray between two genetically identical twins. Decades later, KT has become the standard care for patients with renal failure. Maintaining graft preservation requires immunosuppressive therapy (IST) or immune tolerance in genetically different individuals. To date, an understanding of immunological principles has been critical to successful management of KT patients [4].

After transplantation, a whole cascade of immune reactions of nonspecific (phagocytosis and cytokine release) and specific type (provided by T-cell and B-humoral immunity) occurs in the recipient's body. Antigen-specific response is activated by a huge number of potentially foreign antigens of the donor, including human leukocyte antigens (HLA) [5, 6] and the ABO system. Ischemia and reperfusion of the donor kidney are major factors in the development of graft injury, causing endothelial damage, free radical formation and induction of apoptosis, which is described as ischemia/reperfusion injury (IRI). Damage-associated molecular patterns (DAMPs), released from damaged or dying cells, are endogenous danger signals that activate the innate immune system, leading to inflammation and the release of anti-inflammatory cytokines like tumor necrosis factor, type I interferons, chemokines, and interleukins (IL-1 and IL-6) [7, 8].

Allograft rejection is tissue damage caused by effector mechanisms of the alloimmune response, resulting in impaired graft function. There are two main types of rejection: T cell (or cellular rejection) and antibody-mediated rejection. Both types of rejection may be early or late, fulminant or sluggish, isolated or concomitant, and may share pathomorphological features on biopsy [9]. Kidney allograft biopsies are graded according to the Banff classification, which helps clinicians to manage various allograft pathologies [10].

Corresponding author: Tatiana Lelyavina. Address: 6, Dekabristov str., Strelna, 198515, St. Petersburg, Russian Federation. Phone: (981) 9089018. E-mail: tatianalelyavina@mail.ru

The success of KT is largely due to advances in IST used in the induction and maintenance phases, as well as for the treatment of acute rejection [4]. There are so many foreign and domestic reports indicating the most common and serious complications of chronic IST in recipients, such as infectious diseases [11], malignant tumors, hypertension, leukopenia and thrombocytopenia, and others.

Cancer and infection appear to be the two most dangerous complications of immunosuppression and are often key research priorities for patients and clinicians [12]. To date, the risks of atypical infections and cancer remain high [13]. The cumulative incidence of *de novo* cancer (incidence of new cancer cases) 10 years after KT is about 40%, increasing to 60% after 20 years. The risk of cancer-related death in kidney transplant recipients is three times higher than in patients with cancer in the general population [14].

Infections are also a serious problem and the leading causes of early posttransplant death (within the first 12 months after transplantation), especially in low- and middle-income countries where prophylactic treatments for viral and bacterial infections are not available to all. The timing, severity and etiology of infections in recipients depend on the individual's state of immunosuppression [15]. To date, there are just few studies describing the adverse effects of immunosuppression directly on the kidneys.

The ***aim*** of our work is to study the sources and summarize the information on the adverse effects of immunosuppression, which play an important role in the full functioning of the transplant.

Currently, the main groups of immunosuppression drugs for KT patients are calcineurin inhibitors (cyclosporine A and tacrolimus), mycophenolates, mammalian target of rapamycin (mTOR) inhibitors, corticosteroids, azathioprine, and biologic polyclonal and monoclonal antibody preparations [4, 16–19].

IST protocols differ significantly in the immediate and late posttransplant periods. There are different protocols for initial and maintenance immunosuppression, variable in the number of drugs used (quadruple, triple and double) and their dosage [20–23].

A six-month randomized trial conducted across 47 European countries demonstrated that modern immunosuppressive regimens significantly reduce the incidence of acute rejection in KT recipients. This is achieved by combining calcineurin inhibitors (CNI) such as tacrolimus or cyclosporine with additional immunosuppressive agents like corticosteroids, mycophenolate mofetil (MMF), or azathioprine [24].

Glucocorticoids (GCS) have been a cornerstone in transplant immunosuppression for decades. Despite their numerous side effects, they remain widely used, particularly in pregnant transplant recipients, although there have been reports of fetal adrenal suppression. Among the abundance of widely known side effects of GCS, this report focuses on renal effects. Among them are known disorders of the hypothalamic-pituitary-adrenal (HPA) axis and the renin-angiotensin-aldosterone (RAAS) system – arterial hypertension, hypokalemia, increased glomerular filtration rate (GFR), sodium retention and diuretic resistance [25]. The advantage of using GCS is that their use is not associated with increased cancer risk. Most transplant centers advocate low maintenance doses, since it has been shown that early GCS withdrawal was associated with an increased risk of graft loss, especially in sensitized patients [26].

CNIs – cyclosporine A and tacrolimus – are fat-soluble small molecules derived from fungi (mycotoxins) and serve as the foundation of maintenance immunosuppression in organ transplantation [27]. The drugs selectively inhibit immune response by specifically targeting helper T cells, without affecting other immune cell functions, such as neutrophil phagocytosis or bone marrow activity. Target cells are inhibited but not killed (hence, the effects are reversible when treatment is discontinued). Administration of CNIs – cyclosporin A and later tacrolimus – in the mid-1980s significantly improved short-term kidney graft survival by reducing the incidence of acute rejection, but chronic nephrotoxicity was responsible for the decline in graft function [28]. Cyclosporin A and tacrolimus have similarities and differences in toxicity. But the most common and unpleasant problem with CNIs is nephrotoxicity [29]. Both drugs are nephrotoxic, cause hyperkalemia, hyperuricemia, hypomagnesemia and hypophosphatemia (secondary to urine loss), type 4 renal tubular acidosis, and diuretic resistance.

CNI nephrotoxicity is a result of both reversible hemodynamic effects and irreversible structural damage. Cyclosporin A causes thrombotic microangiopathic vasculitis and intrarenal vasoconstriction. Reversible vasoconstriction is caused by direct vascular effects and activation of the renin-angiotensin system, endothelin, thromboxane, and the sympathetic nervous system. Over time, chronic renal injury, characterized by afferent arterial hyalinosis and tubulointerstitial fibrosis, occurs, presumably as a result of prolonged renal vasoconstriction with ischemia and direct tubular toxicity. In fewer cases, CNIs can cause thrombotic microangiopathy (TMA) leading to direct endothelial cell damage and dysfunction [30].

CNI nephrotoxicity affects all histologic sections of the transplanted kidney. Although not specific for CNI toxicity, lesions include medial arteriolar hyalinosis, interstitial fibrosis, global glomerulosclerosis, and tubular microcalcification unrelated to other causes such as tubular necrosis and hyperparathyroidism. CNI-induced arteriolopathy is characterized by nodular hyaline deposits in afferent arterioles sufficient to cause luminal narrowing. Renal arteriolar hyalinosis is the most reliable diagnostic marker of CNI nephrotoxicity. The diagnosis is valida-

ted by excluding other causes such as donor hyalinosis (which can be detected on a biopsy specimen), diabetes mellitus, and hypertensive nephrosis [4, 30].

MMF is a prodrug of mycophenolic acid (MPA), an inosine monophosphate dehydrogenase inhibitor and provide lymphocyte-specific immunosuppression. MMF or enteric-coated mycophenolate sodium (EC-MPS) are potential components of immunosuppression regimens, and are associated with the most successful outcomes in kidney transplantation [31]. MMF is by far the most commonly used immunosuppressive agent in transplantology, primarily due to its high efficacy and relatively acceptable side effect profile. It is usually used in combination with CNIs. This group of drugs is not nephrotoxic (as does azathioprine), but has gastrointestinal toxicity, suppresses bone marrow function and increases the risk of infections, especially those of a viral nature [32].

mTOR inhibitors (sirolimus and everolimus) work by inhibiting lymphocyte proliferation and differentiation. Although they were originally used in drug regimens to minimize exposure to CNIs with their known side effects, mTOR inhibitors have been associated with their own set of toxic properties that have prevented their widespread use. A 2011 study comparing everolimus (EVR) and mycophenolic acid (MPA/MMF) in kidney transplant recipients did not show a clear superiority of EVR over MMF in terms of mean estimated GFR at 12 months when both were used in combination with similar doses of tacrolimus or cyclosporine A [33]. Many studies using mTOR inhibitors instead of CNIs have found a higher risk of renal allograft rejection with variable improvement in kidney function [34, 35]. Studies have shown that EVR with reduced-exposure CNIs has comparable efficacy to MPA/MMF with standard CNI exposure in KT recipients who have low to moderate immunologic risk [36]. EVR in combination with reduced-exposure CNI and low-dose steroids is an appropriate regimen for preventing kidney graft rejection in most adult patients with low to moderate immunologic risk when managed individually [37].

Although mTOR inhibitors are not inherently nephrotoxic, they cause renal graft injury by several mechanisms. When used in combination with a standard dose of cyclosporin A (and probably tacrolimus), sirolimus potentiates CNI-induced nephrotoxicity [36]. In patients with renal impairment, sirolimus is associated with marked but potentially reversible proteinuria and worsening of pre-existing proteinuria. Sirolimus may also cause delayed recovery from acute tubular necrosis and may be associated with podocyte injury, focal segmental glomerulosclerosis.

Finally, cases of thrombotic microangiopathy have been reported, and there is concern that higher doses of sirolimus may inhibit endothelial cell growth. Interestingly, sirolimus-based treatment regimens have been associated with a reduced incidence of post-transplant malignancies. Sirolimus is often considered the preferred immunosuppressant in post-transplant patients who develop malignancy because mTOR inhibitors have been shown to reduce the risk of malignancy [37, 38]. However, most data are limited to KT recipients with squamous cell carcinoma of the skin. When mTOR inhibitors (sirolimus, everolimus) are used together with CNIs (calcium inhibitors), there is a risk of synergistic nephrotoxicity and other complications, including delayed recovery from acute tubular necrosis, proteinuria, hypokalemia, and hypertension.

Biological agents in the form of polyclonal antibodies and monoclonal antibodies (mAb) are often used in KT, either as induction therapy or to treat rejection. Polyclonal anti-lymphocytic agents are produced by immunizing animals with human thymic lymphoid cells; they bind to numerous elements on the surface of T cells and induce rapid lymphocytopenia by several mechanisms including complement-dependent cytolysis, cell-dependent phagocytosis, and apoptosis. Alemtuzumab is a humanized immunoglobulin G1 (IgG1) monoclonal antibody directed against human CD52, a glycoprotein found in circulating T and B cells, monocytes, macrophages, natural killer cells and granulocytes. Anti-CD25 monoclonal antibodies: the alpha subunit of the IL-2 receptor (CD25) is activated by T cells and leads to the expression of highly sensitive interleukin-2 (IL-2) receptors. Basiliximab is a CD25-specific chimeric monoclonal antibody (mAb) drug; it causes relatively mild immunosuppression and is used as an inducer to prevent rejection but not to treat established rejection. Rituximab (a monoclonal antibody that attaches to CD20, a protein on the surface of B cells, to destroy them) is an engineered chimeric mAb that contains murine variegated heavy and light chain regions and is directed against human IgG1 CD20. Rituximab is used as induction therapy after desensitization therapy for ABO blood group incompatibility and cross-over kidney transplantation. A study of the pharmacokinetics and pharmacodynamics of obinutuzumab, a novel type II, humanized, CD20 mA, in highly sensitized patients with kidney failure, demonstrated good tolerability and effective B cell depletion [16, 19]. However, its effect on reducing HLA alloantibody levels was inconsistent and not clinically significant [39]. No reports of adverse effects of biotechnological drugs on the kidneys were found in available literature. We do not dwell on the side effects of azathioprine because it is now rarely used and there is no reported nephrotoxicity.

Costimulation blockade therapy is an alternative to immunosuppression for KT recipients. Belatacept, a first-in-class co-stimulation blocker, is a fusion protein that binds to CD80 and CD86 to prevent T cell activation and proliferation. The drug primarily affects the CD28 costimulation pathway, preventing T cell activation. On renal biopsy, belatacept has been shown to improve renal function in patients with chronic vascular lesions [40]. As

early as 2003, a retrospective study of a scientific registry of transplant recipients was conducted comparing the outcomes of treatment with belatacept and tacrolimus. This study found no No significant difference in long-term graft survival between belatacept and tacrolimus, but belatacept was associated with better renal function, despite belatacept-treated patients having a higher incidence of acute rejection [41]. Recent studies have shown that belatacept attenuated acute rejection and increased graft survival. The drug may be a good alternative to CNI-based regimens after KT [42–45]. Nevertheless, there is evidence that low-dose tacrolimus maintenance therapy is often necessary when switching to belatacept early after transplantation, especially in steroid-free regimens, to reduce the risk of acute rejection [46].

Costimulators are still being investigated (CD28 receptor T cells in particular are of interest) [47]. Abatacept is another co-stimulator with proven efficacy [48]. Studies initiated several years ago indicated a potentially high efficacy of the drug [49]. Specifically, there has been a case series of 9 kidney transplant recipients who were switched to abatacept as an emergency immunosuppressive therapy due to CNI intolerance when belatacept was unavailable. A retrospective review reported successful allograft recovery and 100% patient and graft survival (median follow-up: 115 months) in kidney transplant recipients who were switched to abatacept. Patients who switched to abatacept had stable long-term renal function (median 82 months on abatacept). Further studies, conducted for the first time in a large patient cohort, showed that once-weekly abatacept administration is feasible and safe for post-KT patients previously receiving belatacept (and the efficacy is comparable) [50].

BK virus-associated nephropathy (BKVN) should be considered as a renal side effect of immunosuppressants. It was first reported in 1995 and is now considered an important cause of kidney graft loss. BK virus (also known as human polyomavirus 1) is a virus with double-stranded DNA that affects 75% of the general population. Primary infection with the virus occurs during childhood, resulting in an indeterminate flu-like illness. The route of transmission varies. The BK virus (BKV) then persists in the urinary tract. The disease is more severe in immunocompromised individuals, especially in KT recipients, due to the effects of immunosuppressants. In KT recipients, BKV disease has a wide range of manifestations, including ureteral stenosis, temporary graft dysfunction, or irreversible allograft failure secondary to BKVN. BKVN was first recognized as a significant cause of kidney allograft dysfunction in KT recipients approximately two decades ago. It presents as progressive deterioration of graft function, associated with histologically distinct allograft infection with BKV [51]. This lesion has been detected in about 8% of KT patients [52], and the incidence is increasing with better diagnostic capabilities, such as detection of decoy cells in urine sediment and polymerase chain reaction (PCR) tests. This may also be partly a result of the use of more potent immunosuppressants and increased awareness and improved diagnostic tools [53]. Definitive diagnosis of BKVN requires allograft biopsy. BKVN in biopsy specimens manifests as intranuclear inclusions in tubular epithelial cells with enlarged nuclei.

Continued viral replication leads to an associated inflammatory response with fibrosis and eventually tubular atrophy. Infected cells are excreted in the urine. Quantitative PCR for BKVN DNA in serum is the most commonly used non-invasive test that has a sensitivity of 100% and a specificity of 88% [52]. Antiviral treatment with cidofovir may be effective, but it is potentially nephrotoxic and the benefit/harm ratio has not yet been evaluated in randomized trials. It is believed that everolimus-treated patients had a lower rate of BKV infection [54].

Immunosuppression in pediatric KT patients is more complex, and treatment regimens based on MMF in combination with low-dose CNIs and corticosteroids are preferred. In KT recipients with chronic allograft dysfunction and excessive immunosuppression leading to recurrent infections, MMF and corticosteroids represent the most appropriate therapy option. Studies have shown that CNI-based immunosuppressive regimens, when combined with MMF and corticosteroids, more than 90% of all renal grafts are functional at 1 year, with 77% and 56% at 5 and 10 years, respectively [29].

Attention should be paid to the choice of therapy in the older age group of patients: the relationship between pharmacokinetics and immunological reactivity in elderly and senile patients should be taken into account when administering IST [55, 56].

Urine biomarkers have emerged as a non-invasive and promising strategy for monitoring kidney allograft status post-transplant. Since urine can be obtained non-invasively and, in the case of KT, its production is closely related to the function of the target organ. However, biomarkers related to immune function/hypoxia/ferroptosis/epithelial-mesenchymal transformation are of much greater interest in predicting allograft rejection. Five diagnostic genes were identified, including CCR5, CD86, CD8A, ITGAM and PTPRC, which positively correlated with allograft rejection after KT [57].

DISCUSSION

Over the past 40 years, immunosuppressive agents have facilitated the development of allogeneic transplantation, which has significantly improved graft survival. However, several problems remain, such as nephrotoxicity (especially CNIs, which are the mainstay of immunosuppressive regimens), and/or increased risk of opportunistic infections and cancer. Most immunosuppressants target T cell activation and may not be effective enough to prevent alloimmunization in the long

term. Many drugs have been tested in the last decade, but very few have found clinical use. The most recent of these is CTLA4-Ig (belatacept), a costimulation blocking molecule that targets a second T cell activation signal and is associated with improved kidney function in the long term compared to CNIs, and abatacept, which has shown comparable efficacy to belatacept. Importantly, these drugs have no nephrotoxic properties and can even improve graft function in the long term. Studies of new long-acting immunosuppressive agents are aimed at costimulation blocking. Agents that inhibit CD40-CD40-ligand interactions may provide good control of both T cell and B cell responses. Anti-CD28 antibodies can stimulate regulatory T cells. Drugs targeting these costimulation pathways are being evaluated in clinical trials. New drugs targeting antibody (imlifidase), B cell and plasmablast depletion (anti-IL-6/IL-6R, anti-CD38) and complement inhibition are being developed, but their evaluation is still an unresolved challenge.

Monitoring of ongoing IST to prevent undesirable effects due to cumulation, polyprogmasy, pharmacokinetic interactions, will help patients from different age groups to better tolerate treatment regimens. A dynamic urine clinical and biochemical study (sediment, leukocyte count, trapped cells, microalbuminuria, protein-creatinine ratio, and AKI/CKD biomarkers) will make this therapy more traceable and safer.

Thus, summarizing the above, IST today is necessary, and it is worth emphasizing the importance of the dynamic effect of IST on transplant function, the need for a reasonable selection of the scheme and dosage of a particular drug or combination of drugs to minimize nephrotoxic effects, the need to monitor the functions of the transplanted kidney in during postoperative patient care.

The authors declare no conflict of interest.

REFERENCES

1. Management of Chronic Kidney Disease. A Clinician's Guide. Second Edition / Editor Mustafa Arıcı. Switzerland: Springer Nature, 2023. 603 p.
2. *Cockwell P, Fisher L-A.* The global burden of chronic kidney disease. *Lancet*. 2020; 395 (10225): 662–664.
3. *Aiyegbusi O, McGregor E, McManus SK, Stevens KI.* Immunosuppression Therapy in Kidney Transplantation. *Urol Clin North Am*. 2022 May; 49 (2): 345–360. doi: 10.1016/j.ucl.2021.12.010. PMID: 35428439.
4. *Johnson RJ, Floege J, Tonelli M.* Comprehensive Clinical Nephrology. Seventh Edition. Elsevier, 2024. 1309 p.
5. *Alegre ML, Lakkis FG, Morelli AE.* Antigen presentation in transplantation. *Trends Immunol*. 2016; 37 (12): 831–843.
6. *Sypek M, Kausman J, Holt S, Hughes P*. HLA epitope matching in kidney transplantation: an overview for the general nephrologist. *Am J Kidney Dis*. 2018; 71 (5): 720–731.
7. Damage-Associated Molecular Patterns in Human Diseases. Volume 3: Antigen-Related Disorders / Walter Gottlieb Land. Springer Nature Switzerland AG, 2023. 667 p.
8. *Granata S, Votrico V, Spadaccino F, Catalano V, Netti GS, Ranieri E et al.* Oxidative stress and ischemia/reperfusion injury in kidney transplantation: focus on ferroptosis, mitophagy and new antioxidants. *Antioxidants (Basel)*. 2022; 11 (4): 769. https://www.mdpi. com/2076-3921/11/4/769.
9. *Roufosse C, Simmonds N, Clahsen-van Groningen M, Haas M, Henriksen KJ, Horsfield C et al.* 2018 reference guide to the Banff classification of renal allograft Pathology. *Transplantation*. 2018; 102 (11): 1795–1814.
10. *Nakagawa K, Tsuchimoto A, Ueki K, Matsukuma Y, Okabe Y, Masutani K et al.* Japan Academic Consortium of Kidney Transplantation Investigators. Significance of revised criteria for chronic active T cell-mediated rejection in the 2017 Banff classification: Surveillance by 1-year protocol biopsies for kidney transplantation. *Am J Transplant*. 2021; 21 (1): 174–185. https://doi.org/10.1111/ajt.16093.
11. *Tong A, Gill J, Budde K, Marson L, Reese PP, Rosenbloom D et al.* Toward establishing core outcome domains for trials in kidney transplantation: report of the Standardized Outcomes in Nephrology-Kidney Transplantation Consensus Workshops. *Transplantation*. 2017; 101 (8): 1887–1896.
12. *Ying T, Shi B, Kelly PJ, Pilmore H, Clayton PA, Chadban SJ.* Death after kidney transplantation: an analysis by era and time post-transplant. *J Am Soc Nephrol*. 2020; 31 (12): 2887–2899.
13. *Au EH, Chapman JR, Craig JC, Lim WH, Teixeira-Pinto A, Ullah S et al.* Overall and site-specific cancer mortality in patients on dialysis and after kidney transplant. *J Am Soc Nephrol*. 2019; 30 (3): 471–480.
14. *Nambiar P, Silibovsky R, Belden KA.* Infection in kidney transplantation. *Contemporary Kidney Transplantation*. 2018: 307–327.
15. *Lim MA, Kohli J, Bloom RD.* Immunosuppression for kidney transplantation: Where are we now and where are we going? *Transplant Rev (Orlando)*. 2017 Jan; 31 (1): 10–17. doi: 10.1016/j.trre.2016.10.006. Epub 2016 Oct 11. PMID: 28340885.
16. *Bauer AC, Franco RF, Manfro RC*. Immunosuppression in Kidney Transplantation: State of the Art and Current Protocols. *Curr Pharm Des*. 2020; 26 (28): 3440–3450. doi: 10.2174/1381612826666200521142448. PMID: 32436821.
17. *Chandra A, Midtvedt K, Åsberg A, Eide IA*. Immunosuppression and Reproductive. Health After Kidney Transplantation. *Transplantation*. 2019 Nov; 103 (11): e325–e333. doi: 10.1097/TP.0000000000002903. PMID: 31397802.
18. *Clayton PA, Lim WH, Wong G, Chadban SJ*. Relationship between eGFR decline and hard outcomes after kidney transplants. *J Am Soc Nephrol*. 2016; 27 (11): 3440–3446.
19. *Ortiz F, Salonsalmi A, Helanterä I.* Associations between dialysis modality and adherence to immunosup-

pression after kidney transplantation-A single-center study. *PLoS One*. 2025 Jan 24; 20 (1): e0317435.
20. *Kamal J, Doyle A.* Immunosuppression and Kidney Transplantation. *Handb Exp Pharmacol*. 2022; 272: 165–179. doi: 10.1007/164_2021_546. PMID: 34697664.
21. *Suslov DN.* The basic principles of immunosuppressive therapy after kidney transplantation. *Transplantologiya. The Russian Journal of Transplantation*. 2018; 10 (1): 42–49. (In Russ.). https://doi.org/10.23873/2074-0506-2018-10-1-42-49.
22. *Vatazin AV, Kildjushevskiy AV, Fedulkina VA, Faenko AP*. Renal allograft rejection mechanisms and immunotolerance. *Nephrology*. 2016; 20 (6): 33–41. (In Russ.).
23. *Cheung CY, Tang SCW.* Personalized immunosuppression after kidney transplantation. *Nephrology (Carlton)*. 2022; 27 (6): 475–483. doi: 10.1111/nep.14035.
24. *Kuppe C, van Roeyen C, Leuchtle K, Kabgani N, Vogt M, Van Zandvoort M et al.* Investigations of glucocorticoid action in GN. *J Am Soc Nephrol*. 2017; 28 (5): 1408–1420.
25. *Bae S, Garonzik Wang JM, Massie AB, Jackson KR, McAdams-DeMarco MA, Brennan DC et al.* Early steroid withdrawal in deceased-donor kidney transplant recipients with delayed graft function. *J Am Soc Nephrol*. 2020; 31 (1): 175–185.
26. *Wojciechowski D, Wiseman A.* Long-Term Immunosuppression Management: Opportunities and Uncertainties. *Clin J Am Soc Nephrol*. 2021 Aug; 16 (8): 1264–1271. doi: 10.2215/CJN.15040920. Epub 2021 Apr.
27. Oxford Handbook of Clinical Immunology and Allergy. Fourth edition / Editor Gavin Spickett. Oxford University Press, 2020. 677 p.
28. *El Hennawy HM, Faifi ASA, El Nazer W, Mahedy A, Kamal A, Al Faifi IS et al*. Calcineurin Inhibitors Nephrotoxicity Prevention Strategies With Stress on Belatacept-Based Rescue Immunotherapy: A Review of the Current Evidence. *Transplant Proc*. 2021 Jun; 53 (5): 1532–1540. doi: 10.1016/j.transproceed.2021.03.028. Epub 2021 May 18.
29. Chapel and Haeney's Essentials of Clinical Immunology. Seventh Edition / Siraj A. Misbah, Gavin P. Spickett, Virgil A.S.H. Dalm. Wiley-Blackwell, John Wiley & Sons Ltd, 2022. 374 p. (P. 158). LCCN 2021061617 (ebook).
30. *Mengel M, Mihatsch M, Halloran PF*. Histological characteristics of calcineurin inhibitor toxicity – there is no such thing as specicity. *Am J Transplant*. 2011; 11 (12): 2549–2550.
31. *Gardiner KM, Tett SE, Staatz CE.* Is conversion from mycophenolate mofetil to enteric-coated mycophenolate sodium justifiable for gastrointestinal quality of life? *Drugs R D*. 2018; 18 (4): 271–282.
32. *Sommerer C, Suwelack B, Dragun D, Schenker P, Hauser IA, Witzke O et al.* An open-label, randomized trial indicates that everolimus with tacrolimus or cyclosporine is comparable to standard immunosuppression in *de novo* kidney transplant patients. *Kidney Int*. 2019; 96 (1): 231–244.
33. *Budde K, Becker T, Arns W, Sommerer C, Reinke P, Eisenberger U et al.* Everolimus-based, calcineurin-inhibitor-free regimen in recipients of de-novo kidney transplants: an open-label, randomised, controlled trial. *Lancet*. 2011; 377 (9768): 837–847.
34. *De Fijter JW, Holdaas H, Øyen O, Sanders JS, Sundar S, Bemelman FJ et al.* Early Conversion from calcineurin inhibitor- to everolimus-based therapy following kidney transplantation: results of the randomized ELEVATE Trial. *Am J Transplant*. 2017; 17 (7): 1853–1867.
35. 3C Study Collaborative Group. Campath, calcineurin inhibitor reduction, and chronic allograft nephropathy (the 3C Study) – results of a randomized controlled clinical trial. *Am J Transplant*. 2018; 18 (6): 1424–1434.
36. *Pascual J, Berger SP, Chadban SJ, Citterio F, Kamar N, Hesselink DA et al*. Evidence-based practice: Guidance for using everolimus in combination with low-exposure calcineurin inhibitors as initial immunosuppression in kidney transplant patients. *Transplant Rev (Orlando)*. 2019 Oct; 33 (4): 191–199. doi: 10.1016/j.trre.2019.07.001. Epub 2019 Jul 23. PMID: 31377099.
37. *Yanik EL, Siddiqui K, Engels EA.* Sirolimus effects on cancer incidence after kidney transplantation: a meta-analysis. *Cancer Med*. 2015; 4 (9): 1448–1459.
38. *Campbell SB, Walker R, Tai SS, Jiang Q, Russ GR*. Randomized controlled trial of sirolimus for renal transplant recipients at high risk for nonmelanoma skin cancer. *Am J Transplant*. 2012; 12 (5): 1146–1156.
39. *Redfield RR, Jordan SC, Busque S, Vincenti F, Woodle ES, Desai N et al.* Safety, pharmacokinetics, and pharmacodynamic activity of obinutuzumab, a type 2 anti-CD20 monoclonal antibody for the desensitization of candidates for renal transplant. *Am J Transplant*. 2019; 19 (11): 3035–3045.
40. *Pérez-Sáez MJ, Yu B, Uffing A, Murakami N, Borges TJ, Azzi J et al.* Conversion from tacrolimus to belatacept improves renal function in kidney transplant patients with chronic vascular lesions in allograft biopsy. *Clin Kidney J*. 2018; 12 (4): 586–591.
41. *Budde K, Prashar R, Haller H, Rial MC, Kamar N, Agarwal A et al*. Conversion from Calcineurin Inhibitor-to Belatacept-Based Maintenance Immunosuppression in Renal Transplant Recipients: A Randomized Phase 3b Trial. *J Am Soc Nephrol*. 2021 Dec 1; 32 (12): 3252–3264. doi: 10.1681/ASN.2021050628. Epub 2021 Dec 1.
42. *El Hennawy H, Safar O, Al Faifi AS, El Nazer W, Kamal A, Mahedy A et al*. Belatacept rescue therapy of CNI-induced nephrotoxicity, meta-analysis. *Transplant Rev (Orlando)*. 2021 Dec; 35 (4): 100653. doi: 10.1016/j.trre.2021.100653. Epub 2021 Sep 21.
43. *Choi M, Bachmann F, Wu K, Lachmann N, Schmidt D, Brakemeier S et al*. Microvascular inflammation is a risk factor in kidney transplant recipients with very late conversion from calcineurin inhibitor-based regimens to belatacept. *BMC Nephrol*. 2020 Aug 20; 21 (1): 354. doi: 10.1186/s12882-020-01992-6. PMID: 32819287; PMCID: PMC7439694.
44. *Ulloa CE, Anglicheau D, Snanoudj R, Scemla A, Martinez F, Timsit MO et al*. Conversion From Calcineurin Inhibitors to Belatacept in HLA-sensitized Kidney Transplant Recipients With Low-level Donor-specific Antibodies. *Transplantation*. 2019 Oct; 103 (10): 2150–

2156. doi: 10.1097/TP.0000000000002592. PMID: 30720681.
45. *Zhang H, Wang Z, Zhang J, Gui Z, Han Z, Tao J et al*. Combined Immunotherapy With Belatacept and BTLA Overexpression Attenuates Acute Rejection Following Kidney Transplantation. *Front Immunol*. 2021 Feb 24; 12: 618737. doi: 10.3389/fimmu.2021.618737.
46. *Tawhari I, Hallak P, Bin S, Yamani F, Safar-Boueri M, Irshad A et al*. Early calcineurin-inhibitor to belatacept conversion in steroid-free kidney transplant recipients. *Front Immunol*. 2022 Dec 19; 13: 1096881. doi: 10.3389/fimmu.2022.1096881.
47. *Kervella D, Blancho G*. New immunosuppressive agents in transplantation. *Presse Med*. 2022 Dec; 51 (4): 104142. doi: 10.1016/j.lpm.2022.104142. Epub 2022 Oct 15. PMID: 36252821.
48. *Uro-Coste C, Atenza A, Heng AE, Rouzaire PO, Garrouste C*. Abatacept Rescue Therapy in Kidney Transplant Recipients: A Case Series of Five Patients. *Transpl Int*. 2022 Aug 12; 35: 10681. doi: 10.3389/ti.2022.10681.
49. *Badell IR, Karadkhele GM, Vasanth P, Farris AB 3rd, Robertson JM, Larsen CP*. Abatacept as rescue immunosuppression after calcineurin inhibitor treatment failure in renal transplantation. *Am J Trans*plant. 2019 Aug; 19 (8): 2342–2349. doi: 10.1111/ajt.15319. Epub 2019 Mar 12. PMID: 30768841.
50. *Bertrand D, Brunel M, Lebourg L, Scemla A, Lemoine M, Amrouche L et al*. Conversion From Intravenous In-Hospital Belatacept Injection to Subcutaneous Abatacept Injection in Kidney Transplant Recipients During the First COVID-19 Stay-at-Home Order in France. *Transpl Int*. 2023 Jul 24; 36: 11328. doi: 10.3389/ti.2023.11328.
51. *Kazory A, Ducloux D.* Renal transplantation and polyomavirus infection: recent clinical facts and controversies. *Transpl Infect Dis*. 2003; 5 (2): 65–71.
52. *Cohen-Bucay A, Ramirez-Andrade SE, Gordon CE, Francis JM, Chitalia VC*. Advances in BK virus complications in organ transplantation and beyond. *Kidney Med*. 2020; 2 (6): 771–786.
53. *Hirsch HH, Randhawa PS; AST Infectious diseases Community of Practice.* BK polyomavirus in solid organ transplantation-guidelinesfrom the American Society of Transplantation infectious diseasesCommunity of Practice. *Clin Transpl.* 2019; 33 (9): e13528.
54. *Spasovski G, Trajceska L, Rambabova-Bushljetik I.* Pharmacotherapeutic options for the prevention of kidney transplant rejection: the evidence to date. *Expert Opin Pharmacother*. 2022 Aug; 23 (12): 1397–1412. doi: 10.1080/14656566.2022.2102418. Epub 2022 Jul 19. PMID: 35835450.
55. *Lehner LJ, Staeck O, Halleck F, Liefeldt L, Bamoulid J, Budde K.* Need for optimized immunosuppression in elderly kidney transplant recipients. *Transplant Rev (Orlando)*. 2015 Oct; 29 (4): 237–239. doi: 10.1016/j.trre.2015.08.001. Epub 2015 Aug 15. PMID: 26411381.
56. *Fedulkina VA, Vatazin AV, Kildyushevskiy AV, Zulkarnayev AB, Gubina DV*. Rational maintenance immunosuppression for elderly renal transplant recipients. The literature review. *Nephrology*. 2022; 26 (2): 25–33. (In Russ.). https://doi.org/10.36485/1561-6274-2022-26-2-25-33.
57. *He L, Wang B, Wang X, Liu Y, Song X, Zhang Y et al*. Uncover diagnostic immunity/hypoxia/ferroptosis/epithelial mesenchymal transformation-related CCR5, CD86, CD8A, ITGAM, and PTPRC in kidney transplantation patients with allograft rejection. *Ren Fail*. 2022 Dec; 44 (1): 1850–1865. doi: 10.1080/0886022X.2022.2141648. PMID: 36330810; PMCID: PMC9639483.

The article was submitted to the journal on 13.03.2024

DOI: 10.15825/1995-1191-2025-1-32-39

FLUORESCENCE-GUIDED LAPAROSCOPIC LIVING-DONOR HEPATECTOMY TO ACQUIRE AN S2 GRAFT

A.R. Monakhov[1, 2], V.R. Salimov[1], S.V. Meshcheriakov[1], I.I. Kurbanov[2], D.I. Bystrov[3], S.V. Gautier[1, 2]

[1] Shumakov National Medical Research Center of Transplantology and Artificial Organs, Moscow, Russian Federation
[2] Sechenov University, Moscow, Russian Federation
[3] Volzhsky Branch of Shumakov National Medical Research Center of Transplantology and Artificial Organs, Volzhsky, Russian Federation

Background. Liver transplantation (LT) in children with low body weight using the left lateral segment from a living donor is associated with large-for-size syndrome (LFSS). We present the first Russian clinical case of laparoscopic living-donor hepatectomy to acquire an S2 graft. **Materials and methods.** A six-month-old child who had biliary atresia-induced liver cirrhosis was prepared for transplantation. The child's 20-year-old mother was the donor. The left lateral segment had a volume of 426 mL (graft-to-recipient weight ratio, GRWR, was 5.9%). Indocyanine green fluorescence-guided laparoscopic intracorporeal reduction up to the S2 segment was performed. **Results.** Donor operation time was 230 minutes, blood loss was 50 ml. The postoperative period was uneventful; the donor was discharged on day 9. The recipient had no surgical complications; a rejection episode was successfully managed. The child was discharged with a satisfactory graft function. **Discussion.** Fluorescence-guided laparoscopic living-donor hepatectomy to acquire an S2 graft is effective and safe. The presented technique may be an effective solution when performing monosegmental LT under the high-risk conditions of LFSS.

Keywords: monosegment liver transplantation, laparoscopic living-donor hepatectomy, pediatric transplantation, indocyanine green.

INTRODUCTION

Pediatric liver transplantation (LT) has seen remarkable advancements over the years, leading to excellent short-term and long-term survival rates [1–3]. For many children with advanced liver disease, it is considered the only curative treatment option, providing a definitive solution to their end-stage liver condition [3, 4]. Certain pediatric cases present significant challenges in transplantation, often carrying higher risks. For instance, children weighing less than 7 kg face increased postoperative mortality [5, 6], primarily due to their small anthropometric parameters and the potential mismatch between graft size and the recipient's abdominal cavity. In living donor liver transplantation, the left lateral segment (LLS) of the liver (Couinaud segments 2 and 3) is commonly used. However, even the LLS may be too large for the recipient, increasing the risk of large-for-size syndrome [7, 8].

The graft-to-recipient weight ratio (GRWR) is a widely used and simple method to assess the suitability of a living related donor for a LT, expressed as a percentage. A GRWR ≥4% is considered a significant risk factor for developing over-sized graft syndrome [9]. This syndrome is characterized by the development of respiratory failure against the background of diaphragmatic excursion disorders, insufficient visceral perfusion, graft compression in the abdominal cavity, which may eventually affect the function and survival of graft and recipient [10–11].

Performing either an "anatomic" or "non-anatomic" reduction of the LLS graft is a potential solution to manage excess graft material in LT [12–16]. Each method has its own advantages and limitations. Non-anatomic reduction may not always adequately address the issue of excess graft thickness. On the other hand, anatomic reduction, which involves removing one of the segments to achieve monosegmental grafting, is considered technically more complex.

Over the past decade, minimally invasive surgery for living donors has become increasingly common in major transplant centers. While initially limited to a few cases in the mid-2010s, by the early 2020s, this approach has been widely recognized as the gold standard, particularly for LLS sectionectomy in living donors [17–19]. Our center adopted this technique in 2016, and it has since become routine practice [20]. Given the need for graft reduction in certain cases and our extensive experience with laparoscopic liver surgery, we have integrated existing technologies and surgical techniques to perform

Corresponding author: Artem Monakhov. Address: 1, Shchukinskaya str., Moscow, 123182, Russian Federation. Phone: (906) 078-16-21. E-mail: a.r.monakhov@gmail.com

laparoscopic liver resection in living donors to obtain an S2 graft. Similar cases have already been reported in global clinical practice [7, 21, 22].

Thus, we present a detailed description of our clinical case, marking the first such intervention performed in Russia.

CLINICAL CASE

The patient, a 6-month-old infant weighing 8 kg, was admitted to our center with cirrhosis due to congenital biliary tract malformation (biliary atresia). At the time of admission, the calculated PELD score was 20. Following a thorough multisystem evaluation, the patient was deemed eligible for a liver transplant, with no absolute contraindications to surgery. Abdominal MSCT revealed a Hiatt 3 variant arterial anatomy, where the left hepatic lobe artery originated from the common hepatic artery and the right hepatic lobe artery arose from the superior mesenteric artery. The portal and hepatic vein anatomy were found to be standard.

The recipient's mother, a 20-year-old woman with a body mass index of 24.4, was assessed as the sole potential related liver donor. A thorough evaluation of her health status, liver function, and parenchymal quality revealed no contraindications to donation. Bolus contrast-enhanced abdominal MSCT was performed to analyze her vascular anatomy. The arterial anatomy was classified as Hiatt 4, where the left hepatic artery bifurcated into branches supplying S4 and S3, while the artery to S2 originated independently from the left gastric artery. Portal vein anatomy followed the standard Nakamura type A configuration, with sequential branching into S3 and S2. The S3 and S2 veins converged to form the left hepatic vein, with all three hepatic veins draining separately into the inferior vena cava (IVC) (Fig. 1).

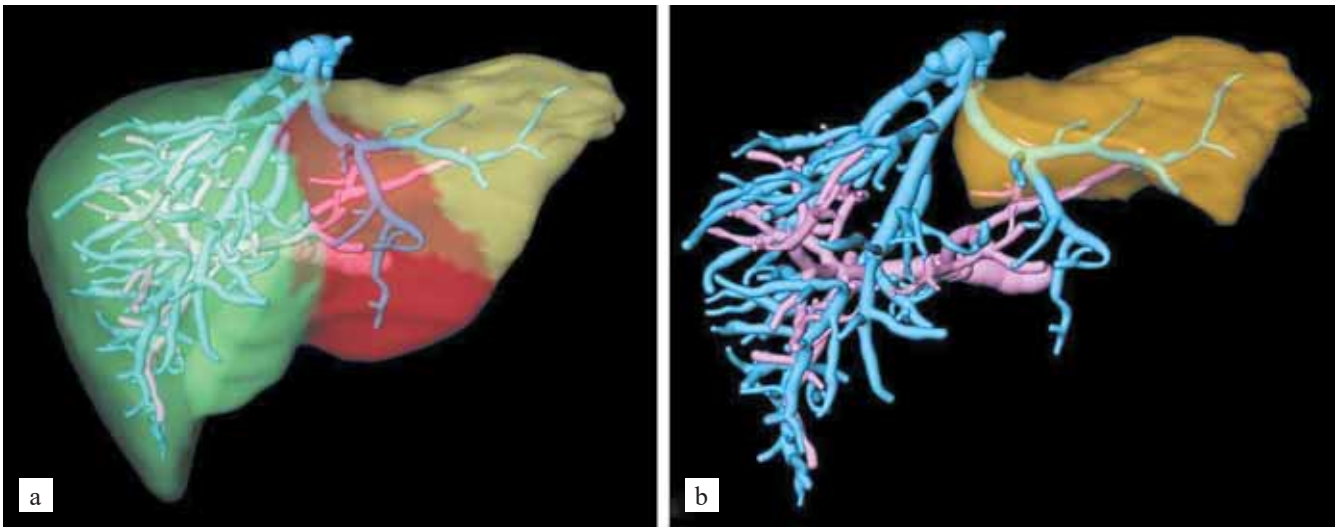

Fig. 1. 3D reconstruction of contrast-enhanced CT images of the hepatic veins (blue) and portal vein branches (pink) 2D CT images. a, whole liver; b, second segment

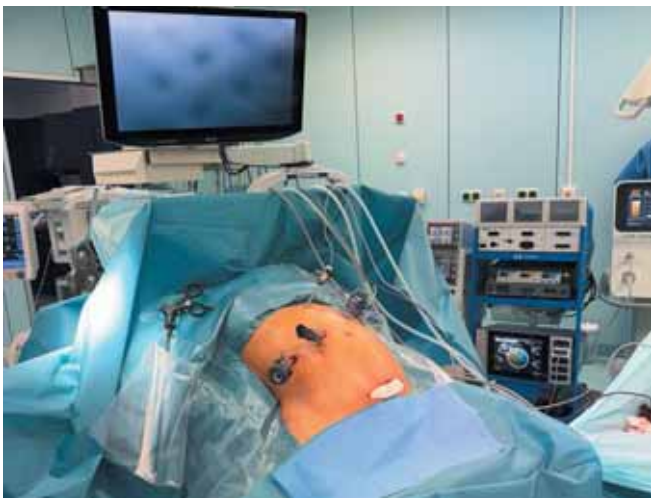

Fig. 2. Donor position and trocar placement on the operating table

Magnetic resonance cholangiopancreatography (MRCP) revealed no biliary tract anomalies. Computer volumetry and 3D modeling estimated the left lateral segment (LLS) volume at 426 mL, with a GRWR of 5.9%. The maximum LLS thickness-to-recipient anteroposterior abdominal dimension ratio was 1.08. The estimated S2 monosegmental volume was 206 mL, with a GRWR of 2.86%. Given these findings, the optimal approach was an intracorporeal anatomic reduction of the donor's LLS under fluorescence guidance to obtain an S2 graft.

SURGICAL TECHNIQUE

Surgery in the donor

The donor was positioned in reverse Trendelenburg (table tilted flat with legs down) with legs spread to maintain the French position (Fig. 2). Four trocars

were inserted into the abdomen (one 10 mm, two 12 mm, and one 5 mm) as illustrated in Fig. 2. The procedure was performed under an intra-abdominal pressure of 12 mmHg using 30-degree optics and a high-resolution laparoscopic system with ICG mapping functionality (Olympus, Japan).

The liver left lobe was mobilized by transecting the round and left triangular ligaments. The falciform ligament was dissected down to the caval gate, exposing the middle and left hepatic veins. The lesser omentum was also divided, allowing for the isolation of the S2 artery along its course. As an additional anatomical landmark, the inferior pubic ligament was identified and transected at the mouth of the left hepatic vein.

Subsequently, the LLS was rotated counterclockwise, facilitating the isolation of key elements of the hepatoduodenal ligament, including the left hepatic artery and the left branch of the portal vein. Parenchymal transection was performed 5 mm lateral to the falciform ligament using an ultrasonic dissector, bipolar coagulation, and a harmonic scalpel. Tubular structures were clipped and transected during the separation process. Following parenchymal division, the left hepatic vein was bypassed, leaving the LLS connected only by the main afferent vessels and the umbilical plate, which contains bile ducts and their vascular supply.

Next, the Glissonean pedicle of segment 3 (G3) was isolated separately, and a bulldog vascular clamp was applied. Indocyanine green (ICG) was then injected intravenously at a dose of 0.05 mg/kg body weight. Under fluorescence navigation, the boundaries of segment 3 were clearly visualized, allowing for precise intracorporeal reduction of the left lateral segment (LLS) (Fig. 3).

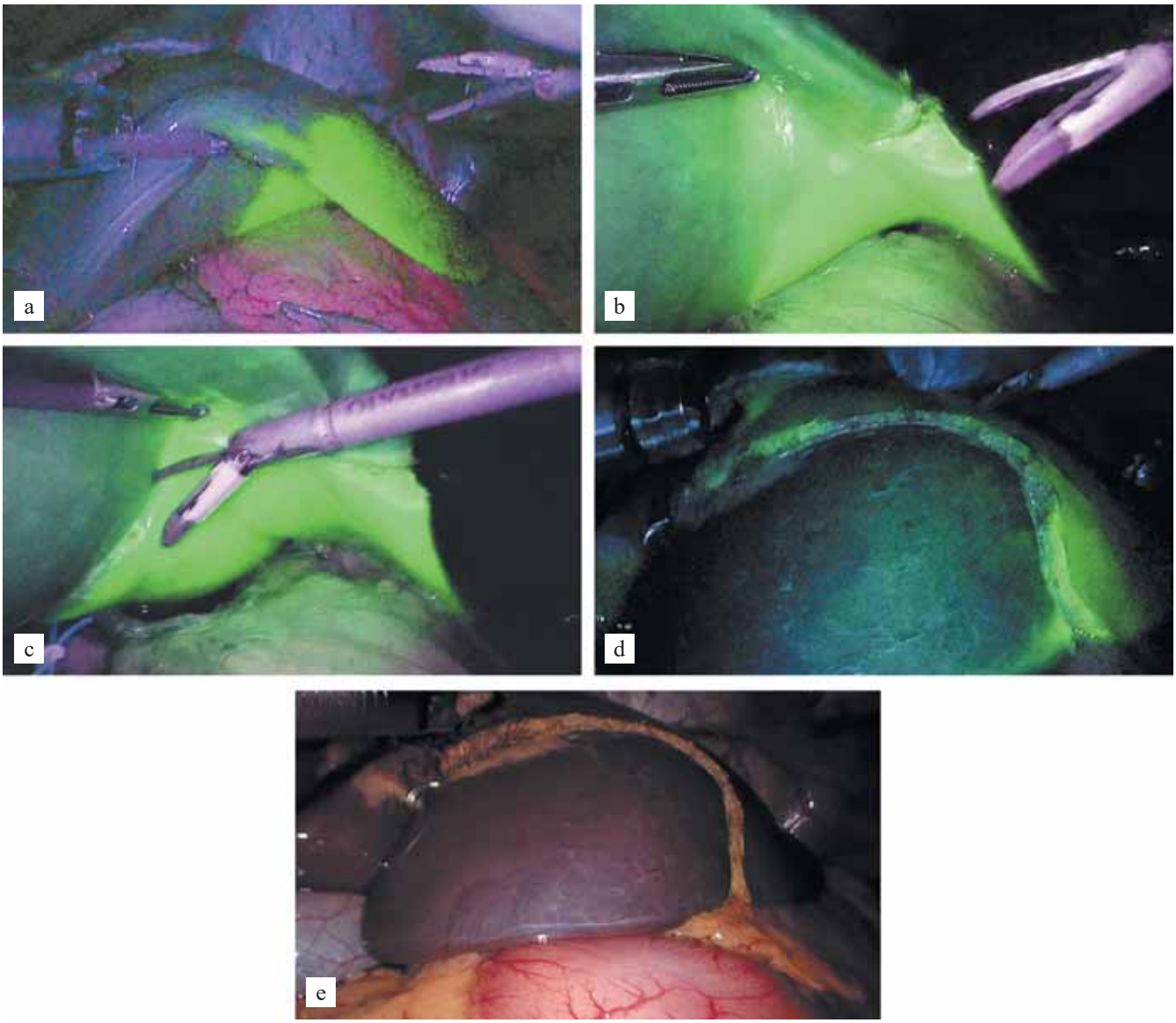

Fig. 3. ICG guided liver resection: a–d, Boundaries of the S2 segment under ICG guidance; e, parenchyma transection line between S2 and S3

During parenchymal dissection, the S3 vein was carefully clipped and transected. In the final stage, segment 3 was completely separated from the future graft, and a hem-o-lok clip was applied to the Glissonean pedicle to ensure vascular control.

Next, a Pfannenstiel laparotomy was performed, and a trocar was placed for the self-opening extraction bag. Using fluorescence navigation, the confluence of the lobular bile ducts was visualized, and the transection line for the left lobular duct was outlined. After that, The left lobular bile duct, aberrant artery to S2, and left branch of the portal vein were sequentially clipped and transected. The left hepatic vein was then divided using a unilateral linear stapler. The S2 graft, along with the separated S3, was placed in a container and extracted through the prepared incision.

The graft was transferred to the dissecting table for preservation and preparation for subsequent implantation. The final mass of the monosegment S2 graft was 180 g.

Surgery in the recipient

Transplantation of the S2 liver fragment was performed using a bisubcostal incision. Following hepatectomy with IVC preservation, the graft was positioned in the recipient's abdominal cavity. The implantation technique followed the standard protocol for LLS revascularization used at the Center.

So, caval anastomosis was established between the graft's hepatic vein and the common confluence of the recipient's three hepatic veins using a continuous twisted suture with a 5/0 polydioxanone monofilament. The portal vein was reconstructed with a 6/0 suture, adapting the difference in vein diameters through longitudinal dissection of the recipient's portal vein, following the Center's standard approach.

Arterial reconstruction was performed end-to-end between the graft artery and the recipient's right hepatic artery using the parachute technique with a 7/0 Prolene suture. Biliary reconstruction was carried out on a Roux-en-Y jejunal loop with a knot suture and an external frame drainage. Notably, no bleeding or bile leakage was observed along the graft reduction plane.

RESULTS

Operation on the donor lasted 230 minutes with a blood loss of 50 mL. The postoperative period was uneventful; the donor was discharged on postoperative day 9. A comprehensive outpatient examination one month later showed no signs of liver dysfunction or any deterioration in the donor's health or quality of life.

The recipient experienced no surgical complications postoperatively but developed an episode of graft rejection. This was successfully managed with glucocorticoid pulse therapy and an adjustment of maintenance immunosuppression. The child was subsequently discharged with satisfactory graft function under outpatient follow-up.

DISCUSSION

In this clinical case, we presented the first Russian experience of using a laparoscopic approach for the removal of a monosegmental graft for pediatric liver transplantation. The combination of fluorescent navigation and the Glissonean approach enabled the intracorporeal separation of segment 3, allowing for the retrieval of a viable segment 2 graft.

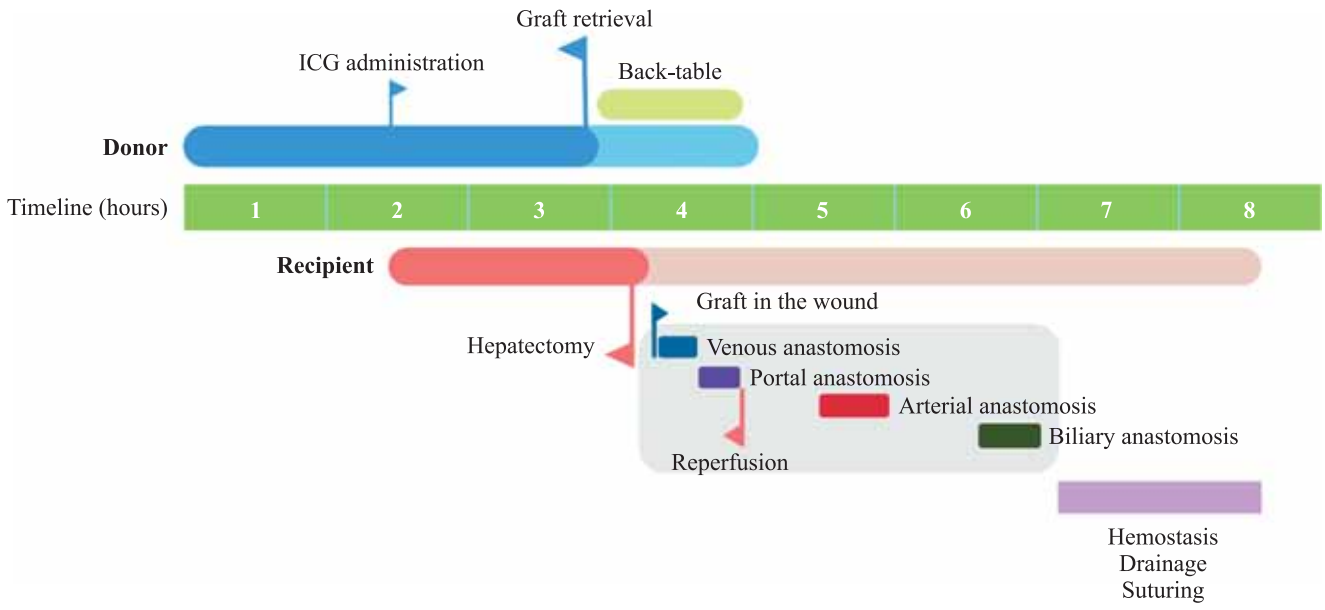

Fig. 4. Sequence of surgical steps of donor and recipient surgery

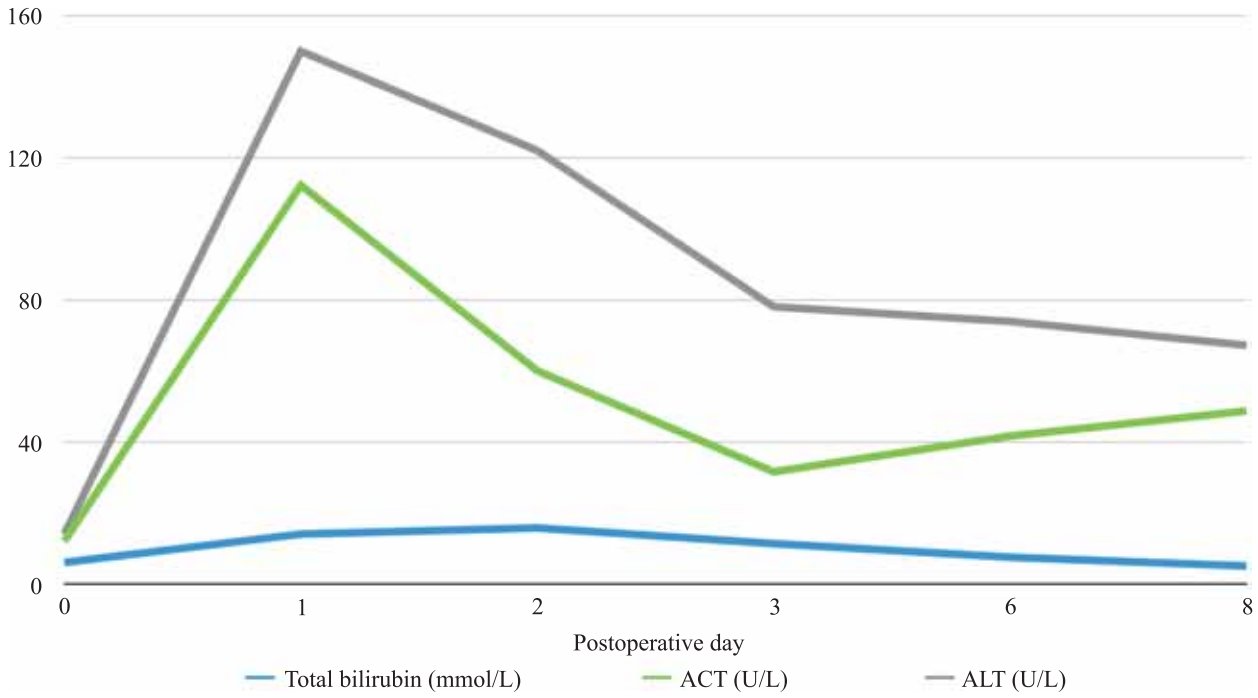

Fig. 5. Dynamics of the main laboratory parameters of the donor in the first 8 days after surgery

LT in children with low body weight is often constrained by the unavailability of an appropriately sized liver fragment from a related donor. Large-for-size syndrome poses a significant risk, potentially leading to complications such as impaired visceral perfusion, graft compression, and restricted diaphragm excursion. Essentially a variant of abdominal compartment syndrome, this condition makes low-weight pediatric patients particularly vulnerable. Anatomic reduction of the left lateral segment of the donor liver is one of the key strategies to mitigate these risks and improve transplant outcomes.

Laparoscopic removal of liver fragments for transplantation is still considered a technically demanding procedure, and is generally performed only at high-volume transplant centers by experienced surgeons [18, 19, 23]. To date, only four such operations using laparoscopic techniques have been reported, including our case [21, 22, 24]. Interestingly, ICG fluorescence imaging and in-situ separation technique were used in each of them, while the Glissonean approach was used in only two cases.

ICG navigation is becoming a prevalent tool in laparoscopic liver surgery, particularly for intraoperative cholangiography, its ability to accumulate in certain tumors and finally for mapping of anatomical fragments of the liver as in our case. And this is by no means a complete list of ways to use this dye [25, 26].

Thus, the presented technique offers several distinct advantages. First, the laparoscopic approach has already been widely recognized as an effective and safe method for donor hepatectomy. According to multiple studies, laparoscopic lateral sectionectomy in living donors is increasingly regarded as the new standard for this procedure [19]. Second, the combination of ICG-negative staining and the Glissonean approach enables precise delineation of the perfusion zone, ensuring that only viable parenchyma is preserved within the graft. Third, performing *in situ* graft reduction minimizes ischemia time compared to reduction on the dissecting table. Additionally, when comparing *in situ* reduction in the donor versus *in situ* reduction in the recipient, donor-stage reduction is preferable as it reduces both blood loss and the surgical complexity for the recipient. Moreover, meticulous preoperative surgical planning plays a crucial role in optimizing outcomes for living donor liver transplantation.

CONCLUSION

In this clinical case, we reported the first Russian experience of laparoscopic liver resection in a living donor to obtain an S2 graft under fluorescence navigation. This technique minimized risks for both the donor and recipient while ensuring high precision and safety. The integration of laparoscopic methods with ICG fluorescence imaging for real-time navigation has significantly enhanced outcomes in segmental liver transplantation for young children with low body weight, a population for whom conventional transplantation techniques may be unsuitable. Our experience underscores the potential of this approach and highlights the need for further research

to establish fluorescence-guided laparoscopic resections as a standard practice in pediatric liver transplantation.

The authors declare no conflict of interest.

REFERENCES

1. *Seda Neto J, Costa CM, Pugliese R, Vincenzi R, Benavides MR, Travassos NPR et al.* Living Donor Whole and Partial Liver Grafts, Deceased Donor Whole Liver and SPLIT: Outcome Comparison. *J Pediatr Surg*. 2024 Sep; 59 (9): 1784–1790. doi: 10.1016/j.jpedsurg.2024.02.010. PMID: 38413259.
2. *Baumann U, Karam V, Adam R, Fondevila C, Dhawan A, Sokal E et al.* European Liver and Intestine Transplant Association (ELITA) and all ELTR contributing centers. Prognosis of Children Undergoing Liver Transplantation: A 30-Year European Study. *Pediatrics*. 2022 Oct 1; 150 (4): e2022057424. doi: 10.1542/peds.2022-057424. PMID: 36111446.
3. *Yamamoto H, Khorsandi SE, Cortes-Cerisuelo M, Kawano Y, Dhawan A, McCall J et al.* Outcomes of Liver Transplantation in Small Infants. *Liver Transpl*. 2019 Oct; 25 (10): 1561–1570. doi: 10.1002/lt.25619. PMID: 31379050; PMCID: PMC6856963.
4. *Cuenca AG, Kim HB, Vakili K*. Pediatric liver transplantation. *Semin Pediatr Surg*. 2017 Aug; 26 (4): 217–223. doi: 10.1053/j.sempedsurg.2017.07.014. Epub 2017 Jul 26. PMID: 28964477.
5. *Arnon R, Annunziato R, Miloh T, Sogawa H, Nostrand KV, Florman S et al.* Liver transplantation in children weighing 5 kg or less: analysis of the UNOS database. *Pediatr Transplant*. 2011 Sep; 15 (6): 650–658. doi: 10.1111/j.1399-3046.2011.01549.x. Epub 2011 Jul 29. PMID: 21797956.
6. *Yeh YT, Liu C, Tsai HL, Chen CY, Lin NC, Chang JW et al.* Living donor liver transplantation for small infants aged less than 6 months: The experience of a single institute. *J Pediatr Surg*. 2021 Jul; 56 (7): 1157–1161. doi: 10.1016/j.jpedsurg.2021.03.022. Epub 2021 Mar 24. PMID: 33840505.
7. *Sakuma Y, Sasanuma H, Miki A, Shimizu A, Sata N, Yasuda Y et al*. Living-Donor Liver Transplantation Using Segment 2 Monosegment Graft: A Single-Center Experience. *Transplant Proc*. 2016 May; 48 (4): 1110–1114. doi: 10.1016/j.transproceed.2015.12.119. PMID: 27320568.
8. *Kasahara M, Sakamoto S, Umeshita K, Uemoto S.* Effect of graft size matching on pediatric living-donor liver transplantation in Japan. *Exp Clin Transplant*. 2014 Mar; 12 Suppl 1: 1–4. doi: 10.6002/ect.25liver.l5. PMID: 24635782.
9. *Sakamoto S, Kanazawa H, Shigeta T, Uchida H, Sasaki K, Hamano I et al.* Technical considerations of living donor hepatectomy of segment 2 grafts for infants. *Surgery*. 2014 Nov; 156 (5): 1232–1237. doi: 10.1016/j.surg.2014.05.003. Epub 2014 Jun 6. PMID: 24909347.
10. *Stefanowicz M, Kowalewski G, Szymczak M, Patkowski W, Zieniewicz K, Grzelak I et al.* Impact of Graft Size Matching on the Early Post-Transplant Complications and Patients Survival in Children after Living Donor Liver Transplantations. *Children (Basel)*. 2021 Jul 6; 8 (7): 579. doi: 10.3390/children8070579. PMID: 34356558; PMCID: PMC8307631.
11. *Li JJ, Zu CH, Li SP, Gao W, Shen ZY, Cai JZ*. Effect of graft size matching on pediatric living-donor liver transplantation at a single center. *Clin Transplant*. 2018 Jan; 32 (1). doi: 10.1111/ctr.13160. Epub 2017 Dec 12. PMID: 29154411.
12. *Kasahara M, Kaihara S, Oike F, Ito T, Fujimoto Y, Ogura Y et al.* Living-donor liver transplantation with monosegments. *Transplantation*. 2003 Aug 27; 76 (4): 694–696. doi: 10.1097/01.TP.0000079446.94204.F9. PMID: 12973111.
13. *Ogawa K, Kasahara M, Sakamoto S, Ito T, Taira K, Oike F et al.* Living donor liver transplantation with reduced monosegments for neonates and small infants. *Transplantation*. 2007 May 27; 83 (10): 1337–1340. doi: 10.1097/01.tp.0000263340.82489.18. PMID: 17519783.
14. *Kanazawa H, Sakamoto S, Fukuda A, Uchida H, Hamano I, Shigeta T et al.* Living-donor liver transplantation with hyperreduced left lateral segment grafts: a single-center experience. *Transplantation*. 2013 Mar 15; 95 (5): 750–754. doi: 10.1097/TP.0b013e31827a93b4. PMID: 23503505.
15. *Namgoong JM, Hwang S, Song GW, Kim DY, Ha TY, Jung DH et al.* Pediatric liver transplantation with hyperreduced left lateral segment graft. *Ann Hepatobiliary Pancreat Surg*. 2020 Nov 30; 24 (4): 503–512. doi: 10.14701/ahbps.2020.24.4.503. PMID: 33234754; PMCID: PMC7691208.
16. *Kitajima T, Sakamoto S, Sasaki K, Narumoto S, Kazemi K, Hirata Y et al.* Impact of graft thickness reduction of left lateral segment on outcomes following pediatric living donor liver transplantation. *Am J Transplant*. 2018 Sep; 18 (9): 2208–2219. doi: 10.1111/ajt.14875. Epub 2018 May 15. PMID: 29673096.
17. *Buell JF, Cherqui D, Geller DA, O'Rourke N, Iannitti D, Dagher I et al.* World Consensus Conference on Laparoscopic Surgery. The international position on laparoscopic liver surgery: The Louisville Statement, 2008. *Ann Surg*. 2009 Nov; 250 (5): 825–830. doi: 10.1097/sla.0b013e3181b3b2d8. PMID: 19916210.
18. *Han HS, Cho JY, Kaneko H, Wakabayashi G, Okajima H, Uemoto S et al*. Expert Panel Statement on Laparoscopic Living Donor Hepatectomy. *Dig Surg*. 2018; 35 (4): 284–288. doi: 10.1159/000479242. Epub 2017 Oct 20. PMID: 29050033.
19. *Soubrane O, de Rougemont O, Kim KH, Samstein B, Mamode N, Boillot O et al.* Laparoscopic Living Donor Left Lateral Sectionectomy: A New Standard Practice for Donor Hepatectomy. *Ann Surg*. 2015 Nov; 262 (5): 757–761; discussion 761–763. doi: 10.1097/SLA.0000000000001485. PMID: 26583663.
20. *Monakhov A, Semash K, Tsiroulnikova O, Djanbekov T, Khizroev K, Kurtak N et al.* Laparoscopic left lateral sectionectomy in living liver donors: from the first experi-

ence to routine usage. *Transplantation*. 2020 Sep; 104 (S3): S241. doi: 10.1097/01.tp.0000699664.06418.8f.

21. *Hong SK, Suh KS, Kim HS, Yoon KC, Ahn SW, Kim H et al.* Pediatric Living Donor Liver Transplantation Using a Monosegment Procured by Pure 3D Laparoscopic Left Lateral Sectionectomy and *In situ* Reduction. *J Gastrointest Surg*. 2018 Jun; 22 (6): 1135–1136. doi: 10.1007/s11605-018-3705-1. Epub 2018 Feb 12. PMID: 29435902.
22. *Umemura A, Nitta H, Takahara T, Hasegawa Y, Katagiri H, Kanno S et al.* Pure laparoscopic left lateral graft procurement with removing segment 3 employing Glissonean approach, indocyanine green fluorescence imaging and *in situ* splitting for a small infant. *J Minim Access Surg*. 2023 Jan-Mar; 19 (1): 165–167. doi: 10.4103/jmas.jmas_290_21. PMID: 36722543; PMCID: PMC10034808.
23. *Kim WJ, Kim KH, Cho HD, Namgoong JM, Hwang S, Park JI, Lee SG.* Long-Term Safety and Efficacy of Pure Laparoscopic Donor Hepatectomy in Pediatric Living Donor Liver Transplantation. *Liver Transpl*. 2021 Apr; 27 (4): 513–524. doi: 10.1002/lt.25910. Epub 2020 Dec 12. PMID: 33021038; PMCID: PMC8246762.
24. *Li H, Zhu Z, Wei L, Tan Y, Zeng Z, Qu W et al.* Laparoscopic Left Lateral Monosegmentectomy in Pediatric Living Donor Liver Transplantation Using Real-Time ICG Fluorescence *In situ* Reduction. *J Gastrointest Surg*. 2020 Sep; 24 (9): 2185–2186. doi: 10.1007/s11605-020-04534-5. Epub 2020 May 12. PMID: 32399671.
25. *Lau NS, Ly M, Liu K, Majumdar A, McCaughan G, Crawford M, Pulitano C.* Current and Potential Applications for Indocyanine Green in Liver Transplantation. *Transplantation*. 2022 Jul 1; 106 (7): 1339–1350. doi: 10.1097/TP.0000000000004024. Epub 2021 Dec 27. PMID: 34966106.
26. *Fortuna L, Buccianti S, Risaliti M, Matarazzo F, Agostini C, Ringressi MN et al.* Indocyanine Green and Hepatobiliary Surgery: An Overview of the Current Literature. *J Laparoendosc Adv Surg Tech A*. 2024 Oct; 34 (10): 921–931. doi: 10.1089/lap.2024.0166. PMID: 39167475.

The article was submitted to the journal on 21.10.2024

DOI: 10.15825/1995-1191-2025-1-40-49

ANALYSIS OF THE PREVALENCE AND ROLE OF MALADAPTIVE LEFT VENTRICULAR REMODELING IN THE RISK OF EARLY RENAL GRAFT DYSFUNCTION

R.A. Ibadov, D.A. Chernov, S.Kh. Ibragimov, Z.U. Abdugafurov, Z.T. Matkarimov

Vakhidov Republican Specialized Research and Practical Medical Center of Surgery, Tashkent, Uzbekistan

Objective: to study the prevalence of maladaptive left ventricular remodeling (MLVR) among kidney transplant (KT) candidates and the role of MLVR in the development of early graft dysfunction (EGD). **Materials and methods.** The study is based on a retrospective analysis of treatment outcomes in 650 patients who underwent a living related KT. Transthoracic echocardiogram revealed different types of left ventricular (LV) remodeling, whose prevalence was studied in the context of influence on the general population and specific "renal" risk factors. Two patient groups were also identified: Group I had EGD (n = 82) and Group II had primary graft function (PGF) (n = 79). These groups were comparable in terms of demographics, clinical data, and laboratory results ($p > 0.1$). The relative risk of developing EGD was calculated depending on whether maladaptive remodeling was present. **Results.** Concentric LV hypertrophy (cLVH) was detected in 341 (52.46%), eccentric (eLVH) in 174 (26.77%) patients. Concentric remodeling (CR) and normal LV geometry were detected in 86 (13.23%) and 49 (7.54%) patients, respectively. MLVR (cLVH + eLVH) was more common in men ($p = 0.003$). Compared to patients in the pre-dialysis stage, the risk of developing MLVR was 5.6 times higher for dialysis therapy durations up to 1 year, 8 times higher for durations 1 to 2 years, and 4.5 times higher for durations greater than 2 years ($p < 0.05$). The likelihood of developing MLVR was 8-fold higher in those with a functioning arteriovenous fistula ($p < 0.001$). As diuresis decreased, the odds of developing MLVR increased 4 to 15.8 times ($p < 0.001$). Depending on the severity of their anemia, patients with anemia had 2.7–13.8 times the chances of developing MLVR compared to those without anemia ($p < 0.05$). According to comparative analysis, the EGD group had a high prevalence of MLVR ($p = 0.01$). MLVR raised the risk of developing EGD in the post-transplant period by 8.5 times for cLVH ($p = 0.049$) and 14.5 times for eLVH ($p = 0.011$). **Conclusion.** The presence of MLVR in a KT candidate indicates the severity of cardiovascular disease brought on by progression of chronic kidney disease, and can also be regarded as one of the risk factors for EGD.

Keywords: kidney transplantation, left ventricular hypertrophy, remodeling, early graft dysfunction.

INTRODUCTION

Today, kidney transplantation (KT) is widely considered the preferred method of replacement therapy for end-stage renal disease" (ESRD). It provides significantly better quality of life for patients and is considered more cost-effective compared to dialysis as a treatment for ESRD.

Cardiovascular health is a major determinant of life expectancy both in patients with chronic kidney disease (CKD) and in renal transplant recipients [1–3]. The diversity and close connection of pathological changes in kidney and cardiovascular damage led to the formation of the concept of cardiorenal syndrome (CRS), the definition and classification of which were first proposed by Ronco et al. in 2010 [4]. CRS is defined as a complex of pathological interdependent conditions involving the heart and kidneys, developing due to acute or chronic dysfunction in one of the organs, which leads to subsequent dysfunction in the other organ. In this article, we focus on CRS type 4, a condition where CKD leads to significant cardiovascular dysfunction.

In ESRD patients, the high risk of adverse cardiovascular events – including decompensated heart failure, arrhythmias, and acute coronary syndrome – is largely attributed to structural remodeling of the left ventricular (LV) myocardium. This remodeling results from increased LV mass, myocardial fibrosis, and geometric disturbances. Left ventricular hypertrophy (LVH) initially serves as a compensatory adaptation in early-stage CKD. However, as CKD progresses, LVH transforms into a pathological, maladaptive remodeling process [5].

In a clinical context, the progression from normal LV geometry to concentric remodeling (CR), then to concentric LV hypertrophy (cLVH) and eccentric LV hypertrophy (eLVH), represents distinct stages of maladaptive cardiac remodeling in CKD [6]. The high prevalence of

Corresponding author: Denis Chernov. Address: 10, Kichik Khalka Yuli str., Chilonzor District, Tashkent, 100115, Uzbekistan. Phone: +998 (91) 185-35-99. E-mail: dionis8501@gmail.com

cLVH in early CKD is primarily due to pressure overload, while the transition to eLVH at dialysis initiation is driven by volume overload and anemia [7]. In addition to hemodynamic causes, specific (renal) risk factors for LVH are common in CKD patients, with anemia having the greatest impact. Renal anemia in CKD primarily results from a deficiency of erythropoietin due to kidney damage. However, several additional factors worsen anemia in CKD, including iron deficiency and chronic inflammation.

LVH prevalence increases progressively from 16–31% in stage 1–3 CKD patients, reaching nearly 90% in dialysis-dependent patients. Meanwhile, CR is considered an adaptive form of LV remodeling, whereas cLVH and eLVH are classified as maladaptive left ventricular remodeling (MLVR) due to their strong association with adverse cardiovascular events (ACEs) [3, 5–9]. In a study by de Roij van Zuijdewijn CL et al. (2015), the risk of sudden death among patients with eLVH was 5.2 times higher than in the group of patients with cLVH and 10.2 times higher than in patients with normal LV geometry [10].

MLVR before KT is a strong predictor of ACEs and all-cause mortality in both the perioperative and long-term postoperative periods [11, 12].

KT can significantly improve cardiac function in most patients, but it takes time to trigger reverse remodeling processes [13, 14]. An experimental study by Hagmayer et al. (2023) demonstrated that KT in CKD rats led to improved cardiac function, but LVH persisted in most animals at 16 weeks post-transplant [15].

At the same time, decreased LV stroke volume, circulatory minute volume, cardiac index, increased total peripheral vascular resistance (PVR), arrhythmias, diastolic and systolic dysfunction caused by MLVR may have an adverse effect on kidney graft function in the early post-transplant period.

Thus, LVH prevalence among KT candidates is a crucial area of investigation due to its direct impact on transplant outcomes, particularly the risk of early graft dysfunction. We found no studies addressing this issue in available scientific databases.

Objective: to investigate MLVR prevalence among KT candidates, to determine its significance in the development of early graft dysfunction (EGD).

MATERIALS AND METHODS

The study is based on a retrospective analysis of the treatment outcomes of 650 patients with ESRD who underwent a living-related kidney transplantation (LRKT) at Vakhidov Republican Specialized Research and Practical Medical Center of Surgery from January 2018 to August 2022.

Patients were included in the study using a continuous method. Inclusion criteria for the study were stage 5 CKD and LRKT. The sample did not include patients who did not have a histocompatible donor or were not allowed for transplantation due to chronic underlying diseases in the decompensation stage.

The patients were examined at the outpatient and hospital stage of preparation for KT surgery according to the approved national protocol for examining KT candidates (Order of the Ministry of Health of the Republic of Uzbekistan, No. 179 dated June 27, 2022, Appendix No. 2 “List of tests for medical examination of a living donor and recipient”).

A donor-recipient pair was selected taking into account histocompatibility on the basis of HLA I–II analysis; lymphocytotoxic test was also performed. Determination of markers of hepatitis B, C, HIV, TORCH complex, biochemical and hematological studies were performed at the laboratory of Vakhidov Republican Specialized Research and Practical Medical Center of Surgery in Tashkent, Uzbekistan, on automatic analyzers BC-5300 (Mindray, China), Vitros-350 (G&G, USA), and Maglumi-800 (China).

An echocardiogram was performed on ultrasound scanners GE LOGIQ P6 (General Electric Health Care, USA), Philips HD11 XE (Philips Healthcare, USA), and Toshiba Xario 200 (Toshiba Medical Systems Corp., Japan) using 3–5 MHz phased array probes. A standard transthoracic echocardiogram (TTE) was performed according to the guidelines of the American Society of Echocardiography [16]. In patients receiving hemodialysis sessions, the study was performed mainly on the day after hemodialysis procedure, thus leveling the factor of volume overload associated with interdialysis increase in the volume of extracellular fluid.

As a result of measurements from parasternal, apical, subcostal accesses, in M-, B-modes, structural-geometric parameters, systolic heart function parameters, assessment of the valve apparatus state (using pulsed-wave, constant-wave Doppler mode) were determined.

Linear parameters were studied in M-mode according to the standard Penn convention method, and the following were determined: left ventricular end-diastolic diameter (LVEDD, cm); left ventricular end-systolic diameter (LVESD, cm); interventricular septum thickness at systole and diastole (IVSs, IVSd, cm); left ventricular posterior wall thickness at systole and diastole (LVPWs, LVPWd, cm). The LV relative wall thickness (RWT) was calculated using the formula:

$$RWT = 2 \times LVPWd / LVEDD.$$

Based on the obtained data, left ventricular myocardial mass (LVMM) was calculated using the formula developed by Devereux et al. (1986), recommended by the American Society of Echocardiography (ASE), based on linear measurements and the LV model as an elongated ellipsoid of revolution:

$$LVMM = 0.8 \times (1.04 \times [(EDD + LVPWd + IVSd)^3 - (EDD)^3]) + 0.6 \text{ gr.}$$

The result was weighed against body surface area (BSA) in m^2 to obtain the LVMM. BSA was calculated using the Gehan & George method in accordance with European Renal Best Practice Guideline on kidney donor and recipient evaluation and perioperative care [17]:

$$BSA\ (m^2) = 0.0235 \times \text{growth (cm)}^{0.42246} \times \times \text{weight (kg)}^{0.51456}.$$

An LVMM of more than 115 g/m^2 in men and 95 g/m^2 in women was considered as LVH criterion according to ASE and European Association of Echocardiography (EAE) guidelines. Types of LV hypertrophy and remodeling were determined depending on LVMM and RWT according to the classification proposed by Antonello Ganau (1992):

- normal geometry (normal LVMM; RWT ≤0.42)
- concentric remodeling (normal LVMM; RWT >0.42)
- concentric hypertrophy (increased LVMM; RWT >0.42)
- eccentric hypertrophy (increased LVMM and RWT ≤0.42).

Primary graft function (PGF) was observed in 539 (82.92%) patients. Delayed graft function (the need for dialysis within the first 7 days after KT) was observed in 48 (7.38%) patients. Delayed graft function was determined by a 2-fold increase in plasma creatinine within the first 5 days after operation, and was observed in 34 (5.23%) patients. Acute renal graft rejection was observed in 9 (1.38%) cases, and infectious and surgical complications leading to graft dysfunction or loss were observed in 12 (1.85%) cases.

Patients with delayed graft function were grouped into study group I (n = 82) with early graft dysfunction (EGD). For comparison, group II (n = 79), comparable in terms of clinical and demographic parameters, was selected among patients with PGF (n = 539).

Statistical processing was carried out using parametric and nonparametric analysis methods. Accumulation, adjustment, systematization of initial information and visualization of the obtained results were done in Microsoft Office Excel 2016 spreadsheets. Statistical analysis was performed using the IBM SPSS Statistics v.26 program developed by IBM Corporation, USA.

Conformity of quantitative indicators to normal distribution was measured using the Kolmogorov–Smirnov test. In the case of describing the indicators having normal distribution, the obtained data were presented in the form of arithmetic mean (M) and standard deviation (SD); for indicators that did not follow a normal distribution, data were presented as median (Me) with lower and upper quartiles (Q1; Q3). Nominal data were described with absolute values and percentages.

When comparing mean values in normally distributed sets of quantitative data, the Student t-test was calculated; in cases of no signs of normal distribution, we used Mann–Whitney U test.

Nominal data were compared using Pearson's chi-squared test; where the expected phenomenon was less than 10, we calculated the chi-squared test with a Yates correction to reduce the probability of type 1 error.

As a quantitative measure of effect when comparing relative measures, we used the odds ratio (OR), defined as the ratio of the probability of an event occurring in the exposed group to the probability of the event occurring in the control group. In order to project the obtained OR values to the general population, we calculated the boundaries of the 95% confidence interval (95% CI). Statistical significance of differences was recognized at a significance level of $p < 0.05$.

RESULTS

The median age of the study cohort was 33 (27–39) years, with a predominance of young people (18–44 years), n = 543 (83.54%). In terms of gender composition, males predominated – 476 (73.23%) versus 174 (26.7%) females. Body mass index (BMI) was calculated using the formula: body weight (kg) / height (m^2). Median BMI was 22.7 kg/m^2 (20.2; 25.3). Renal replacement therapy by long-term hemodialysis was received by 565 (86.92%) patients. Median duration of CKD was 24 (12; 50) months and median length of dialysis was 9 (5; 16) months. Vascular access was via arteriovenous fistula (AVF) (n = 507; 89.73%) or central venous catheter (CVC) (n = 58; 10.27%). In 85 (13.08%) cases, KT was performed in the pre-dialysis stage of the disease.

The structure of clinical entities of renal diseases that were the cause of ESRD in our study is presented in Fig. 1. In most cases, the cause of ESRD in the studied patient cohort was chronic glomerulonephritis (n = 554; 85.23%). Among other pathology: 3 (0.46%) cases each of diabetic and gouty nephropathy; 2 (0.31%) cases each of neurogenic bladder, interstitial nephritis in pregnancy, lupus nephritis; one patient was diagnosed with Alport syndrome, a rare hereditary pathology of basal membranes, which is manifested by hematuria and progressive decline in renal function.

When studying the prevalence of various forms of LV remodeling in the studied patient cohort, it was revealed that the most common form was cLVH, detected in 341 (52.46%) patients. It is also worth noting the relatively high prevalence of the most unfavorable form of remodeling – eLVH (n = 174; 26.77%). Normal LV geometry was detected only in 49 (7.54%) patients (Fig. 2).

Table 1 presents the results of analysis of the influence of traditional (gender, age, BMI) and renal (length of dialysis therapy, type of vascular access, residual diuresis, renal anemia) risk factors on the prevalence of maladaptive remodeling (cLVH + eLVH).

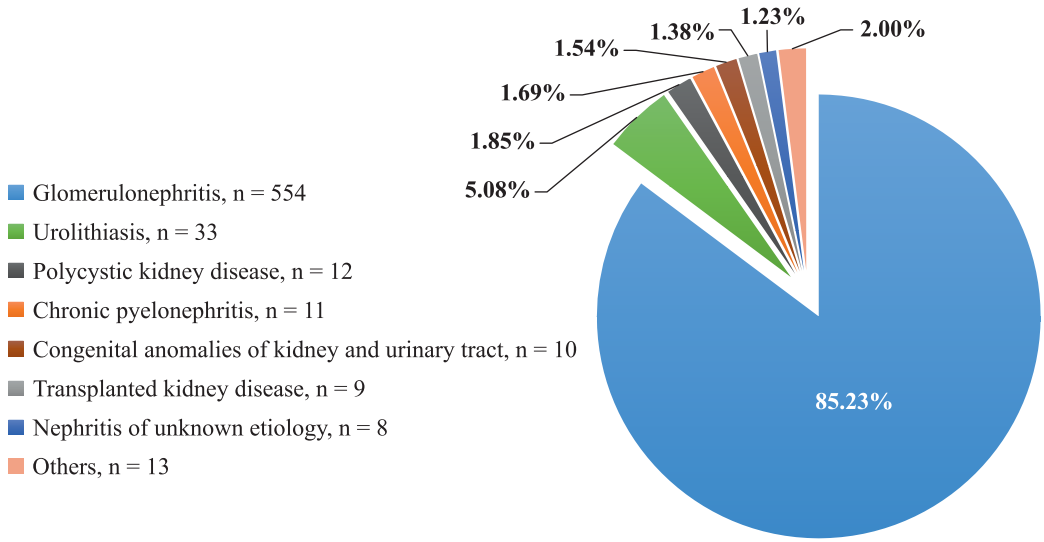

Fig. 1. Classification of kidney diseases

Table 1

Factor analysis of the prevalence of maladaptive left ventricular remodeling among kidney transplant candidates

	Patients with maladaptive remodeling (cLVH + eLVH)						Normal geometry	
	n	%	χ^2	p	OR	95% CI	n	%
Entire cohort (n = 650)	515	79.2					49	7.5
Sex								
Male (n = 476)	395	83	9.13	0.003	2.469	1.353–4.505	28	5.9
Female (n = 174)	120	69					21	12.1
Age								
≤20 years (n = 37)	20	54.1					7	18.9
21–44 years (n = 524)	431	82.3	9.686	0.002	4.571	1.802–11.594	33	6.3
45–59 years (n = 70)	50	71.4	2.143	0.144	2.917	0.872–9.756	6	8.6
60–74 years (n = 19)	14	73.7	0.072	0.789	1.633	0.359–7.432	3	15.8
BMI								
BMI < 18.4 (n = 86)	62	72.1	0.237	0.627	0.722	0.300–1.737	7	8.1
BMI 18.5–24.9 (n = 385)	319	82.9					26	6.8
BMI 25–29.9 (n = 139)	108	77.7	0.157	0.692	0.8	0.383–1.674	11	7.9
BMI >30 (n = 40)	26	65	1.757	0.186	0.424	0.150–1.196	5	12.5
Duration of dialysis								
≤12 months (n = 364)	308	84.6	23.473	0.001	5.600	2.717–11.543	22	6.0
1–2 years (n = 122)	100	82	16.215	0.001	8.000	2.747–23.301	5	4.1
>2 years (n = 79)	67	84.8	7.896	0.005	4.467	1.616–12.347	6	7.6
Pre-dialysis (n = 85)	40	47.1					16	18.8
Vascular access								
AVF (n = 507)	440	86.8	38.223	0.001	8.000	3.891–16.448	22	4.3
CVC (n = 58)	35	60.3	0.282	0.596	1.273	0.522–3.105	11	19.0
Residual urine output								
Anuria (n = 93)	86	92.5	21.575	0.001	15.809	3.617–69.101	2	2.2
≤500 mL/day (n = 304)	264	86.8	34.828	0.001	7.466	3.630–15.358	13	4.3
500–1500 mL/day (n = 129)	97	75.2	11.828	0.001	3.962	1.741–9.020	9	7.0
>1500 mL/day (n = 124)	68	54.8					25	20.2
Renal anemia								
Mild (n = 193)	138	71.5	7.276	0.007	2.684	1.288–5.595	19	9.8
Moderate (n = 255)	219	85.9	27.483	0.001	8.093	3.482–18.810	10	3.9
Severe (n = 121)	112	92.6	21.866	0.001	13.797	3.857–49.350	3	2.5
No anemia (n = 81)	46	56.8					17	21.0

Note: cLVH, concentric left ventricular hypertrophy; eLVH, eccentric left ventricular hypertrophy; BMI, body mass index; AVF, arteriovenous fistula; CVC, central venous catheter.

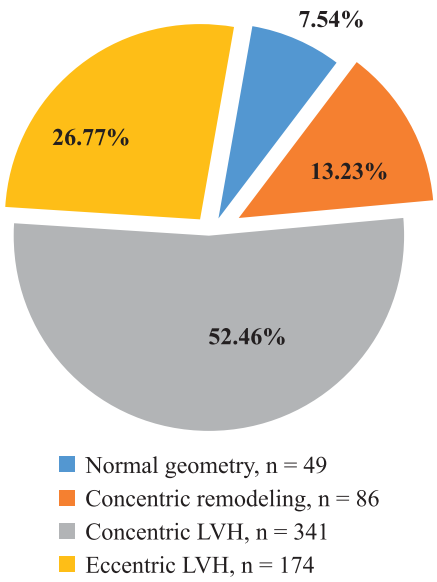

Fig. 2. Prevalence of left ventricular remodeling types

As shown in the presented table, male gender was associated with a high chance of developing cLVH and eLVH (OR 2.469; CI 95% 1.353–4.505; p = 0.003). Patient age and weight had no significant effect. Renal risk factors had a significant impact on the prevalence of maladaptive remodeling. For example, the odds of developing cLVH and eLVH were 5.6 times (p < 0.001) higher for dialysis lasting for less than 1 year, 8 times (p < 0.001) for 1 to 2 years, and 4.5 times (p = 0.005) for more than 2 years compared to pre-dialysis patients. The presence of a functioning AVF was associated with an 8-fold increase in the odds of developing cLVH and eLVH (p < 0.001) compared to pre-dialysis patients, where the influence of shunt blood flow was absent. We also found that progressive decrease in diuresis significantly increased the odds of maladaptive remodeling by 4 to 16 times (p < 0.001) compared to patients with preserved diuresis (>1500 mL/day). We consider renal anemia as a specific renal risk factor, but it is worth noting that anemia is also a risk factor for LVH in the general population [8]. The chances of developing MLVR in persons with anemia, depending on its degree, are 2.7 to 13.8 times (p < 0.001) higher than in the anemia-free group.

For the next stage of the study, we selected a group of PGF patients comparable in terms of the main clinical and demographic parameters in comparison with the EGD patient group; the obtained data are presented in Table 2.

The absence of statistically significant differences in the presented parameters allowed us to level their potential influence on the prevalence of various forms of remodeling and graft function between the study groups. This condition was necessary to study the possible influence of MLVR on the risk of early renal graft dysfunction.

A comparative analysis of transthoracic echocardiogram results between the study groups is presented in Table 3.

The presented results suggest that patients who developed EGD exhibited distinct cardiac abnormalities on preoperative echocardiography (EchoCG), including LV dilatation, reduced myocardial contractility, severe

Table 2

Comparative analysis by primary clinical and demographic indicators

	Group I (n = 82) (EGD)		Group II (n = 79) (PGF)		p
Age (Me; Q1; Q3)	32.5	27; 38	33	26; 37.5	0.907
Male (n/%)	66	80.49%	63	79.75%	0.908
Female (n/%)	16	19.51%	16	20.25%	
BMI (M ± SD)	22.99	3.41	22.51	3.41	0.384
Duration of dialysis					
Pre-dialysis (n/%)	6	7.32%	7	8.86%	
≤12 months (n/%)	51	62.20%	41	51.90%	0.741
12–24 months (n/%)	17	20.73%	15	18.99%	0.925
>24 months (n/%)	8	9.76%	16	20.25%	0.445
Residual urine output					
Anuria (n, %)	18	21.95%	17	21.52%	0.964
≤500 mL/day (n, %)	41	50.00%	34	43.04%	0.904
500–1500 mL/day (n, %)	15	18.29%	22	27.85%	0.455
>1500 mL/day (n, %)	8	9.76%	6	7.59%	
Renal anemia					
No anemia (n, %)	8	9.76%	10	12.66%	
Mild (n, %)	22	26.83%	19	24.05%	0.713
Moderate (n, %)	26	31.71%	28	35.44%	0.786
Severe (n, %)	26	31.71%	22	27.85%	0.670

Note: EGD, early graft dysfunction; PGF, primary graft function; BMI, body mass index.

left LVH, increased prevalence of mitral and tricuspid regurgitation, and severe pulmonary hypertension.

The comparative prevalence of maladaptive remodeling in the study groups is presented in Fig. 3. Differences between groups evaluated using Pearson's chi-squared test were statistically significant ($\chi^2 = 11.497$; $p = 0.01$), which allowed us to conclude that cLVH and eLVH are highly prevalent in the group of patients with EGD.

Quantitative analysis of the effect of MLVR on EGD demonstrated that the presence of cLVH increased the odds of EGD 8.5-fold (95% CI: 1.027–71.134; p = 0.049), while eLVH increased the odds 14.5-fold (95% CI: 1.661–126.57; p = 0.011). In contrast, CR did not have a statistically significant effect on EGD development (Table 4).

DISCUSSION

Our study revealed that MLVR was highly prevalent (79.23%) among the study population, with cLVH being the most common subtype (52.46%). These findings align with previously reported data, indicating that LVH is present in 48–84% of patients with CKD at the

Table 3

Comparative analysis of transthoracic echocardiogram results in patients depending on kidney graft function

	Group I (n = 82) (EGD)		Group II (n = 79) (PGF)		p
EDV, mL (M ± SD)	170.74	41.97	154.51	44.76	0.016
ECV, mL (Me; Q1; Q3)	79	59; 99	64	46.5; 89	0.002
SV, mL (M ± SD)	87.77	23.42	84.70	21.82	0.362
EF % (M ± SD)	51.35	10.45	56.05	8.08	0.002
IVSd, cm (Me; Q1; Q3)	1.5	1.3; 1.8	1.4	1.2; 1.6	0.060
LVPWd, cm (Me; Q1; Q3)	1.5	1.3; 1.8	1.4	1.2; 1.65	0.058
RWT (Me; Q1; Q3)	0.52	0.41; 0.6	0.52	0.42; 0.62	0.450
LVMM (Me; Q1; Q3)	245.13	184.79; 325.33	197.28	150.49; 265.95	0.001
EDD (M ± SD)	5.92	0.87	5.39	0.96	<0.001
ESD (Me; Q1; Q3)	4	3.5; 4.5	3.7	3.3; 4.2	0.009
MR II, III (n, %)	47	57.32%	28	35.44%	0.006
TR II, III (n, %)	41	50.00%	15	18.99%	<0.001
AR II (n, %)	3	3.66%	1	1.27%	0.640
mPAP, mmHg (M ± SD)	48.26	18.63	31.92	16.11	<0.001

Note: EDV, end-diastolic volume; ECV, end-systolic volume; SV, stroke volume; EF, ejection fraction; IVSd, interventricular septum thickness at diastole; LVPWd, left ventricular posterior wall thickness at diastole; RWT, relative wall thickness; LVMM, left ventricular myocardial mass; EDD, end-diastolic diameter; ESD, end-systolic diameter; MR, mitral regurgitation; TR, tricuspid regurgitation; AR, aortic regurgitation; mPAP, mean pulmonary artery pressure.

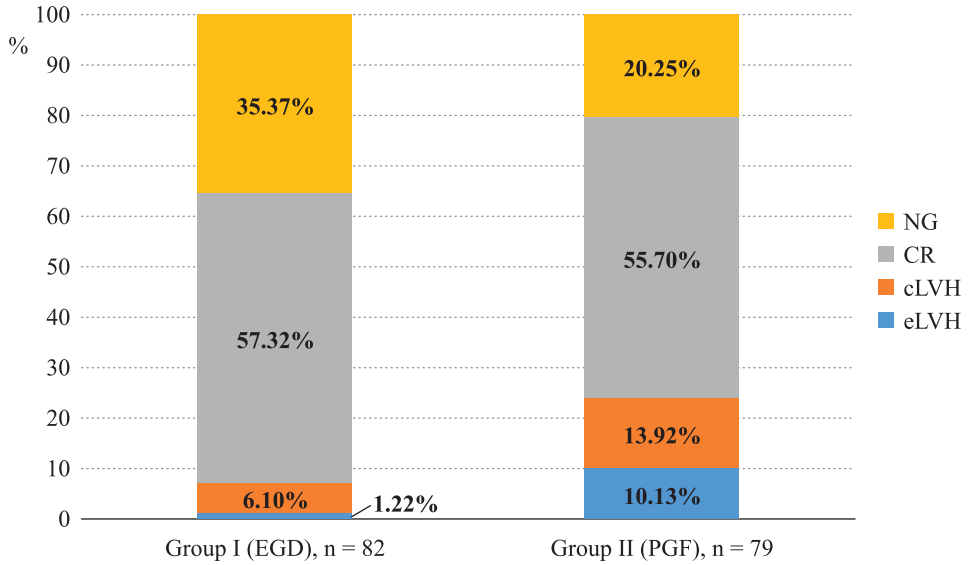

Fig. 3. Prevalence of left ventricular remodeling types in the study groups. NG, normal geometry; CR, concentric remodeling; cLVH, concentric LV hypertrophy; eLVH, eccentric LV hypertrophy; EGD, early graft dysfunction; PGF, primary graft function

Table 4

Risks of developing early allograft dysfunction depending on types of left ventricular remodeling

	Group I (n = 82) (EGD)	Group II (n = 79) (PGF)	χ^2	p	OR	95% CI
Normal LV geometry	1 (1.22%)	8 (10.13%)				
Concentric remodeling	5 (6.1%)	11 (13.92%)	1.281	0.52	3.64	0.353–37.458
Concentric LV remodeling	47 (57.32%)	44 (55.7%)	3.89	0.049	8.55	1.027–71.134
Eccentric LV remodeling	29 (35.37%)	16 (20.25%)	6.615	0.011	14.50	1.661–126.570

Note: EGD, early graft dysfunction; PGF, primary graft function; OR, odds ratio; LV, left ventricular.

pre-dialysis stage and up to 90% of patients on long-term hemodialysis [7–9].

Among the identified risk factors, male gender ($p = 0.003$), longer duration of dialysis therapy ($p < 0.001$), presence of a functioning AVF ($p < 0.001$), decreased diuresis ($p < 0.001$), and renal anemia ($p < 0.001$) were significantly associated with a higher prevalence of MLVR. Information about the influence of the above factors on MLVR development according to reports is contradictory, except for renal anemia, whose role in the development of LVH has been confirmed by most studies [5–9, 18, 19]. In addition, renal anemia is a modifiable risk factor for MLVR, and its effective treatment may significantly promote LVH regression [20]. Evidence also suggests that in ESRD patients, anemia has a greater influence on myocardial remodeling than blood pressure [18].

We investigated the prevalence of various forms of LV remodeling among KT candidates, particularly in relation to their potential impact on transplant outcomes, including the risk of EGD. Our findings indicate that the likelihood of developing EGD is 8.5-fold higher in cLVH and 14.5-fold higher in eLVH compared to patients with normal LV geometry. These results suggest that patients with MLVR should be considered at increased risk for EGD.

KT eliminates the need for long-term dialysis and improves renal function, which contributes to regression of LVH and other structural cardiac changes. These improvements ultimately enhance overall survival and quality of life in transplant recipients. Despite advancements in modern transplantology, EGD remains a concern, occurring in approximately 15–30% of cadaveric transplants and 5–10% of living donor transplants. Various donor- and recipient-related risk factors for EGD are still under investigation. Similarly, EGD significantly impacts long-term graft survival in the postoperative period [21–23].

Based on both literature data and our own research findings, this relationship underscores the critical importance of eliminating modifiable risk factors for LVH, particularly symptomatic hypertension and renal anemia. Effective control of these factors can significantly reduce the risk of MLVR development and progression, ultimately leading to improved immediate post-transplant renal outcomes. In addition, evidence suggests that optimizing dialysis therapy – specifically, achieving the patient's dry weight and maintaining interdialytic weight gain below 5% of body weight – can contribute to LVH regression [19].

A promising area for further investigation is the role of the endogenous cardiotonic steroid marinobufagenin (MBG) in LVH development and progression in CKD patients, including those who have undergone KT. A study by Bolignano et al. demonstrated that MBG levels in KT recipients are lower than those observed in hemodialysis patients but remain elevated compared to healthy individuals. MBG levels were found to directly correlate with left ventricular myocardial mass and serve as a significant predictor of post-KT cardiovascular and renal complications. The authors proposed considering MBG as a unifying factor in pathological cardiac remodeling and kidney graft dysfunction. Its measurement holds significant prognostic value in enhancing cardiorenal risk assessment [24].

CONCLUSION

The identification of MLVR in KT candidates is a crucial component of preoperative comorbidity assessment. Early detection can help reduce the risk of postoperative complications, including EGD. Further investigation into the impact of MLVR on immediate KT outcomes necessitates multicenter randomized clinical trials to provide robust evidence.

The authors declare no conflict of interest.

REFERENCES

1. *Xu C, Tsihlis G, Chau K, Trinh K, Rogers NM, Julovi SM.* Novel Perspectives in Chronic Kidney Disease-Specific Cardiovascular Disease. *Int J Mol Sci*. 2024; 25 (5): 2658. https://doi.org/10.3390/ijms25052658.
2. *Reggiani F, Moroni G, Ponticelli C.* Cardiovascular Risk after Kidney Transplantation: Causes and Current Approaches to a Relevant Burden. *J Pers Med*. 2022; 12 (8): 1200. https://doi.org/10.3390/jpm12081200.
3. *Aalten J, Hoogeveen EK, Roodnat JI, Weimar W, Borm GF, de Fijter JW, Hoitsma AJ.* Associations between pre-kidney-transplant risk factors and post-transplant cardiovascular events and death. *Transpl Int.* 2008 Oct; 21 (10): 985–991. doi: 10.1111/j.1432-2277.2008.00717.x.
4. *Ronco C, McCullough P, Anker SD, Anand I, Aspromonte N, Bagshaw SM et al.* Cardio-renal syndromes: report

from the consensus conference of the acute dialysis quality initiative. *Eur Heart J.* 2010; 31 (6): 703–711. doi: 10.1093/eurheartj/ehp507.

5. *Kalyuzhin VV, Teplyakov AT, Solovtsov MA, Kalyuzhina EV, Bespalova ID, Terentyeva NN.* Remodeling of the left ventricle: one or several scenarios? *Bulletin of Siberian Medicine.* 2016; 15 (4): 120–139. [in Russ, English abstract]. https://doi.org/10.20538/1682-0363-2016-4-120-139.
6. *Ievlev EN, Kazakova IA, Rudenko IB, Shamova LL.* Anemia and structural and functional heart conditions in patients undergoing renal replacement therapy. *Ul'yanovskiy mediko-biologicheskiy zhurnal.* 2023; 1: 14–26. [in Russ, English abstract]. doi: 10.34014/2227-1848-2023-1-14-26.
7. *Maqbool S, Shafiq S, Ali S, Rehman MEU, Malik J, Lee KY.* Left Ventricular Hypertrophy (LVH) and Left Ventricular Geometric Patterns in Patients with Chronic Kidney Disease (CKD) Stage 2–5 With Preserved Ejection Fraction (EF): A Systematic Review to Explore CKD Stage-wise LVH Patterns. *Curr Probl Cardiol.* 2023; 48 (4): 101590. doi: 10.1016/j.cpcardiol.2023.101590.
8. *Sedov DS, Rebrov AP.* Cardiac remodeling in patients with chronic kidney disease (review). *Saratov Journal of Medical Scientific Research*. 2019; 15 (2): 217–221. [in Russ, English abstract].
9. *Law JP, Pickup L, Pavlovic D, Townend JN, Ferro CJ.* Hypertension and cardiomyopathy associated with chronic kidney disease: epidemiology, pathogenesis and treatment considerations. *J Hum Hypertens.* 2023; 37 (1): 1–19. doi: 10.1038/s41371-022-00751-4.
10. *De Roij van Zuijdewijn CL, Hansildaar R, Bots ML, Blankestijn PJ, van den Dorpel MA, Grooteman MP et al.* Eccentric Left Ventricular Hypertrophy and Sudden Death in Patients with End-Stage Kidney Disease. *Am J Nephrol.* 2015; 42 (2): 126–133. doi: 10.1159/000439447.
11. *Malyala R, Rapi L, Nash MM, Prasad GVR.* Pre-Transplant Left Ventricular Geometry and Major Adverse Cardiovascular Events After Kidney Transplantation. *Ann Transplant.* 2019; 24: 100–107. doi: 10.12659/AOT.913649.
12. *Pecoits-Filho R, Calice-Silva V.* Unchain the heart: impact of left ventricular myocardial hypertrophy regression in kidney transplant outcomes. *Nephrol Dial Transplant.* 2016; 31 (7): 1025–1026. doi: 10.1093/ndt/gfv424.
13. *Zhidkova DA, Tomilina NA, Storozhakov GI, Gendlin GE, Kim IG, Fedorova ND.* The dynamics and risk factors of left ventricular hypertrophy at the first and the second years after renal transplantation. *Nephrology and Dialysis.* 2007; 9 (4): 408–421. [In Russ, English abstract].
14. *Qi L, Ni X, Schoepf UJ, Varga SA, McGill L, Wang W et al.* Time-dependent cardiac structural and functional changes after kidney transplantation: a multi-parametric cardiac magnetic resonance study. *Eur Radiol.* 2022; 32 (8): 5265–5275. doi: 10.1007/s00330-022-08621-w.
15. *Hagmayer L, Mayer C, Ebert N, Amann K, Daniel C.* Experimental renal transplantation in rats improves cardiac dysfunction caused by chronic kidney disease while LVH persists. *Front Cardiovasc Med.* 2023; 10: 1200323. doi: 10.3389/fcvm.2023.1200323.
16. *Mitchell C, Rahko PS, Blauwet LA, Canaday B, Finstuen JA, Foster MC et al.* Guidelines for performing a comprehensive transthoracic echocardiographic examination in adults: recommendations from the American society of echocardiography. *J Am Soc Echocardiogr.* 2019; 32 (1): 1–64. doi: 10.1016/j.echo.2018.06.004.
17. *Abramowicz D, Cochat P, Claas FH, Heemann U, Pascual J, Dudley C et al.* European Renal Best Practice Guideline on kidney donor and recipient evaluation and perioperative care. *Nephrol Dial Transplant.* 2015 Nov; 30 (11): 1790–1797. doi: 10.1093/ndt/gfu216.
18. *Di Lullo L, Gorini A, Russo D, Santoboni A, Ronco C.* Left Ventricular Hypertrophy in Chronic Kidney Disease Patients: From Pathophysiology to Treatment. *Cardiorenal Med*. 2015; 5 (4): 254–266. doi: 10.1159/000435838.
19. *Strokov AG, Gavrilin VA, Terehov VA.* Left ventricular hypertrophy in patients on chronic haemodialysis. *Russian Journal of Transplantology and Artificial Organs.* 2010; 12 (3): 48–51. [In Russ, English abstract]. https://doi.org/10.15825/1995-1191-2010-3-48-51.
20. *Tian Z, Bergmann K, Kaufeld J, Schmidt-Ott K, Melk A, Schmidt BMW.* Left Ventricular Hypertrophy After Renal Transplantation: Systematic Review and Meta-analysis. *Transplant Direct.* 2024; 10 (6): e1647. doi: 10.1097/TXD.0000000000001647.
21. *Ahlmark A, Sallinen V, Eerola V, Lempinen M, Helanterä I.* Characteristics of Delayed Graft Function and Long-Term Outcomes After Kidney Transplantation From Brain-Dead Donors: A Single-Center and Multicenter Registry-Based Retrospective Study. *Transpl Int*. 2024; 37: 12309. doi: 10.3389/ti.2024.12309.
22. *Ponticelli C, Reggiani F, Moroni G.* Delayed Graft Function in Kidney Transplant: Risk Factors, Consequences and Prevention Strategies. *J Pers Med.* 2022 Sep 21; 12 (10): 1557. doi: 10.3390/jpm12101557.
23. *Shabunin AV, Drozdov PA, Nesterenko IV, Makeev DA, Astapovich SA, Zhuravel OS, Karapetyan LR.* Effect of delayed graft function on immediate and long-term kidney transplant outcomes. *Russian Journal of Transplantology and Artificial Organs.* 2024; 26 (1): 20–25. [In Russ, English abstract]. https://doi.org/10.15825/1995-1191-2024-1-20-25.
24. *Bolignano D, Greco M, Presta P, Caglioti A, Carullo N, Zicarelli M et al.* Marinobufagenin, Left Ventricular Hypertrophy and Residual Renal Function in Kidney Transplant Recipients. *J Clin Med.* 2023; 12 (9): 3072. doi: 10.3390/jcm12093072.

The article was submitted to the journal on 01.06.2024

DOI: 10.15825/1995-1191-2025-1-50-54

ENDOSCOPIC TREATMENT OF KAPOSI'S SARCOMA IN A HEART TRANSPLANT PATIENT

M.T. Bekov[1], I.V. Pashkov[1], N.P. Mozheiko[1], N.N. Koloskova[1], K.S. Smirnov[1], Ya.S. Yakunin[1], M.V. Olkhovskaya[1], O.M. Tsirulnikova[1, 2], S.V. Gautier[1, 2]

[1] Shumakov National Medical Research Center of Transplantology and Artificial Organs, Moscow, Russian Federation

[2] Sechenov University, Moscow, Russian Federation

Kaposi's sarcoma (KS) is a malignant tumor caused by human herpesvirus 8. Due to etiological and pathogenetic factors, this type of tumor is common among patients with immunodeficiency of various genesis. Solid organ recipients are at a high risk of developing malignant tumors in various locations due to the peculiarities of subsequent drug immunosuppressive therapy. Because KS is so common in this patient cohort, methods for early detection, efficient treatment, and prevention of the neoplastic process must be developed. This paper presents a clinical case of a successful surgical treatment of KS of the aryepiglottic fold using an endoscopic electrosurgical station with an argon complex.

Keywords: endoscopy, heart transplantation, heart recipients, Kaposi's sarcoma.

INTRODUCTION

The number of solid organ transplants performed globally has been increasing over the years. In 2022, 157,494 organ transplants were performed worldwide. Kaposi sarcoma (KS) is a malignant poorly differentiated vascular tumor and is directly linked to human herpesvirus 8 (HHV-8). KS incidence is significantly higher in solid organ transplant recipients receiving immunosuppressive therapy for vital indications than, ranging from 0.2–11% in transplant recipients, compared to rare cases in the general population [2, 3].

KS has several distinct forms. The four main types are:

– Classical KS (idiopathic, sporadic, European KS);
– Endemic KS (African KS);
– Epidemic KS (AIDS-related KS);
– Immunosuppressive KS (occurs in individuals on chronic immunosuppressive therapy, including those taking cytostatic drugs) [4, 5].

CLINICAL CASE

Patient B, a 40-year-old male, was diagnosed with dilated cardiomyopathy prior to transplantation. In August 2022, he underwent orthotopic heart transplantation using the biatrial technique. His post-transplant immunosuppressive regimen included tacrolimus and mycophenolate mofetil at tailored dosages.

In the fall of 2022, he developed an acute upper respiratory infection (URTI), prompting a temporary adjustment in immunosuppressive therapy – mycophenolate mofetil was discontinued for three days before being resumed. In the spring of 2023, he experienced another episode of URTI, but no modifications were made to his immunosuppressive regimen.

In June 2023, the patient developed conjunctivitis accompanied by a low-grade fever. Laboratory tests conducted in August 2023 detected no DNA from cytomegalovirus, Epstein–Barr virus, or human herpesvirus types 1, 2, and 6; however, HHV-8 was positive.

During a routine esophagogastroduodenoscopy, an epithelial tumor was identified in the projection of the right aryepiglottic fold, measuring 30×10×15 mm (Fig. 1). Consultation with an ENT specialist was advised. Laryngoscopy was subsequently performed, and a tissue sample was obtained for morphological examination. The final diagnosis from the morphological study confirmed a cavernous hemangioma.

The patient was invited again on an outpatient basis at Shumakov National Medical Research Center of Transplantology and Artificial Organs for another examination with taking material for histopathology. Fibrolaryngoscopy was performed, biopsy was taken. Histopathological findings: morphological picture is characteristic of Kaposi's sarcoma (Fig. 2).

York et al. reported a clinical case of a heart recipient with incidentally diagnosed KS localized in the upper gastrointestinal tract [6]. The article demonstrates the occurrence of profuse bleeding from the stomach, which was the reason for endoscopic intervention for hemostatic purposes. During the therapeutic and diagnostic

Corresponding author: Maksat Bekov. Address: 1, Shchukinskaya str., Moscow, 123182, Russian Federation. Phone: (926) 399-49-75. E-mail: doctorbekov@gmail.com

endoscopic manipulation, an vascular epithelial formation was visualized. Upon completion of endoscopic hemostasis, a biopsy of the tumor was performed. Histopathology carried out detected KS.

This clinical case highlights several key aspects regarding the development, progression, and diagnosis of such tumors. Firstly, it underscores the absence of clinical manifestations, making early detection challenging. Secondly, it points to the lack of screening for KS, which may delay diagnosis and treatment in transplant recipients.

According to the available world literature, no endoscopic techniques for KS removal have been documented. Existing studies primarily focus on observational endoscopy for generalized forms, utilizing gastroscopy and colonoscopy for diagnostic purposes [7]. Cutaneous forms of KS in a kidney recipient have also been reported.

To suppress active vascular proliferation, the immunosuppressive regimen was modified: tacrolimus was discontinued, and everolimus was introduced at a daily dose of 3.5 mg, maintaining blood levels within 4–8 ng/

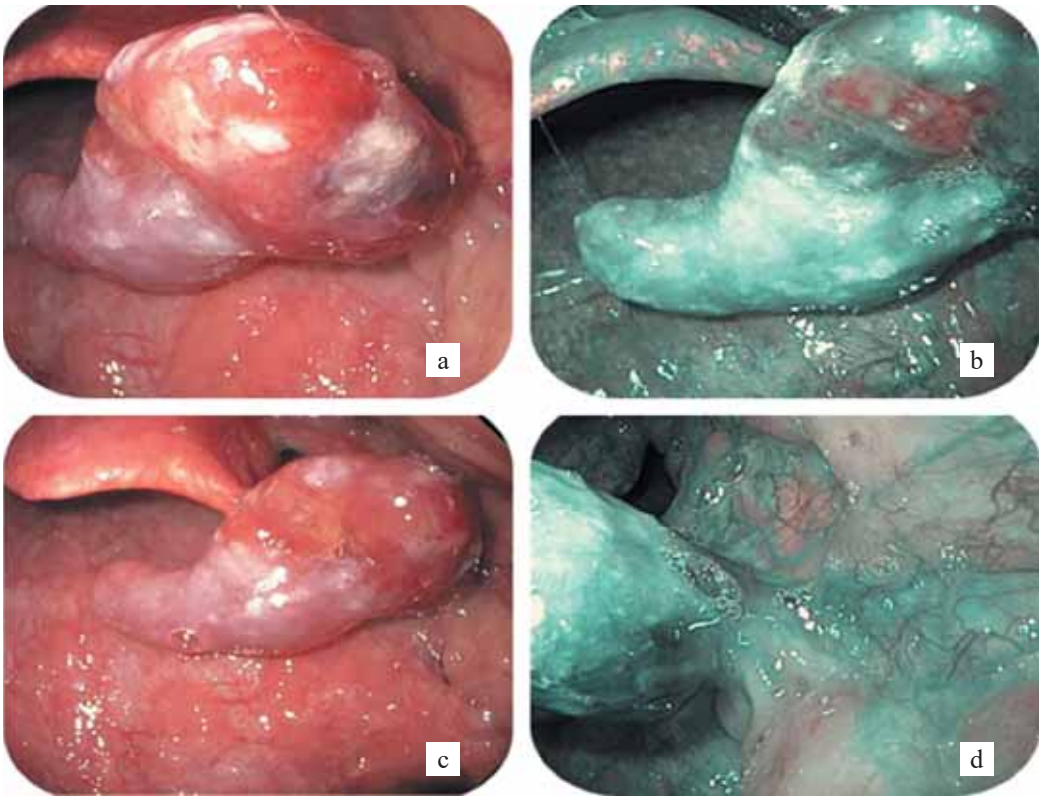

Fig. 1. Kaposi's sarcoma: a, c – white color diagnosis; b, d – narrow band imaging (NBI), visualization of the base area

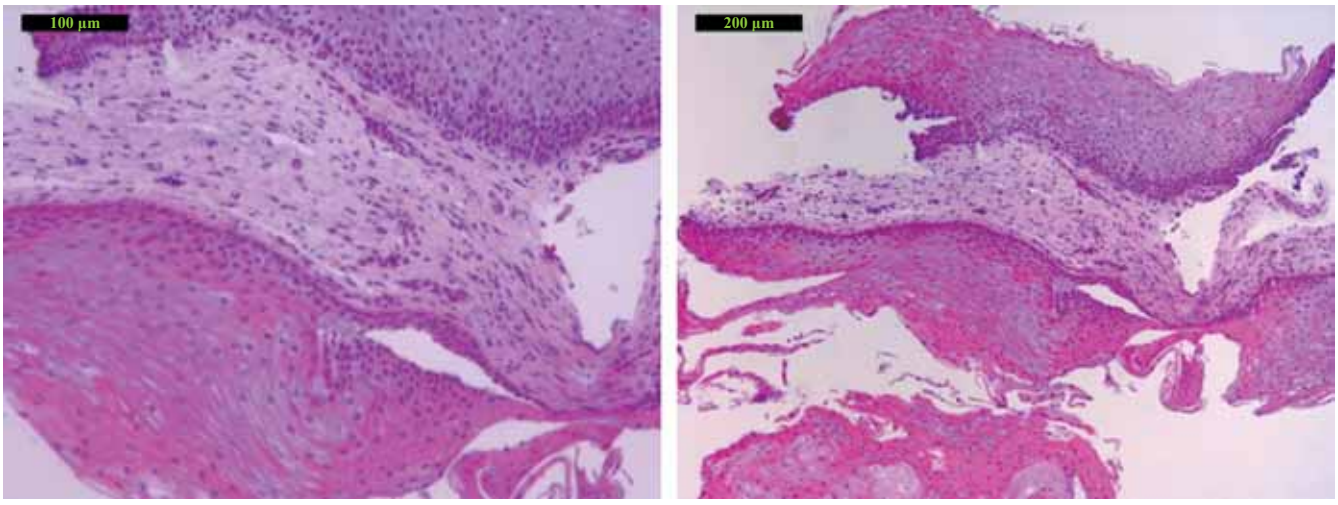

Fig. 2. Histologic picture of Kaposi's sarcoma

mL. However, no positive response was observed. Due to declining graft function, a transplantectomy was performed, and immunosuppressive therapy was discontinued. Chronic hemodialysis was resumed. Following the withdrawal of immunosuppressive therapy, complete regression of KS skin manifestations was achieved [8].

According to the 2020 clinical guidelines for the management of KS, isolated forms of the disease can be treated using electrosurgical methods or local cryotherapy.

In October 2023, the surgical intervention was performed in the operating room under general anesthesia, using a flexible endoscope of the OLYMPUS EXERA III 190 PLUS endoscopic stand, using NBI and DUAL FOCUS modes. KS was removed using ERBE VIO 300D electrosurgical station with ERBE APC2 argon complex in "CUT" and "COAG" modes (Fig. 3). There was no bleeding.

FOLLOW-UP RESULTS

A follow-up diagnostic examination was conducted three months after KS removal, revealing a whitish scar at the excision site (Fig. 4). A biopsy taken from the scar area for histopathological analysis showed no evidence of recurrent KS.

Ten months post-removal, the surgical site was re-evaluated using an OLYMPUS EVIS X1 endoscopic system with a GIF-H290EC endocytoscope, utilizing TXI, NBI, and magnification modes of 100× and 520× (Fig. 5). Staining with an aqueous methylene blue solution was performed, and the absence of dye uptake at the surgical site indicated no pathological epithelial tissue. At the time of writing, the follow-up period exceeded 10 months, with no signs of recurrence.

CONCLUSION

Endoscopic removal of localized KS is a relatively safe and effective treatment option. The use of advanced endoscopic equipment with various optical modes enhances the diagnosis of tumors in solid organ transplant recipients in the late postoperative period. The integration of magnification technology, such as endocytoscopy, provides a real-time method for identifying pathological areas with greater accuracy.

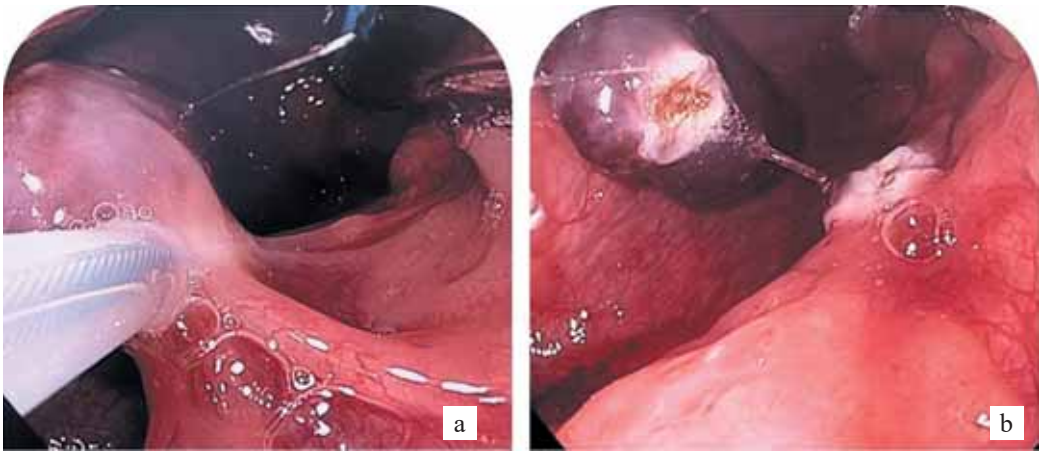

Fig. 3. Stages of Kaposi's sarcoma removal: a, diathermy loop fixed for removal; b, whitish necrosis after removal

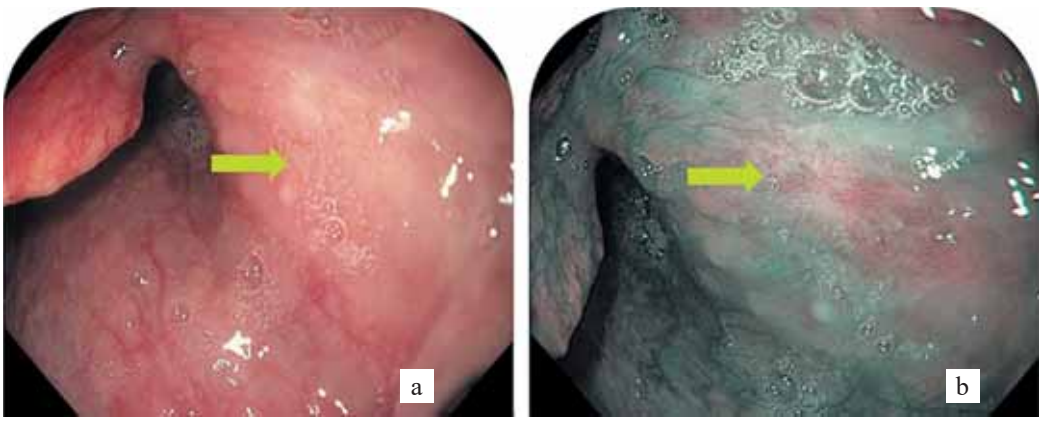

Fig. 4. Kaposi's sarcoma removal area 3 months after surgery: a, white light examination, a whitish scar is clearly visualized; b, narrow-band imaging (NBI) – no evidence of recurrence. The arrow indicates the postoperative scar area

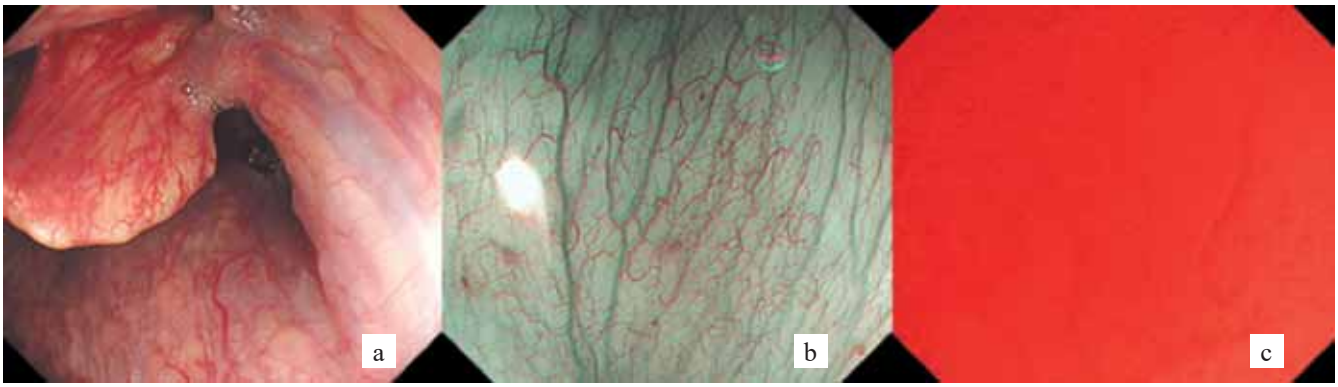

Fig. 5. Kaposi's sarcoma removal area 10 months after surgery: a, examination in TXI mode, scar area; b, examination in narrow-band imaging (NBI) mode at ×100 magnification; c, examination at ×520 magnification – no pathologic cellular structures were detected, no evidence of recurrence

Unlike other transplanted organs, discontinuation of immunosuppressive therapy in heart transplant recipients is fatal. Therefore, endoscopic KS removal may serve as a viable alternative to the standard practice of withdrawing immunosuppressive treatment in transplant patients.

The authors declare no conflict of interest.

REFERENCES

1. www.statista.com [Internet]. Estimated number of organ transplantations worldwide in 2022 [cited October 2023]. Available from: http:// www.statista.com/statistics /398645/global-estimation-of-organ-transplantations.
2. *Munoz P, Alvarez P, de Ory F, Pozo F, Rivera M, Bouza E.* Incidence and clinical characteristics of Kaposi sarcoma after solid organ transplantation in Spain: importance of seroconversion against HHV-8. *Medicine (Baltimore).* 2002; 81 (4): 293–304. doi: 10.1097/00005792-200207000-00005.
3. *Gobitti C, De Vivo F, Franchin G, Minatel E, Innocente R, Trovò MG*. Kaposi's sarcoma in a heart transplant patient. *Acta Oncol*. 1998; 37 (7–8): 769–770. doi: 10.1080/028418698430188.
4. *Esser S, Schöfer H, Hoffmann C, Claßen J, Kreuter A, Leiter U et al.* S1 Guidelines for the Kaposi Sarcoma. *J Dtsch Dermatol Ges.* 2022; 20 (6): 892–904. doi: 10.1111/ddg.14788.
5. *Fu L, Tian T, Wang B, Lu Zh, Gao Y, Sun Y et al.* Global patterns and trends in Kaposi sarcoma incidence: a population-based study. *Lancet Glob Health*. 2023; 11 (10): e1566–e1575. doi: 10.1016/S2214-109X(23)00349-2.
6. *York C, Stratton L, Hodges J, Lei Y, Doran A.* S2598 Gastric Kaposi Sarcoma Presenting as Acute Upper Gastrointestinal Hemorrhage in a Heart Transplant Patient. *The American Journal of Gastroenterology.* 2022; 117 (10S): e1723. doi: 10.14309/01.ajg.0000867032.40405.0a.
7. *Weprin L, Zollinger R, Clausen K, Thomas FB.* Kaposi's sarcoma: endoscopic observations of gastric and colon involvement. *J Clin Gastroenterol*. 1982; 4 (4): 357–360.
8. *Sapozhnikov AD, Perlina AD, Dymkov IN*. Kaposi's sarcoma regression after long term treatment of m-TOR inhibitors and cancellation of immunosuppressive therapy in patient after kidney transplantation. *Russian Journal of Transplantology and Artificial Organs*. 2019; 21 (2): 121–124. (In Russ.). https://doi.org/10.15825/1995-1191-2019-2-121-124.

The article was submitted to the journal on 22.07.2024

DOI: 10.15825/1995-1191-2025-1-55-62

CLINICAL CASE OF LIVER TRANSPLANTATION IN A KIDNEY TRANSPLANT RECIPIENT WITH HEPATOCELLULAR CANCER AND CORONARY ARTERY DISEASE

A.V. Shabunin[1, 2], Z.A. Bagatelia[1, 2], P.A. Drozdov[1, 2], A.G. Komarova[1], S.A. Bliznyuk[1], G.S. Michailyants[2], S.A. Astapovich[1], E.Yu. Astapovich[1], V.A. Tsurkan[1], Yu.I. Mitchenko[1], P.E. Pazenko[3]

[1] Botkin Hospital, Moscow, Russian Federation
[2] Russian Medical Academy of Continuing Professional Education, Moscow, Russian Federation
[3] Sechenov University, Moscow, Russian Federation

Objective: organ transplantation is a highly effective and often the only possible definitive treatment for terminal diseases, significantly improving patient survival and quality of life. However, recipients have a higher risk of developing cardiovascular and oncological diseases, and are susceptible to decompensation of pre-existing diseases. Prevention and treatment of these conditions are becoming critical tasks in transplantology, requiring multidisciplinary collaboration. **Materials and methods.** This article presents a clinical case of the treatment of a patient with stage 5 chronic kidney disease, concomitant cardiologic pathologies and subsequently diagnosed hepatocellular cancer on the background of hepatitis C-related liver cirrhosis. Competent interaction and bridge therapy yielded successful consecutive kidney and liver transplantation with satisfactory outcomes. **Conclusion.** Our treatment experience has shown the effectiveness and necessity of a multidisciplinary approach, early diagnosis, therapy modification during transplantation and further treatment of patients with end-stage multiple organ dysfunction.

Keywords: transplantation, chronic kidney disease, hepatocellular cancer, hemodialysis, bridge therapy.

INTRODUCTION

Transplantation is a highly effective treatment for terminal diseases affecting various organ systems. Kidney transplantation (KT) can double the five-year survival rate of patients with stage 5 chronic kidney disease (CKD) compared to other renal replacement therapies (RRT) while significantly enhancing their quality of life [1–3]. Similarly, liver transplantation (LT) remains the only definitive treatment for many end-stage liver diseases, offering excellent immediate and long-term outcomes with no equally effective alternatives [4, 5]. Just over half a century ago, solid organ transplantation was an experimental field, with only isolated cases of clinical success. However, advancements in science, technology, immunology, genetics, and surgical techniques have transformed transplantation into a standard clinical practice in many transplant centers worldwide. Modern immunosuppressive therapy enables targeted suppression of the alloimmune response without causing severe immunodeficiency. While generally well tolerated by recipients, it is associated with adverse effects [6–8]. Solid organ transplant recipients face an increased risk of cardiovascular disease and cancer and are more susceptible to both the progression of preexisting conditions and the development of new ones. Managing these risks is a critical challenge in modern transplant medicine, requiring a multidisciplinary approach. The presented clinical case underscores the significance of these considerations.

MATERIALS AND METHODS

Patient B., a 65-year-old man, was admitted to the cardiology ward at Botkin Hospital in Moscow on December 20, 2023, with complaints of irregular heart function, general weakness, and recurrent episodes of high blood pressure.

His medical history indicates that he has had arterial hypertension since 2005, with blood pressure reaching 200/100 mmHg. In 2014, he began experiencing leg swelling, progressive weakness, nausea, and vomiting. An outpatient examination revealed an elevated creatinine level of 1300 μmol/L, necessitating hospitalization for urgent medical care. He was diagnosed with stage 5 CKD due to hypertensive arteriolar nephrosclerosis.

In August 2014, an arteriovenous fistula was created, and chronic hemodialysis was initiated. The patient was informed about the irreversible nature of his condition and the advantages of kidney allotransplant over other

Corresponding author: Pavel Drozdov. Address: 15/8, Brusilova str., Moscow, 117148, Russian Federation.
Phone: (962) 985-04-41. E-mail: dc.drozdov@gmail.com

RRTs. Following a comprehensive evaluation, he was placed on the transplant waiting list.

During pre-transplant screening, the patient tested positive for hepatitis C virus (HCV) RNA, though there were no clinical, laboratory, or imaging signs of liver damage.

On November 21, 2015, the patient underwent deceased-donor kidney allotransplantation (DKAT) from a brain-dead donor. The early postoperative period was uneventful, with immediate and satisfactory graft function. The patient was discharged with a creatinine level of 120 μmol/L.

For long-term follow-up, a triple-drug maintenance immunosuppressive regimen was prescribed following the standard protocol: prolonged-release tacrolimus (target concentration 7–10 ng/mL), mycophenolic acid (360 mg twice daily), and methylprednisolone (4 mg once daily). Throughout follow-up, the patient showed no signs of significant kidney graft dysfunction or acute rejection.

The patient's medical history indicates that his blood pressure remained within the target range (130–139/70–79 mmHg) for an extended period while taking amlodipine (5 mg twice daily) and doxazosin (4 mg twice daily). In 2015, coronary angiography was performed as part of the pre-transplant evaluation, revealing no hemodynamically significant coronary artery stenoses.

Post-transplant diabetes mellitus was diagnosed in 2015, and the patient had been on vildagliptin for an extended period. However, due to sustained glycemic control, he discontinued anti-diabetic medication in mid-2023. Given his history of secondary hyperparathyroidism and electrolyte imbalances related to CKD and ongoing immunosuppressive therapy, the patient had also been on long-term supplementation, including calcium (1000 mg/day), potassium (99 mg/day), magnesium (500 mg/day), and vitamin D (10,000 IU every other day).

Given the previously diagnosed dyslipidemia, the patient has been on pitavastatin (4 mg daily) and ezetimibe (10 mg daily) for cardiovascular risk prevention. In 2017, routine outpatient biochemical testing revealed elevated hepatic transaminases (up to 200 U/L) and total bilirubin (56 mmol/L). Liver ultrasound findings were suggestive of cirrhosis, and HCV replication was confirmed in the blood.

Following hepatology consultation, liver function was deemed compensated with hepatoprotective therapy. An infectious disease specialist prescribed antiviral therapy (AVT) with sofosbuvir and daclatasvir. After six months of AVT, a sustained virological response was achieved, with an HCV RNA test on February 1, 2018, confirming viral clearance.

Upon admission, the patient was in a moderate but stable condition and fully conscious. His vital signs were as follows: height 170 cm, weight 70 kg (BMI 24.2 kg/m^2), body temperature 36.7 °C, blood pressure (BP) 142/93 mmHg, and heart rate (HR) 62 beats per minute with a regular pulse. Bilateral pedal edema was noted. Auscultation revealed vesicular breath sounds and clear heart tones.

***Electrocardiogram (ECG) conducted on December 20, 2023**, showed sinus rhythm with a heart rate of 66 beats per minute. There was a marked leftward deviation of the electrical axis, a blockade of the anterior branch of the left bundle branch of His, and a first-degree atrioventricular (AV) block. Additionally, a single atrial extrasystole of the bigeminy type was observed.*

***Echocardiography conducted on December 20, 2023**, revealed preserved global systolic function of the left ventricle (Simpson ejection fraction: 67%) with no local contractility impairments. Concentric left ventricular hypertrophy was observed (interventricular septum: 12 mm, posterior wall: 12 mm, LV mass index: 119 g/m^2). Diastolic dysfunction was noted, following the abnormal relaxation pattern. Valve leaflets appeared thickened, with calcification of the non-coronary aortic valve leaflet. Minor pulmonary, mitral, and tricuspid regurgitation were present. The heart chambers were not dilated, and signs of hypovolemia were noted. Pulmonary artery pressure was within normal limits (systolic pulmonary artery pressure: 28 mmHg). No pericardial or pleural effusion was detected.*

***Daily blood pressure monitoring on December 21, 2023**, revealed persistent systolic-diastolic arterial hypertension throughout the day. The degree of nocturnal BP decrease classified systolic BP as a "nightpeaker" pattern and diastolic BP as a "dipper". The 24-hour average BP values were as follows: mean systolic BP – 156 mmHg, mean diastolic BP – 87 mmHg, and pulse pressure – 69 mmHg (elevated). Given the presence of uncontrolled hypertension, antihypertensive therapy was adjusted as follows: amlodipine was replaced with lercanidipine 20 mg once daily, doxazosin 4 mg twice daily was continued, and valsartan/sacubitril 50 mg twice daily was introduced.*

***Holter ECG monitoring on December 22, 2023**, recorded a predominantly sinus rhythm with an average HR of 54 beats/min (maximum 85 bpm at 13:17, minimum 42 bpm at 06:25). Against this background, 213 polymorphic ventricular extrasystoles (two distinct morphologies) were recorded, including 6 paired and 10 episodes of bigeminy. Additionally, 674 supraventricular extrasystoles were observed, comprising 21 paired and 7 short runs of supraventricular tachycardia (up to 9 complexes), with a maximum HR of 144 beats/min. At 4:17 and 5:22, against the background of persistent first-*

degree AV block (PQ interval up to 0.25 sec), episodes of third-degree AV block were recorded, characterized by idioventricular rhythm lasting up to 5 complexes at a frequency of 40 beats/min with AV dissociation. No diagnostically significant ST segment changes were observed during prolonged pauses. The maximum RR interval was 1.738 sec at 0:22.

***Consultation with an arrhythmologist** determined that there were no current indications for pacemaker implantation. However, it was recommended to conduct a repeat Holter ECG monitoring before any surgical intervention. If extensive surgical treatment is required, the possibility of temporary pacemaker placement should be considered based on indications. No antiarrhythmic therapy was deemed necessary at this time.*

Laboratory findings indicated elevated creatinine (319 μmol/L) and urea (29 mmol/L) levels. Tacrolimus trough level on December 21, 2023, was 10.3 ng/mL. Kidney graft ultrasound on the same date showed no fluid accumulation in the transplant bed and no significant enlargement of the pelvicalyceal system. The kidney graft measured 99×57 mm, with clear and even contours. Doppler ultrasound revealed no signs of stenosis or thrombosis in the renal artery and vein, though cortical blood flow was somewhat reduced. The resistive index at the segmental arteries was 0.9. To determine the cause of graft dysfunction, a biopsy performed on December 21, 2023, confirmed acute tubular necrosis and signs of chronic transplant nephropathy, with no evidence of acute rejection. The findings suggested prerenal acute kidney injury and calcineurin inhibitor nephrotoxicity. Infusion therapy was initiated, and the tacrolimus dose was reduced. By discharge on December 29, 2023, creatinine and urea levels had improved to 146 μmol/L and 13 mmol/L, respectively.

***Lipid profile as of December 20, 2023**, showed total triglycerides at 0.86 mmol/L, HDL at 1.45 mmol/L, LDL at 3.57 mmol/L, and total cholesterol at 5.11 mmol/L. Despite ongoing therapy with pitavastatin 4 mg and ezetimibe 10 mg, LDL cholesterol remained above target levels, necessitating an adjustment in lipid-lowering treatment. Considering the potential for drug interactions in a kidney transplant recipient, inclisiran was identified as the preferred therapeutic option.*

Taking into account the history of post-transplant diabetes mellitus and the increase in fasting glucose levels to 7.9 mmol/L recorded during hospitalization, the patient was evaluated by an endocrinologist. As a result, dapagliflozin therapy at a dose of 10 mg once daily was prescribed, along with recommendations for a balanced diet with restricted intake of fast-digesting carbs.

A hepatology consultation was also conducted regarding liver cirrhosis secondary to chronic hepatitis C. Hepatobiliary ultrasound on December 24, 2023, revealed diffuse liver changes characteristic of cirrhosis, signs of portal hypertension, liver asymmetry due to significant reduction in the left lobe, and a volumetric formation in segments 4–5, raising suspicion of hepatocellular carcinoma (HCC). Additionally, splenomegaly was noted.

An abdominal CT scan with intravenous contrast performed on December 25, 2023, showed a liver of normal size with an uneven, finely bumpy contour and normal density (55–65 HU). In the left lobe of the liver, early contrast enhancement of the portal vein branches was observed, indicative of arteriovenous shunting due to fibrotic changes. An inhomogeneous formation in segment 5 measuring 52×61 mm was identified, showing weak peripheral contrast uptake with washout in the delayed phase. No dilation of intrahepatic or extrahepatic bile ducts was noted. However, portogastric and portosplenal collaterals, as well as esophageal vein dilation, were present. The portal vein measured 19 mm (Fig. 1).

On December 26, 2023, the alpha-fetoprotein (AFP) level was 67.02 ng/mL. Based on the presence of cirrhosis, a characteristic CT appearance, and elevated AFP levels, a diagnosis of hepatocellular carcinoma (HCC) was established. Given the clear radiological and biochemical findings, a puncture biopsy was not indicated.

Laboratory tests on December 26, 2023, revealed an elevated alpha-fetoprotein (AFP) level of 67.02 ng/mL. Based on the presence of cirrhosis, a characteristic CT appearance, and increased AFP levels, HCC of the liver was diagnosed. A puncture biopsy was deemed unnecessary.

Due to the newly detected malignant tumor, an oncological consultation was held, and a PET/CT scan was recommended to assess the presence of distant metas-

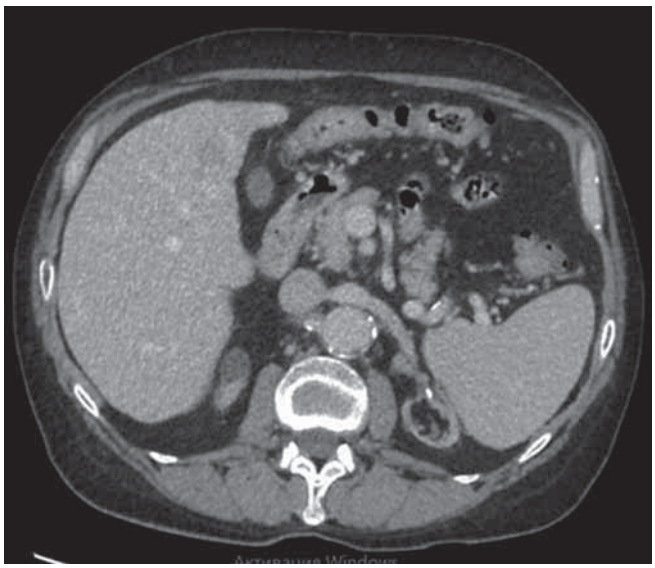

Fig. 1. Contrast-enhanced abdominal CT scan. Signs of liver cirrhosis, hepatocellular carcinoma, portal hypertension

tases. The PET/CT findings confirmed the absence of distant metastases.

According to current treatment guidelines for HCC, surgical intervention is the preferred approach in eligible patients. In cases of compensated liver cirrhosis (Child–Turcotte–Pugh (CTP) class A), both surgical resection and liver transplantation (LT) offer comparable long-term oncological outcomes. However, given the tumor's localization, achieving an R0 resection (complete removal with negative margins) would require extensive liver resection, posing a high risk of complications due to the underlying cirrhosis, potential liver decompensation, and worsening portal hypertension.

Furthermore, the tumor size exceeds the "Milan criteria", which many transplant centers use as a benchmark for LT eligibility [9]. Nevertheless, the Metroticket 2.0 prognostic model estimates a five-year post-LT survival rate of 78.3%, which is considered an acceptable outcome [10]. Additionally, LT is acknowledged as the most suitable radical treatment of HCC for this patient because lifelong de novo immunosuppressive therapy is not required.

The patient was re-hospitalized on January 9, 2024, at Botkin Hospital for evaluation as a candidate for orthotopic liver transplantation (OLT). Comprehensive pre-transplant screening, including esophagogastroduodenoscopy, fibrocolonoscopy, and ultrasound of the lower limb veins, revealed no contraindications to OLT.

Given the patient's age and medical history – including stage 5 CKD, dyslipidemia, post-transplant diabetes mellitus, long-term smoking, arterial hypertension, and prolonged immunosuppressive therapy – a thorough cardiovascular assessment was warranted. A bicycle stress echocardiogram was performed, showing no initial signs of impaired local contractility. The end-diastolic volume was 95 mL, and the ejection fraction was 60%. At peak exercise, arrhythmias were recorded on ECG, including unstable runs of supraventricular tachycardia (up to 6 complexes), ventricular extrasystoles, and one short (3-complex) unstable run of ventricular tachycardia. Following rhythm restoration, two zones of impaired local contractility were identified: hypokinesis of the basal and middle posterolateral segments, which were clinically painless.

Coronary angiography performed on January 1, 2024, revealed hemodynamically significant stenoses: 80% in the middle segment of the anterior descending artery, 70% in the proximal third of the right coronary artery, and a subtotal lesion of the posterior interventricular branch (Fig. 2, a). Based on these findings, the patient was diagnosed with coronary artery disease with painless myocardial ischemia.

Based on coronary angiography and stress echocardiography findings, a decision was made to proceed with percutaneous coronary intervention. Transluminal balloon angioplasty and stenting were performed on the posterior descending artery (PDA) and right coronary artery (RCA) using Promus Premier 2.25×28 mm and Promus Premier 4.0×28 mm stents, respectively, with a favorable angiographic outcome (Fig. 2, b).

To evaluate the functional significance of the atherosclerotic lesion in the anterior descending artery (ADA), another stress echo was conducted, yielding a negative result. No indications for additional revascularization were identified at the time of assessment. The patient was prescribed dual antiplatelet therapy (DAPT) for a minimum of three months.

The prolonged waiting time for transplantation due to coronary artery stenting and the need for DAPT posed a risk of tumor progression and potentially poor oncologic outcomes. Consequently, a decision was made to initiate bridge therapy. Selective transarterial chemoembolization (TACE) was chosen as the preferred method. The procedure was performed on January 16, 2024, using

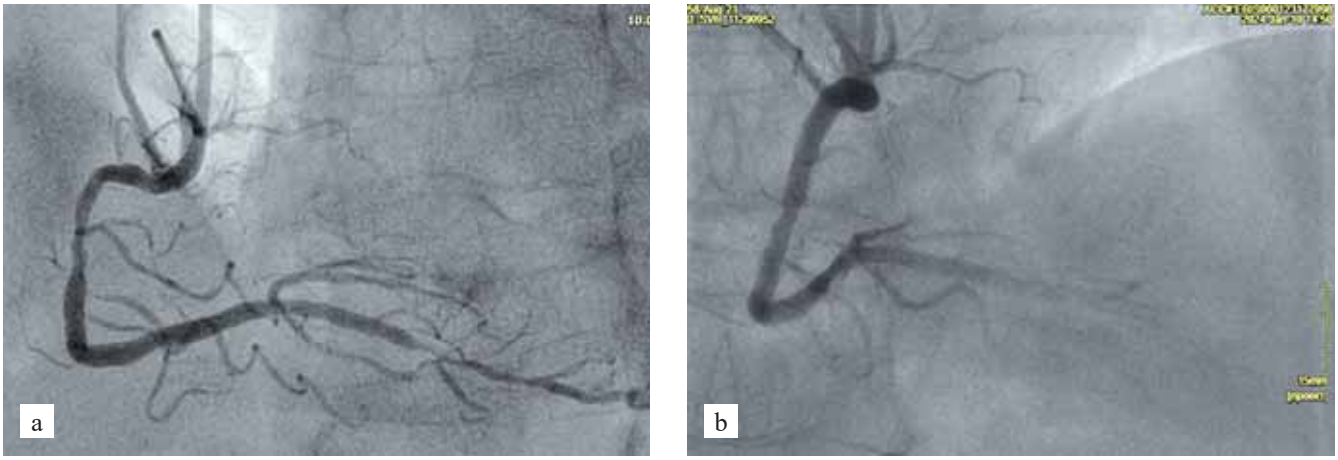

Fig. 2. Coronary angiogram: a, multilevel stenoses of RCA, PDA and ADA are detected; b, Promus Premier 2.25×28 mm and Promus Premier 4.0×28 mm coronary stents were positioned and implanted in the area of PDA and RCA stenoses

DC Bead microspheres (100–300 microns) loaded with doxorubicin (50 mg) to target the liver tumor. The angiographic findings are presented in Fig. 3.

Three months after undergoing percutaneous coronary intervention, the patient was placed on the active LT waiting list. A multidisciplinary consultation with a cardiologist, transplantologist, nephrologist, and hepatologist was conducted, leading to adjustments in the immunosuppressive therapy regimen, including the withdrawal of mycophenolic acid preparations in preparation for extensive surgery. Kidney transplant function was satisfactory.

Fig. 3. Selective transarterial chemoembolization of liver tumor

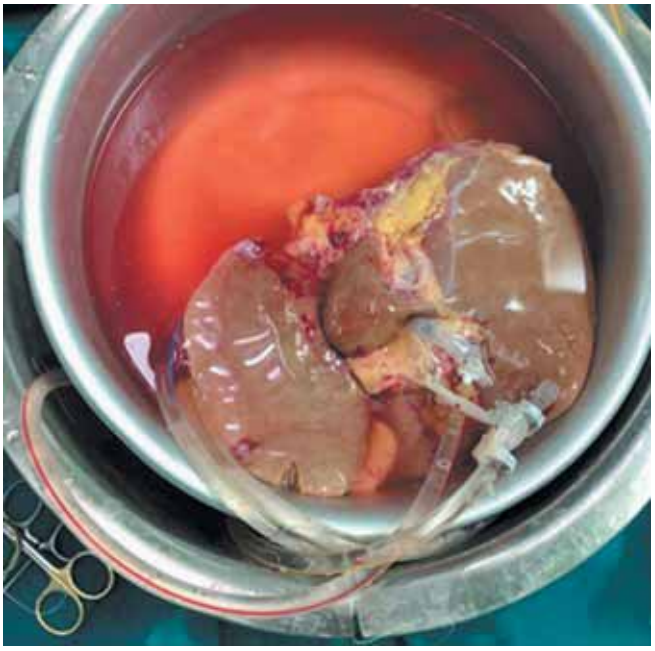

Fig. 4. Dual hypothermic oxygenated machine perfusion (DHOPE)

LIVER TRANSPLANTATION

On May 18, 2024, the transplant ward was notified of a potential brain-dead donor. The donor was a 66-year-old man, 180 cm tall and weighing 92 kg, who had died from acute ischemic stroke. Laboratory parameters, including aspartate transaminase (AST), alanine transaminase (ALT), total bilirubin, creatinine, and urea levels, were within normal limits. The donor had been on mechanical ventilation for 72 hours.

During visual assessment at multi-organ retrieval, the liver appeared medium-sized, with a smooth, shiny surface and a yellowish trace upon palpation. Its consistency was dense and elastic, and vascular anatomy was standard (Michel's type I). Instant histopathology revealed macrovesicular steatosis of 40–50%. The organ was deemed suitable for transplantation and was immediately offered to the patient (Fig. 4).

Given the donor's classification as suboptimal and the borderline characteristics of the liver graft, indications were established for dual hypothermic oxygenated perfusion (DHOPE) using a heart-lung machine upon organ delivery to the transplant ward's operating room. The total cold ischemia time was 5 hours and 13 minutes, with the final 2 hours and 10 minutes dedicated to DHOPE. Perfusate AST and ALT levels at 30 minutes of perfusion were 934 U/L and 523 U/L, respectively.

During surgical planning, it was evident that complete inferior vena cava (IVC) clamping, as required in the classical OLT technique, could cause significant hemodynamic instability in a patient with a complex cardiac history. To mitigate this risk, a decision was made to perform hepatectomy while preserving the IVC, followed by caval reconstruction using the Belghiti technique (Fig. 5).

Hepatectomy was performed without technical difficulties. The graft was placed into the surgical field, and

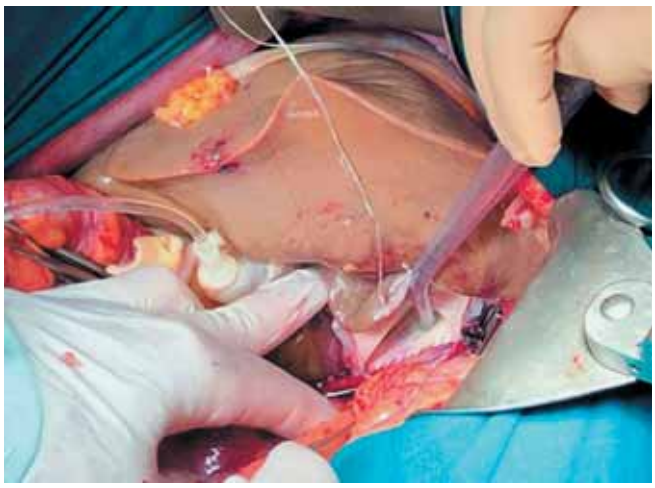

Fig. 5. Liver transplantation: caval reconstruction using the Belghiti technique

sequential anastomoses of the IVC and portal vein were completed. Following an intravenous injection of methylprednisolone 500 mg, reperfusion was initiated. The liver rapidly turned cherry-colored and exhibited satisfactory turgor, with no signs of postreperfusion syndrome.

Arterial reconstruction was performed using an end-to-end technique with ligation of the gastroduodenal artery. Biliary reconstruction was completed via end-to-end choledochoduodenostomy with interrupted PDS 6-0 sutures. The surgery lasted 5 hours and 38 minutes, with a total blood loss of 900 mL. The early postoperative period was uneventful, and the patient stayed in the intensive care unit for 48 hours. Peak AST and ALT levels reached 1232 U/L and 1923 U/L, respectively, indicating a moderate degree of ischemia-reperfusion injury. No signs of early graft dysfunction were observed. Immunosuppressive therapy followed a standard protocol, with basiliximab induction and reintroduction of prolonged-release tacrolimus from postoperative day 3. The total hospital stay was 13 days, with both grafts functioning satisfactorily.

Three weeks after wound healing, mTOR inhibitor everolimus was introduced into the immunosuppressive regimen, maintaining a target level of 4–6 ng/mL, while the tacrolimus target level was reduced to 3–5 ng/mL. Oral methylprednisolone therapy was continued at 4 mg once daily.

RESULTS

At 3-month follow-up, the patient remained in stable and satisfactory condition with no complaints. Despite prior interventions and a complex comorbid background, he maintains an active lifestyle. Liver and kidney transplant functions were stable, with a creatinine level of 120 μmol/L and an AFP level of 4 ng/mL. A contrast-enhanced abdominal CT scan revealed no signs of recurrent HCC.

DISCUSSION

This clinical case illustrates the complex medical journey of a patient whose prognosis would have been extremely poor without comprehensive and well-coordinated care. Long-standing uncontrolled hypertension led to nephroangiosclerosis and, ultimately, end-stage CKD. KT was the optimal treatment, allowing the patient to regain a high quality of life for over eight years – an outcome unlikely to be achieved with chronic hemodialysis.

However, prolonged immunosuppressive therapy, despite adequate prophylaxis, contributed to the development of obstructive coronary artery disease (CAD), diabetes mellitus, and the progression of chronic hepatitis C to cirrhosis and HCC. During hospitalization for cardiovascular pathology, the patient required a multidisciplinary care from at least seven specialists, including a cardiologist, transplant surgeon, hepatologist, nephrologist, endocrinologist, oncologist, and interventional radiologist. These specialists not only managed existing conditions but also diagnosed two additional life-threatening diseases: multivessel CAD with hemodynamically significant stenoses and a malignant liver tumor.

LT was identified as the optimal treatment for cirrhosis and HCC, but proceeding without prior correction of obstructive CAD would have posed a high risk of cardiovascular complications. The use of minimally invasive percutaneous coronary intervention provided effective treatment and rapid rehabilitation. Moreover, bridge therapy with TACE controlled tumor progression, allowing LT to be performed within acceptable criteria and ensuring favorable overall and recurrence-free survival.

Solid organ recipients face a heightened risk of specific complications, stemming both from their underlying disease and the long-term immunosuppressive regimen. In response, the global trend is shifting toward integrating transplant programs within multidisciplinary hospitals, where patients can receive comprehensive, specialized care across multiple medical disciplines simultaneously [11].

Organ transplantation is no longer confined to isolated, highly specialized institutions; it has evolved into a high-tech yet accessible therapeutic option for patients. However, availability of transplant care remains closely tied to efficient organization of organ donation processes and adoption of advanced technologies that maximize the viability of each organ. In this case, the use of cold oxygenated perfusion played a crucial role in reducing the risk of early graft dysfunction and primary non-function, ensuring the successful transplantation of an organ from a suboptimal donor.

CONCLUSION

Transplantation is a highly effective treatment for end-stage diseases of various organ systems. However, solid organ transplant recipients face an elevated risk of complications due to both the underlying disease that necessitated the transplant and the lifelong need for immunosuppressive medications. Prevention and management of these complications represent a primary challenge that requires a coordinated effort from a multidisciplinary team of specialists.

The authors declare no conflict of interest.

REFERENCES

1. *Abecassis M, Bartlett ST, Collins AJ, Davis CL, Delmonico FL, Friedewald JJ et al.* Kidney transplantation as primary therapy for end-stage renal disease: a National Kidney Foundation/Kidney Disease Outcomes Quality Initiative (NKF/KDOQI™) conference. *Clin J*

Am Soc Nephrol. 2008; 3 (2): 471–480. doi: 10.2215/CJN.05021107.
2. United States Renal Data System. 2021 USRDS annual data report: epidemiology of kidney disease in the United States. https://www.usrds.org/adr.aspx.2021.
3. *Andrusev AM, Tomilina NA, Peregudova NG, Shinkarev MB*. Kidney replacement therapy for end Stage Kidney Disease in Russian Federation, 2015–2019. Russian National Kidney Replacement Therapy Registry Report of Russian Public Organization of Nephrologists «Russian Dialysis Society». *Nephrology and Dialysis*. 2021; 23 (3): 255–329. [In Russ, English abstract]. doi: 10.28996/2618-9801-2021-3-255-329.
4. *Müller PC, Kabacam G, Vibert E, Germani G, Petrowsky H*. Current status of liver transplantation in Europe. *Int J Surg*. 2020; 82S: 22–29. PMID: 32454252. doi: 10.1016/j.ijsu.2020.05.062.
5. *Hughes CB, Humar A*. Liver transplantation: current and future. *Abdom Radiol (NY)*. 2021; 46 (1): 2–8.
6. *Kasiske BL, Zeier MG, Chapman JR, Craig JC, Ekberg H, Garvey CA et al.* KDIGO clinical practice guideline for the care of kidney transplant recipients: a summary. *Kidney Int.* 2010; 77 (4): 299–311. PMID: 19847156. doi: 10.1038/ki.2009.377.
7. *Yu M, Liu M, Zhang W, Ming Y*. Pharmacokinetics, pharmacodynamics and pharmacogenetics of tacrolimus in kidney transplantation. *Curr Drug Metab.* 2018; 19 (6): 513–522. doi: 13892002196661801291519 48.
8. *Parlakpinar H, Gunata M*. Transplantation and immunosuppression: a review of novel transplant-related immunosuppressant drugs. *Immunopharmacol Immunotoxicol*. 2021; 43 (6): 651–665. doi: 10.1080/08923973.2021.1966033.
9. *Mazzaferro V, Bhoori S, Sposito C, Bongini M, Langer M, Miceli R, Mariani L*. Milan criteria in liver transplantation for hepatocellular carcinoma: an evidence-based analysis of 15 years of experience. *Liver Transpl*. 2011; 17 (S2): S44–S57. doi: 10.1002/lt.22365.
10. *Cucchetti A, Serenari M, Sposito C, Di Sandro S, Mosconi C, Vicentin I et al.* Including mRECIST in the Metroticket 2.0 criteria improves prediction of hepatocellular carcinoma-related death after liver transplant. *J Hepatol*. 2020; 73 (2): 342–348. doi: 10.1016/j.jhep.2020.03.018.
11. *Bagatelia ZA, Dukhanina IV*. Analiz hirurgicheskoj pomoshchi bol'nym s zabolevanijami organov brjushnoj polosti. *Vrach-aspirant*. 2015; 69 (2.2): 208–212.

The article was submitted to the journal on 28.08.2024

DOI: 10.15825/1995-1191-2025-1-63-73

RENAL TRANSPLANT PATHOLOGY AND FACTORS DETERMINING THE RATE OF ITS PROGRESSION

E.S. Stolyarevich[1–3], E.T. Egorova[1], N.P. Mozheiko[1], D.A. Saydulaev[1]

[1] Shumakov National Medical Research Center of Transplantology and Artificial Organs, Moscow, Russian Federation

[2] Municipal Clinical Hospital No. 52, Moscow, Russian Federation

[3] Moscow State University of Medicine and Dentistry, Moscow, Russian Federation

The structure of allograft dysfunction is heterogeneous, and the peculiarities of its course depend on the underlying pathological process as well as other factors that influence how quickly it progresses. The most significant of these factors are the prevalence of interstitial fibrosis and tubular atrophy. **Objective:** to evaluate the factors influencing the rate of nephropathy progression depending on the nature of dysfunction. **Materials and methods.** The study included 189 kidney transplant recipients with morphologically verified renal graft dysfunction. Patients were divided into five categories based on their morphological pictures: Group 1, acute tubular necrosis (ATN) (n = 20); Group 2, cellular rejection (CR) (n = 50); Group 3, antibody-mediated rejection (AMR) (n = 61); Group 4, interstitial fibrosis and tubular atrophy (IFTA) (n = 41); Group 5, recurrent or *de novo* glomerulonephritis (GN) (n = 17). **Results.** Even though graft function tended to improve with treatment, The CR and AMR groups had the lowest long-term graft survival rates at 12 months, amounting to 64% and 54%, respectively, while the IFTA and GN groups had the highest, 79% and 86%, respectively. ATN patients (94%) showed the best 1-year survival. In the multivariate analysis performed in the Cox regression model, only two factors – creatinine level at the time of biopsy and IFTA prevalence – were found to be independent predictors of prognosis, regardless of the underlying mechanism of injury. A prognostic model that incorporates both characteristics demonstrated significantly higher prognostic accuracy. A combination of creatinine level ≥200 μmol/L and an interstitial fibrosis prevalence ≥20% of the parenchyma area showed the strongest correlation with prognosis. This model had a 91% sensitivity and a 28% specificity ($p < 0.01$ 95% CI: 0.74–0.89). **Conclusion.** When assessing the risk of graft loss, it is necessary to consider the entire set of potential prognostic factors, such as the nature of the underlying disease, severity of graft dysfunction and prevalence of background interstitial fibrosis.

Keywords: kidney transplantation, renal graft pathology, graft survival, risk factors for graft loss.

INTRODUCTION

Allograft dysfunction is heterogeneous in its structure, and its development is determined by a number of factors, the severity of which can vary significantly depending on the immunosuppressive therapy (IST) used and the course of the postoperative period. Thus, in the pre-cyclosporine era, acute graft rejection was considered the main cause of dysfunction. The widespread use of calcineurin inhibitors as basic immunosuppressants has significantly reduced acute rejection rates and severity of acute rejection and, consequently, has increased in the relative proportion of pathology unrelated to immune response activation in the structure of late kidney transplant (KT) dysfunction. However, the results of the DeKAF study, a multicenter study of the causes of late graft dysfunction have again forced us to talk about the decisive significance of rejection for the long-term fate of the graft. This study found that more than half of all patients with late graft dysfunction exhibited signs of acute or chronic rejection, with 57% showing evidence of activation of humoral immune response (donor-specific antibodies (DSA) or C4d complement fragment deposition in peritubular capillaries) [1–4].

Subsequent studies confirm the ideas about antibody-mediated rejection (AMR) as the main cause of graft loss. Nevertheless, some of its variants are characterized by a long subclinical course or slowly progressive dysfunction [5–7]. Thus, identifying factors associated with poor prognosis in AMR remains a pressing issue.

The role of cell-mediated rejection in the development of irreversible graft dysfunction is less pronounced, as it typically occurs early after KT, is often responsive to corticosteroid therapy, and has a limited impact on long-term graft survival [8, 9]. Nevertheless, there are works indicating that even being reversible, cellular rejection (CR) can initiate processes that subsequently lead to graft loss [10–12]. In particular, the role of CR as a trigger for DSA synthesis and as a factor having a

Corresponding author: Ekaterina Stolyarevich. Address: 1, Shchukinskaya str., Moscow, 123182, Russian Federation. Phone: (499) 196-17-94. E-mail: Stolyarevich@yandex.ru

negative effect on the rate of AMR progression has been demonstrated [13].

It is widely recognized that interstitial fibrosis resulting from non-immune causes progresses slowly over an extended period. It remains clinically silent until it reaches a critical threshold, at which point it manifests as progressive graft dysfunction, eventually leading to end-stage renal disease (ESRD). However, the rate of progression of nephrosclerosis can vary widely depending on the cause of nephrosclerosis and signs of persistent activity of the underlying process, as well as individual characteristics of the patient.

One of the main causes of interstitial fibrosis and tubular atrophy (IFTA) is rejection [15–17]. Shimizu et al. examined the characteristics of fibrosis in renal transplants and identified signs of acute or chronic rejection in 34% of cases. Conversely, according to Lefaucheur, 61% of patients who experienced CR show infiltration in areas of sclerosis and tubulitis in atrophic tubules in subsequent biopsies (i-IFTA). The 2017 Banff classification categorized these changes as chronic cellular graft rejection. However, in later stages, persistent interstitial inflammation in the presence of interstitial fibrosis no longer meets the CR criteria [18], yet it can still accelerate the progression of nephrosclerosis.

A strong correlation has been established between *de novo* DSA production and subsequent sclerosis formation in the context of AMR [19]. Conversely, IFTA presence at the time of AMR diagnosis is the most significant predictor of further disease progression [20].

Most studies examining the morphological patterns of KT dysfunction have focused on a single primary cause of graft dysfunction, and, consequently, its long-term loss. Nevertheless, it is well established that in the late post-transplant period, graft pathology often results from the cumulative impact of multiple damaging factors over time. According to Van Loon, 25% of biopsies revealed the presence of two or more coexisting pathologies, each potentially contributing to graft dysfunction. At the same time, 33% of biopsies showed signs of both acute and chronic process [21]. Thus, IFTA prevalence and glomerulosclerosis may be both a consequence of the underlying pathological process and the background on which this process developed.

In the work of Naesens et al., it was shown that not only the nature of the underlying pathological process, but also the severity of the background nonspecific graft injury determine its further fate [22–24]. The prognostic influence of nonspecific interstitial fibrosis was also demonstrated according to the protocol biopsy data [25]. In addition to the severity of nephrosclerosis, the extent of graft injury at the onset of the pathological process also holds prognostic significance. Traditionally, this is evaluated using serum creatinine levels at the time of biopsy, which many studies have identified as a key predictor of KT loss [26–30]. Other research has assessed injury severity through molecular profiling, specifically by analyzing injury-repair response-associated transcripts (IRRATs) [31–34]. Moreover, in the early post-transplant period, this indicator correlated with the severity of acute tubular necrosis (ATN) but had no significant impact on long-term graft survival [33]. However, in later stages, particularly in the presence of AMR or other specific causes, it served as a predictor of accelerated disease progression [20, 24, 34].

Thus, progression of renal graft dysfunction, leading to nephrosclerosis, is influenced by various damaging factors, which, with increasing prevalence, becomes the main cause of graft loss.

MATERIALS AND METHODS

The retrospective study included 189 KT recipients with morphologically verified allograft dysfunction, who were monitored at Shumakov National Medical Research Center of Transplantology and Artificial Organs in Moscow. Graft biopsy was performed within 2 days to 25 years from the time of KT (median 24.6 months). Recipient mean age was 37.3 ± 15.2 years. Male/female ratio was 54/46. Most recipients received triple-drug IST including tacrolimus (178 patients) or cyclosporine (11 patients) in combination with corticosteroids and mycophenolate.

In all patients, the indication for biopsy was allograft dysfunction, characterized by increased serum creatinine levels (averaging 287.1 ± 218.9 μmol/L), either in isolation or in combination with proteinuria.

Morphological examination of biopsy specimens included light microscopy on 3–4 μm thick sections, stained with hematoxylin and eosin, Masson's trichrome, and Schiff's reagent. Immunofluorescence analysis was conducted on 4 μm frozen sections using monoclonal FITC-labeled antibodies targeting IgG, IgM, IgA, and complement component C3 (DAKO, Denmark). C4d detection was performed on frozen sections by indirect immunofluorescence, using FITC-labeled monoclonal antibodies specific to the C4d complement fragment (Quidel Corporation, San Diego, CA). Morphological diagnosis was established according to the Banff classification.

In statistical data processing, variables with a normal distribution were expressed as mean ± standard deviation ($X \pm \sigma$). For variables that did not follow a normal distribution, the median and interquartile range were calculated. Differences in means for normally distributed variables were assessed using the Student's t-test, while the Mann–Whitney U test and Kruskal–Wallis test were applied to variables that did not follow a normal distribution. Results were considered statistically significant at $p < 0.05$. Actuarial survival was analyzed using the

Kaplan–Meier method. Data processing was conducted with the SPSS statistical software package.

RESULTS

Depending on the features of morphological picture and the main mechanism of nephropathy progression, five groups of patients were identified. Group 1 included 20 patients with acute tubular epithelial injury and morphological picture of ATN. Group 2 featured 50 patients with CR. Most of them were cases of acute (n = 21) and chronic (n = 5) cellular interstitial graft rejection, 19 patients had borderline changes, 5 experienced acute vascular cellular graft rejection. Group 3 consisted of 61 patients with acute (n = 34) or chronic (n = 27) AMR. In 13 of them, there were also signs of activation of cellular immune response (mixed-type rejection). Group 4 included 41 IFTA cases without signs of immune response activation. Group 5 included 17 patients with recurrent or *de novo* GN, in most cases represented by IgA nephropathy (n = 12) and focal segmental glomerulosclerosis (n = 3) (Fig. 1).

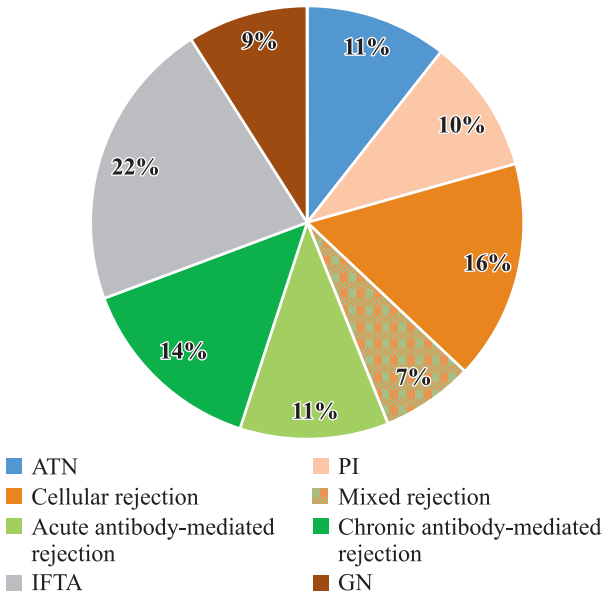

Fig. 1. Distribution of histological diagnosis of late allograft dysfunction. ATN, acute tubular necrosis; IFTA, interstitial fibrosis and tubular atrophy; BC, borderline changes; GN, glomerulonephritis

Patients across the groups showed no significant differences in terms of sex, age, or severity of dysfunction. However, in the ATN group, the time after KT was the shortest, while dysfunction severity was the highest compared to all other groups.

Excluding ATN patients, the severity of azotemia at the time of biopsy did not differ significantly between groups. Tacrolimus levels were highest in ATN patients ($p < 0.05$ compared to all other groups), whereas differences in tacrolimus levels between the remaining groups did not reach statistical significance (Table 1, Fig. 2).

When assessing the morphological findings IFTA prevalence and glomerulosclerosis severity were analyzed separately from the characteristic manifestations of each selected nosological category. This distinction was made because nephrosclerosis in a renal graft can arise from multiple injurious processes acting on the graft from the time of transplantation to the time of biopsy.

The prevalence of IFTA and glomerulosclerosis was minimal in the ATN group ($p < 0.001$ than in all other groups) and maximal in nonspecific nephrosclerosis of non-immune nature ($p < 0.05$ compared to all other groups) (Fig. 3).

The subsequent trajectory of graft function varied depending on the underlying mechanism of injury. For instance, in ATN patients, creatinine levels significantly decreased as ischemia-reperfusion injury resolved. CR and AMR patients also exhibited improved graft function following targeted treatment. Meanwhile, in patients with nonspecific nephrosclerosis and glomerular pathology, graft function remained stable throughout the follow-up period (Fig. 4).

However, despite the tendency for graft function to improve with treatment, long-term graft survival was lowest in the AMR group, with a 45% survival rate at 3 years. In contrast, graft survival was 75% in the CR group, 70% in the IFTA group, and 83% in the GN group. The best 1-year survival rate was observed in ATN patients, reaching 94% (Fig. 5).

In order to identify factors associated with accelerated progression of dysfunction, a comparative analysis of

Table 1

Clinical, laboratory and demographic data of patients included in the study

Group		n	Male	Age (years)	Duration (months)	Baseline creatinine	End creatinine	Tac level
1	ATN	20	61%	35.4	0.95	488.2	236.6	8.3
2	CR	50	59%	35.0	12.6	186.0	160.1	7.6
3	AMR	61	49%	40.3	32.9	247.0	173.0	5.6
4	IFTA	41	51%	44.3	39.1	184.0	177.0	7.9
5	GN	17	67%	38.0	70.3	184.8	196.1	6.0

Note: Tac, tacrolimus; ATN, acute tubular necrosis; CR, cellular rejection; AMR, antibody-mediated rejection; IFTA, interstitial fibrosis and tubular atrophy; GN, glomerulonephritis.

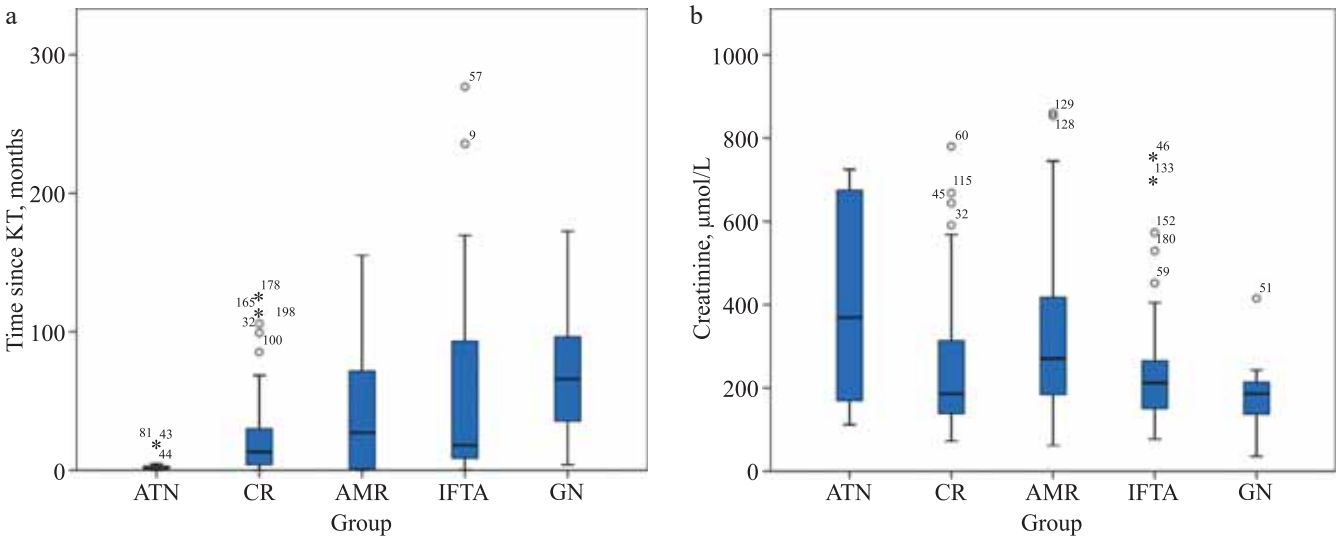

Fig. 2. Differences in the timing of dysfunction (a) and baseline creatinine level at the time of biopsy (b) according to histological diagnosis. Hereinafter in the Figs.: ATN, acute tubular necrosis; CR, cellular rejection; AMR, antibody-mediated rejection; IFTA, interstitial fibrosis and tubular atrophy; GN, glomerulonephritis

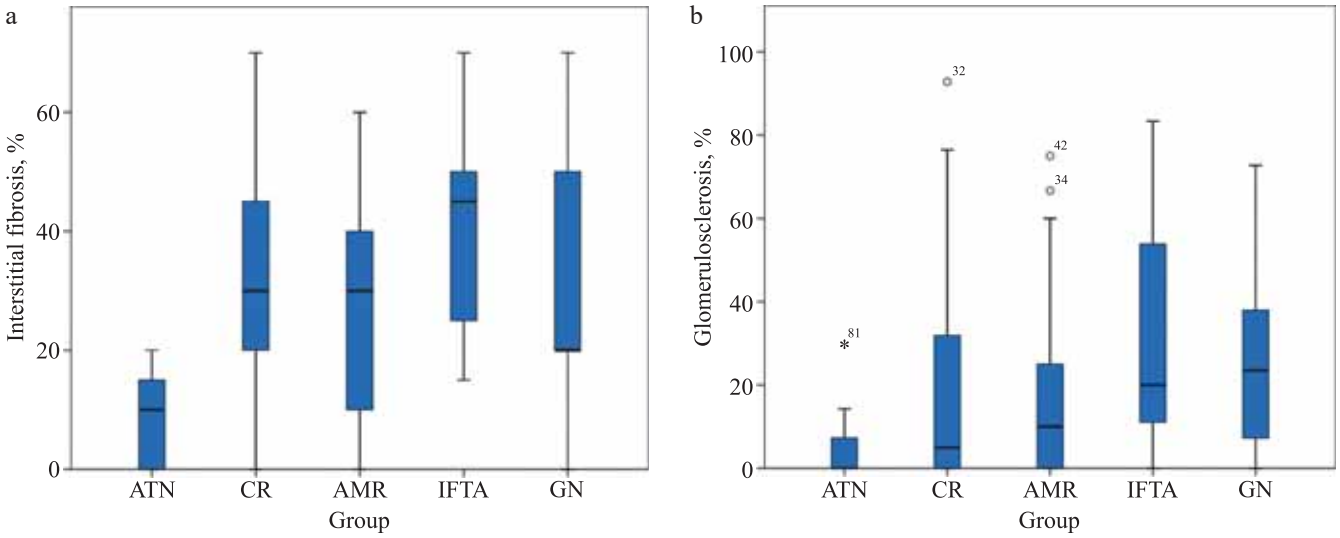

Fig. 3. Severity of interstitial fibrosis (a) and glomerulosclerosis (b) at the time of biopsy

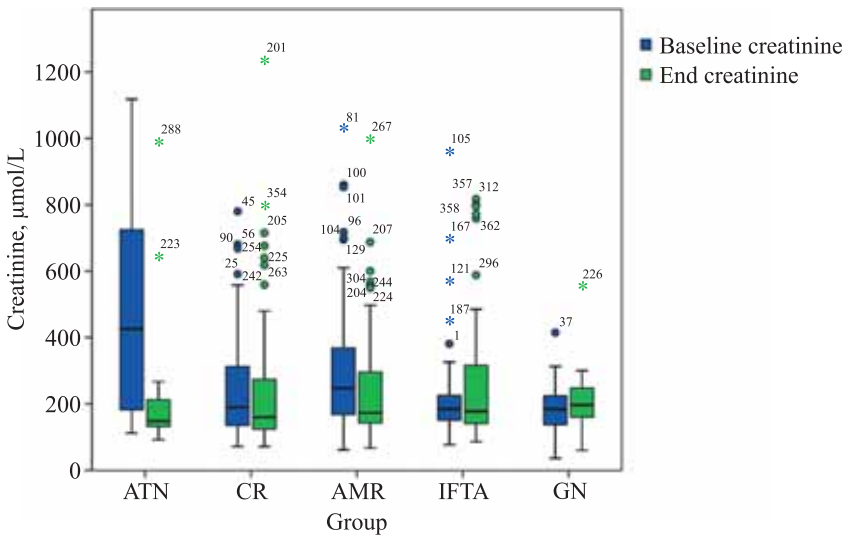

Fig. 4. Changes in graft function during treatment

clinical, demographic, laboratory, and morphological characteristics was performed in patients with relapsed ESRD and with a functioning graft (Table 2).

In a multivariate analysis performed in a Cox regression model, only two factors – creatinine level at the time of biopsy and IFTA prevalence – were found to be independent predictors of prognosis, regardless of the underlying mechanism of injury (Table 3).

Moreover, no correlation was found between the severity of azotemia at the time of biopsy and the prevalence of interstitial fibrosis. Additionally, the nature of this relationship varied depending on the underlying mechanism of injury, demonstrating a multidirectional pattern across different patient groups (Fig. 6).

So, in ATN and AMR, there was an inverse relationship between creatinine levels and severity of interstitial fibrosis. Conversely, in other mechanisms of injury,

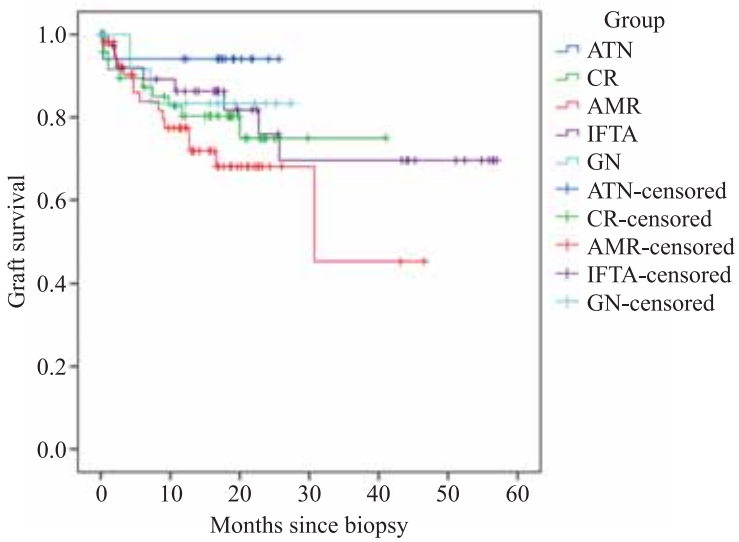

Fig. 5. Death-censored graft survival depending on the cause of dysfunction

Table 2

Clinical, laboratory and morphological features in patients with stabilized graft function and relapse of ESRD

	Age	Time since KT	Baseline creatinine	Tac level	IFTA	Glomerulosclerosis
Preserved function	37.1 ± 15.4	42.8 ± 51.7	262 ± 216.4	9.39 ± 17.6	27.5 ± 18.1	19.0 ± 21.8
Relapse of ESRD	88.7 ± 15.8	45.9 ± 60	427.6 ± 211.5	7.89 ± 10.5	40.6 ± 19.7	27.9 ± 25.3
p	0.54	0.76	<0.001	0.66	<0.001	0.05

Note: ESRD, end-stage renal disease; KT, kidney transplant; Tac, tacrolimus; IFTA, interstitial fibrosis and tubular atrophy.

Table 3

Risk factors for graft loss (multivariate Cox regression model)

	B	SE	Wald	df	Sig.	Exp(B)
Duration (months)	0,006	0,005	1,696	1	0,193	1,006
Age (years)	0,018	0,018	0,968	1	0,325	1,018
Tac level (ng/mL)	–0,304	0,094	10,461	1	0,001	0,738
Creatinine (μmol/L)	0,007	0,001	29,648	1	0,000	1,007
IFTA (%)	0,058	0,017	11,355	1	0,001	1,060
Glomerulosclerosis (%)	–0,005	0,010	0,263	1	0,608	0,995
Group 1 (reference)			3,016	4	0,555	
Group 2	0,323	0,964	0,112	1	0,738	10,381
Group 3	0,005	0,875	0,000	1	0,995	10,005
Group 4	–0,972	1,221	0,633	1	0,426	0,378
Group 5	–0,615	1,401	0,193	1	0,661	0,541

Note: KT, kidney transplant; Tac, tacrolimus; IFTA, interstitial fibrosis and tubular atrophy.

dysfunction severity correlated with interstitial fibrosis prevalence, though a statistically significant association ($R^2 = 0.545$, $p < 0.01$) was only found in the GN group.

Overall, graft survival differed significantly depending on severity of interstitial fibrosis at the time of biopsy, being 95.3%, 72.5% and 54.2%, with a prevalence of <25%, 25–50% and >50% respectively ($p < 0.01$). A similar trend was observed for dysfunction severity at biopsy, with survival rates of 97% 69% and 34% for creatinine levels <200 μmol/L, 200–300 μmol/L, and >300 μmol/L, respectively (Fig. 7).

ROC analysis was conducted to evaluate the prognostic significance of creatinine levels and interstitial fibrosis prevalence in predicting graft loss probability (Fig. 8). The resulting ROC curve indicates that both markers demonstrate strong predictive reliability, as reflected by the area under the curves (Table 4).

In order to predict graft loss probability on the basis of these parameters, the predictive value of several potential models including these parameters was analyzed.

Model 1: Pcr >150 IFTA >20 (AUC = 0.46).

Model 2: Pcr >200 IFTA >20 (AUC = 0.814).

Model 3: Pcr >200 IFTA >25 (AUC = 0.8).

Model 4: Pcr >300 IFTA >25 (AUC = 0.72).

Model 1 demonstrated the highest predictive value, with 91% sensitivity and 28% specificity ($p < 0.01$, 95% CI: 0.74–0.89). Based on the findings, a combination of azotemia >200 μmol/L at onset and IFTA prevalence >20% is considered prognostically unfavorable for renal graft survival.

DISCUSSION

In this study, as in the DeKAF study and numerous other investigations, AMR patients had the worst prognosis. However, the long-term prognosis for CR patients was only slightly better. Despite initial improvements with treatment, 14% of CR patients experienced a progressive decline in graft function, ultimately leading to recurrent ESRD in 10% of cases. These findings align with the understanding of CR as a trigger for other pathological processes, including the accelerated progression of interstitial fibrosis. Similar results were reported by Lefaucheur et al., who observed a high prevalence of persistent infiltration in sclerotic areas, persisting in 61% of patients post-CR. This persistent inflammation contributed to a reduced long-term graft survival rate of 70.8%, compared to 83.5% in patients without ongoing interstitial inflammation [15].

IFTA prevalence and glomerulosclerosis can serve both as consequences of the underlying pathological process and as pre-existing conditions that contribute to its development. Naesens et al. demonstrated that not only the nature of the primary pathological process but also the severity of background nonspecific graft inju-

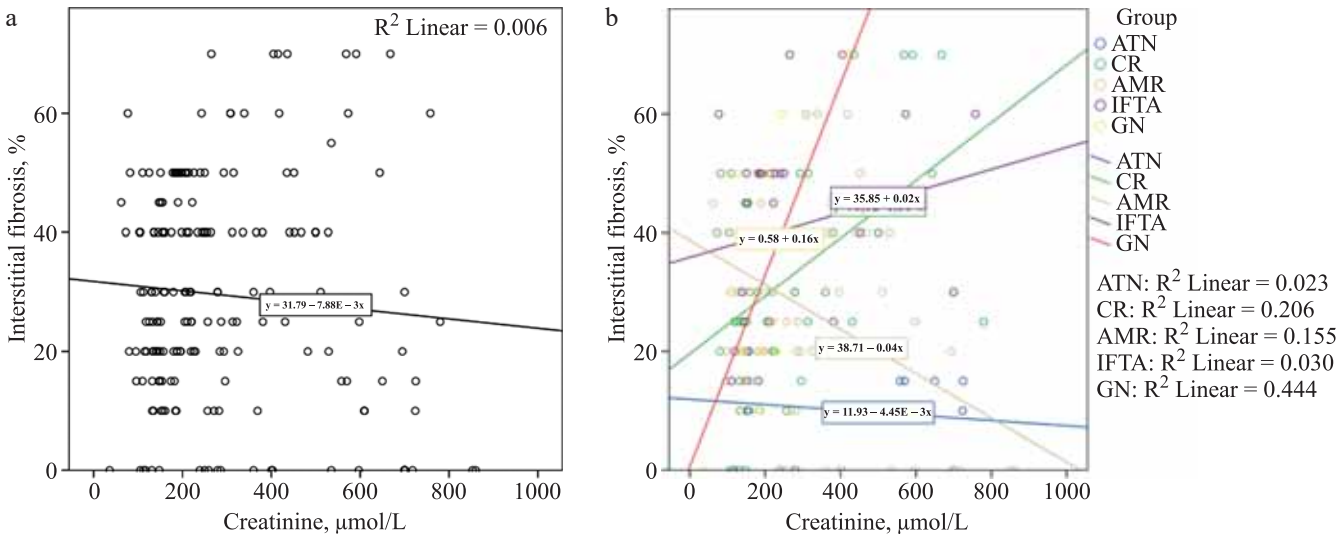

Fig. 6. Correlation between severity of dysfunction at the time of biopsy and prevalence of tubulointerstitial fibrosis (TIF): a, overall; b, depending on morphological diagnosis

Table 4

Area under ROC-curve for prognosis of graft loss by the severity of dysfunction at the time of biopsy and the degree of interstitial fibrosis

Test Result Variable(s)	Area	Std. Error	Asymptotic Sig.	Asymptotic 95% Confidence Interval	
				Lower Bound	Upper Bound
Creatinine	0.799	0.042	0.000	0.717	0.881
IFTA	0.744	0.048	0.000	0.649	0.838

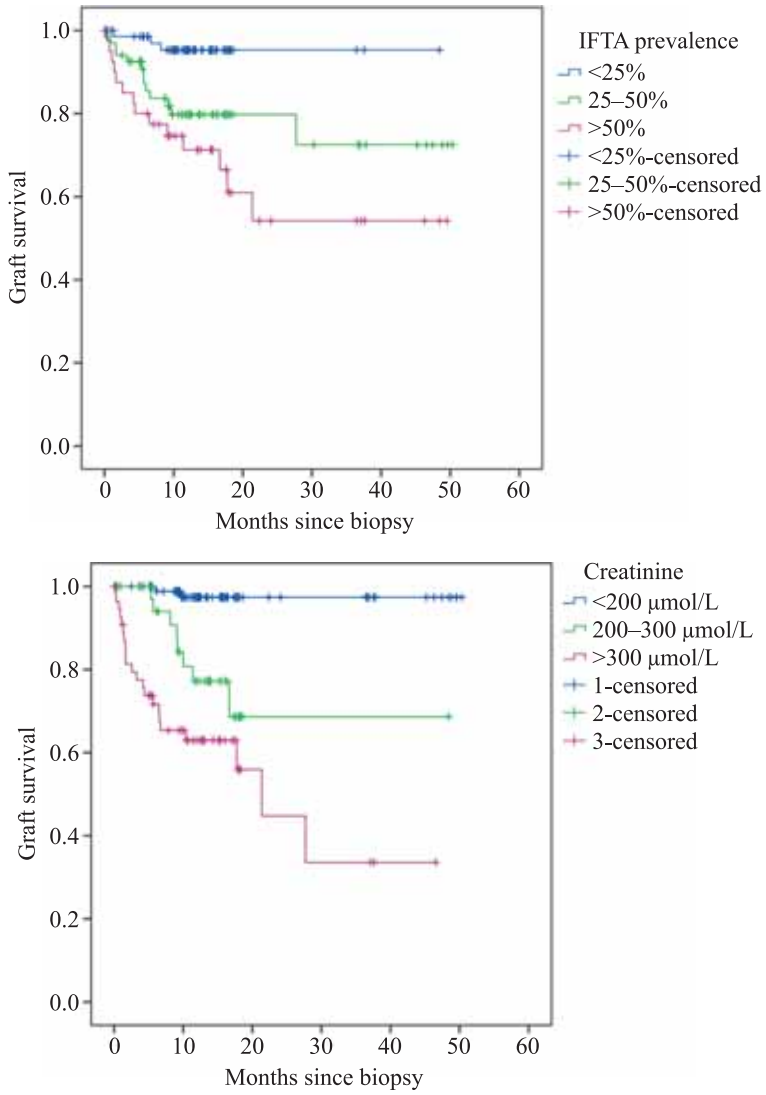

Fig. 7. Death-censored graft survival depending on prevalence of interstitial fibrosis

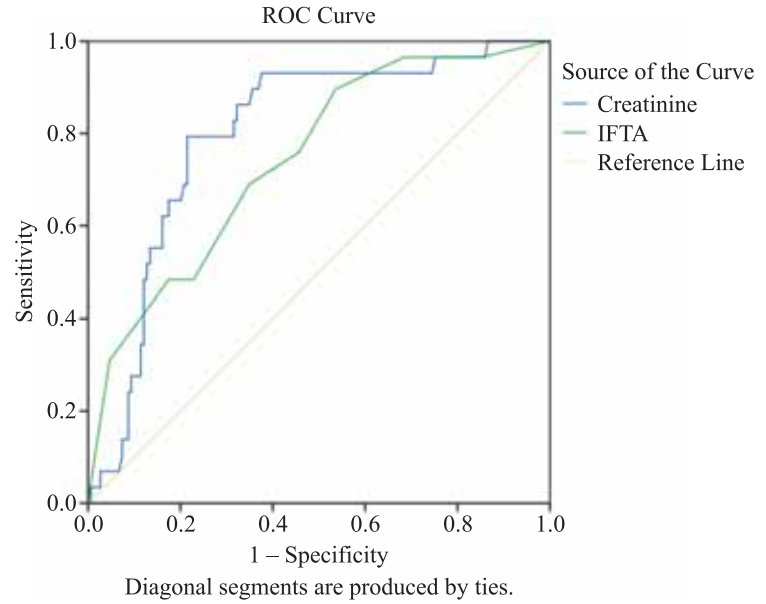

Fig. 8. ROC graft loss prediction curve depending on creatinine level at the time of biopsy and prevalence of interstitial fibrosis

ry plays a crucial role in determining long-term graft survival [22–24]. The prognostic impact of nonspecific interstitial fibrosis was further supported by protocol biopsy data [25].

Given these insights, our study assessed the significance of these factors both in the entire sample, regardless of the underlying pathology, and within each group separately.

In all groups, except for ATN, interstitial fibrosis of varying severity was observed at the time of biopsy. Its highest prevalence was found in nonspecific nephrosclerosis of non-immune origin ($p < 0.05$ compared to all other groups). A possible explanation for this phenomenon is that, in the absence of other damaging mechanisms, the sclerosing process remains subclinical for an extended period, only becoming apparent when graft dysfunction emerges at the stage of widespread nephrosclerosis. As in previous studies, IFTA prevalence was identified as a significant independent predictor of prognosis, alongside the severity of dysfunction at onset.

Traditionally, graft injury severity is assessed using creatinine levels at the time of biopsy, which – consistent with our findings – largely determines the probability of KT loss [26–30]. However, other studies have evaluated injury severity using molecular profiles, such as IRRATs [31–34]. In the early post-KT period, IRRATs correlate with ATN severity but have no impact on long-term survival [33]. However, in later stages, particularly in cases of AMR, these markers serve as predictors of accelerated disease progression [34].

In our study, creatinine levels and their subsequent dynamics varied depending on the underlying pathological process, aligning with the findings of Famulski et al. The multidirectional correlation between creatinine levels and interstitial fibrosis severity further supports this variability.

Thus, when estimating the risk of graft loss, it is essential to consider a comprehensive set of prognostic factors, including nature of the underlying disease, severity of allograft dysfunction, and extent of background interstitial fibrosis.

The authors declare no conflict of interest.

REFERENCES

1. *El-Zoghby ZM, Stegall MD, Lager DJ, Kremers WK, Amer H, Gloor JM, Cosio FG*. Identifying specific causes of kidney allograft loss. *Am J Transplant*. 2009 Mar; 9 (3): 527. doi: 10.1111/j.1600-6143.2008.02519.x.
2. *Sellarés J, de Freitas DG, Mengel M, Reeve J, Einecke G, Sis B et al.* Understanding the causes of kidney transplant failure: the dominant role of antibody-mediated rejection and nonadherence. *Am J Transplant*. 2012 Feb; 12 (2): 388-399. doi: 10.1111/j.1600-6143.2011.03840.x. Epub 2011 Nov 14.
3. *Gaston RS, Cecka JM, Kasiske BL, Fieberg AM, Leduc R, Cosio FC et al.* Evidence for antibody-mediated injury as a major determinant of late kidney allograft failure. *Transplantation*. 2010 Jul 15; 90 (1): 68–74. doi: 10.1097/TP.0b013e3181e065de.
4. *Gourishankar S, Leduc R, Connett J, Cecka JM, Cosio F, Fieberg A et al*. Pathological and clinical characterization of the 'troubled transplant': data from the DeKAF study. *Am J Transplant*. 2010 Feb; 10 (2): 324–330. doi: 10.1111/j.1600-6143.2009.02954.x. Epub 2010 Jan 5. PMID: 20055809; PMCID: PMC3538367.
5. *Aubert O, Higgins S, Bouatou Y, Yoo D, Raynaud M, Viglietti D et al*. Archetype Analysis Identifies Distinct Profiles in Renal Transplant Recipients with Transplant Glomerulopathy Associated with Allograft Survival. *J Am Soc Nephrol*. 2019 Apr; 30 (4): 625–639. doi: 10.1681/ASN.2018070777. Epub 2019 Mar 14. PMID: 30872323; PMCID: PMC6442337.
6. *Halloran PF, Merino Lopez M, Barreto Pereira A.* Identifying Subphenotypes of Antibody-Mediated Rejection in Kidney Transplants. *Am J Transplant*. 2016 Mar; 16 (3): 908–920. doi: 10.1111/ajt.13551. Epub 2016 Jan 6. PMID: 26743766.
7. *Lefaucheur C, Nochy D, Hill GS, Suberbielle-Boissel C, Antoine C, Charron D, Glotz D.* Determinants of poor graft outcome in patients with antibody-mediated acute rejection. *Am J Transplant*. 2007 Apr; 7 (4): 832–841. doi: 10.1111/j.1600-6143.2006.01686.x. PMID: 17391126.
8. *He X, Johnston A.* Early acute rejection does not affect chronic allograft nephropathy and death censored graft failure. *Transplant Proc*. 2004 Dec; 36 (10): 2993–2996. doi: 10.1016/j.transproceed.2004.10.070. PMID: 15686679.
9. *Halloran PF, Chang J, Famulski K, Hidalgo LG, Salazar ID, Merino Lopez M et al*. Disappearance of T Cell-Mediated Rejection Despite Continued Antibody-Mediated Rejection in Late Kidney Transplant Recipients. *J Am Soc Nephrol*. 2015 Jul; 26 (7): 1711–1720. doi: 10.1681/ASN.2014060588. Epub 2014 Nov 6. PMID: 25377077; PMCID: PMC4483591.
10. *Cooper JE, Gralla J, Cagle L, Goldberg R, Chan L, Wiseman AC.* Inferior kidney allograft outcomes in patients with *de novo* donor-specific antibodies are due to acute rejection episodes. *Transplantation*. 2011 May 27; 91 (10): 1103–1109. doi: 10.1097/TP.0b013e3182139da1. PMID: 21403588.
11. *El Ters M, Grande JP, Keddis MT, Rodrigo E, Chopra B, Dean PG et al*. Kidney allograft survival after acute rejection, the value of follow-up biopsies. *Am J Transplant*. 2013 Sep; 13 (9): 2334–2341. doi: 10.1111/ajt.12370. Epub 2013 Jul 19. PMID: 23865852.
12. *Cherukuri A, Mehta R, Sharma A, Sood P, Zeevi A, Tevar AD et al*. Post-transplant donor specific antibody is associated with poor kidney transplant outcomes only when combined with both T-cell-mediated rejection and non-adherence. *Kidney Int*. 2019 Jul; 96 (1): 202–213. doi: 10.1016/j.kint.2019.01.033. Epub 2019 Mar 20. PMID: 31029504.

13. *Matignon M, Muthukumar T, Seshan SV, Suthanthiran M, Hartono C.* Concurrent acute cellular rejection is an independent risk factor for renal allograft failure in patients with C4d-positive antibody-mediated rejection. *Transplantation*. 2012 Sep 27; 94 (6): 603–611. doi: 10.1097/TP.0b013e31825def05. PMID: 22932115; PMCID: PMC3621127.
14. *Vanhove T, Goldschmeding R, Kuypers D*. Kidney Fibrosis: Origins and Interventions. *Transplantation*. 2017 Apr; 101 (4): 713–726. doi: 10.1097/TP.0000000000001608.
15. *Lefaucheur C, Gosset C, Rabant M, Viglietti D, Verine J, Aubert O et al*. T cell-mediated rejection is a major determinant of inflammation in scarred areas in kidney allografts. *Am J Transplant*. 2018 Feb; 18 (2): 377–390. doi: 10.1111/ajt.14565. Epub 2017 Nov 21. PMID: 29086461.
16. *Gago M, Cornell LD, Kremers WK, Stegall MD, Cosio FG*. Kidney allograft inflammation and fibrosis, causes and consequences. *Am J Transplant*. 2012 May; 12 (5): 1199–1207. doi: 10.1111/j.1600-6143.2011.03911.x. Epub 2012 Jan 5. PMID: 22221836.
17. *Shimizu T, Toma H, Hayakawa N, Shibahara R, Ishiyama R, Hayashida A et al*. Clinical and pathological analyses of interstitial fibrosis and tubular atrophy cases after kidney transplantation. *Nephrology (Carlton)*. 2016 Jul; 21 Suppl 1: 26–30. doi: 10.1111/nep.12766. PMID: 26972969.
18. *Haas M, Loupy A, Lefaucheur C, Roufosse C, Glotz D, Seron D et al*. The Banff 2017 Kidney Meeting Report: Revised diagnostic criteria for chronic active T cell-mediated rejection, antibody-mediated rejection, and prospects for integrative endpoints for next-generation clinical trials. *Am J Transplant*. 2018 Feb; 18 (2): 293–307. doi: 10.1111/ajt.14625. Epub 2018 Jan 21. PMID: 29243394; PMCID: PMC5817248.
19. *Gosset C, Viglietti D, Rabant M, Vérine J, Aubert O, Glotz D et al*. Circulating donor-specific anti-HLA antibodies are a major factor in premature and accelerated allograft fibrosis. *Kidney Int*. 2017 Sep; 92 (3): 729–742. doi: 10.1016/j.kint.2017.03.033. Epub 2017 May 26. PMID: 28554738.
20. *Einecke G, Reeve J, Gupta G, Böhmig GA, Eskandary F, Bromberg JS et al*. Factors associated with kidney graft survival in pure antibody-mediated rejection at the time of indication biopsy: Importance of parenchymal injury but not disease activity. *Am J Transplant*. 2021 Apr; 21 (4): 1391–1401. doi: 10.1111/ajt.16161. Epub 2020 Jul 31. PMID: 32594646.
21. *Van Loon E, Senev A, Lerut E, Coemans M, Callemeyn J, Van Keer JM et al*. Assessing the Complex Causes of Kidney Allograft Loss. *Transplantation*. 2020 Dec; 104 (12): 2557–2566. doi: 10.1097/TP.0000000000003192. PMID: 32091487.
22. *Naesens M, Kuypers DR, De Vusser K, Vanrenterghem Y, Evenepoel P, Claes K et al*. Chronic histological damage in early indication biopsies is an independent risk factor for late renal allograft failure. *Am J Transplant*. 2013 Jan; 13 (1): 86–99. doi: 10.1111/j.1600-6143.2012.04304.x. Epub 2012 Nov 8. PMID: 23136888.
23. *Naesens M, Kuypers DR, De Vusser K, Evenepoel P, Claes K, Bammens B et al.* The histology of kidney transplant failure: a long-term follow-up study. *Transplantation*. 2014 Aug 27; 98 (4): 427–435.
24. *Toki D, Inui M, Ishida H, Okumi M, Shimizu T, Shirakawa H et al*. Interstitial fibrosis is the critical determinant of impaired renal function in transplant glomerulopathy. *Nephrology (Carlton)*. 2016 Jul; 21 Suppl 1: 20–25. doi: 10.1111/nep.12765. PMID: 26970313.
25. *De Vusser K, Lerut E, Kuypers D, Vanrenterghem Y, Jochmans I, Monbaliu D et al*. The predictive value of kidney allograft baseline biopsies for long-term graft survival. *J Am Soc Nephrol*. 2013 Nov; 24 (11): 1913–1923. doi: 10.1681/ASN.2012111081. Epub 2013 Aug 15. PMID: 23949799; PMCID: PMC3810080.
26. *Khalkhali HR, Ghafari A, Hajizadeh E, Kazemnejad A.* Risk Factors of Long-Term Graft Loss in Renal Transplant Recipients with Chronic Allograft Dysfunction. *Exp Clin Transplant*. 2010 Dec; 8 (4): 277–282.
27. *Ponticelli C, Villa M, Cesana B, Montagnino G, Tarantino A.* Risk factors for late kidney allograft failure. *Kidney Int*. 2002; 62 (5): 1848–1854.
28. *Sijpkens YWJ, Zwinderman AH, Mallat MJK, Boom H, Fijter JWde, Paul LC.* Intercept and slope analysis of risk factors in chronic renal allograft nephropathy. *Graft*. 2002 Mar; 5 (2): 108–113.
29. *Gourishankar S, Hunsicker LG, Jhangri GS, Cockfield SM, Halloran PF.* The stability of the glomerular filtration rate after renal transplantation is improving. *J Am Soc Nephrol*. 2003 Sep; 14 (9): 2387–2394.
30. *First MR.* Renal function as a predictor of long-term graft survival in renal transplant patients. *Nephrol Dial Transplant*. 2003 May; 18 Suppl 1: i3–i6. doi: 10.1093/ndt/gfg1027. PMID: 12738756.
31. *Halloran PF, Reeve J, Akalin E, Aubert O, Bohmig GA, Brennan D et al*. Real Time Central Assessment of Kidney Transplant Indication Biopsies by Microarrays: The INTERCOMEX Study. *Am J Transplant*. 2017 Nov; 17 (11): 2851–2862. doi: 10.1111/ajt.14329. Epub 2017 May 30. PMID: 28449409.
32. *Einecke G, Reeve J, Sis B, Mengel M, Hidalgo L, Famulski KS et al.* A molecular classifier for predicting future graft loss in late kidney transplant biopsies. *J Clin Invest*. 2010; 120 (6): 1862–1872.
33. *Famulski KS, de Freitas DG, Kreepala C, Chang J, Sellares J, Sis B et al*. Molecular phenotypes of acute kidney injury in kidney transplants. *J Am Soc Nephrol*. 2012 May; 23 (5): 948–958. doi: 10.1681/ASN.2011090887. Epub 2012 Feb 16. PMID: 22343120; PMCID: PMC3338297.
34. *Famulski KS, Reeve J, de Freitas DG, Kreepala C, Chang J, Halloran PF.* Kidney transplants with progressing chronic diseases express high levels of acute kidney injury transcripts. *Am J Transplant*. 2013; 13 (3): 634–644.

The article was submitted to the journal on 25.06.2024

DOI: 10.15825/1995-1191-2025-1-74-83

COMPREHENSIVE ASSESSMENT OF THE QUALITY OF LIFE IN HEART TRANSPLANT RECIPIENTS: EXPERIENCE AT SHUMAKOV NATIONAL MEDICAL RESEARCH CENTER OF TRANSPLANTOLOGY AND ARTIFICIAL ORGANS

I.I. Muminov[1], A.A. Yusova[1], N.N. Koloskova[1], A.O. Shevchenko[1–3], R.Yu. Bangarov[1], M.S. Nesterova[1]

[1] Shumakov National Medical Research Center of Transplantology and Artificial Organs, Moscow, Russian Federation

[2] Sechenov University, Moscow, Russian Federation

[3] Pirogov Russian National Research Medical University, Moscow, Russian Federation

Heart transplant (HT) is an effective treatment option for patients with end-stage chronic heart failure, as it can restore their ability to work, facilitate physical and social rehabilitation, and significantly improve their long-term survival. **Objective:** to evaluate the psychological and physical well-being of HT recipients using a comparative analysis of the TxEQ, PTGI, and SF-36 questionnaires and the impact of the obtained results on the frequency of visits to health care facilities. **Materials and methods.** The findings of the study were derived by analyzing the data of recipients by random randomization, who were observed on an outpatient basis at Shumakov National Medical Research Center of Transplantology and Artificial Organs. The TxEQ, SF-36, and PTGI questionnaires were used to assess recipients' psychological and physical well-being. For comparative analysis, HT recipients were divided into three equal groups based on the total score obtained when assessing each factor in the TxEQ questionnaire. Results. A comparative evaluation of factors from the TxEQ questionnaire and scores from the SF-36 questionnaire revealed that recipients who scored poorly on a particular factor had better mental health ($p = 0.02$). Recipients who are more eager to inform others about their surgery show better vitality ($p = 0.019$). Analysis of the "Medication adherence" factor found that there was a significantly high compliance of recipients to taking their medications ($p = 0.01$). Subsequent data analysis showed that the total PTGI score strongly correlated with the factors "Responsibility", "New life perspectives", "Disclosure" and "Medication adherence" ($p < 0.005$). While analyzing factors from the TxEQ questionnaire and the frequency of recipients' outpatient visits to health care facilities, it was revealed that recipients who were more worried about their surgery and those who exhibited high medication adherence during the follow-up year visited health care facilities more often ($p < 0.005$). **Conclusion.** Regularly assessing the quality of life in HT recipients is a key factor of outpatient follow-up, which allows to significantly improve physical and psychological well-being, and ultimately preventing the risk of negative health complications.

Keywords: heart transplantation, quality of life, SF-36 questionnaire, PTGI questionnaire, TxEQ questionnaire, outpatient follow-up.

INTRODUCTION

For patients with end-stage chronic heart failure, a heart transplant (HT) is widely considered the primary and often only option for a radical treatment, significantly improving their life expectancy [1]. However, not only the life expectancy of HT recipients is important, but also their quality of life, which depends on various factors often not directly related to the general state of health [2]. These include socio-demographic characteristics, daily activity levels, comorbid conditions, frequency of hospitalizations, medication side effects, and personal traits [3]. Given these complexities, regular clinical and diagnostic assessments must be complemented by psychosocial evaluations, as disruptions in psychosocial well-being can lead to poor treatment adherence, increased morbidity and mortality, and difficulties in post-transplant adaptation [4]. As a result, the number of studies assessing the physical and psychological health of HT recipients and analyzing their quality of life is steadily increasing. However, there is no single internationally recognized methodology for evaluating post-transplant quality of life. Instead, a variety of standardized questionnaires are used, including the Transplant Effects Questionnaire (TxEQ), Post-Traumatic Growth Inventory (PTGI), and the Short Form Health Survey (SF-36).

Corresponding author: Nadezda Koloskova. Address: 1, Shchukinskaya str., Moscow, 123182, Russian Federation. Phone: (926) 651-40-64. E-mail: nkrasotka@mail.ru

These tools assess both physical and psycho-emotional well-being, as well as patients' satisfaction with their functional status. Their use enables early identification of potential risks in long-term follow-up, allowing for timely interventions to enhance the quality of life for HT recipients.

The objective of our study was to assess the psychological and physical well-being of HT recipients through a comparative analysis of the TxEQ, PTGI, and SF-36 questionnaires and to evaluate how these results influence the frequency of healthcare visits.

MATERIALS AND METHODS

Study participants were randomly selected from HT recipients receiving outpatient care at the Shumakov National Medical Research Center of Transplantology and Artificial Organs ("Shumakov Center"). Their health status was monitored by cardiologists and psychologists at the Shumakov Center's consulting and diagnostic department, as well as by specialists at their place of residence. Remote consultations were also conducted via telemedicine.

All recipients received a standard immunosuppressive regimen consisting of tacrolimus, mycophenolate mofetil, and methylprednisolone. Routine postoperative assessments included clinical evaluations, laboratory tests (general and biochemical bloodwork, immunosuppressive drug levels), echocardiography, and annual coronary angiography with endomyocardial biopsy.

Additionally, we collected data on recipients' social status (living conditions, marital status, and education), as well as medical records and outpatient charts from the Shumakov Center. All patients were treated in accordance with established clinical guidelines.

The TxEQ (Transplant Effects Questionnaire) [5] was used to assess the psychological status of HT recipients. This questionnaire was translated and adapted for HT recipients in collaboration with a psychologist from the Shumakov Center. It consists of 26 items divided into 5 sections; each item is scored from 1 (completely disagree) to 5 (completely agree). The sections are outlined in Table 1.

The TxEQ evaluates key psychological aspects experienced by HT recipients, including concerns about

Table 1

Transplant Effects Questionnaire

	Points
Factor 1: Worry about the transplant	
I am worried about how reliable my new heart is	1–5
I feel like my heart is "fragile"	1–5
I hesitate to do certain activities for fear of harming my new heart	1–5
I wonder how long my new heart will last	1–5
I have started to take better care of myself since the transplant	1–5
I worry every time my doctor adjusts my medications	1–5
I find it hard to trust doctors	1–5
Factor 2: Disclosure	
I avoid telling other people that I have a transplant	1–5
I feel uncomfortable when other people know that I have had a heart transplant	1–5
I find it hard to talk about the fact that I had a transplant	1–5
I am not ready to tell everyone that life after a transplant is just beginning	1–5
Factor 3: Medication adherence	
Sometimes I deliberately do not take my medication	1–5
Sometimes I forget to take my medication	1–5
I might get distracted and forget to take my medication	1–5
Sometimes I think I can do without medication	1–5
I find it inconvenient for me to take my medication at the same time	1–5
I don't always follow my doctor's instructions	1–5
Factor 4: Responsibility	
I feel a sense of duty to the doctors who performed my successful surgery	1–5
I feel a sense of duty to my family and other people close to me	1–5
I am sometimes haunted by guilt	1–5
I usually try not to do things that could cause condemnation from my family and other close people.	1–5
Factor 4: New life perspectives after transplant	
I have a sense of purpose in my life after the heart transplant	1–5
I have become more interested in playing sports after the transplant	1–5
I feel that my quality of life has improved after the transplant	1–5
I feel energized after the transplant to pursue my dreams	1–5
I have returned to my normal routine after the transplant	1–5

the transplant, willingness to disclose their transplant status (renamed "Disclosure" for clarity), adherence to medication, and feelings of obligation toward family, friends, and medical staff. Higher scores indicate a stronger presence of the corresponding factor, except for "Medication adherence" and "Disclosure", which exhibit a negative correlation.

All patients provided informed voluntary consent before undergoing psychological assessment. For comparative analysis, recipients were divided into three equal groups based on their total scores for each TxEQ factor.

The PTGI questionnaire [6] was used to assess positive psychological and emotional changes in individuals following psychological trauma or stressful experiences. It comprises 21 items divided into five domains: Relating to Others (7 items), New Possibilities (5 items), Personal Strength (4 items), Existential and Spiritual Change (2 items), and Appreciation of Life (3 items). Each item is rated on a 6-point Likert scale, reflecting the extent to which the respondent has experienced these changes due to the trauma.

The SF-36 questionnaire was used to evaluate both the physical and psychoemotional components of quality of life. The results provide insights into overall well-being and the level of satisfaction in health-dependent aspects of daily life [7]. This questionnaire consists of 36 questions covering the following eight key health domains:

1. *Physical functioning.* Measures limitations in daily physical activities like self-care, walking, climbing stairs, carrying heavy objects, etc. Lower score signifies greater limitations in daily physical activities due to the disease.
2. *Role limitations due to physical health problems.* Measures how much a person's physical health issues interfere with their ability to perform their usual roles and responsibilities in daily life, such as work, household chores, or other activities.
3. *Role limitations due to emotional problems.* Measures how much a person's daily activities and responsibilities are restricted or impacted by their emotional state (including more time, less work, lower quality, etc.). A lower score signifies greater impact of emotional problems on daily activities, indicating significant impairment in work and role functioning.
4. *Social functioning.* Measures how physical and emotional health problems affect a person's ability to engage in social activities (communication). Lower score indicate restrictions in social interactions due to physical or emotional health issues, potentially indicating reduced level of communication.
5. *Bodily pain.* Measures the intensity of pain and its impact on daily activities, including housework. Lower score signifies severe pain that significantly affects daily function and work capacity.
6. *Vitality (energy or fatigue).* Measures overall energy level and fatigue, essentially gauging how "worn out" or "vigorous" they feel. Lower score suggests experiencing more fatigue and exhaustion.
7. *Mental health.* Lower score suggests emotional distress, anxiety, or depressive symptoms.
8. *General health perceptions.* Measures an individual's current state of health and overall view of their health status. Lower score suggests poor health perceptions.

The SF-36 questionnaire generates scores ranging from 0 to 100, where a higher score indicates a better perceived quality of life across the various health domains.

The data are presented as the arithmetic mean and standard deviation (M ± SD). Pearson's chi-square test was used to assess the statistical significance of relationships between two categorical variables. For comparative analysis, the one-way nonparametric Kruskal–Wallis test was employed to evaluate variance. When significant differences were identified, pairwise multiple comparisons were conducted using the least significant difference (LSD) criterion test. Statistical analyses were performed using IBM SPSS Statistics, with hypotheses tested at a significance level of $p < 0.005$.

Cronbach's alpha coefficient was calculated to measures the reliability of the TxEQ questionnaire.

RESULTS

A representative sample was drawn from patients under outpatient follow-up at the Shumakov Center between 2009 and 2022. A randomized selection process identified a cohort of 607 recipients with a mean age of 46.74 ± 10.72 years, including 509 men (83.8%). The study excluded cases of heart retransplantation, in-hospital mortality, and recipients younger than 18 years. The mean follow-up period was 9.4 ± 3.5 years.

Cronbach's alpha coefficient was calculated for each section of the TxEQ questionnaire, with the results presented in Table 2.

Analysis of the results indicated that the Cronbach's alpha coefficient for each section of the TxEQ questionnaire was satisfactory, confirming the questionnaire's reliability as an assessment tool.

Comparisons of TxEQ factors based on gender, marital status, and education level revealed statistically signi-

Table 2

Calculation of Cronbach's alpha for each section of the TxEQ questionnaire

Factor	Cronbach's alpha
Worried about the heart transplant performed	0.766
Disclosure	0.759
Adherence to immunosuppression	0.758
Responsibility	0.759
New life perspectives after transplant	0.794

ficant trends. Married recipients exhibited greater anxiety about their HT surgery, demonstrated higher adherence to drug therapy, showed a stronger motivation to inform others about their transplant, and felt a greater sense of duty toward their family, friends, and physicians for the success of their surgery.

Men reported greater concern about their surgical treatment and displayed greater responsibility in adhering to drug therapy ($p < 0.005$). Furthermore, recipients who scored high on the factor "Worried about the heart transplant performed" tended to have a higher level of education than those with lower scores ($p < 0.005$).

COMPARATIVE EVALUATION OF THE TXEQ QUESTIONNAIRE FACTORS AND SF-36 INDICATORS

Analysis using the TxEQ indicated that transplant recipients who score lower on the "Worry about the transplant" subscale tend to demonstrate a higher level of mental health ($p = 0.02$). The results suggest that recipients who exhibit less anxiety about their HT surgery are also less prone to depressive and anxiety-related states.

Subsequently, the SF-36 questionnaire results were analyzed in relation to the "Disclosure" factor to assess its impact on quality of life. It was revealed that recipients who are more motivated to share their surgery experience have higher Vitality scores, as shown in Fig. 1. The findings demonstrate that recipients who are able to talk openly about their heart transplant surgery and related experiences show better vitality ($p = 0.019$).

Analyzing the data obtained for the factor "Medication adherence", a reliably high compliance of recipients to taking prescribed medications was revealed. Fig. 2, indicates a statistically significant negative relationship between high medication adherence scores and lower mental health scores ($p = 0.01$).

Individuals with higher "Mental health" scores tend to have lower adherence to therapy. The obtained result indicates the presence of depressive, anxious feelings, and mental distress, which reflects the instability of psycho-emotional state due to irregular intake of medications and possible complications arising from the lack of adequate drug treatment.

When evaluating the factor "Responsibility" from the TxEQ questionnaire, a negative correlation was established: as "Responsibility" scores increased, scores for "Physical Functioning" ($p = 0.008$), "Role limitations due to emotional problems" ($p = 0.047$) and "General health perceptions" ($p = 0.05$) from the SF-36 questionnaire decreased. Based on these findings, it can be concluded that recipients who experience an increased sense of responsibility for the success of their HT surgery may face limitations in daily life due to a decline in physical health, exacerbated by emotional distress and psycho-emotional destabilization.

In further assessment of the factor "New life perspectives after transplant", individuals who score higher on measures of "New life perspectives after transplant" tend to exhibit higher "Physical functioning" scores compared to those with lower ($p = 0.004$) or average ($p = 0.007$) scores. This indicates the importance of forming a posi-

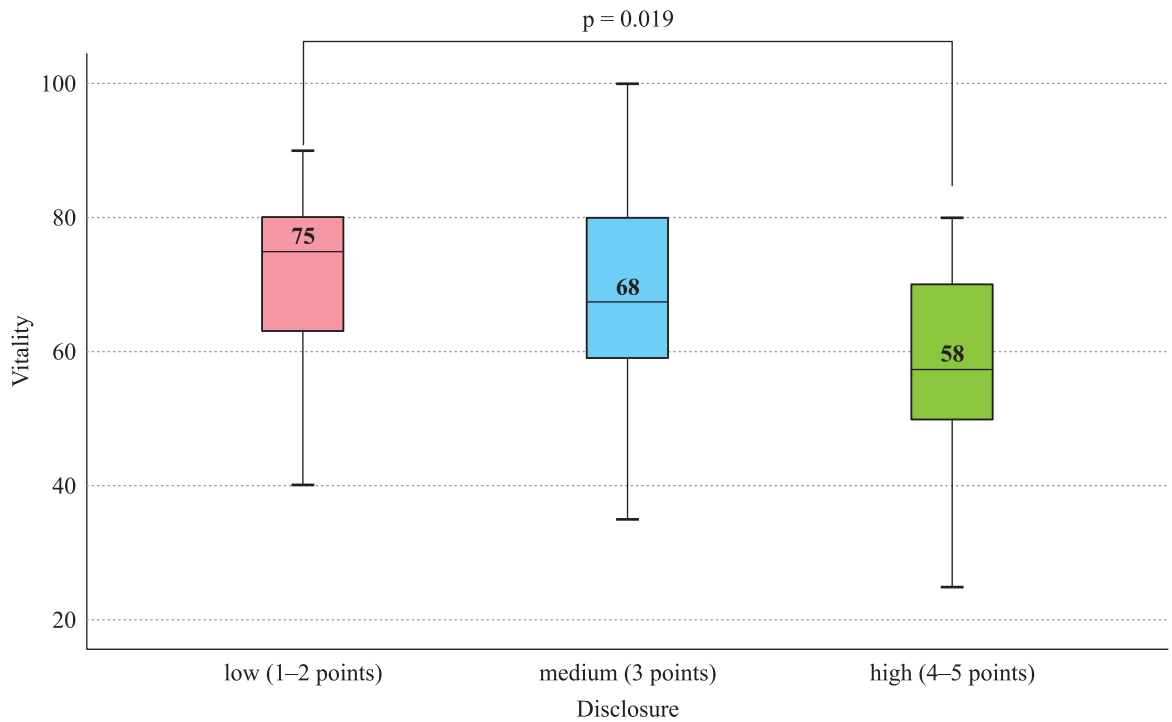

Fig. 1. Comparative analysis of the factor "Disclosure" (TxEQ questionnaire) and the indicator "Vitality" (SF-36 questionnaire)

tive image of the future and vision of new perspectives within the framework of improving the general physical condition (Fig. 3).

Further analysis assessed the impact of the total PTGI score on TxEQ factors, revealing a significant positive correlation between the PTGI total score and the factors "Responsibility" and "New life perspectives after transplant". These findings suggest that transplant recipients undergo profound life changes, often marked by an existential crisis, personalization of life and death issues, internal conflict, and a search for new meaning and redefinition of existence ($p < 0.005$).

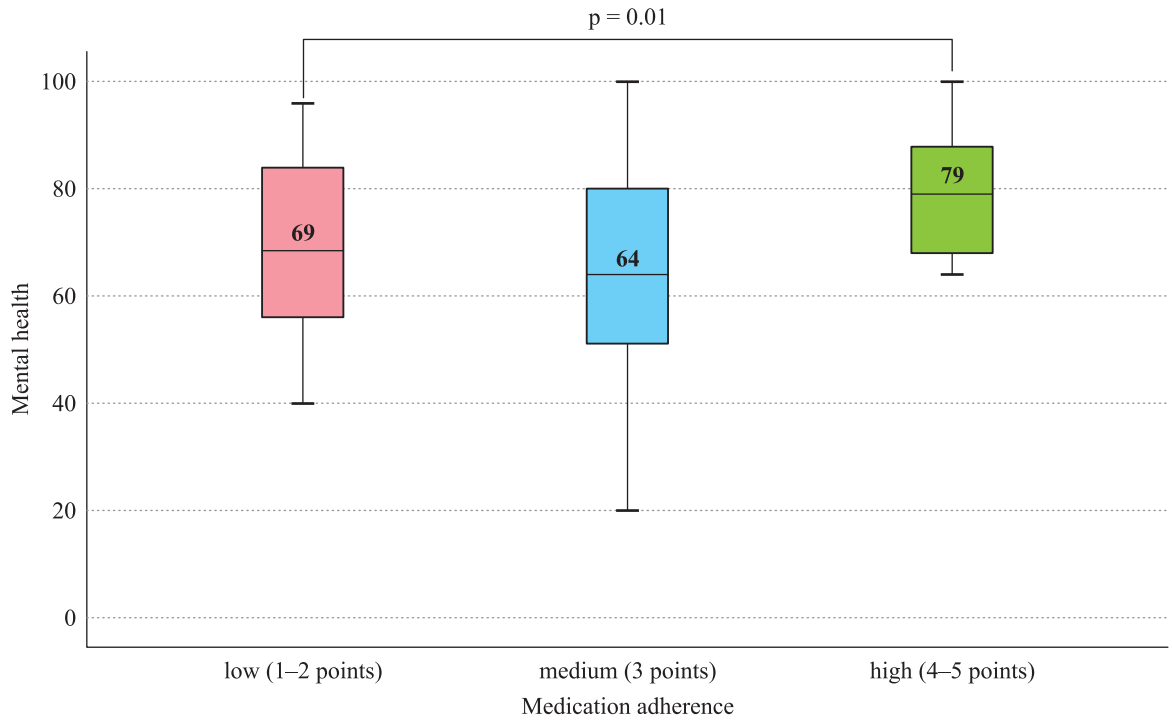

Fig. 2. Comparative analysis of the factor "Medication adherence" (TxEQ questionnaire) and the indicator "Mental health" (SF-36 questionnaire)

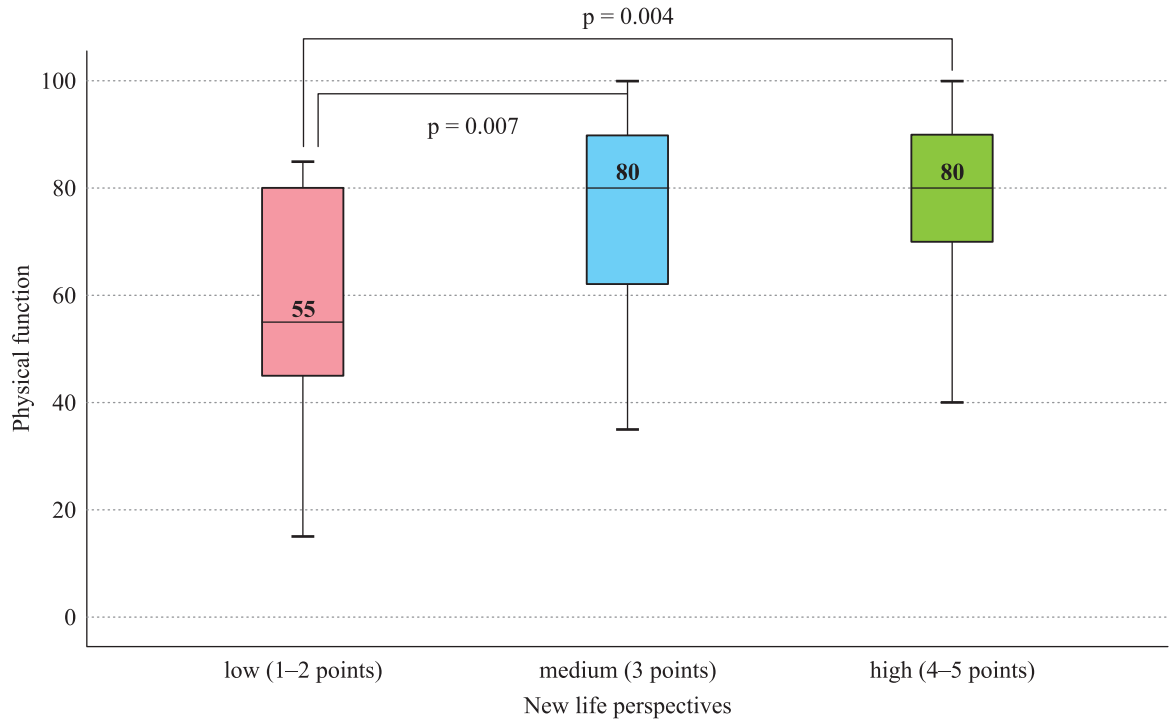

Fig. 3. Comparative analysis of the factor "New life perspectives" from the TxEQ questionnaire and the indicator "Physical function" from the SF-36 questionnaire

A comparison of "Medication adherence" with the total PTGI score indicated a statistically significant inverse correlation, where recipients with higher adherence to drug therapy tended to have lower PTGI scores, while those with higher PTGI scores exhibited lower adherence ($p = 0.017$). Additionally, recipients who openly shared their transplant experience demonstrated significantly higher PTGI scores, highlighting the role of disclosure in psychological growth after HT.

The analysis revealed a correlation between TxEQ factors and the frequency of recipients' outpatient visits to medical facilities. Recipients who exhibited greater anxiety about their HT surgery and demonstrated high adherence to drug therapy during the first year of follow-up were more likely to visit clinical and diagnostic departments, both at the Shumakov Center and other healthcare institutions.

Notably, the high frequency of outpatient visits was not associated with adverse events but rather with increased patient vigilance regarding their health condition ($p < 0.005$).

DISCUSSION

This study is the first in Russian literature to provide a detailed assessment of quality-of-life indicators in a large cohort of HT recipients, utilizing a comparative analysis of three standardized questionnaires – key tools for evaluating treatment outcomes [7].

Our comparative evaluation of sex, marital status, and TxEQ factors revealed that married men demonstrated greater adherence to drug therapy. These findings align with results from a study conducted by Jia-Rong Wu et al. [8]. However, similar patterns were not confirmed in the findings of other researchers [9, 10].

Our study provided compelling evidence that recipients who exhibited greater concern about their HT surgery demonstrated better mental health. This finding is likely explained by the fact that these recipients more frequently sought medical consultations, leading to greater awareness of their health status, which may positively influence their mental well-being.

Similarly, Richard Klaghofer et al. [5] highlight the importance of specialist consultations in assessing not only the physical but also the mental health of recipients. However, their study found that better mental health was observed in patients who were less concerned about their surgery.

Thus, early detection of psychological issues in transplant recipients plays a crucial role in maintaining emotional stability and reducing the risk of complications [11].

A study conducted in Poland reported that recipients who were more motivated to inform others about their HT surgery demonstrated higher vitality scores [10]. These scores are linked to positive lifestyle changes and improved quality of life post-transplant, findings that are also supported by the results of our study.

Further assessment of psycho-emotional status revealed that recipients with lower medication adherence exhibited greater emotional instability and were more prone to depressive and anxious experiences. Similarly, Brocks et al. [12] found that recipients who adhered to their medication regimen had higher mental health scores. Our study yielded comparable results, demonstrating a significant association between the "Medication adherence" factor from the TxEQ questionnaire and the "Mental health" indicator from the SF-36 questionnaire.

Our study also provided strong evidence that recipients who felt an increased sense of responsibility for the success of their HT surgery – toward their family, relatives, and physicians – experienced a decline in physical health and psycho-emotional destabilization. However, a study by Natalie Engelbrecht found that personal responsibility was not a predictor of quality of life [13].

When assessing the "New life perspectives after transplant" factor from the TxEQ questionnaire, our findings demonstrated that HT recipients experienced improved quality of life and social adaptation, driven by a positive perception of future prospects and life goals post-transplant. These results are consistent with findings from international studies [14, 15].

Further evaluation of the influence of total PTGI score on TxEQ factors revealed that recipients with the highest PTGI scores were those who were highly motivated to inform others about their surgery, exhibited strong adherence to drug therapy, and demonstrated a high level of personal responsibility. These findings align with results from previous studies confirming the impact of the PTGI score on TxEQ factors [9, 5, 16, 17].

Moreover, successful post-transplant recovery has been shown to be directly linked to several key factors: personal responsibility, adherence to prescribed therapy, and a positive outlook. These elements play a crucial role in facilitating significant cognitive and emotional transformations following a major traumatic event such as transplant surgery [18, 19].

A study by Samar Tharwat et al. found that patients with high medication adherence had more frequent outpatient visits compared to those with lower adherence to therapy [20]. Our study similarly confirms that recipients with higher adherence to prescribed treatments tend to visit healthcare facilities more frequently for follow-ups and monitoring.

CONCLUSION

Following HT, recipients experience significant improvements in both psychological and physical quality of life, largely due to a personalized approach to outpatient follow-up. Regular check-ups, continuous health monitoring, and enhanced adherence to treatment play a crucial role in improving mental and physical health indicators while also reducing the risk of adverse events.

Therefore, to maintain a high quality of life among HT recipients, it is essential to provide consistent medical supervision, conduct regular psycho-emotional assessments, implement strategies to enhance social adaptation.

The authors declare no conflict of interest.

REFERENCES

1. Transplantology: results and prospects. Vol. XIII. 2021 / Ed. by S.V. Gautier. M.–Tver: Triada, 2022; 416.
2. *Shevchenko AO, Khalilulin TA, Mironkov BL, Saitgareev RSh, Zakharevich VM, Kormer AYa et al.* Quality of life assessment in cardiac transplant recipients. *Russian Journal of Transplantology and Artificial Organs*. 2014; 16 (4): 11–16. (In Russ.). https://doi.org/10.15825/1995-1191-2014-4-11-16.
3. *White-Williams C, Wang E, Rybarczyk B, Grady KL.* Factors associated with work status at 5 and 10 years after heart transplantation. *Clin Transplant*. 2011 Nov-Dec; 25 (6): E599–E605.
4. *Simonenko MA, Fedotov PA, Sitnikova MYu, Bart VA, Vasilieva LA, Berezina AV, Karpenko MA*. Changes of mental and physical components of quality of life in patients after heart transplantation: experience of the Almazov National Medical Research Center. *Russian Journal of Cardiology*. 2024; 29 (9): 5749. (In Russ.). https://doi.org/10.15829/15604071-2024-5749.
5. *Klaghofer R, Sarac N, Schwegler K, Schleuniger M, Noll G, Muellhaupt B et al.* Fragebogen zur psychischen Verarbeitung einer Organtransplantation: Deutsche Validierung des Transplant Effects Questionnaire (TxEQ) [Questionnaire on emotional response after organ transplantation: German validation of the Transplant Effect Questionnaire (TxEQ-D)]. *Z Psychosom Med Psychother*. 2008; 54 (2): 174–188. [German]. doi: 10.13109/zptm.2008.54.2.174. PMID: 18510834.
6. *Pravdina LR, Ulyanova NYu*. Co-operative behavior and posttraumatic stress in servicemen. *Psychology and psychotechnics*. 2017; 2: 59–73.
7. *Ahmadzai RLM*. Assessment of quality of life in donor heart recipients: diss. … candidate of medical sciences. M., 2018; 102.
8. *Wu JR, Lennie TA, Chung ML, Frazier SK, Dekker RL, Biddle MJ, Moser DK.* Medication adherence mediates the relationship between marital status and cardiac event-free survival in patients with heart failure. *Heart Lung*. 2012 Mar-Apr; 41 (2): 107–114. doi: 10.1016/j.hrtlng.2011.09.009. Epub 2011 Nov 3. PMID: 22054720; PMCID: PMC3288268.
9. *Pérez-San-Gregorio MÁ, Martín-Rodríguez A, Sánchez-Martín M, Borda-Mas M, Avargues-Navarro ML, Gómez-Bravo MÁ, Conrad R.* Spanish Adaptation and Validation of the Transplant Effects Questionnaire (TxEQ-Spanish) in Liver Transplant Recipients and Its Relationship to Posttraumatic Growth and Quality of Life. *Front Psychiatry*. 2018 Apr 18; 9: 148. doi: 10.3389/fpsyt.2018.00148. PMID: 29720952; PMCID: PMC5915644.
10. *Milaniak I, Wilczek-Rużyczka E, Wierzbicki K, Sadowski J, Przybyłowski P.* The influence of sense of coherence on emotional response in heart transplant recipients – a preliminary report. *Kardiochir Torakochirurgia Pol*. 2014 Jun; 11 (2): 220–224. doi: 10.5114/kitp.2014.43856. Epub 2014 Jun 29. PMID: 26336426; PMCID: PMC4283861.
11. *Denhaerynck K, Dobbels F, Cleemput I, Desmyttere A, Schäfer-Keller P, Schaub S, De Geest S.* Prevalence, consequences, and determinants of nonadherence in adult renal transplant patients: a literature review. *Transpl Int*. 2005 Oct; 18 (10): 1121–1133. doi: 10.1111/j.1432-2277.2005.00176.x. PMID: 16162098.
12. *Chui MA, Deer M, Bennett SJ, Tu W, Oury S, Brater DC, Murray MD*. Association between adherence to diuretic therapy and health care utilization in patients with heart failure. *Pharmacotherapy*. 2003 Mar; 23 (3): 326–332. doi: 10.1592/phco.23.3.326.32112.
13. *Engelbrecht N.* The Role of Personal Responsibility, Agency, and Resourcefulness, in Improving Quality of Life in Survivors of Trauma. Masters of Applied Psychology. Liverpool, August 2014.
14. *Kugler C, Bara C, von Waldthausen T, Einhorn I, Haastert B, Fegbeutel C, Haverich A.* Association of depression symptoms with quality of life and chronic artery vasculopathy: a cross-sectional study in heart transplant patients. *J Psychosom Res*. 2014; 77 (2): 128–134.
15. *Carvalho WDN, Alves Maria GDS, Gonçalves KC, Miranda AL, Moreira MDCV*. Health-Related Quality of Life of Heart Transplant Recipients Living in a Developing Country. *Transplant Proc*. 2021 Jan-Feb; 53 (1): 358–363. doi: 10.1016/j.transproceed.2020.05.027. Epub 2020 Jun 30. PMID: 32620391.
16. *Tedeschi RG, Calhoun LG*. The Posttraumatic Growth Inventory: measuring the positive legacy of trauma. *J Trauma Stress*. 1996 Jul; 9 (3): 455–471. doi: 10.1007/BF02103658. PMID: 8827649.
17. *Tedeschi RG, Calhoun LG.* Posttraumatic Growth: Conceptual Foundations and Empirical Evidence. *Psychol Inq*. 2004; 15 (1): 1–18.
18. *Scrignaro M, Sani F, Wakefield JR, Bianchi E, Magrin ME, Gangeri L.* Post-traumatic growth enhances social identification in liver transplant patients: A longitudinal study. *J Psychosom Res*. 2016 Sep; 88: 28–32. doi: 10.1016/j.jpsychores.2016.07.004. Epub 2016 Jul 11. PMID: 27521649.
19. *Anand-Kumar V, Kung M, Painter L, Broadbent E.* Impact of organ transplantation in heart, lung and liver recipients: assessment of positive life changes. *Psychol Health*. 2014; 29 (6): 687–697. doi: 10.1080/08870446.2014.882922.
20. *Tharwat S, Shaker EA.* Adherence patterns to medications and their association with subsequent hospitalization in adult Egyptian patients with systemic lupus erythematosus. *Lupus*. 2023 Oct; 32 (11): 1335–1344. doi: 10.1177/09612033231198826. Epub 2023 Aug 26. PMID: 37632454.

The article was submitted to the journal on 4.01.25

DOI: 10.15825/1995-1191-2025-1-84-89

USE OF CRYOPRESERVED AORTIC HOMOGRAFT FOR SUBCLAVIAN ARTERIAL CANNULATION DURING EXTRACORPOREAL MEMBRANE OXYGENATION

G.B. Moroz, D.A. Sirota, A.V. Guseva, A.V. Fomichev, E.E. Kliver
Meshalkin National Medical Research Center, Novosibirsk, Russian Federation

Extracorporeal membrane oxygenation (ECMO) is a vital tool in the treatment of patients with severe cardiovascular failure during heart surgery. The femoral artery is the most common access for veno-arterial ECMO in adults. Where there are contraindications to traditional cannulation techniques, the subclavian artery is an alternative access site, despite its many peculiarities. This paper presents a clinical case where peripheral ECMO connection with cannulation into the subclavian artery using a cryopreserved homovital abdominal aortic homograft was performed in a patient.

Keywords: extracorporeal membrane oxygenation, cannulation, subclavian artery, homograft.

INTRODUCTION

Extracorporeal membrane oxygenation (ECMO) is a life support system that temporarily takes over the function of a patient's heart and lungs by circulating their blood through a machine that adds oxygen and removes carbon dioxide, allowing the patient's own organs to rest and potentially recover from a reversible failure. According to the latest ELSO (Extracorporeal Life Support Organization) report, postcardiotomy syndrome patients have survival rates ranging from 25% to 50%. Additionally, 31% to 76% of patients are successfully weaned off ECMO [1].

Femoral artery cannulation (FAC) remains the most traditional and widely used approach for venoarterial ECMO (VA-ECMO) in adults. However, is associated with significant risks, such as arterial occlusion, limb ischemia, reperfusion injury leading to compartment syndrome, thrombosis, embolism, bleeding and hematoma formation [2]. In patients with peripheral artery disease, the risks of these complications are significantly higher and may be considered a contraindication to femoral artery cannulation.

Subclavian artery cannulation (SAC) is a viable alternative to FAC in patients with contraindications. However, it has technical peculiarities and usually requires surgical expertise [2]. Synthetic prostheses offer significant advantages over direct cannulation of peripheral vessels in VA-ECMO, particularly in reducing complications like damage to the artery by the cannula, vessel dissection, limb ischemia, and the need for post-decannulation arterial reconstruction. However, achieving hemostasis with synthetic prostheses in ECMO patients is challenging, especially in the setting of pronounced hypocoagulation. The porosity of synthetic grafts contributes to persistent bleeding from suture lines and puncture sites, leading to significant blood loss.

This article presents a clinical case in which ECMO was initiated via peripheral cannulation using a homovital cryopreserved abdominal aortic homograft. The homograft was obtained from a brain-dead donor during a multi-organ retrieval procedure. The retrieval and preservation technique ensured the absence of warm ischemia and included a controlled freezing protocol, preserving tissue viability, strength, and elasticity – critical factors for surgical manipulation [3]. According to available reports, cannulation using a homograft has not been previously performed.

CLINICAL CASE

Patient K., a 62-year-old man, underwent valve-sparing aortic root replacement (David procedure), radiofrequency ablation of atrial fibrillation zones, and coronary artery bypass grafting (CABG) as indicated. Following surgery, the patient was weaned from mechanical ventilation while receiving moderate doses of norepinephrine, epinephrine, and dobutamine. After extubation, transesophageal echocardiography revealed reduced contractility of both the left and right ventricular myocardium.

The early postoperative period was marked by worsening heart failure, a tendency toward hypotension, severe acid-base imbalances that were difficult to correct (metabolic acidosis, hypokalemia, hyperglycemia), and decreased urine output. Given the clinical deterioration, ECG changes, and overall negative dynamics, the

Corresponding author: Anastasiya Guseva. Address: 15, Rechkunovskaya str., 630055, Novosibirsk, Russian Federation. Phone: (913) 016-81-31. E-mail: gusevaanastasya@mail.ru

patient underwent urgent CABG evaluation. No further deterioration was observed, and the coronary grafts remained patent.

On the second postoperative day, the patient's condition deteriorated significantly, with worsening heart failure, episodes of ventricular tachycardia, and an elevated lactate level reaching 20 mmol/L. Despite the use of inotropes at extremely high doses, hemodynamic instability persisted, necessitating VA-ECMO initiation. Due to the small diameter of the common femoral arteries and the presence of diffuse atherosclerosis, as confirmed by ultrasound, FAC was deemed unsuitable. Instead, a resternotomy was performed, with arterial cannulation of the ascending aorta and venous cannulation guided by ultrasound through the femoral vein. ECMO support led to stabilization of the patient's condition.

Given the anticipated need for prolonged mechanical circulatory support and the increased risk of infectious complications and bleeding associated with surgical diastasis of the sternum, a decision was made on the second day of ECMO to close the chest and transition to peripheral cannulation. Cannulation of the right subclavian artery was performed using a cryopreserved homovital abdominal aortic homograft, measuring 10 mm in diameter and 40 mm in length (Fig. 1).

Fig. 1. Cryopreserved homovital abdominal aortic homograft

Cryopreserved grafts are stored at temperatures ranging *from –150 °C to –170 °C, requiring approximately 1.5 to 2 hours for thawing.*

A 4 cm oblique incision provided access to the right subclavian artery, which measured 7 mm in diameter. The abdominal aortic homograft was prepared by suturing and clipping the lumbar branches. A proximal end-to-side anastomosis was then formed between the homograft and the subclavian artery using a continuous locking stitch with a 6.0 suture.

To ensure structural integrity, the distal end of the homograft was attached to a 3/8–3/8 connector, which was reinforced with a Dacron vascular prosthesis to prevent wall rupture. The connector was secured with a lavsan thread (Figs. 2, 3). The volumetric perfusion rate (VPR) achieved was 5.1 L/min, and activated clotting time (ACT) during ECMO was maintained between 160–190 seconds.

By day 9 of ECMO, progressive renal failure and oliguria necessitated the initiation of continuous renal replacement therapy (hemodialysis) via the ECMO circuit. By day 14, the VPR was gradually reduced to 2.2–1 L/min.

An attempt was made to gradually discontinue ECMO, but it was unsuccessful. Following ECMO cessation, the patient exhibited hypotension (BP 80/40–70/30 mmHg), paroxysmal atrial fibrillation, and required high-dose inotropic support. Given these hemodynamic instabilities, the decision was made to continue ECMO support.

On day 19 of ECMO, the arterial cannula became dislodged from the anastomosis site between the homograft and the subclavian artery. Immediate interventi-

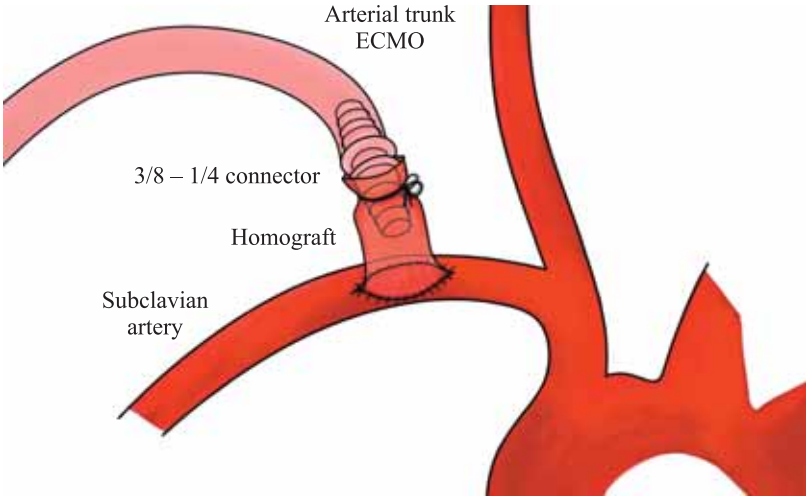

Fig. 2. Scheme of subclavian arterial cannulation using a homograft

on was required – a clamp was applied to the arterial ECMO line, and the surgeon performed re-cannulation into the homograft, securing it with a ligature knot. During ECMO cessation, cardiopulmonary resuscitation (CPR) was performed for 7 minutes before ECMO was successfully resumed. The patient's condition stabilized, with VPR restored to 4.3 L/min. Consciousness was regained, and treatment continued.

By day 27, mechanical circulatory support was reduced in response to stable systemic hemodynamics, with no signs of tissue hypoperfusion at a VPR of 1 L/min. A decision was made to discontinue ECMO and proceed with decannulation. The patient remained on ECMO for a total of 27 days.

After ECMO was discontinued, the patient continued to experience liver failure (blood bilirubin 261 mmol/L) and renal dysfunction. In response, hemodialysis with citrate anticoagulation was maintained. Despite the gradual reduction in inotropic therapy, there was no worsening of cardiovascular failure. The patient remained in the intensive care unit, receiving mechanical ventilation via tracheostomy.

It should be noted that throughout the entire ECMO support period, there were no complications related to arterial cannula patency, graft function, or bleeding at the cannulation site.

On day 14 after disconnection from ECMO, the patient succumbed to multiple organ failure.

Histological analysis of a fragment of the thawed cryopreserved homovital graft revealed moderate inflammatory changes in the intimal layer (Fig. 4).

Immunohistochemistry (IHC) analysis of the endothelial factor CD34, a well-known marker for blood vessel progenitor cells and stromal tissues, demonstrated a tendency for capacitive-type vessel formation in the adventitial layer (Fig. 5). Additionally, IHC staining with an antibody to ASM revealed positive expression of alpha-actin smooth muscle cells in the wall of the cryopreserved homograft, with focal absence observed in the middle layer.

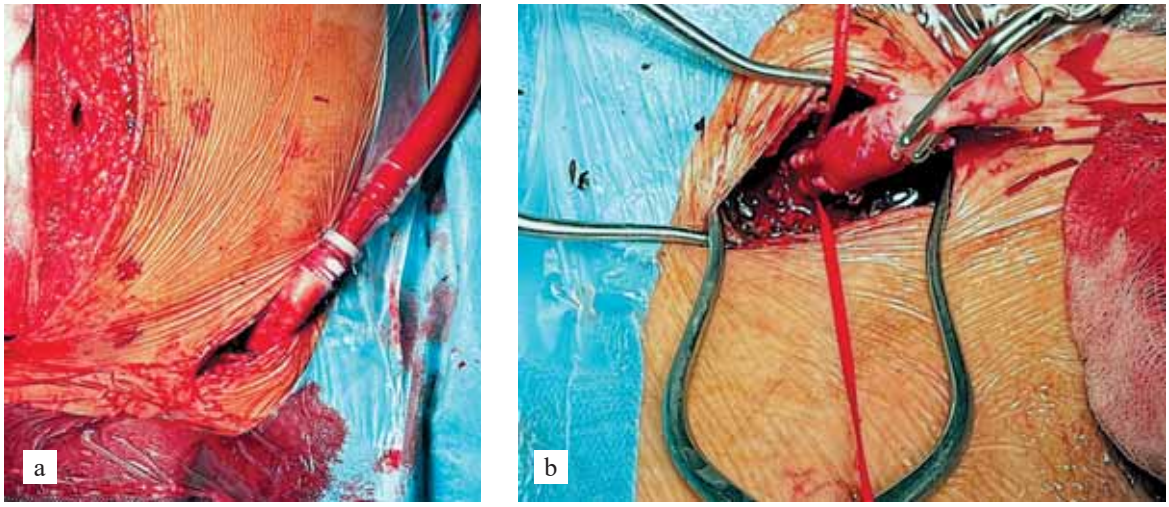

Fig. 3. Intraoperative photo: a, connection between the arterial trunk and homograft sutured to the subclavian artery; b, anastomosis between the subclavian artery and homograft

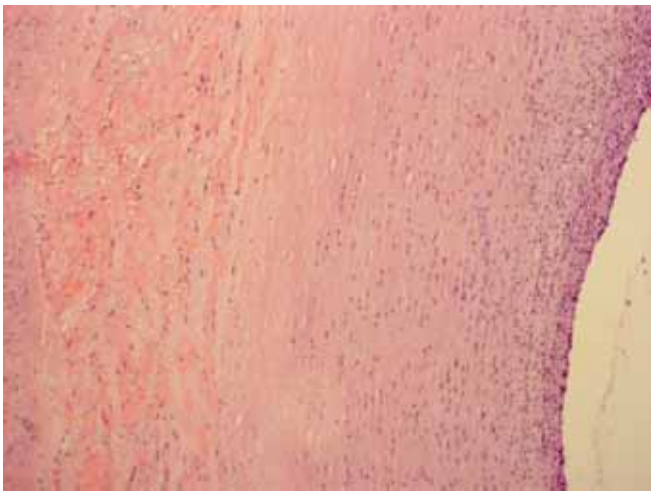

Fig. 4. Fragment of cryopreserved homograft. Inflammatory changes in the intima. H&E staining. ×400 magnification

DISCUSSION

ECMO plays a critical role in supporting patients with severe cardiovascular failure, especially during or after cardiac surgery [4, 5]. Cannulation in VA-ECMO can be central, or it can be peripheral [4]. The central cannulation technique is associated with a higher bleeding rate, increased need for blood transfusions, frequent reoperations, and surgical sternal diastasis, which requires delayed chest closure [6, 7]. When central cannulation is used for ECMO, the possibility of patient activation and mobilization is virtually nonexistent. According to

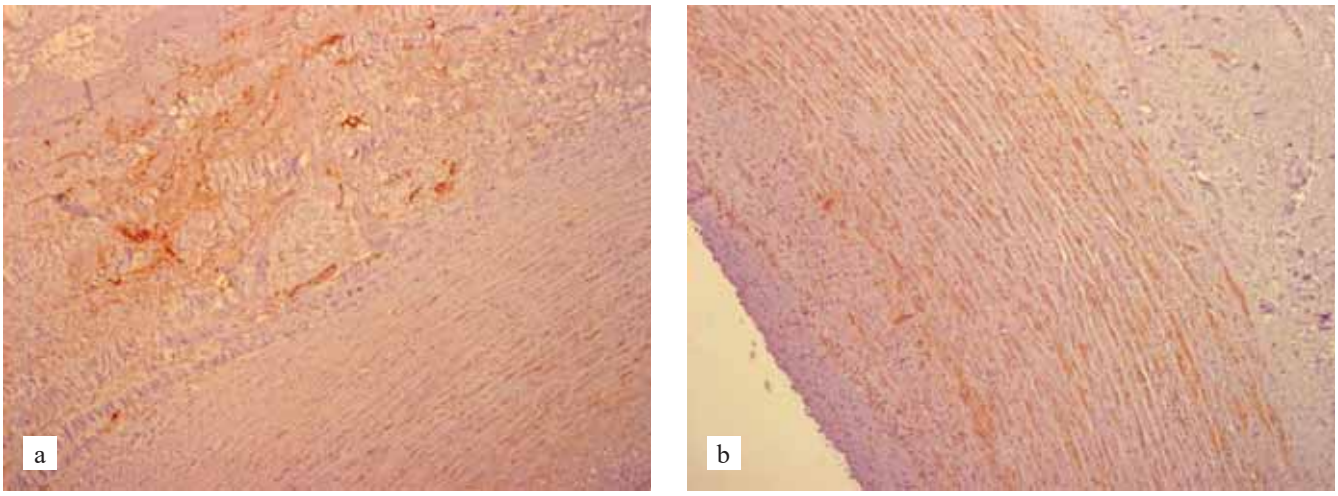

Fig. 5. Fragment of a cryopreserved homograft; a, formation of capacitance-type vessels, expression (CD34) in the adventitial layer; b, uneven positive actin expression (ASM). ×400 magnification. Immunohistochemistry

a multicenter registry analysis of 781 patients on ECMO and a meta-analysis, 30-day mortality was significantly higher in central ECMO compared to peripheral ECMO (72% *vs.* 61%, p = 0.004) [7].

Yes, peripheral VA-ECMO cannulation offers several advantages over central VA-ECMO, including less surgical trauma, quicker deployment, and greater potential for patient mobilization.

Peripheral VA-ECMO cannulation technique is able provides less surgical trauma, can be connected without the involvement of a surgical team, and has greater potential for patient mobilization [2]. At Meshalkin National Medical Research Center, over the past two years, peripheral VA-ECMO cannulation was applied in 61% of cases.

The common femoral artery and femoral vein are the standard vascular access points for peripheral VA-ECMO cannulation [2]. However, femoral cannulation has a unique challenge: its retrograde flow direction can, in some cases, increase left ventricular (LV) pressure, worsen LV dysfunction, promote pulmonary edema, elevate the risk of LV thrombosis, and significantly reduce the likelihood of myocardial recovery [9]. This scenario often necessitates additional interventions to unload the LV [10]. Various LV unloading methods exist, but they are generally invasive and may require supplementary mechanical support devices, depending on the chosen strategy [10].

When cannulating the subclavian artery, the most common approach involves inserting the arterial cannula through a vascular prosthesis (graft) that has been anastomosed to the artery. This technique preserves the integrity of the arterial lumen compared to direct cannulation through the arterial wall. It also simplifies the decannulation procedure, lowers the risk of limb ischemia, minimizes the chance of arterial dissection, and reduces the need for vascular wall grafting after ECMO discontinuation [11].

When cannulating the subclavian artery, the majority of nonpulsatile ECMO blood flow follows an antegrade direction through the aortic arch into the descending aorta. This approach is more physiologic and avoids increasing LV afterload, unlike femoral cannulation, where blood flow opposes the natural direction from the left ventricle [9, 12].

We have presented a clinical case of ECMO application in the peripheral venoarterial variant over 27 days, utilizing cannulation through a cryopreserved abdominal aortic homograft. The homograft was anastomosed to the subclavian artery, marking the first known clinical application of this technique. A review of literature databases (PubMed, Google Scholar, eLIBRARY) revealed no previously reported cases of homograft use for subclavian artery cannulation in ECMO procedures.

Cannulation into the homograft provided several advantages. First, it significantly reduced bleeding at the arterial cannula insertion site, even under high pressure (up to 250 mmHg) at the anastomosis level. This was due to the vascular graft's natural elasticity and the absence of anastomosis deformation. In contrast, synthetic prostheses, with their rigid walls and porosity, often present challenges in achieving satisfactory hemostasis – not only along the anastomosis line but also at puncture sites and due to prosthesis wall leakage. Second, the use of a homograft improved the positional maneuverability of the cannula.

The quality of a cryopreserved homograft is directly influenced by its preparation technique, with warm ischemia time before preservation being a critical factor. The term "homovital" refers to the preservation of viability in a significant portion of the endothelium, fibroblasts, and interstitial structures even after graft preservation.

It should be noted that the cryopreservation process itself does not cause significant damage to intact tissue. The strongest and most elastic graft walls are observed in homografts retrieved from brain-dead donors during multi-organ procurement, as these tissues experience no warm ischemia. In contrast, grafts obtained from cadavers hours or days after biological death have a significantly higher risk of structural failure and rupture due to degradation of vascular integrity [3].

Studies have demonstrated that cellular metabolism remains unchanged during cold ischemia for up to 24 hours and warm ischemia of no more than 12 hours. However, Yankah and Hetzer (1987) found that only 24% of endothelial cells survive after 2 hours of warm ischemia, and that prolonged warm ischemia of 12 hours results in cell apoptosis. The histological findings in this study align with previously published literature, confirming the preservation of a significant portion of the morphological structures in a homovital cryopreserved homograft.

The primary drawback of the presented technique is the inability to perform an emergency ECMO connection, as the graft thawing process (approximately 1.5–2 hours) and anastomosis formation require a certain amount of time. Additionally, in the context of organ shortages, maintaining a consistent stock of homografts with the required diameter may not always be feasible. From a legal perspective, the use of a homograft constitutes the transplantation of a "section of the vascular bed", necessitating compliance with all procedural and documentation requirements, which may be challenging to fulfill in enmergency cases.

CONCLUSION

The presented clinical case highlights the successful use of a cryopreserved vascular homograft for peripheral ECMO connection. Effective control of hemorrhagic complications during prolonged mechanical support is a crucial factor in achieving positive outcomes. This underscores the importance of accumulating further clinical experience with this technique to draw definitive conclusions regarding its effectiveness.

The authors declare no conflict of interest.

REFERENCES

1. *Whitman GJR.* Extracorporeal membrane oxygenation for the treatment of postcardiotomy shock. *J Thorac Cardiovasc Surg*. 2017 Jan; 153 (1): 95–101. https://doi.org/10.1016/j.jtcvs.2016.08.024.
2. *Kervan U, Kocabeyoglu SS, Sert DE, Aygün E, Kavasoglu K, Karahan M et al.* A novel technique of subclavian artery cannulation for venoarterial extracorporeal membrane oxygenation. *Exp Clin Transplant*. 2017 Dec; 15 (6): 658–663. doi: 10.6002/ect.2016.0002.
3. *Ostrovsky YuP, Spiridonov SV, Muratov RM, Yudina OA*. Technology of manufacturing and technique of using cryopreserved allografts in surgery of aortic valve malformations. Minsk: Belarusian Science, 2016. 232 p.
4. *Jacob S, MacHannaford JC, Chamogeorgakis T, Gonzalez-Stawinski GV, Felius J, Rafael AE et al.* Ambulatory extracorporeal membrane oxygenation with subclavian venoarterial cannulation to increase mobility and recovery in a patient awaiting cardiac transplantation. *Proc (Bayl Univ Med Cent)*. 2017 Apr; 30 (2): 224–225. https://doi.org/10.1080/08998280.2017.11929596.
5. *Wallinder A, Pellegrino V, Fraser JF, McGiffin DC*. ECMO as a bridge to non-transplant cardiac surgery. *J Card Surg*. 2017 Aug; 32 (8): 514–521. https://doi.org/10.1111/jocs.13172.
6. *Raffa GM, Kowalewski M, Brodie D, Ogino M, Whitman G, Meani P et al.* Meta-analysis of peripheral or central extracorporeal membrane oxygenation in postcardiotomy and non-postcardiotomy shock. *Ann Thorac Surg*. 2019 Jan; 107 (1): 311–321. https://doi.org/10.1016/j.athoracsur.2018.05.063.
7. *Mariscalco G, Salsano A, Fiore A, Dalén M, Ruggieri VG, Saeed D et al.* Peripheral versus central extracorporeal membrane oxygenation for postcardiotomy shock: multicenter registry, systematic review, and meta-analysis. *J Thorac Cardiovasc Surg*. 2020 Nov; 160 (5): 1207–1216.e44. https://doi.org/10.1016/j.jtcvs.2019.10.078.
8. *Saeed D, Stosik H, Islamovic M, Albert A, Kamiya H, Maxhera B, Lichtenberg A*. Femoro-femoral versus atrio-aortic extracorporeal membrane oxygenation: selecting the ideal cannulation technique. *Artif Organs*. 2014 Jul; 38 (7): 549–555. https://doi.org/10.1111/aor.12245.
9. *Ahmed Y, Lynch SR, Haft JW, Moll FL, van Herwaarden JA, Burris NS et al.* Patient-specific computational modeling of different cannulation strategies for extracorporeal membrane oxygenation. *ASAIO J*. 2022 Nov 1; 68 (11): e179–e187. doi: 10.1097/MAT.0000000000001819.
10. *Ezad SM, Ryan M, Donker DW, Pappalardo F, Barrett N, Camporota L et al.* Unloading the left ventricle in venoarterial ECMO: in whom, when, and how? *Circulation*. 2023 Apr 18; 147 (16): 1237–1250. https://doi.org/10.1161/CIRCULATIONAHA.122.062371.
11. *Gautier SV, Poptsov VN, Spirina EA.* Extracorporeal membrane oxygenation in cardiac surgery and transplantology. M.–Tver: Triada, 2013. 272 p.
12. *Kinsella JP, Gerstmann DR, Rosenberg AA*. The effect of extracorporeal membrane oxygenation on coronary perfusion and regional blood flow distribution. *Pediatr Res*. 1992 Jan; 31 (1): 80–84. doi: 10.1203/00006450-199201000-00015.
13. *Smit FE, Bester D, van den Heever JJ, Schlegel F, Botes L, Dohmen PM*. Does prolonged post-mortem cold ischemic harvesting time influence cryopreserved pulmonary homograft tissue integrity? *Cell Tissue Bank*. 2015 Dec; 16 (4): 531–544. doi: 10.1007/s10561-015-9500-2.

The article was submitted to the journal on 22.07.2024

DOI: 10.15825/1995-1191-2025-1-90-102

DECELLULARIZED PORCINE LIVER SCAFFOLD FOR MAINTAINING THE VIABILITY AND CAPACITY OF PANCREATIC ISLETS

N.V. Baranova[1], A.S. Ponomareva[1], A.D. Belova[1], L.A. Kirsanova[1], D.D. Filin[1, 2], E.A. Nemets[1], Yu.B. Basok[1], V.I. Sevastianov[1, 3]

[1] Shumakov National Medical Research Center of Transplantology and Artificial Organs, Moscow, Russian Federation
[2] Mendeleev University of Chemical Technology of Russia, Moscow, Russian Federation
[3] Institute of Biomedical Research and Technology, Moscow, Russian Federation

Bioengineered pancreatic constructs based on scaffolds made from decellularized tissues and pancreatic islets (PIs) may be used to extend the functional activity of transplanted PIs in patients with type I diabetes. Objective: to investigate *in vitro* the effect of decellularized porcine liver scaffold (DPLS) on the viability and insulin-producing capacity of isolated human PIs. **Materials and methods.** The resulting DPLS was subjected to histological examination, DNA quantification, and cytotoxic effect testing. The PIs were isolated from human pancreas fragments using the collagenase technique. Under standard conditions, PIs were cultured in three different environments: monoculture (control group), with DPLS present (experimental group 1) or with decellularized human pancreas scaffold (DHPS) present (experimental group 2). Vital fluorescent dyes were used to evaluate the viability of PIs. Basal and glucose-loaded insulin concentrations were determined by enzyme immunoassay. **Results.** The basic composition and structure of the extracellular matrix of liver tissue in DPLS samples were preserved thanks to the selected decellularization procedure. The samples had no cytotoxic effect, and the residual amount of DNA in the scaffold did not exceed 1.0%. PIs from the experimental groups showed no significant signs of degradation and fragmentation during the 10-day incubation period compared to PIs from the control group. On day 10, the viability of PIs from experimental group 1 was 64%, that of experimental group 2 was 72%, and that of the control group was less than 20%. After the first day of culturing, insulin concentration were 29.0% higher in experimental group 1 and 39.1% higher in experimental group 2 compared to the control group. On day 10 of the experiment, insulin levels in experimental groups 1 and 2 differed by 124.8% and 150.9%, respectively, from the control group. Under a glucose load, the insulin level in experimental group 1 was 1.7 times higher than in the control group, whereas that of experimental group 2 was 2.2 times higher. **Conclusion.** The resulting DPLS has a positive effect on the viability and insulin-producing capacity of PIs. When creating a bioengineered construct of PIs, DPLS can be used as a component obtained in sufficient quantity from an available source.

Keywords: decellularization, porcine liver, scaffold, pancreatic islets.

INTRODUCTION

Transplantation of functionally active pancreatic islets (PIs) is generally considered one of the safest and least invasive transplantation methods for treating severe cases of type I diabetes mellitus (T1D) [1]. A major focus in cell therapy research in the treatment of T1D is to maintain the viability and functional activity of transplanted beta cells as long as possible. Several key challenges impact islet graft survival, including hypoxia, oxidative stress, partial portal vein thrombosis, and the immediate blood-mediated inflammatory response. In addition, the isolation process itself significantly compromises PI viability and function before transplantation even occurs. PIs vascularization and innervation are disturbed, and the signaling interaction between islet cells and components of extracellular matrix (ECM) is fundamentally changed.

Recent advances in tissue engineering have opened new possibilities for improving the long-term survival and function of transplanted PIs [2–4]. One of the most promising strategies involves bioengineered endocrine pancreas constructs that utilize decellularized scaffolds recellularized with insulin-producing cells [5]. To obtain scaffolds, organs or tissues undergo a decellularization process to remove immunogenic cellular components, while preserving the ECM (proteins and growth factors) composition as much as possible [6, 7].

Three-dimensional (3D) scaffolds, purified from DNA and retaining essential proteins, create a microenvironment that supports functional cell survival and activity. This allows optimizing conditions for their prolonged viability [3]. In addition, decellularized tissue scaffolds provide efficient repopulation by functional cells, as they contain the appropriate 3D architecture and preserved

Corresponding author: Anna Ponomareva. Address: 1, Shchukinskaya str., Moscow, 123182, Russian Federation. Phone: (499) 196-26-61; (926) 585-23-73. E-mail: a.s.ponomareva@gmail.com

spatial framework of ECM components to maintain cell adhesion and functional activity.

Decellularized pancreas scaffolds (DPS) provide a highly supportive environment for PIs by maintaining their structural integrity, prolonging viability, and enhancing insulin secretion compared to standard culture conditions. Research has demonstrated that culturing islets in the presence of DPS prolonges survival and functioning *in vivo* [10, 11].

The liver and pancreas are known to share a similar embryonic developmental pathway (arising from the same part of the foregut entoderm). The ECM of the liver and pancreas share similar components, including type I, III, and IV collagen, elastin, laminin, fibronectin, and glycosaminoglycans [4, 7]. Given these similarities, a decellularized liver scaffold (DLS) may serve as an alternative framework for bioengineered constructs, offering a supportive environment for insulin-producing cells.

Furthermore, the transplantation of islets into the liver parenchyma via the portal vein remains the primary clinically approved site for islet transplantation [12, 13]. DLS have shown great potential in preserving both liver cells [14, 15] and endocrine islet cells [16]. For instance, studies have demonstrated that 3D scaffolds obtained from decellularized whole mouse liver lobes significantly enhance the survival and function of isolated mouse PIs *in vitro* [17].

Goh et al. demonstrated that mouse DLS can be successfully repopulated with insulin-producing cell aggregates derived from differentiated pluripotent human embryonic stem cells. The extensive vascular network of DLS allowed for even distribution of cell aggregates, unlike DPS, enabling efficient nutrient and oxygen supply to the insulin-producing cells during cultivation in a bioreactor for nine days [18].

The potential of scaffolds from other decellularized organs to prolong the function of PIs has also been demonstrated. In [19], it was shown that decellularized rat spleen scaffolds can serve as a promising carrier for beta-cell transplantation. When MIN6 cells (a mouse insulinoma beta-cell line) were seeded onto these scaffolds, insulin production was significantly increased compared to traditional 2D culture. Bioartificial PIs created using decellularized pig lung scaffolds and human PIs exhibited high viability and insulin production *in vitro* comparable to freshly isolated islets. This makes them a promising platform for real-time drug screening [20].

This strategy for creating a bioengineered pancreatic construct is expected to find potential applications in preclinical trials, drug development, and diabetes therapy.

When creating a bioengineered construct based on functional human cells and decellularized allogeneic scaffold, the problem of organ shortage cannot be avoided, which makes it necessary to obtain scaffold from xenogeneic material, for example, porcine. In addition, implants derived from decellularized porcine tissues and organs, such as skin, bladder, heart valves, and small intestine, have been successfully used in clinical practice [21]. We also note that the exocrine activity of the pancreas, and, accordingly, the possibility of self-digestion of pancreatic tissue complicates the collection and transportation of the xenogeneic organ. The liver is devoid of this disadvantage, which makes it attractive for pancreatic tissue engineering.

The **objective** of our work was to obtain decellularized porcine liver scaffold (DPLS) and to study *in vitro* its effect on the viability and insulin-producing function of isolated human islets of Langerhans.

MATERIALS AND METHODS

Objects of research

Pancreatic tissue fragments obtained during pancreatic resection in patients were used to isolate PIs and obtain a decellularized human pancreas scaffold (DHPS). All manipulations were performed according to the World Medical Association's (WMA) Declaration of Helsinki "Recommendations Guiding Physicians in Biomedical Research Involving Human Subjects", adopted by the 18th World Medical Assembly, held in Helsinki, Finland in 1964 according to the current revised text. A report (dated March 16, 2018, Protocol No. 160318-1/1/1e) approving the experimental studies was obtained from the Local Ethics Committee of Shumakov National Medical Research Center of Transplantology and Artificial Organs.

Pancreatic tissue fragments were placed in Hanks' Balanced Salt solution (+4 °C) with antibiotic/antimycotic and stored at +4 °C…+6 °C for no more than 10 hours before the islet isolation procedure.

DHPS obtained by decellularization of human pancreatic tissue fragments according to our previously developed protocol [22] was used in the experiments.

DPLS was obtained using pig liver (weight 20 kg, age 3 months, Promagro, Stary Oskol).

Obtaining and studying decellularized porcine liver scaffold

Porcine liver was decellularized (Fig. 1) guided by a protocol including treatment of mechanically chopped tissue (fragment size no larger than 2×2×2×2 mm) in three shifts (24 hours for each shift) of phosphate-buffered saline (PBS) containing 0.1% sodium dodecyl sulfate (SDS) and increasing concentrations of Triton X-100 (1%, 2%, and 3%), and treatment with deoxyribonuclease I (DNase I) (Sci-Store, Russia) [23]. Porcine liver fragments were processed at room temperature under continuous stirring on a magnetic stirrer at a speed of 300 rpm. To achieve complete removal of cellular components, measured by the residual amount of DNA, DPLS was treated in a DNase I solution. Next, DPLS were washed of residual surfactants for 72 hours

by incubating the samples in PBS containing antibiotic/antimycotic. DPLS samples were sterilized by gamma irradiation with a dose of 1.5 Mrad.

Sterile DPLS samples were stored at –20 °C and, immediately before the experiment, were crushed to a particle size of 500 ± 45 μm to reduce the degree of microheterogeneity.

DNA content in the original and decellularized porcine liver tissue was determined. For this purpose, DNA was isolated from the samples using DNeasy Blood & Tissue Kit (QIAGEN, Germany) according to the manufacturer's instructions. For DNA quantification, we used fluorescent dye Quant-iT PicoGreen (Thermo Fisher Scientific, USA) and microplate reader Spark 10M (Tecan Trading, Switzerland), which was used to analyze the resulting thermionic emission at 520 nm wavelength.

For histological examination, the original tissue and DPLS samples were fixed in 10% buffered formalin (Biovitrum, Russia), washed in running water, dehydrated in ethanol of ascending concentration (70%, 80%, 90% and 96%), incubated in a mixture of 96% ethanol and chloroform and embedded in paraffin. Histological sections were deparaffinized, rehydrated, and stained with Mayer's hematoxylin (Dako, Denmark) and 1% eosin solution (Biovitrum, Russia) and according to the Masson trichrome method for total collagen. The stained sections were encapsulated in Bio Maunt balm (Bio-Optica, Italy). The preparations were analyzed and photographed using a Nikon Eclipse Ti inverted microscope (Nikon, Japan).

In vitro cytotoxicity of the DPLS samples was evaluated by direct contact method in accordance with the standard GOST ISO 10993-5-2011 [24] on a culture of the NIH/3T3 mouse embryonic fibroblasts. Cells were seeded into 24-well flat-bottom culture plates and incubated at +37 °C under standard conditions until a monolayer with an 80–85% confluence was formed. The tested samples were placed on the surface of the formed cell monolayer. Cell morphology was evaluated after 24 hours of incubation. Complete growth medium for NIH/3T3 cells served as a negative control, and a standard zinc solution in nitric acid (9.95 mg Zn in 1–2 wt.% HNO_3, dilution 1:200 with 0.9% NaCl solution for injection) served as a positive control. The cell culture was visually evaluated using a Nikon Eclipse Ti light microscope (Nikon, Japan).

Isolation and identification of human pancreatic islets

Islets were isolated by focusing on the collagenase technique using collagenase NB1 (activity 20 PZ U/g tissue) and neutral protease NP (activity 1.5 DMC U/g tissue) (Serva, Germany) [9, 22].

Freshly isolated islets were identified using dithizone staining (Sigma-Aldrich, USA), which labels zinc in insulin granules. For this purpose, part of the suspension was mixed with the dye solution in a 2:1 ratio and incubated for 20–30 min at +37 °C. Staining and islet counting were performed using a Nikon Eclipse Ti light microscope (Nikon, Japan). The resulting islet suspension was resuspended in complete growth medium and used in the experiment within 24 hours of isolation.

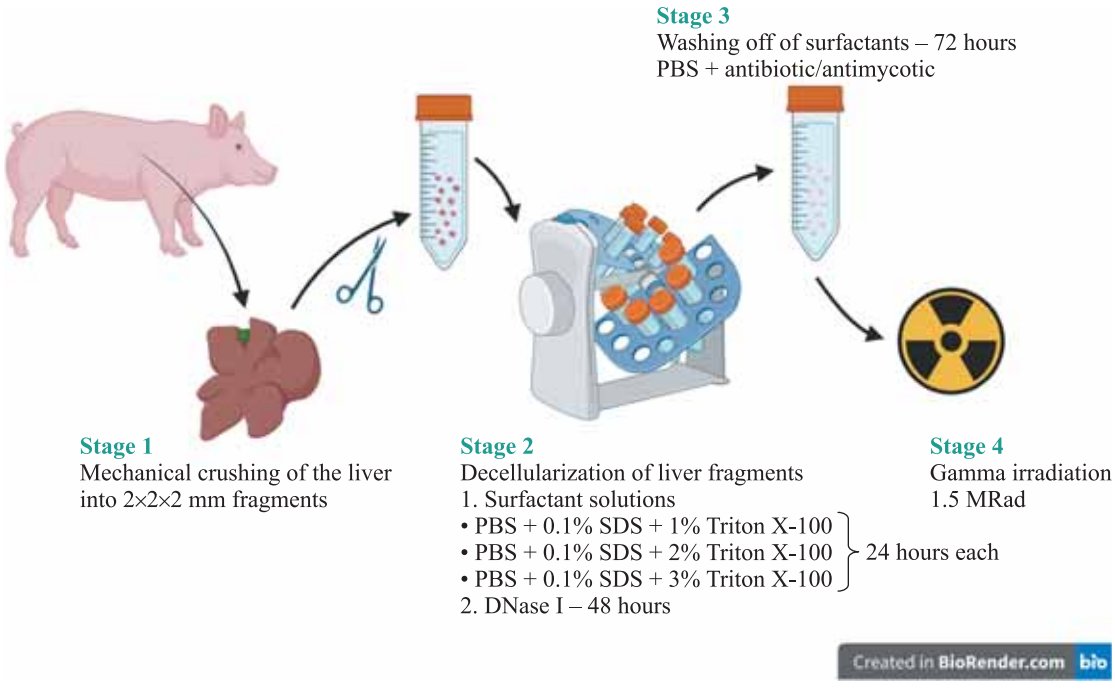

Fig. 1. Schematic representation of how a decellularized porcine liver scaffold (DPLS) is obtained

Cultivation of human pancreatic islets in monoculture and in the presence of scaffolds

Approximately equal amounts of isolated islets (n = 250 ± 10) were added to three 25 cm^2 culture vials (Greiner bio-one, Germany). No scaffolds were added to the first culture vial (control group). In the second culture vial, 20.0 ± 0.1 mg of DPLS was added (experimental group 1). In the third culture vial, 20.0 ± 0.1 mg DHPS was added (experimental group 2). Islets from control and experimental groups were cultured in complete growth medium containing DMEM (1.0 g/L glucose) (PanEco, Russia), 10% ETS (HyClone, USA), Hepes (Gibco, USA), 2 mM L-glutamine (PanEco, Russia), 1% antibiotic/antimycotic (Gibco, USA). Islets were cultured under standard conditions at +37 °C in a humidified atmosphere containing 5% CO_2, with daily visual monitoring and photography using a Nikon Eclipse Ti inverted microscope (Nikon, Japan) equipped with a digital camera. The culture medium was changed at days 1, 3, 7, and 10 in order to collect samples for further investigation of insulin content by enzyme-linked immunosorbent assay (ELISA).

Determination of pancreatic islet viability

To assess the viability of freshly isolated and cultured human PIs, fluorescent staining was performed using the LIVE/DEAD Cell Viability/Cytotoxicity Kit (Molecular Probes, USA). A portion of the islet suspension (either in monoculture or with scaffolds) was placed in a Petri dish, mixed with the prepared working dye solution at a 2:1 ratio, and incubated in the dark for 15–30 minutes. Viable islets, indicated by green fluorescence, were counted using a Nikon Eclipse 50i fluorescent microscope (Nikon, Japan).

Determination of insulin-producing function of pancreatic islets

The basal concentration of insulin in control and experimental groups at day 1, 3, 7 and 10 was determined using the ELISA Kit for insulin Human CEA448 Hu-96 (Cloud-Clone Copr., USA) according to the manufacturer's instructions. For this purpose, growth medium containing 2.8 mmol/L glucose was replaced in culture vials. After 1 hour of incubation under the same conditions (+37 °C, 5% CO_2), the culture medium was sampled.

Changes in hormone levels under glucose loading (up to 25 mmol/L) were assessed on the second day of incubation. The growth medium was first replaced with fresh medium containing a low glucose concentration (2.8 mmol/L). After a 60-minute incubation under standard conditions, culture medium samples were collected and frozen at –23 °C. The growth medium was then replaced with fresh medium containing a high glucose concentration (25 mmol/L), followed by another 60-minute incubation. Culture medium samples were again collected (two per cultivation period) and frozen at –23 °C for further ELISA analysis.

Quantification was performed by measuring optical density using a Spark 10M microplate reader (Tecan Trading, Switzerland) with Spark Control Magellan V1.2.20 software. Readings were taken at wavelengths of 450 nm and 550 nm to correct for optical defects in the microplate. Statistical analysis was conducted using Microsoft Office Excel (2016), with differences considered statistically significant at $p < 0.05$.

RESULTS AND DISCUSSION

Decellularized porcine liver scaffold

Decellularization of porcine liver fragments was achieved using a combination of chemical (SDS and Triton X-100) and enzymatic (DNAse I) treatments. This process resulted in finely dispersed decellularized porcine liver scaffold (DPLS) with a residual DNA content of no more than 10.3 ± 1.5 ng/mg – less than 1% of the DNA present in native liver. Additionally, the fine fiber structure and essential extracellular matrix (ECM) components of the porcine liver were preserved.

Native porcine liver tissue is characterized by a pronounced division of the parenchyma into lobules bounded by connective tissue layers (Fig. 2, a). In Masson's trichrome stain, blue collagen fibers are well identified in connective tissue strands (Fig. 2, b).

DPLS specimens are characterized by preserved fibrous structure with the presence of clearly distinguishable thin ECM fibers. In the structure of the scaffold, both interlobular and intralobular stroma are determined (Fig. 2, c, d). At the same time, the samples are free of cells and cellular detritus, which is also confirmed by quantification of the content of preserved DNA.

In vitro evaluation confirms that the biocompatibility of DPLS meets biosafety criteria regarding cytotoxicity. Cytotoxicity results were assessed based on the degree of cell response after incubation with the samples. Fibroblast morphology and viability remained unchanged upon contact with DPLS samples, relative to the negative control (response degree 0) (Fig. 2, e, f). These findings indicate that the studied samples exhibit no cytotoxic effects.

According to *in vitro* evaluation, the biocompatible properties of DPLS meet the biosafety criteria for cytotoxicity. Cytotoxicity results were analyzed according to the evaluation scale of the degree of cell response after incubation with the samples. Upon contact with DPLS samples, the morphology and viability of fibroblasts relative to the negative control did not change (response degree 0) (Fig. 2, e, f). Thus, the studied samples have no cytotoxic effect.

Freshly isolated human pancreatic islets

After isolation, we observed a significant number of islets of various sizes with predominantly round shape and smooth surface. Selective dithizone red-orange staining of β-cells allowed identification of PIs (Fig. 3, a). LIVE/DEAD staining demonstrated green fluorescence in 95–98% of freshly isolated islets (Fig. 3, b).

Viability of pancreatic islets

After isolation, most PIs in the control group retained their shape and structural integrity during the first three days of incubation, with only a few exhibiting signs of fragmentation and degradation. Fluorescent microscopy analysis revealed that 78% of PIs remained viable in the control group after one day of culturing, decreasing to

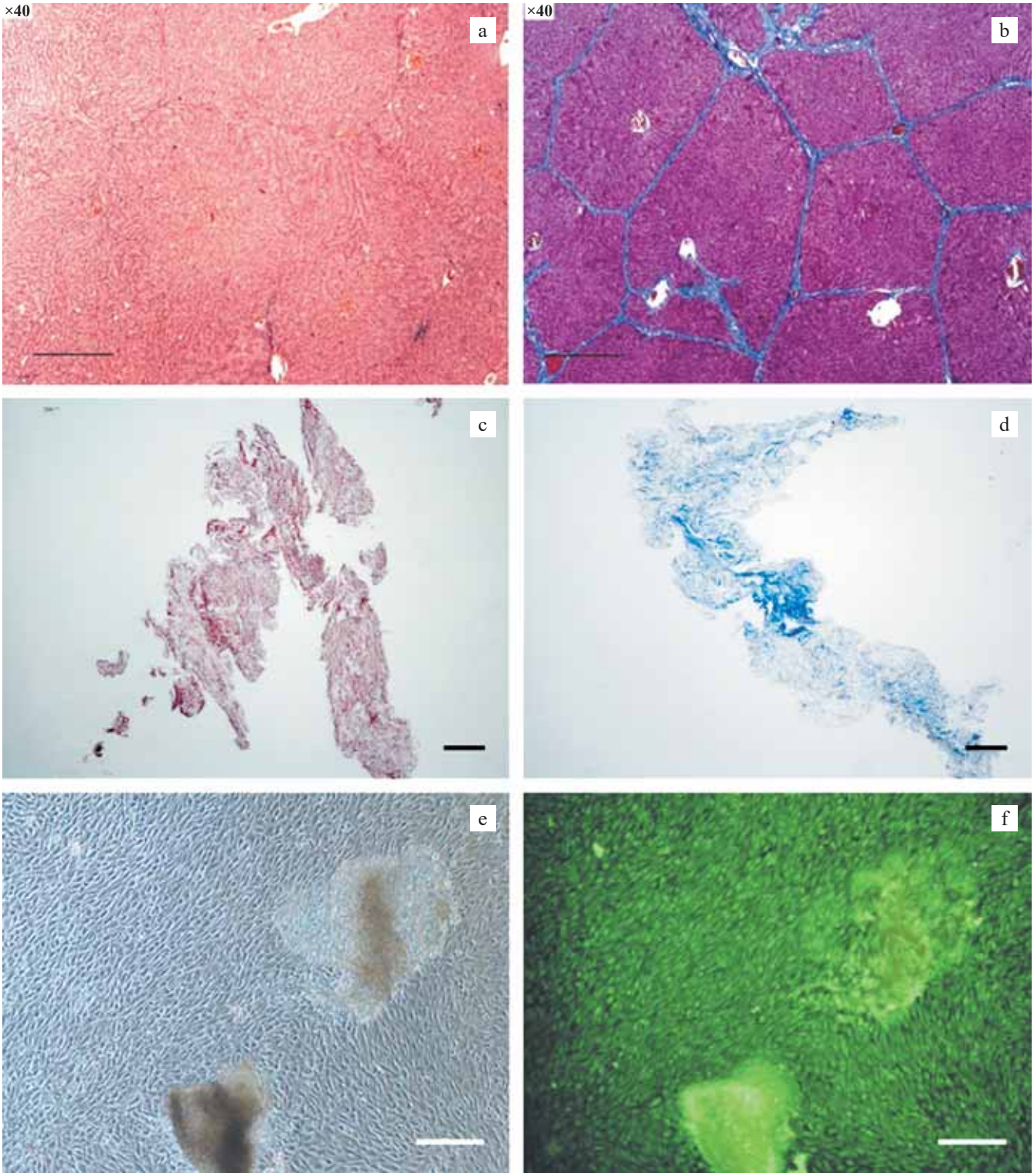

Fig. 2. Native porcine liver (a, b) and DPLS (c, d): a, c – H&E staining; b, d – Masson trichrome staining. NIH/3T3 fibroblasts cultured with DPLS: e, phase-contrast microscopy; f, LIVE/DEAD fluorescent staining. Scale bar 100 μm

approximately 60% by day three (Fig. 4). However, by the third day, noticeable morphological changes were observed, including cavity formation, fragmentation, and irregular surface contours in many PIs. By the end of the first week, significant structural deterioration had occurred, reducing PI viability to below 30%, and by day 10, viability dropped to less than 20% (Fig. 5, a, b).

Isolated islets cultured with DPLS (experimental group 1) and DHPS (experimental group 2) exhibited no signs of destruction or fragmentation throughout the 10-day observation period. Most islets showed adhesive properties, attaching to the fibrous scaffold surface, while those remaining in the culture medium continued to float. LIVE/DEAD staining on day 1 of incubation confirmed the viability of most islets, with 83% viability in experimental group 1 and 85% in experimental group 2. By day 3, islet viability was 77% and 82% for experimental groups 1 and 2, respectively (Fig. 4). A gradual decline in viability was observed by day 7, with 71% in experimental group 1 and 78% in experimental group 2. By day 10, islet viability decreased to 64% (Fig. 5, c, d) and 72% (Fig. 5, e, f), respectively. Notably, enhancing viability may be achievable through the use of a perfusion bioreactor, as the continuous circulation of culture medium could optimize nutrient and gas exchange while facilitating metabolic waste removal. This approach is

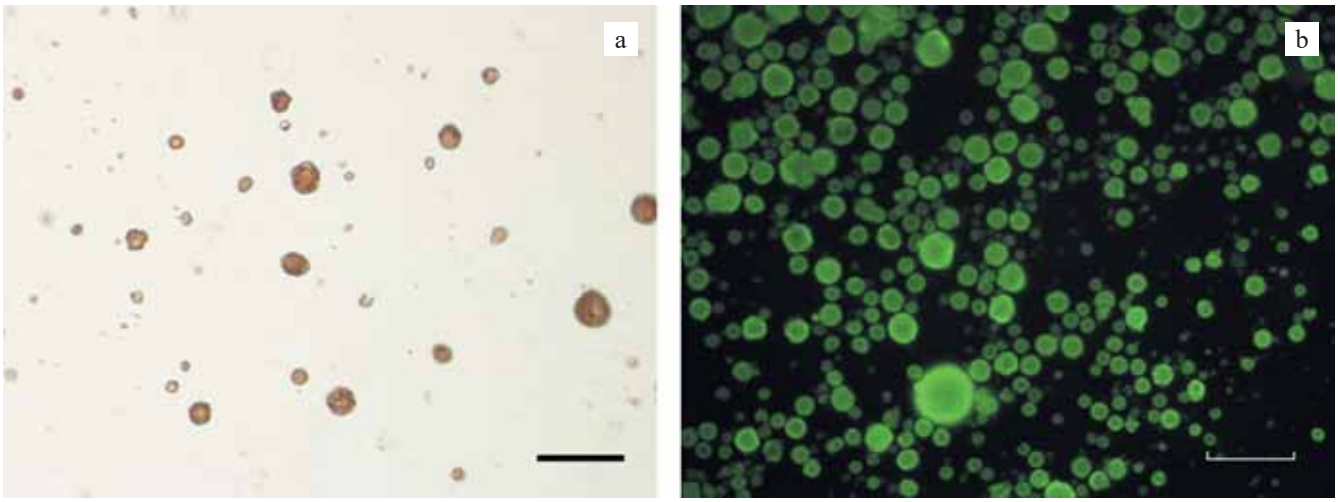

Fig. 3. Isolated human pancreatic islets: a, dithizone staining; b, LIVE/DEAD fluorescent staining. Scale bar 100 μm

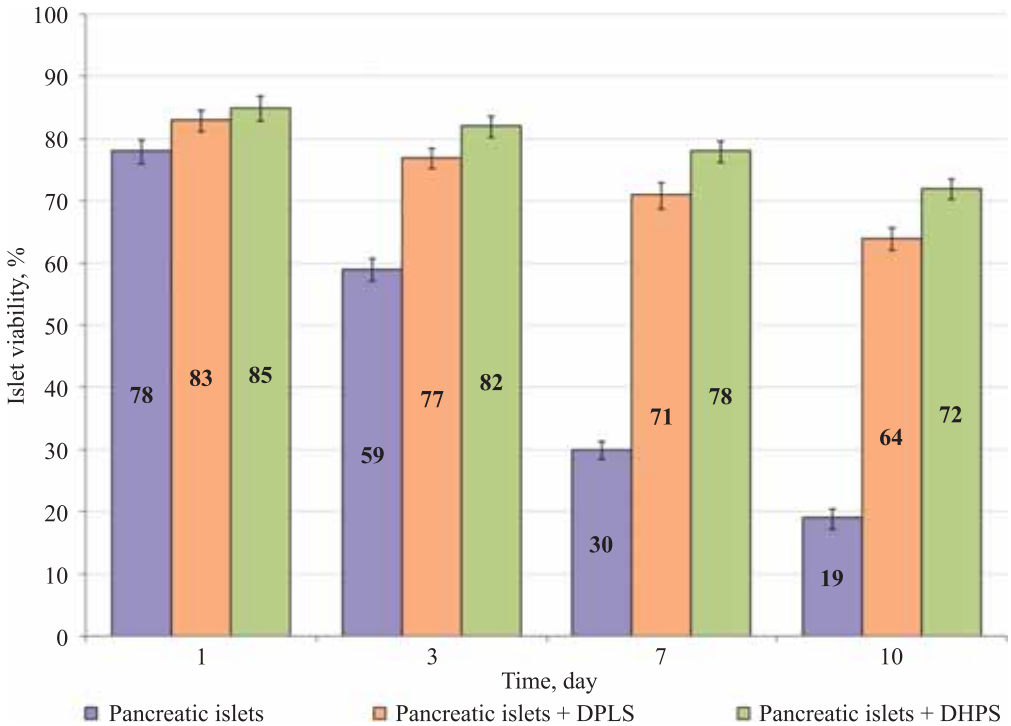

Fig. 4. Comparative analysis of the viability of pancreatic islets cultured in monoculture, with DPLS present and with DHPS present

particularly relevant for PIs embedded within the scaffold structure [25, 26].

Comparative analysis of insulin-producing function of human pancreatic islets in monoculture and in culture with scaffolds

The secretory capacity of human PIs in the control and experimental groups was determined at days 1, 3, 7 and 10, estimating the basal concentration of insulin in the culture medium.

After the first day of culturing, insulin levels were significantly higher in both experimental groups compared to the control. In experimental group 1, the insulin level increased by 29.0% (73.9 ± 8.0 pg/mL), while in experimental group 2, it rose by 39.1% (79.7 ± 7.6 pg/mL), compared to the control group (57.3 ± 6.1 pg/mL).

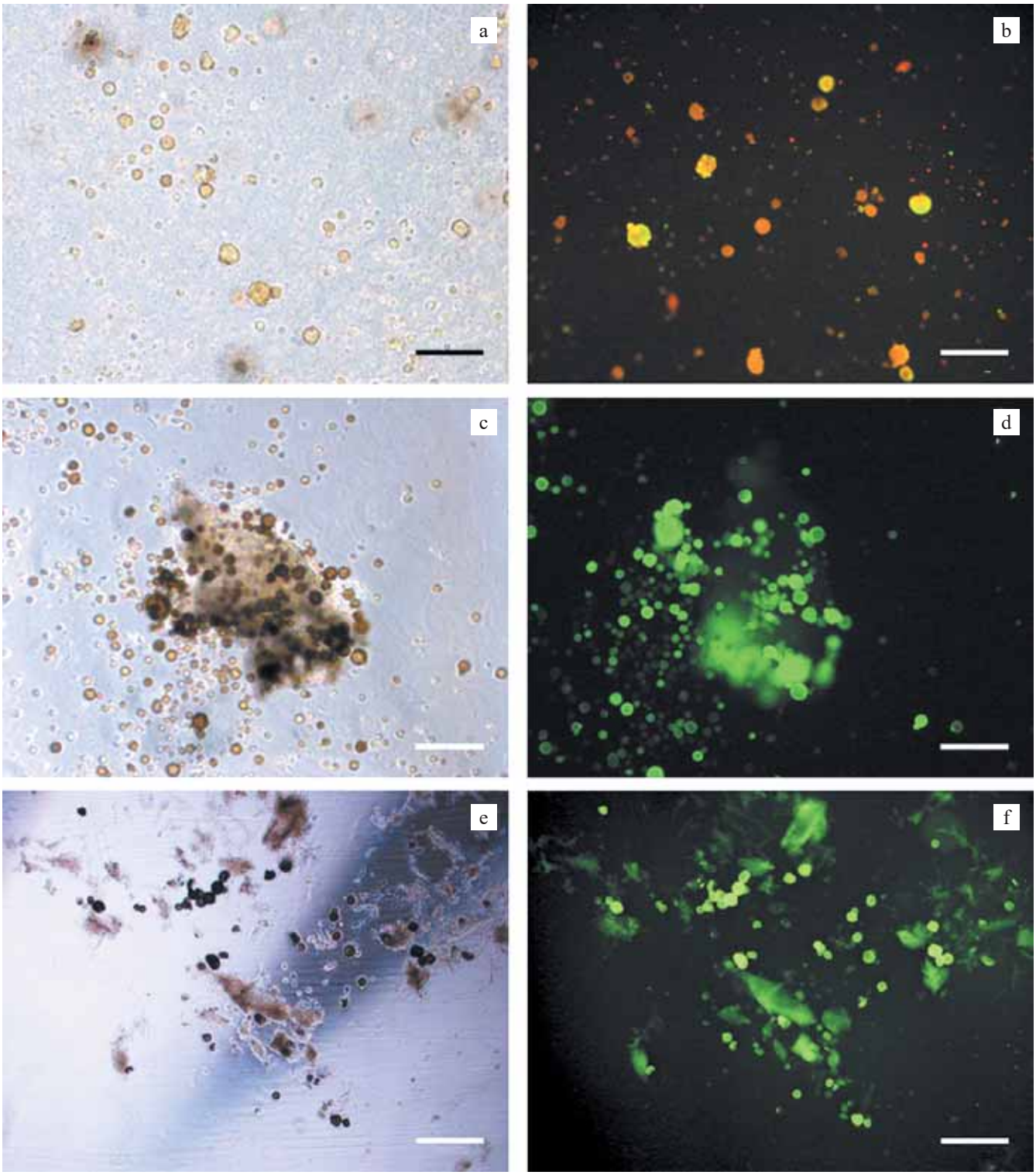

Fig. 5. Human pancreatic islets cultured in monoculture (a, b), with DPLS present (c, d) and with DHPS present (e, f). 10 days of culturing: a, c, e – inverted phase-contrast microscopy; b, d, f – LIVE/DEAD fluorescent staining. Scale bar 100 μm

By day 3 of incubation, insulin levels remained elevated, with experimental group 1 showing a 49.0% increase (62.0 ± 7.4 pg/mL) and experimental group 2 exhibiting a 69.0% increase (70.3 ± 7.0 pg/mL) relative to the control group (41.6 ± 4.9 pg/mL). By day 7, the difference in insulin levels between the experimental and control groups became even more pronounced. Insulin concentration in experimental group 1 (58.4 ± 6.9 pg/mL) was 70.8% higher than in the control group (34.2 ± 5.1 pg/mL), while experimental group 2 (63.3 ± 7.2 pg/mL) exhibited an 85.1% increase. At day 10, basal insulin production in experimental groups 1 and 2 was 124.8% and 150.9% higher than in the control group, respectively (Fig. 6, a). This corresponds to insulin secretion levels that were 2.25 and 2.51 times greater in experimental groups 1 and 2 compared to the control group. Thus, insulin secretion levels in experimental groups 1 and 2 were 2.25 and 2.51 times higher than in the control group, respectively (Fig. 6, b).

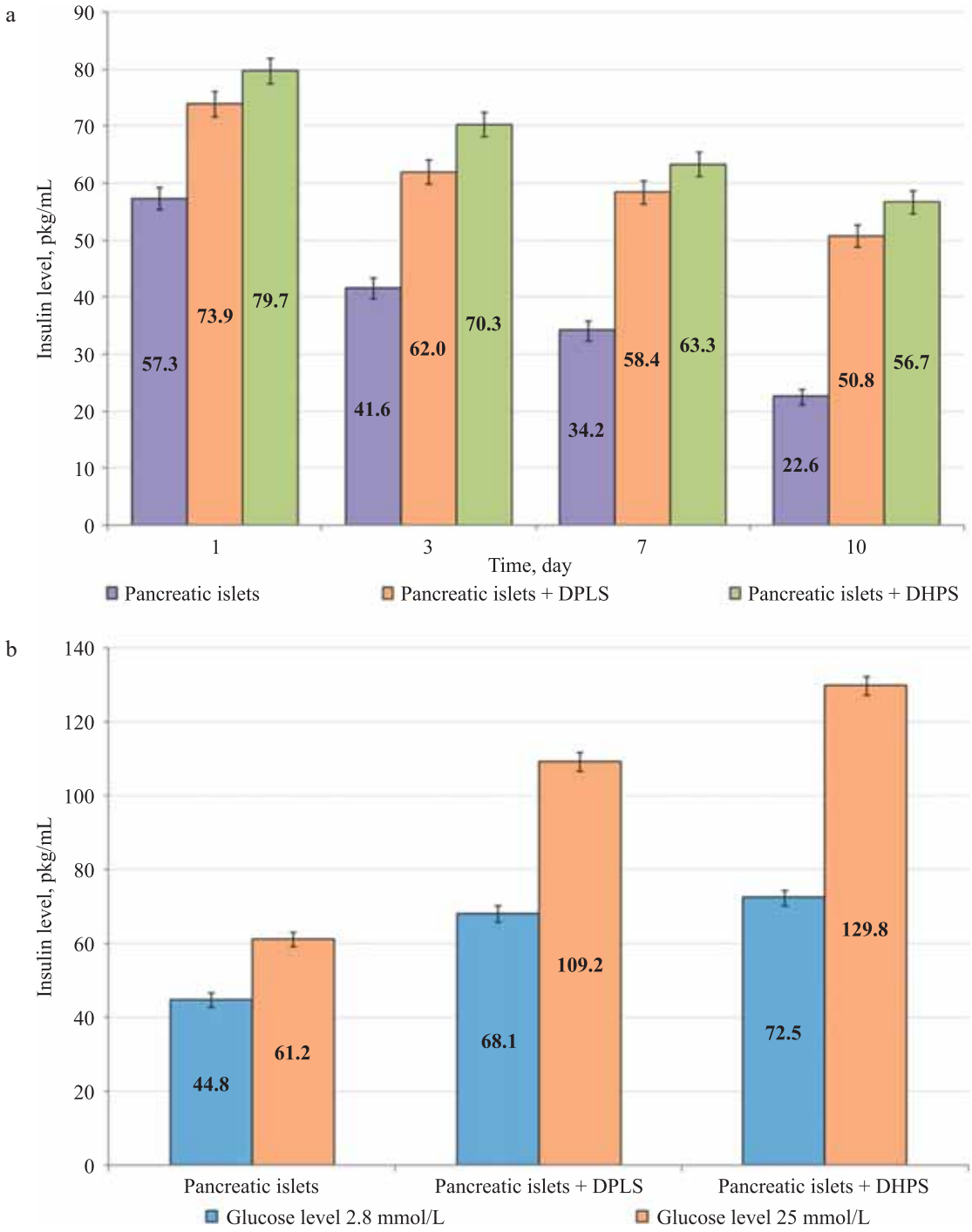

Fig. 6. Comparative analysis of the secretory capacity (a) and functional activity under glucose stimulation (b) of human pancreatic islets in monoculture (control group), cultured with DPLS (experimental group 1) and cultured with DHPS (experimental group 2)

The analysis of culture medium samples collected on day 2 of incubation, both before and after glucose stimulation (25 mmol/L), confirmed the functional activity of the cultured PIs. In the control group, insulin levels increased by 36.6% following glucose stimulation (from 44.8 ± 1.88 to 61.2 ± 1.98 pg/mL). In experimental group 1, insulin secretion rose by 60.4% (from 68.1 ± 2.13 to 109.2 ± 2.53 pg/mL), which was 1.7 times higher than in the control group. In experimental group 2, insulin levels increased by 79.0% (from 72.5 ± 2.07 to 129.8 ± 2.47 pg/mL), which was 2.2 times higher than in the control group and 1.2 times higher than in experimental group 1.

It is important to note that the relative basal insulin levels in the studied culture systems on day 2 of incubation were consistent with the values observed on days 1 and 3 when assessing islet secretory ability. This consistency confirms the reliability of the results obtained.

A comparative analysis of human PI viability and insulin secretion in the presence of DHPS or DPLS demonstrated that both scaffolds support PI survival and insulin production under standard culture conditions for 10 days, outperforming monoculture. Although DPLS had a slightly less pronounced effect on cultured PIs, its advantage lies in its availability and the ease of obtaining it in sufficient quantities compared to DHPS. The use of both DHPS and DPLS scaffolds for *in vitro* islet preservation may contribute to extending PI functionality *in vivo*.

In the future, DPLS may serve as a source for developing new biomaterials, such as macroporous sponges and hydrogels. The porous structure of these scaffolds not only enhances nutrient and gas transport but also promotes cellular colonization, vascular ingrowth, and nerve integration [27–29]. One potential approach for fabricating macroporous sponges with tailored mechanical properties is cryostructuring of DPLS hydrolysis products [30]. For instance, cryogenically structured biopolymer substrates, such as sponge agarose cryogel modified with gelatin, have demonstrated full biocompatibility and effectively supported long-term insulin secretion in cultured mouse islet cells [31, 32]. Additionally, a DPLS-based hydrogel could enable the development of injectable encapsulated cell-engineered constructs and be applied in 3D bioprinting technologies [33].

CONCLUSION

DPLS exhibits slightly lower efficacy than DHPS in supporting the viability, insulin secretion, and functional activity of human PIs. However, in the development of cell-engineered constructs, further studies exploring the use of decellularized liver scaffold – an abundant and readily available biomaterial – could contribute to advancements in both bioartificial liver and bioartificial pancreas technologies. This could enhance beta-cell maintenance and function *in vitro* and *in vivo*.

The authors declare no conflict of interest.

REFERENCES

1. *Ludwig B, Ludwig S, Steffen A, Saeger HD, Bornstein SR.* Islet versus pancreas transplantation in type 1 diabetes: Competitive or complementary? *Curr Diab Rep.* 2010; 10 (6): 506–511. doi: 10.1007/s11892-010-0146-y. PMID: 20830612.
2. *Abadpour S, Wang C, Niemi EM, Scholz H.* Tissue Engineering Strategies for Improving Beta Cell Transplantation Outcome. *Curr Transpl Rep*. 2021; 8 (3): 205–219. doi: 10.1007/s40472-021-00333-2.
3. *Abualhassan N, Sapozhnikov L, Pawlick RL, Kahana M, Pepper AR, Bruni A et al*. Lung-Derived Microscaffolds Facilitate Diabetes Reversal after Mouse and Human Intraperitoneal Islet Transplantation. *PLoS One.* 2016; 11 (5): e0156053. doi: 10.1371/journal.pone.0156053. PMID: 27227978; PMCID: PMC4881949.
4. *Damodaran GR, Vermette P*. Decellularized pancreas as a native extracellular matrix scaffold for pancreatic islet seeding and culture. *J Tissue Eng Regen Med.* 2018; 12 (5): 1230–1237. doi: 10.1002/term.2655. PMID: 29499099.
5. *Napierala H, Hillebrandt KH, Haep N, Tang P, Tintemann M, Gassner J et al.* Engineering an endocrine Neo-Pancreas by repopulation of a decellularized rat pancreas with islets of Langerhans. *Sci Rep*. 2017; 7: 41777. doi: 10.1038/srep41777. PMID: 28150744; PMCID: PMC5288794.
6. *Orlando G, Farney AC, Iskandar SS, Mirmalek-Sani SH, Sullivan DC, Moran E et al.* Production and implantation of renal extracellular matrix scaffolds from porcine kidneys as a platform for renal bioengineering investigations. *Annals of Surgery.* 2012; 256 (2): 363–370. doi: 10.1097/SLA.0b013e31825a02ab. PMID: 22691371.
7. *Song JJ, Ott HC*. Organ engineering based on decellularized matrix scaffolds. *Trends Mol Med.* 2011; 17 (8): 424–432. doi: 10.1016/j.molmed.2011.03.005. PMID: 21514224.
8. *Mirmalek-Sani SH, Orlando G, McQuilling JP, Pareta R, Mack DL, Salvatori M et al.* Porcine pancreas extracellular matrix as a platform for endocrine pancreas bioengineering. *Biomaterials.* 2013; 34 (22): 5488–5495. doi: 10.1016/j.biomaterials.2013.03.054. PMID: 23583038; PMCID: PMC3680884.
9. Biomimetics of Extracellular Matrices for Cell and Tissue Engineered Medical Products / Ed. V.I. Sevastianov, Yu.B. Basok. Newcastle upon Tyne, UK: Cambridge Scholars Publishing, 2023; 339.
10. *Lim LY, Ding SSL, Muthukumaran P, Teoh SH, Koh Y, Teo AKK.* Tissue engineering of decellularized pancreas scaffolds for regenerative medicine in diabetes. *Acta biomater.* 2023; 157: 49–66. doi: 10.1016/j.actbio.2022.11.032. PMID: 36427686.
11. *Wu D, Wan J, Huang Y, Guo Y, Xu T, Zhu M et al.* 3d Culture of MIN-6 Cells on Decellularized Pancreatic Scaffold: *in vitro* and *in vivo* Study. *Biomed Res Int.* 2015; 2015: 432645. doi: 10.1155/2015/432645. PMID: 26688810; PMCID: PMC4672115.
12. *Shapiro AM.* Strategies toward single-donor islets of Langerhans transplantation. *Curr Opin Or-*

gan Transplant. 2011; 16 (6): 627–631. doi: 10.1097/MOT.0b013e32834cfb84. PMID: 22068022; PMCID: PMC3268080.
13. *Pepper AR*, *Gala-Lopez B, Ziff O, Shapiro AJ*. Current status of clinical islet transplantation. *World J Transplant*. 2013; 3 (4): 48–53. doi: 10.5500/wjt.v3.i4.48. PMID: 24392308; PMCID: PMC3879523.
14. *Yang W, Xia R, Zhang Y, Zhang H, Bai L.* Decellularized liver scaffold for liver regeneration. *Methods Mol Biol.* 2018; 1577: 11–23. doi: 10.1007/7651_2017_53. PMID: 28856614.
15. *Rossi EA, Quintanilha LF, Nonaka CKV, Souza BSF.* Advances in hepatic tissue bioengineering with decellularized liver bioscaffold. *Stem Cells Int.* 2019; 2019: 2693189. doi: 10.1155/2019/2693189. PMID: 31198426; PMCID: PMC6526559.
16. *Zhou P, Guo Y, Huang Y, Zhu M, Fan X, Wang L et al*. The dynamic three-dimensional culture of islet-like clusters in decellularized liver scaffolds. *Cell Tissue Res.* 2016; 365 (1): 157–171. doi: 10.1007/s00441-015-2356-8. PMID: 26796204.
17. *Xu T, Zhu M, Guo Y, Wu D, Huang Y, Fan X et al.* Three-dimensional culture of mouse pancreatic islet on a liver-derived perfusion-decellularized bioscaffold for potential clinical application. *J Biomater Appl.* 2015; 30 (4): 379–387. doi: 10.1177/0885328215587610. PMID: 26006767.
18. *Goh SK, Bertera S, Richardson T, Banerjee I.* Repopulation of decellularized organ scaffolds with human pluripotent stem cell-derived pancreatic progenitor cells. *Biomed Mater*. 2023; 18 (2). doi: 10.1088/1748-605X/acb7bf. PMID: 36720168.
19. *Khorsandi L, Orazizadeh M, Bijan Nejad D, Heidari Moghadam A, Nejaddehbashi F, Asadi Fard Y.* Spleen extracellular matrix provides a supportive microenvironment for β-cell function. *Iran J Basic Med Sci.* 2022; 25 (9): 1159–1165. doi: 10.22038/IJBMS.2022.65233.14360. PMID: 36246063; PMCID: PMC9526894.
20. *Goldman O, Puchinsky D, Durlacher K, Sancho R, Ludwig B, Kugelmeier P et al.* Lung Based Engineered Micro-Pancreas Sustains Human Beta Cell Survival and Functionality. *Horm Metab Res*. 2019; 51 (12): 805–811. doi: 10.1055/a-1041-3305. PMID: 31826275.
21. *Crapo PM, Gilbert TW, Badylak SF.* An overview of tissue and whole organ decellularization processes. *Biomaterials*. 2011; 32 (12): 3233–3243. doi: 10.1016/j.biomaterials.2011.01.057. PMID: 21296410; PMCID: PMC3084613.
22. *Sevastianov VI, Ponomareva AS, Baranova NV, Kirsanova LA, Basok YuB, Nemets EA et al.* Decellularization of Human Pancreatic Fragments with Pronounced Signs of Structural Changes. *Int J Mol Sci.* 2022; 24 (1): 119. doi: 10.3390/ijms24010119.28. PMID: 36613557; PMCID: PMC9820198.
23. *Kirillova AD, Basok YuB, Lazhko AE, Grigoryev AM, Kirsanova LA, Nemets EA, Sevastianov VI*. Creating a tissue-specific microdispersed matrix from a decellularized porcine liver. *Physics and Chemistry of Materials Processing*. 2020; 4: 41–50.
24. GOST ISO 10993-5-2011. Medical devices. Biological evaluation of medical devices. Part 5. Tests for *in vitro* cytotoxicity. M.: Standartinform, 2014; 9.
25. *Daoud J, Heileman K, Shapka S, Rosenberg L, Tabrizian M.* Dielectric spectroscopy for monitoring human pancreatic islet differentiation within cell-seeded scaffolds in a perfusion bioreactor system. *Analyst*. 2015; 140 (18): 6295–6305. doi: 10.1039/c5an00525f. PMID: 26280028.
26. *Sevastianov VI, Basok YuB, Grigoriev AM, Kirsanova LA, Vasilets VN.* Application of tissue engineering technology for formation of human articular cartilage in perfusion bioreactor. *Russian Journal of Transplantology and Artificial Organs.* 2017; 19 (3): 81–92. [In Russ, English abstract]. doi: 10.15825/1995-1191-2017-3-81-92.
27. *Watanabe T, Sassi S, Ulziibayar A, Hama R, Kitsuka T, Shinoka T.* The Application of Porous Scaffolds for Cardiovascular Tissues. *Bioengineering (Basel).* 2023; 10 (2): 236. doi: 10.3390/bioengineering10020236. PMID: 36829730; PMCID: PMC9952004.
28. *Flores-Jiménez MS, Garcia-Gonzalez A, Fuentes-Aguilar RQ.* Review on Porous Scaffolds Generation Process: A Tissue Engineering Approach. *ACS Appl Bio Mater.* 2023; 6 (1): 1–23. doi: 10.1021/acsabm.2c00740. PMID: 36599046.
29. *Sevastianov VI, Grigoriev AM, Basok YuB, Kirsanova LA, Vasilets VN, Malkova AP et al.* Biocompatible and matrix properties of polylactide scaffolds. *Russian Journal of Transplantology and Artificial Organs.* 2018; 20 (2): 82–90. [In Russ, English abstract]. doi: 10.15825/1995-1191-2018-2-82-90.
30. C*arriero VC, Di Muzio L, Petralito S, Casadei MA, Paolicelli P.* Cryogel Scaffolds for Tissue-Engineering: Advances and Challenges for Effective Bone and Cartilage Regeneration. *Gels*. 2023; 9 (12): 979. doi: 10.3390/gels9120979. PMID: 38131965; PMCID: PMC10742915.
31. *Ioch K, Lozinsky VI, Galaev IY, Yavriyanz K, Vorobeychik M, Azarov D et al.* Functional activity of insulinoma cells (INS-1E) and pancreaTEC islets cultured in agarose cryogel sponges. *J Biomed Mater Res A*. 2005; 75 (4): 802–809. doi: 10.1002/jbm.a.30466. PMID: 16138321.
32. *Lozinsky VI, Damshkaln LG, Bloch RO, Vardi P, Grinberg NV, Burova TV, Grinberg VYa.* Cryostructuring of polymer systems. Preparation and characterization of supermacroporous (spongy) agarose-based cryogels used as three-dimensional scaffolds for culturing insulin-producing cell aggregates. *J Appl Polym Sci.* 2008; 108 (5): 3046–3062. doi: 10.1002/app.27908.
33. *Saldin LT, Cramer MC, Velankar SS, White LJ, Badylak SF.* Extracellular matrix hydrogels from decellularized tissues: Structure and function. *Acta Biomater.* 2017; 49: 1–15. doi: 10.1016/j.actbio.2016.11.068. PMID: 27915024; PMCID: PMC5253110.

The article was submitted to the journal on 16.07.2024

DOI: 10.15825/1995-1191-2025-1-103-113

CHEMICAL DECELLULARIZATION OF PORCINE LIVER BY TWO-STAGE TREATMENT WITH SURFACTANTS AND OSMOREGULATORS ENHANCES PRESERVATION OF LIVER EXTRACELLULAR MATRIX STRUCTURE

A.D. Belova[1], E.A. Nemets[1], D.D. Filin[1], A.S. Ponomareva[1], L.A. Kirsanova[1], Yu.B. Basok[1], V.I. Sevastianov[1, 2]

[1] Shumakov National Medical Research Center of Transplantology and Artificial Organs, Moscow, Russian Federation

[2] Institute of Biomedical Research and Technology, Moscow, Russian Federation

Objective: to develop and investigate a tissue-specific matrix obtained using a modified chemical porcine liver decellularization regime in order to effectively increase preservation of extracellular matrix (ECM) structure, reduce decellularization time and improve purification of the ECM from cellular elements. **Materials and methods.** Original porcine liver was minced to obtain tissue fragments. Five decellularization regimes were used, with the concentrations and timing of surfactant treatments varied: 0.1% sodium dodecyl sulfate (SDS) and 0.1% or 1% Triton X-100, without and in combination with phosphate-buffered saline (PBS). The glycosaminoglycan (GAG) content of the resulting fragments was determined by lysing the samples for 12 hours in papain solution at +65 °C and then incubating them in 1,9-dimethylmethylene blue. DNA quantification was carried out using DNeasy Blood&Tissue Kit and Quant-iT PicoGreen dye. The morphology of the samples was studied using histological staining techniques. Cytotoxicity of the samples *in vitro* was evaluated on an NIH/3T3 mouse fibroblast culture by direct contact. **Results.** Treatment with 0.1% SDS for 2.5 hours with additional treatment with 1% Triton X-100 containing PBS for 21.5 hours (regime 4) increased GAG content to 11.66 ± 0.61 μg/mg compared to 0.68 ± 0.06 μg/mg (regime 5). The DNA content of samples obtained in regime 4 decreased from 99.75 ± 3.93 ng/mg to 14.93 ± 4.91 ng/mg after additional treatment with type I DNase, indicating that cellular components were effectively removed. This matrix showed no cytotoxicity. **Conclusion**. By optimizing the chemical decellularization regime for porcine liver, we were able to improve preservation of ECM structures, shorten decellularization time and effectively reduce the content of cellular elements. The modified decellularization protocol allowed to obtain a non-cytotoxic tissue-specific matrix with a low potential immunogenicity and a more preserved ECM structure and higher GAG content.

Keywords: porcine liver, decellularization, glycosaminoglycans, tissue engineering.

INTRODUCTION

Over the last decade, tissue engineering has advanced significantly, with cell-free matrices obtained through decellularization becoming a cornerstone among biodegradable materials used as cellular carriers in cell-engineered constructs. Bioequivalents of liver tissue serve as both a promising alternative to liver transplantation – helping address the global donor organ shortage – and as effective *in vitro* models for drug screening and personalized medicine.

The primary advantages of using matrices derived from decellularized organs include: their ability to preserve the native extracellular matrix (ECM) structure and biochemistry, effectively providing a near-native microenvironment for cells to repopulate and function within; low immunogenicity achieved by removing cellular components; high biocompatibility; potential for xenogeneic organ utilization for decellularization [1, 2]. In this context, matrices derived from decellularized tissues and organs serve not only as physical scaffolds for cells but also actively support their proliferation and function [3, 4]. A key objective in developing decellularization protocols is the preservation of glycosaminoglycans (GAGs), a major ECM component. GAGs are essential for cell adhesion, proliferation, and differentiation [5], largely due to their ability to interact with cytokines, growth factors, enzymes, and proteins [6].

The choice of a decellularization method depends on several factors, including the specific organ type, species origin, tissue structure, and density. Decellularization techniques are generally classified into physical, chemical, and enzymatic methods [7, 8].

Among chemical approaches, Triton X-100 and sodium dodecyl sulfate (SDS) are commonly used to dis-

Corresponding author: Aleksandra Belova. Address: 1, Shchukinskaya str., Moscow, 123182, Russian Federation. Phone: (963) 633-94-34. E-mail: sashak1994@mail.ru

rupt cell membranes and denature proteins effectively. Triton X-100, a non-ionic detergent, is considered less aggressive toward collagen, elastin, and GAGs in ECM compared to SDS [9, 10]. Due to its ionic nature, SDS requires extensive washing to prevent cytotoxic residues from remaining deep within the tissue, as their removal can be challenging [11–13].

To enhance cell membrane permeability and improve surfactant penetration deep into the tissue, decellularization protocols often leverage a synergistic approach by combining multiple methods [14, 15].

For instance, to enhance the efficiency of the decellularization process in mouse liver tissue, Kobes et al. combined surfactants with osmotic shock-inducing substances [16]. Osmotic shock, achieved through alternating hypertonic and hypotonic solutions, promotes cell lysis while minimally affecting the ECM and facilitates the removal of cell debris post-lysis [17, 18]. Similarly, Suss et al. employed an SDS solution supplemented with EDTA and ultrasound to decellularize nervous tissue [19].

Previously, we proposed a protocol for generating a tissue-specific microdispersed matrix from decellularized liver using a prolonged (72-hour) treatment with three surfactant solutions containing SDS and increasing Triton X-100 concentrations, followed by DNase treatment [20, 21]. This approach effectively removes cellular components while leveraging Triton X-100 to aid in the removal of SDS residues [12]. However, drawbacks include the extended duration of the decellularization process and the use of a magnetic stirrer, which may negatively impact the ECM's composition and structural integrity.

This study aimed to develop and evaluate a tissue-specific matrix derived from porcine liver using a modified chemical decellularization protocol. The proposed approach focuses on enhancing ECM preservation, shortening decellularization time, and improving the removal of cellular components from ECM.

MATERIALS AND METHODS

Object of study

For decellularization we used porcine liver obtained at a slaughterhouse (PROMAGRO, Stary Oskol) after slaughtering the healthy animals. The original tissue was frozen at –20 °C. Before the experiments, the liver was defrosted and mechanically minced using a scalpel and scissors to obtain porcine liver fragments (PLF) no larger than 1.5×1.5 mm.

PLF decellularization regimes

PLF were processed using 5 decellularization regimes at +25 °C and constant stirring at 90 rpm using an ES-20/60 incubator shaker (Biosan, Latvia). The decellularization regimes are presented in Table.

In all protocols, the PLF underwent sequential treatment with a surfactant-containing solution in distilled water, followed by phosphate-buffered saline (PBS; 137 mM NaCl, 2.67 mM KCl, 1.47 mM KH_2PO_4, 8.1 mM Na_2HPO_4, pH 7.4) containing surfactant (low ionic strength solution) for a specified duration.

PLF treatment with DNase

To achieve complete removal of cellular components, as assessed by the residual DNA, after decellularization of samples in regime 4, we included an additional PLF treatment with a type I DNAase solution (SayStorLab, Russia). Samples (0.5 ml) were placed in 1.0 mL of 10 mM Tris-HCl pH 7.6 solution containing 2.5 mM $MgCl_2$, 0.5 mMol $CaCl_2$, and 50 U/mL DNAase I and incubated for 48 hours at +37 °C.

Determination of glycosaminoglycan content in native liver and decellularized PLF

For quantification of GAG content in native and decellularized PLF (DPLF), samples were lyophilized at –80 °C (FreeZone, Labconco, USA). After lyophilization, 30 mg samples each (n = 3) were lysed in papain solution (Sigma-Aldrich, USA) at +65 °C for 12 hours. GAG concentration was measured using 1,9-dimethylmethylene blue (DMMB) dye (Sigma-Aldrich, USA) and a Tecan Spark 10M tablet reader (Tecan Trading, Switzerland), measuring absorbance at 525 nm wavelength.

Double-stranded DNA staining with DAPI dye in native liver and DPLF

For preliminary assessment of DNA content in native porcine liver (n = 3) and DPLF (n = 3), samples were pre-frozen at –20 °C, embedded in freezing medium (Leica, Germany), and sectioned into 10-μm-thick slices using a Leica CM1900 UV cryostat microtome (Leica,

Table

Porcine liver decellularization regimes

Regime	Stage I	Stage II
1	H_2O + SDS 0.1% – 2.5 hours	PBS + SDS 0.1% – 21.5 hours
2	H_2O + Triton X-100 0.1% – 2.5 hours	PBS + Triton X-100 0.1% – 21.5 hours
3	H_2O + Triton X-100 1% – 2.5 hours	PBS + Triton X-100 1% – 21.5 hours
4	H_2O + SDS 0.1% – 2.5 hours	PBS + Triton X-100 1% – 21.5 hours
5	H_2O + Triton X-100 1% – 18 hours	PBS + SDS 0.1% – 6 hours

Note: SDS, sodium dodecyl sulfate; PBS, phosphate-buffered saline.

Germany). The sections were then stained with the blue-fluorescent DNA stain 4′,6-diamidino-2-phenylindole (DAPI) (Sigma-Aldrich, USA) at a concentration of 1 μg/mL. Each sample was visually examined for DNA preservation using a Leica THUNDER Imager fluorescence microscope (Leica, Germany).

Quantification of DNA in native liver and DPLF

To quantify DNA content in native liver and DPLF samples, the DNeasy Blood & Tissue Kit (QIAGEN, Germany) was used following the manufacturer's instructions. A 10 mg sample of native liver (n = 3) or DPLF (n = 3) was processed for analysis. Double-stranded DNA quantification was performed using the Quant-iT PicoGreen dsDNA Assay Kit and dsDNA Reagents (Invitrogen, USA) according to the manufacturer's protocol. DNA content in the samples was measured using a Tecan Spark 10M microplate reader (Tecan Trading AG, Switzerland) at a wavelength of 520 nm.

Determination of *in vitro* cytotoxicity of DPLF

In vitro cytotoxicity of DPLF samples was assessed following the interstate standard GOST ISO 10993-5-2011 [22] using NIH/3T3 mouse fibroblasts (ATCC® CRL-1658™, American Type Culture Collection) and the direct contact method. Fibroblasts were cultured in standard 25 cm^2 culture flasks (CELLSTAR Greiner Bio-One, Germany) with complete growth medium (CGM) containing DMEM (Dulbecco's Modified Eagle's Medium) with high glucose (4.5 g/L, DMEM high glucose c HEPES, PanEco, Russia), 10% calf serum (Biosera, Germany), Anti-Anti antibiotic-antimycotic (Gibco, Thermo Fisher Scientific, USA), and 2 mM glutamine (PanEco, Russia). Cultures were maintained in a CO_2 incubator at 37 °C under a humidified atmosphere with (5 ± 1)% CO_2. Cells were detached using TrypLE Express Enzyme dissociation reagent (Gibco, Thermo Fisher Scientific, USA), and the initial cell count was determined using a TC 20™ Automated Cell Counter (Bio-Rad Laboratories Inc., USA). The initial cell count in the suspension was determined using a TC 20™ Automated Cell Counter (Bio-Rad Laboratories Inc., USA). To assess cytotoxic effects, fibroblasts were seeded into 96-well flat-bottomed culture plates (CELLSTAR Greiner Bio-One, Germany) at a concentration of 1–2 × 10^6 cells per well and incubated in CGM under standard conditions until an (80 ± 10)% monolayer was established. Test samples (n = 8) were then introduced into wells containing the fibroblast monolayer and incubated for 24 hours. Morphological changes in fibroblasts were assessed using a Nikon Eclipse TS100 microscope (Nikon, Japan).

To evaluate the effect of DPLF samples on NIH/3T3 cell viability, cells were stained using the LIVE/DEAD Cell Viability/Cytotoxicity Kit (Molecular Probes by Life Technologies, USA) following the manufacturer's protocol. Fluorescence analysis was conducted using a Nikon Eclipse Ti fluorescence microscope (Nikon, Japan).

As controls, nutrient medium DMEM with a high glucose content of 4.5 g/L (PanEco, Russia) served as the negative control to establish baseline cellular responses, while a single-element aqueous zinc standard (10,000 μg/mL, Sigma-Aldrich, USA) was used as the positive control.

Histological examination of native liver and DPLF

Samples of native liver tissue and DPLF were fixed in a 10% formalin solution, washed in running water, and dehydrated using a graded ethanol series. They were then treated sequentially with an ethanol-chloroform mixture, pure chloroform, and finally embedded in paraffin.

Histological sections were deparaffinized, rehydrated, and stained using hematoxylin and eosin for general tissue structure, Masson's method for total collagen content, and alcian blue for GAGs. The stained sections were analyzed and photographed using a Nikon Eclipse Ti inverted microscope (Nikon, Japan).

Statistical analysis of obtained results

Data analysis was performed using Microsoft Office Excel (2021). Mean values and standard deviations were calculated, and statistical significance was assessed using Student's t-test. A p-value of <0.05 was considered statistically significant.

RESULTS AND DISCUSSION

Fig. 1 illustrates the impact of different porcine liver decellularization protocols (outlined in Table) on GAG concentration in DPLF samples. For comparison, the figure also includes data from DPLF obtained using a previously developed protocol involving magnetic stirring [20, 21]. It is known that GAG content in native porcine liver tissue is lower (0.59 ± 0.03 μg/mg dry tissue) than in decellularized samples, likely due to the high cellular mass fraction in the liver (comprising up to 80% of the organ's total mass) [23].

When liver fragments were treated with 0.1% SDS for 24 hours (regime 1), only a small amount of GAG was retained (3.42 ± 1.03 μg/mg dry tissue), which was not significantly different from the previously developed protocol (3.03 ± 0.24 μg/mg dry tissue) [20, 21]. Notably, several studies have also reported the detrimental effect of SDS on GAG retention during decellularization of various tissues and organs [24, 25]. An evaluation of the effect of Triton X-100 at 0.1% (regime 2) and 1% (regime 3) concentrations – used to enhance cell membrane permeability and promote cell lysis – revealed no significant difference in GAG retention, with values of 9.38 ± 0.67 μg/mg dry tissue and 10.74 ± 0.95 μg/mg dry tissue, respectively.

After decellularization under regimes 3 and 4, residual GAG content did not differ significantly (10.74 ± 0.95 μg/mg dry tissue and 11.66 ± 0.61 μg/mg dry tissue, respectively). However, in regime 5 – where 1% Triton X-100 was used in the first stage (18 hours) followed by 0.1% SDS in the second stage (6 hours) – GAG retention was the lowest, at 0.68 ± 0.06 μg/mg dry tissue.

Beyond maintaining ECM structure and key components, effective decellularization requires the thorough removal of cells and cellular debris. A key indicator of successful decellularization is the absence of nuclear material, as confirmed by DAPI staining. DAPI selectively binds to double-stranded DNA, producing fluorescence that is twenty times more intense upon binding, making it a reliable marker for residual nuclear content (Fig. 2, a–e) [18].

As shown in Fig. 2, a, the characteristic fluorescence of nuclei was clearly detected in the original porcine liver tissue. In DPLF samples, the intensity of fluorescence varied depending on the decellularization regime and the effectiveness of cellular removal. In regime 1 (Fig. 2, b), a moderate number of visible nuclei remained, indicating partial decellularization. Similarly, regimes 2 and 3 (Fig. 2, c, d), which used only Triton X-100, resulted in multiple observable nuclei, demonstrating that this surfactant alone is insufficient for complete cellular removal. In contrast, regime 4 (Fig. 2, e), which involved sequential treatment with 0.1% SDS followed by 1% Triton X-100, showed a significant reduction in nuclear content. Notably, regime 5, which reversed the order – starting with 1% Triton X-100 followed by 0.1% SDS – resulted in the complete absence of visible nuclei, indicating the most effective decellularization.

Application of all decellularization regimes significantly reduced the DNA content in DPLF compared to the original liver tissue (Fig. 2, g), an essential factor in minimizing the potential immunogenicity of the matrix. According to the criteria proposed by Crapo et al., a decellularized matrix is considered adequately processed if it contains no more than 50 ng of DNA per mg of tissue. Triton X-100 and SDS are known to remove up to 90% of DNA from tissue [18, 26].

In regime 1, where the sample was treated with 0.1% SDS solution, the DNA content was reduced to 34.78 ± 3.82 ng/mg dry tissue – just 2.18% of the DNA present in the original liver tissue (1595.10 ± 96.80 ng/mg dry tissue). The significant reduction in DNA observed with regime 1 likely results from the synergistic effect of SDS-induced changes in osmotic strength, which enhances cell membrane destruction and promotes more efficient cell lysis.

The use of other decellularization regimes did not achieve the minimum DNA removal threshold of 50 ng/mg tissue. This suggests that additional steps are needed to improve the penetration of decellularizing agents deep into the matrix, facilitating cell membrane destruction and cell lysis.

It is worth noting that treating tissue with only 0.1% or 1.0% Triton X-100 solutions is often insufficient for complete cell removal. While these treatments preserve high GAG content (9.38 ± 0.67 μg/mg dry tissue and 10.74 ± 0.95 μg/mg dry tissue, respectively), they fail to eliminate sufficient amounts of genetically active material. A similar trend was observed in decellularization regime 4, where sequential exposure to 0.1% SDS and 1% Triton X-100 reduced DNA levels only to

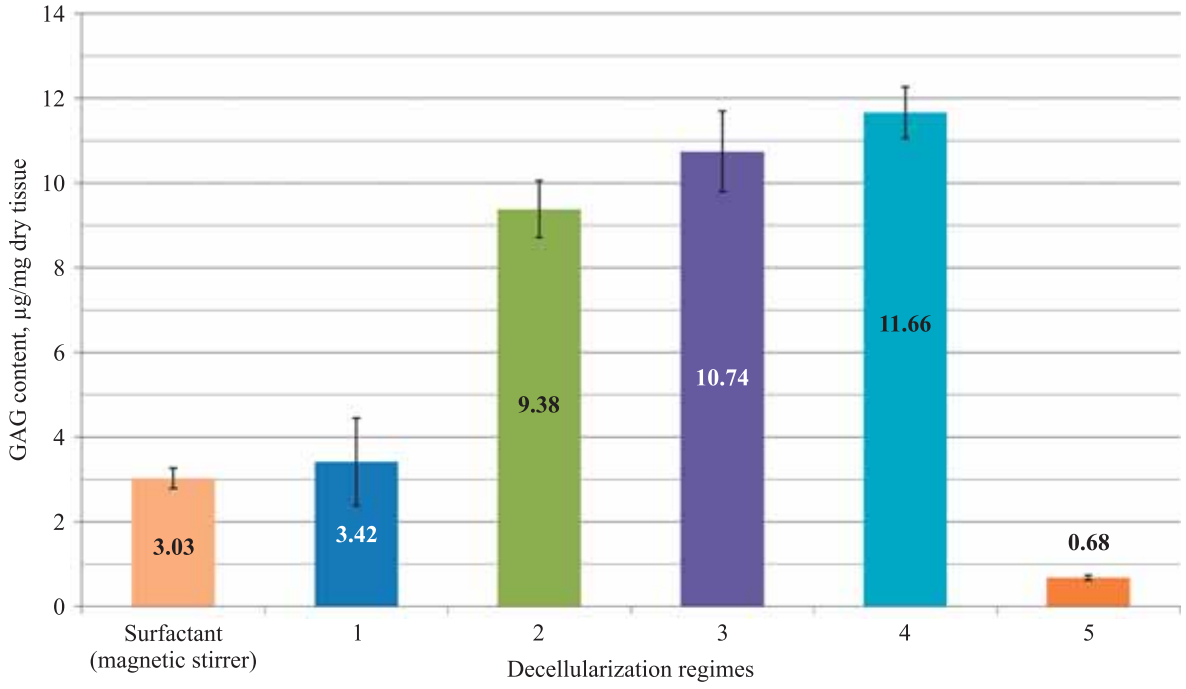

Fig. 1. Effect of porcine liver decellularization regime on GAG content

99.75 ± 3.93 ng/mg dry tissue – well above the required threshold. However, this protocol retained the highest GAG content (11.66 ± 0.61 μg/mg dry tissue).

Histological staining of DPLF samples was performed to validate the results obtained. Two samples were selected for examination based on their distinct characteristics: regime 1, which achieved the lowest residual DNA content, ensuring effective cell removal, and regime 4, which preserved the highest amount of GAG within the DPLF-based matrix (Fig. 3).

When stained with hematoxylin and eosin, as well as using the Masson method, the sample treated under regime 1 exhibited polymorphic fragments of decellularized liver with a well-preserved intra-lobular structure and pronounced porosity (Fig. 3, a, b). This structural integrity could positively impact DPLF recellularization, as high porosity facilitates nutrient diffusion to cells within the matrix and supports neovascularization.

Additionally, no preserved cell nuclei or cellular debris were observed in the sample, corroborating the quantification of residual DNA, which indicated minimal genetic material remaining post-decellularization. However, GAG staining with alcian blue was very weak (Fig. 3, c), aligning with the low quantified GAG content. This suggests that regime 1 – while effective in DNA removal – led to significant loss of GAG, a crucial ECM component.

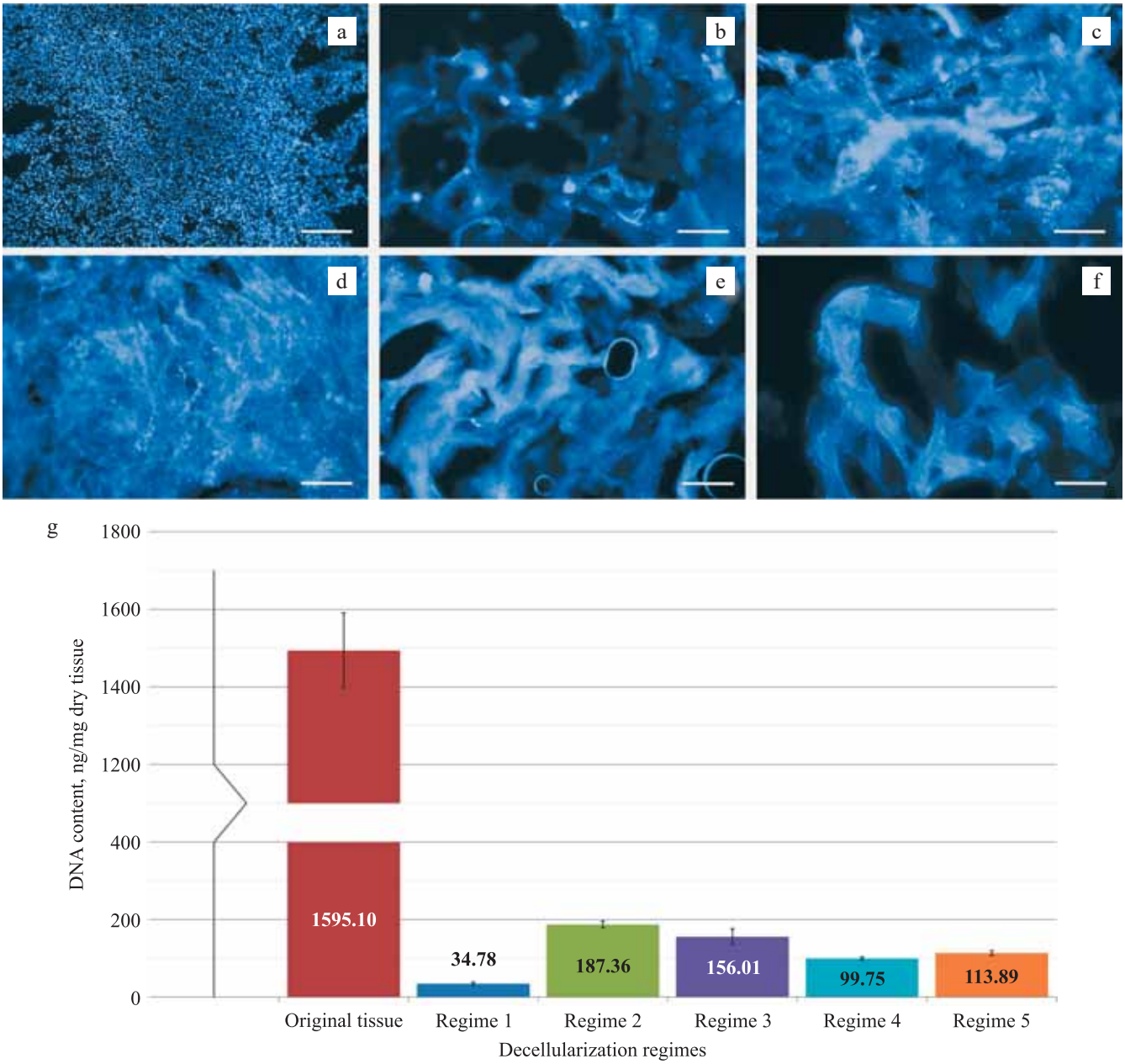

Fig. 2. Effect of porcine liver decellularization regime on DNA content. DAPI staining: a, original porcine liver tissue; b, regime 1; c, regime 2; d, regime 3; e, regime 4; f, regime 5. Scale bar, 100 μm. g, quantitative DNA content in porcine liver fragments

DPLF treated under regime 4 (Fig. 3, d–f) exhibited dense fiber arrangement with reduced porosity due to the formation of liver fragment conglomerates. The sample stained positively for total collagen (Masson's method) and GAG (Alcian blue) (Fig. 3, e, f). However, preserved cellular detritus was observed.

Histological analysis aligned with DNA and GAG quantification data, demonstrating high GAG retention but insufficient DNA removal in DPLF obtained under regime 4.

To address this, additional treatment with type I DNAase solution was applied. Fig. 4 shows that this further reduced DNA levels to 0.94% of the original amount (14.93 ± 4.91 ng/mg dry tissue from 1595.10 ± 96.80 ng/mg dry tissue), significantly enhancing.

Based on these findings, decellularization regime 4 was selected as the optimal protocol due to its ability to maximize ECM structure preservation, retain high GAG content, and enhance cell and cellular debris removal.

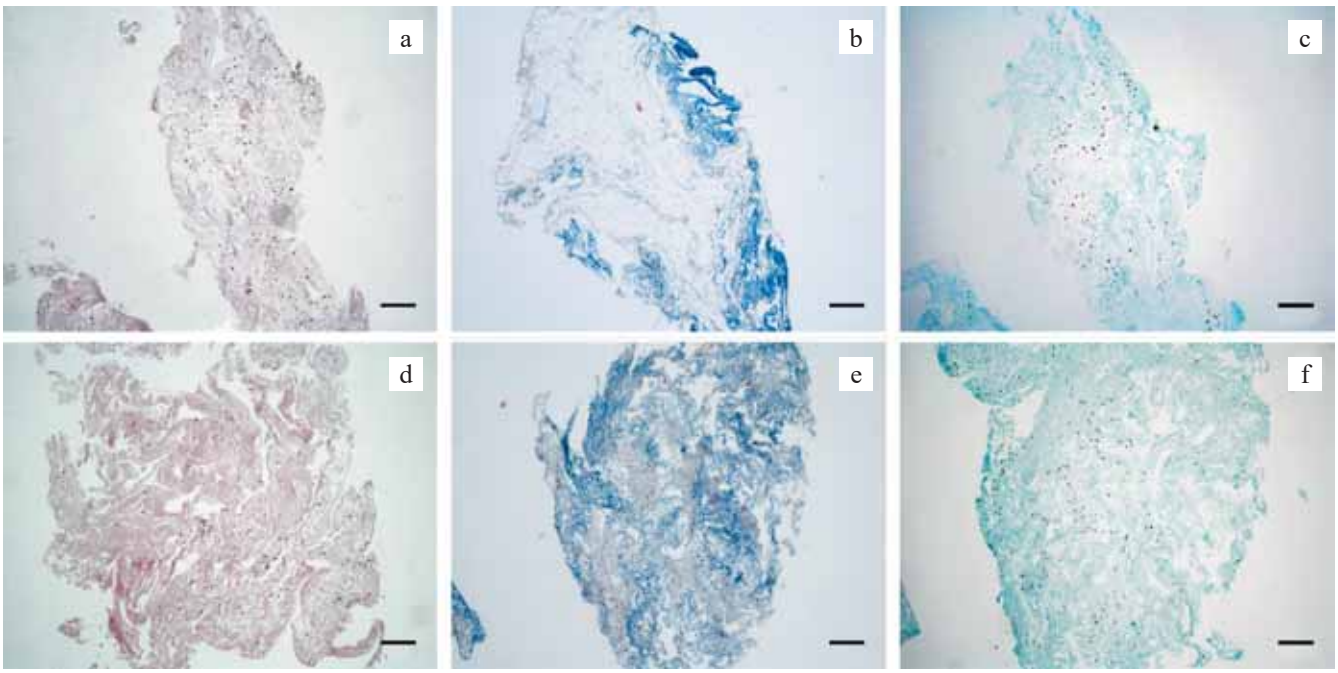

Fig. 3. Effect of porcine liver treatment regime on decellularization efficiency. H&E stain: a, regime 1; d, regime 4. Masson's trichrome stain: b, regime 1; e, regime 4. Alcian blue stain: c, regime 1; f, regime 4. Scale bar, 100 μm

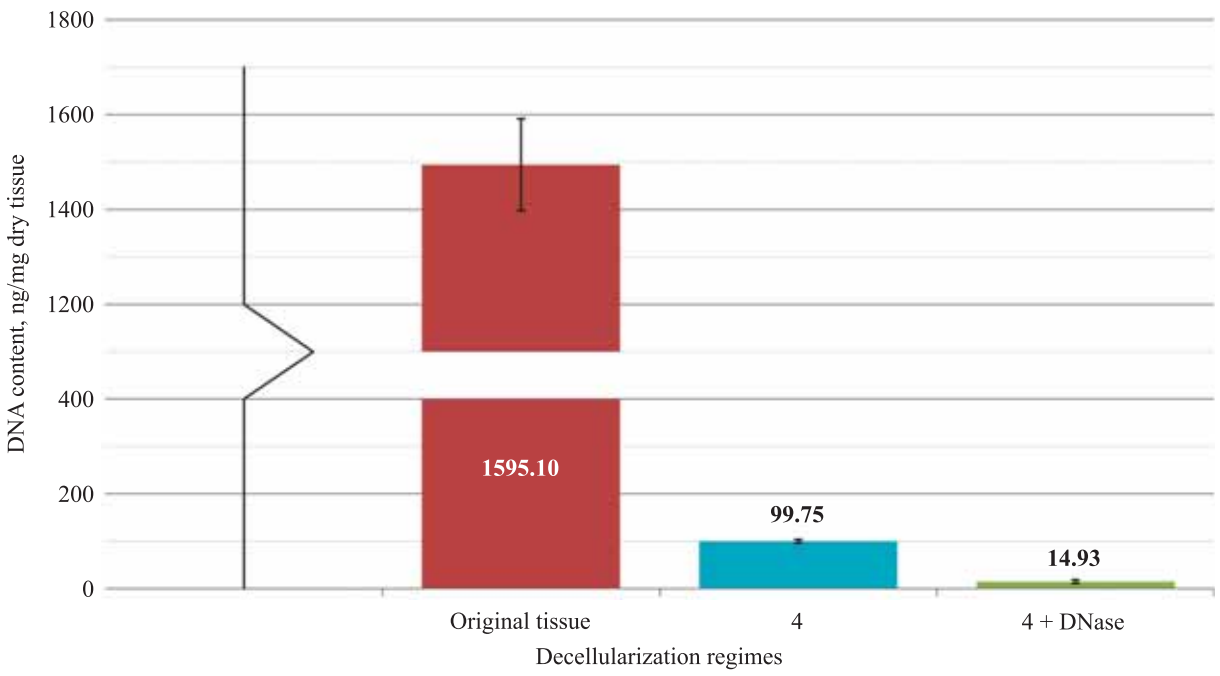

Fig. 4. Effect of DNase treatment on porcine liver decellularization efficiency

Cytotoxicity assessment of DPLF using the direct contact method on NIH/3T3 mouse fibroblast cultures demonstrated no adverse effects on cell morphology or viability. As shown in Fig. 5, a, the number of viable fibroblasts was comparable to the negative control (Fig. 5, c). A cytotoxic effect was observed in the positive

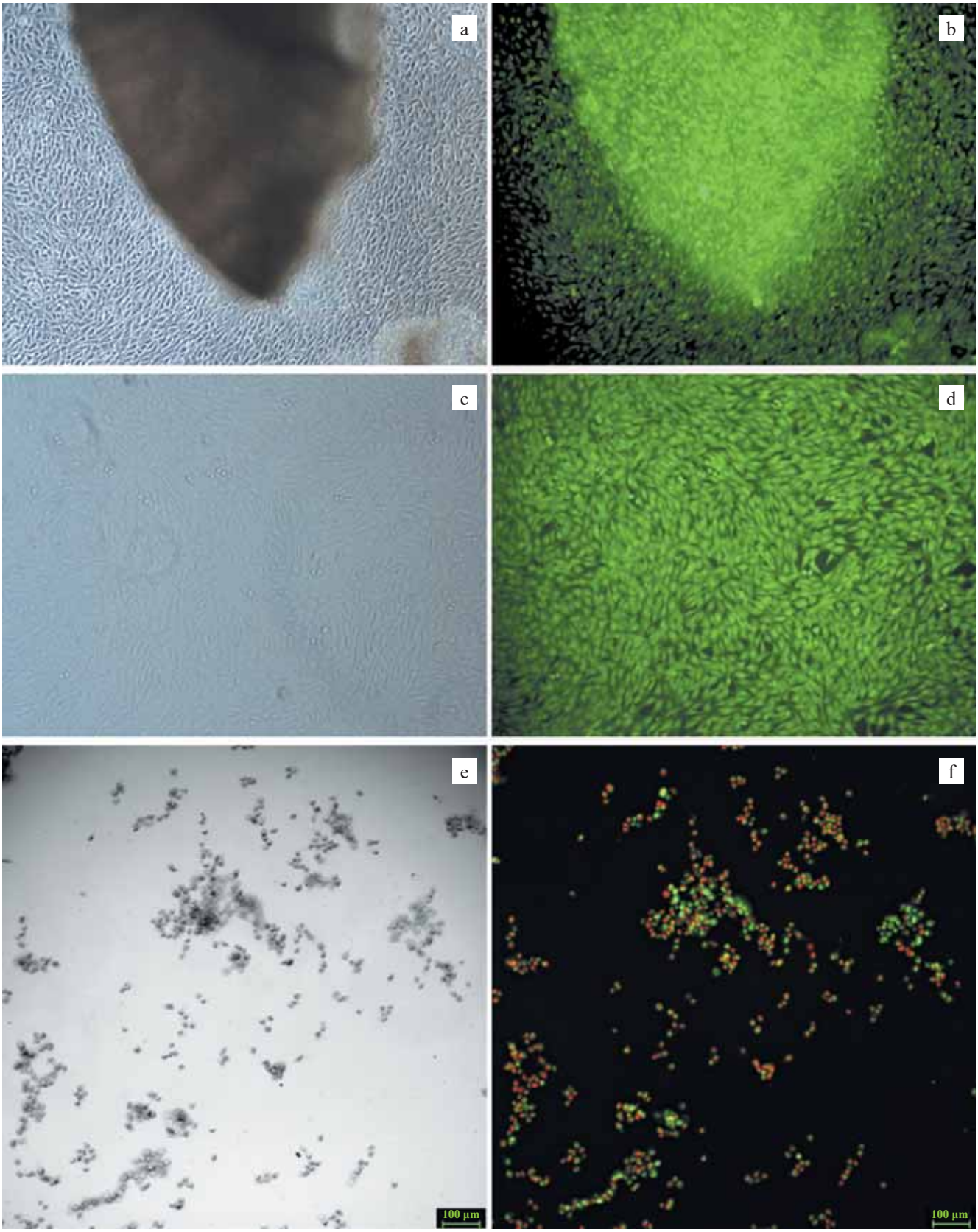

Fig. 5. Degree of cytotoxicity of matrix based on decellularized porcine liver fragments (DPLF) obtained in regime 4, *in vitro*. (a, b), test sample of DPLF; (c, d), negative control; (e, f), positive control. (a, c, e), phase-contrast microscopy; (b, d, f), fluorescence microscopy with LIVE/DEAD vital dye. 40× magnification

control sample, where cells exhibited a spherical shape, indicating loss of viability (Fig. 5, e).

The absence of cytotoxicity in DPLF obtained via decellularization regime 4 was further confirmed by LIVE/DEAD staining (Fig. 5, b). A large number of viable cells, forming a monolayer comparable to the negative control, were observed in contact with the samples (Fig. 5, d). The positive control (Fig. 5, e) exhibited dead cells with red fluorescence.

Based on these findings, it was concluded that DPLF has no cytotoxic effect *in vitro*.

CONCLUSION

Thus, our study revealed that SDS treatment negatively affected preservation of GAG, a key component of the natural ECM. However, optimization of the chemical porcine liver decellularization regime – through a two-stage application of surfactants and osmoregulators – successfully reduced tissue processing time by nearly half, enhanced ECM structure preservation, and reduced cellular component content, ensuring low potential immunogenicity and eliminating cytotoxic effects.

The authors declare no conflict of interest.

REFERENCES

1. *Dai Q, Jiang W, Huang F, Song F, Zhang J, Zhao H*. Recent advances in liver engineering with decellularized scaffold. *Front Bioeng Biotechnol*. 2022; 10: 831477. doi: 10.3389/fbioe.2022.831477.
2. *Zhang X, Chen X, Hong H, Hu R, Liu J, Liu C*. Decellularized extracellular matrix scaffolds: Recent trends and emerging strategies in tissue engineering. *Bioact Mater*. 2021; 10: 15–31. doi: 10.1016/j.bioactmat.2021.09.014.
3. *Isaeva EV, Beketov EE, Arguchinskaya NV, Ivanov SA, Shegay PV, Kaprin AD*. Decellularized Extracellular Matrix for Tissue Engineering (Review). *Sovrem Tekhnologii Med*. 2022; 14 (3): 57–68. doi: 10.17691/stm2022.14.3.07.
4. *García-Gareta E, Abduldaiem Y, Sawadkar P, Kyriakidis C, Lali F, Greco KV.* Decellularised scaffolds: just a framework? Current knowledge and future directions. *J Tissue Eng*. 2020; 11: 2041731420942903. doi: 10.1177/2041731420942903.
5. Biomimetics of Extracellular Matrices for Cell and Tissue Engineered Medical Products / Ed. V.I. Sevastianov, Yu.B. Basok. Newcastle upon Tyne, UK: Cambridge Scholars Publishing, 2023; 339.
6. *Sodhi H, Panitch A*. Glycosaminoglycans in tissue engineering: a review. *Biomolecules*. 2020; 11 (1): 29. doi: 10.3390/biom11010029.
7. *Huang Z, Godkin O, Schulze-Tanzil G*. The challenge in using mesenchymal stromal cells for recellularization of decellularized cartilage. *Stem Cell Rev Rep*. 2017; 13 (1): 50–67. doi: 10.1007/s12015-016-9699-8.
8. *Neishabouri A, Soltani Khaboushan A, Daghigh F, Kajbafzadeh AM, Majidi Zolbin M.* Decellularization in tissue engineering and regenerative medicine: evaluation, modification, and application methods. *Front Bioeng Biotechnol*. 2022; 10: 805299. doi: 10.3389/fbioe.2022.805299.
9. *Jeong W, Kim MK, Kang HW*. Effect of detergent type on the performance of liver decellularized extracellular matrix-based bio-inks. *J Tissue Eng*. 2021; 12: 2041731421997091. doi: 10.1177/2041731421997091.
10. *Willemse J, Verstegen MMA, Vermeulen A, Schurink IJ, Roest HP, van der Laan LJW, de Jonge J*. Fast, robust and effective decellularization of whole human livers using mild detergents and pressure controlled perfusion. *Mater Sci Eng C Mater Biol Appl*. 2020; 108: 110200. doi: 10.1016/j.msec.2019.110200.
11. *Nemets EA, Malkova AP, Duhina GA, Lazhko AJe, Basok YuB, Kirillova AD, Sevastianov VI.* Effect of supercritical carbon dioxide on the *in vivo* biocompatible and resorptive properties of tissue-specific scaffolds from decellularized pig liver fragments. *Promising materials*. 2021; 11: 20–31. [In Russ, English abstract]. doi: 10.30791/1028-978X-2021-11-20-31.
12. *Gilpin A, Yang Y*. Decellularization strategies for regenerative medicine: from processing techniques to applications. *Biomed Res Int*. 2017; 2017: 9831534. doi: 10.1155/2017/9831534.
13. *Syed O, Walters NJ, Day RM, Kim HW, Knowles JC*. Evaluation of decellularization protocols for production of tubular small intestine submucosa scaffolds for use in oesophageal tissue engineering. *Acta Biomater*. 2014; 10 (12): 5043–5054. doi: 10.1016/j.actbio.2014.08.024.
14. *Sevastianov VI, Basok YuB, Grigoriev AM, Nemets EA, Kirillova AD, Kirsanova LA et al*. Decellularization of cartilage microparticles: Effects of temperature, supercritical carbon dioxide and ultrasound on biochemical, mechanical, and biological properties. *J Biomed Mater Res A*. 2023; 111 (4): 543–555. doi: 10.1002/jbm.a.37474.
15. *Bakhtiar H, Rajabi S, Pezeshki-Modaress M, Ellini MR, Panahinia M, Alijani S et al.* Optimizing methods for bovine dental pulp decellularization. *J Endod*. 2021; 47 (1): 62–68. doi: 10.1016/j.joen.2020.08.027.
16. *Kobes JE, Georgiev GI, Louis AV, Calderon IA, Yoshimaru ES, Klemm LM et al*. A comparison of iron oxide particles and silica particles for tracking organ recellularization. *Mol Imaging*. 2018; 17: 1536012118787322. doi: 10.1177/1536012118787322.
17. *Kim JK, Koh YD, Kim JO, Seo DH*. Development of a decellularization method to produce nerve allografts using less invasive detergents and hyper/hypotonic solutions. *J Plast Reconstr Aesthet Surg*. 2016; 69 (12): 1690–1696. doi: 10.1016/j.bjps.2016.08.016.
18. *Crapo PM, Gilbert TW, Badylak SF*. An overview of tissue and whole organ decellularization processes. *Biomaterials*. 2011; 32 (12): 3233–3243. doi: 10.1016/j.biomaterials.2011.01.057.
19. *Suss PH, Ribeiro VST, Motooka CE, de Melo LC, Tuon FF*. Comparative study of decellularization techniques to obtain natural extracellular matrix scaffolds of human peripheral-nerve allografts. *Cell Tissue Bank*. 2022; 23 (3): 511–520. doi: 10.1007/s10561-021-09977-x.
20. *Nemets EA, Kirsanova LA, Basok JB, Schagidulin MJ, Volkova EA, Metelsky ST, Sevastianov VI.* Technology

features of decellularization of human liver fragments as tissue-specific fine-grained matrix for cell-engineering liver construction. Russian *Journal of Transplantology and Artificial Organs*. 2017; 19 (4): 70–77. [In Russ, English abstract]. doi: 10.15825/1995-1191-2017-4-70-77.

21. *Kirillova AD, Basok YB, Lazhko AE, Grigoryev AM, Kirsanova LA, Nemets EA, Sevastianov VI.* Creating a tissue-specific microdispersed matrix from a decellularized porcine liver. *Physics and Chemistry of Materials Processing*. 2020; 4: 41–50. [In Russ, English abstract]. doi: 10.30791/0015-3214-2020-4-41-50.
22. GOST ISO 10993-5-2011. Medical devices. Biological evaluation of medical devices. Part 5. Tests for *in vitro* cytotoxicity. M.: Standartinform, 2014; 9.
23. *Gordillo M, Evans T, Gouon-Evans V*. Orchestrating liver development. *Development*. 2015; 142 (12): 2094–2108. doi: 10.1242/dev.114215.
24. *Zhou J, Fritze O, Schleicher M, Wendel HP, Schenke-Layland K, Harasztosi C et al.* Impact of heart valve decellularization on 3-D ultrastructure, immunogenicity andthrombogenicity. *Biomaterials*. 2010; 31 (9): 2549–2554. doi: 10.1016/j.biomaterials.2009.11.088.
25. *O'Neill JD, Anfang R, Anandappa A, Costa J, Javidfar J, Wobma HM et al.* Decellularization of human and porcine lung tissues for pulmonary tissue engineering. *Ann Thorac Surg*. 2013; 96 (3): 1046–1056. doi: 10.1016/j.athoracsur.2013.04.022.
26. *Sullivan DC, Mirmalek-Sani SH, Deegan DB, Baptista PM, Aboushwareb T, Atala A, Yoo JJ.* Decellularization methods of porcine kidneys for whole organ engineering using a high-throughput system. *Biomaterials*. 2012; 33 (31): 7756–7764. doi: 10.1016/j.biomaterials.2012.07.023.

The article was submitted to the journal on 17.08.2024

DOI: 10.15825/1995-1191-2025-1-114-134

USE OF MESENCHYMAL STEM CELLS IN SOLID ORGAN TRANSPLANTATION: CHALLENGES AND PROSPECTS (SYSTEMATIC REVIEW)

Yu.B. Basok[1], A.S. Ponomareva[1], N.V. Grudinin[1], D.N. Kruglov[1], V.K. Bogdanov[1], A.D. Belova[1], V.I. Sevastianov[1, 2]

[1] Shumakov National Medical Research Center of Transplantology and Artificial Organs, Moscow, Russian Federation

[2] Institute of Biomedical Research and Technology, Moscow, Russian Federation

Organ transplantation continues to be the gold standard for saving the lives of patients with end-stage organ diseases. Its goal is to help recipients live longer and better lives. However, despite advancements, organ transplantation still faces serious challenges, such as organ shortage and the effects of chronic immunosuppression. In this regard, there is ongoing vigorous search for therapeutic strategies that can improve the efficacy of allogeneic organ transplantation. Mesenchymal stems cells (MSCs) can significantly enhance and accelerate regenerative processes in damaged organs, can angiogenesis angiogenesis and inhibit cell apoptosis, inflammation and fibrosis formation, and have immunomodulatory properties. Researchers and physicians are interested in MSCs because of a set of unique properties that could be useful in solid organ transplantation. This review critically analyzes and summarizes the actual clinical data related to the study of the therapeutic effects of MSCs in organ transplantation. Electronic databases Medline/PubMed (www/ncbi.nlm.nih.gov/pubmed) and eLIBRARY/Russian Science Citation Index (https://www.elibrary.ru) were searched for relevant literature. Inclusion criteria were clinical use of MSCs to improve the condition of kidney, liver, lung, heart and pancreas recipients, and to enhance graft quality. Exclusion criteria for articles included the use of MSCs for the treatment of non-transplant patients, as well as articles detailing the effects of MSCs products (exosomes, vesicles and conditioned media) and research studies conducted *in vitro* and *in vivo* (without patient participation), conference proceedings, reviews and preprints of articles. Thirty-one original articles in English and Russian languages were selected for literature review. The prospects of MSCs in transplantology are also covered in the paper.

Keywords: mesenchymal stem cells, kidney transplantation, liver transplantation, lung transplantation, ex vivo perfusion, regenerative medicine.

INTRODUCTION

Organ transplantation continues to be the gold standard treatment for end-stage organ diseases. It is aimed at prolonging and improving the quality of life of recipients. In 2022, the number of organ transplants in the Russian Federation increased by 10.0% compared to 2021 [1]. While organ transplantation has significantly advanced in medical technology, it still faces serious challenges, such as organ shortage and the potentially harmful side effects associated with long-term immunosuppressive medications needed to prevent organ rejection in the recipient's body [2–5]. In this regard, the search for therapeutic approaches that can improve the effectiveness of allogeneic organ transplantation is actively pursued.

Mesenchymal stem/stromal cells (MSCs) have garnered significant interest in research and clinical practice because of their unique properties. By their nature, MSCs can be directed to differentiate into various mesenchymal tissues like cartilage, fat, and bone [6]. MSCs are also known to have immunomodulatory properties that make their allogeneic transplantation possible [7]. In addition, MSCs are accessible and there are no ethical restrictions in their use [8]. However, many researchers attribute the therapeutic potential of MSCs to the production of numerous regulatory and growth-stimulating factors, exosomes, microvesicles, lipoproteins, microRNAs, and apoptotic cells into the surrounding environment, which significantly enhance and accelerate tissue repair in damaged organs, stimulate angiogenesis, and prevent cell apoptosis, inflammation, and fibrosis formation [9]. The use of MSCs for the treatment of a wide range of pathologies has been reported, including cardiovascular [10, 11], neurodegenerative [12, 13], autoimmune [14, 15], lung [16], liver [17], kidney [18], orthopedic diseases [19], and coronavirus infection COVID-19 [20].

These properties highlight the significant potential of MSCs in solid organ transplantation. Incorporating MSCs into machine perfusion systems can enhance do-

Corresponding author: Yulia Basok. Address: 1, Shchukinskaya str., Moscow, 123182, Russian Federation. Phone: (499) 190-45-90. E-mail: bjb2005@mail.ru

nor organ viability and function by mitigating ischemia-reperfusion injury (IRI) and promoting post-transplant tissue recovery [21]. At the same time, MSCs may serve as an adjunct immunosuppressive (immune-tolerizing) therapy to reduce postoperative complications [22].

This systematic review critically evaluates and summarizes the current clinical evidence on the therapeutic effects of MSCs in organ transplantation. Data were sourced from electronic databases, including Medline/PubMed (www.ncbi.nlm.nih.gov/pubmed) and eLIBRARY/Russian Science Citation Index (https://www.elibrary.ru).

DATABASES REVIEWED AND SEARCH RESULTS

The literature search was conducted in electronic databases Medline/PubMed (www/ncbi.nlm.nih.gov/pubmed) and eLIBRARY/Russian Science Citation Index (https://www.elibrary.ru).

The following terms were used as search query in Medline/PubMed: mesenchym*[ti] AND transpl*[ti] AND organ*[ti] (search query 1); mesenchym*[ti] AND transpl*[ti] AND liver*[ti] (search query 2); mesenchym*[ti] AND transpl*[ti] AND hepat*[ti] (search query 3); mesenchym*[ti] AND transpl*[ti] AND kidn*[ti] (search query 4); mesenchym*[ti] AND transpl*[ti] AND renal*[ti] (search query 5); mesenchym*[ti] AND transpl*[ti] AND heart*[ti] (search query 6); mesenchym*[ti] AND transpl*[ti] AND cardio*[ti] (search query 7); mesenchym*[ti] AND transpl*[ti] AND pancr*[ti] (search query 8); mesenchym*[ti] AND transpl*[ti] AND lung*[ti] (search query 9). Date of last search: 29.07.2024.

The following terms were used as search query in eLIBRARY: mesenchym* transpl* organ* (search query 1); мезенхим* транспл* орган* (search query 2); mesenchym* transpl* liver* (search query 3); mesenchym* transpl* hepat* (search query 4); мезенхим* транспл* печен* (search query 5); mesenchym* transpl* kidn* (search query 6); mesenchym* transpl* renal* (search query 7); мезенхим* транспл* поч* (search query 8); mesenchym* transpl* heart* (search query 9); mesenchym* transpl* cardio* (search query 10); мезенхим* транспл* серд* (search query 11); mesenchym* transpl* pancr* (search query 12); мезенхим* транспл* поджелуд* (search query 13); mesenchym* transpl* lung* (search query 14); мезенхим* транспл* легк* (search query 15). Date of last search: July 30, 2024.

The inclusion criteria for this analysis encompassed clinical studies investigating the use of MSCs to improve outcomes in kidney, liver, lung, heart, and pancreas transplant recipients, as well as to enhance graft quality. Only full-text original articles published in English and Russian were considered. Exclusion criteria included studies where MSCs were used for conditions unrelated to organ transplantation, research focusing on MSC-derived products (such as exosomes, vesicles, or conditioned media), and *in vitro* or *in vivo* studies that did not involve human patients. In addition, conference proceedings, review articles, and preprints were excluded.

The flow chart of literature search process is shown in Fig. 1.

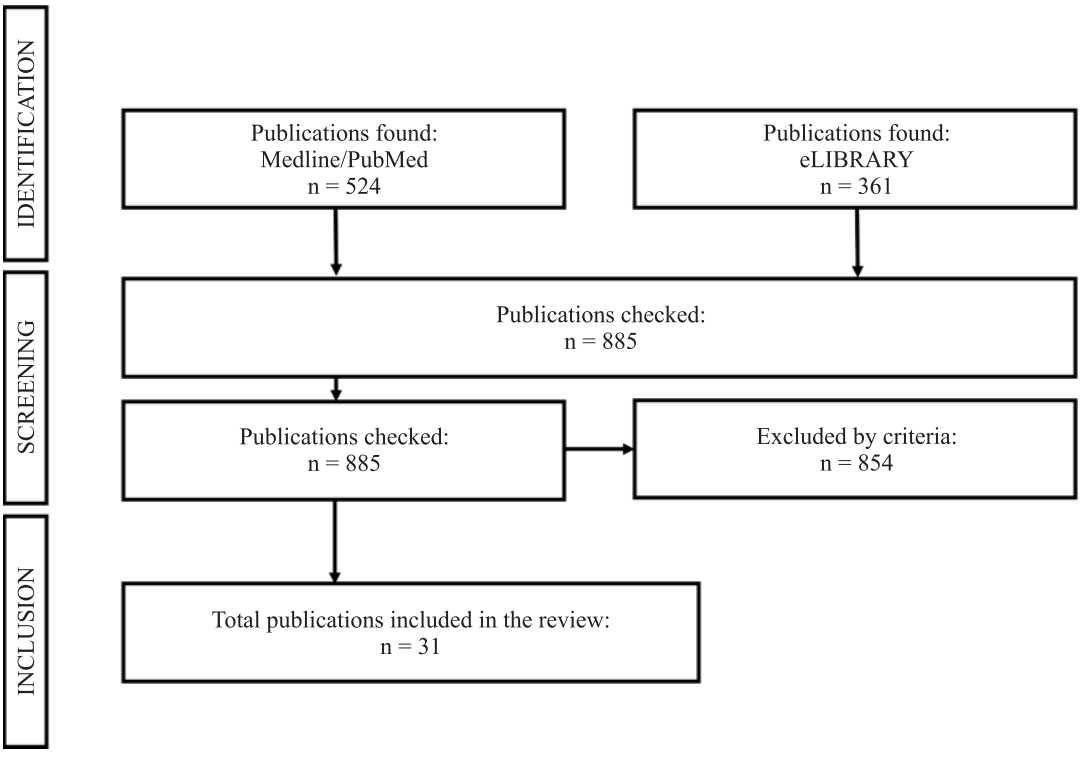

Fig. 1. Literature search flow diagram employed for this review

The initial search identified 885 publications. First, articles were manually excluded if they focused on MSC use in patients who had not undergone solid organ transplantation. Additionally, studies examining the effects of MSC-derived products, such as exosomes, vesicles, and conditioned media, were removed. Next, literature reviews and studies conducted under *in vitro* and *in vivo* conditions were excluded. In the final stage, 16 duplicate publications found in both PubMed and eLIBRARY databases were removed. As a result, 31 articles were included in the study [23–53]. Among the selected studies, 24 articles focused on patients who underwent kidney transplants [23–46], while 6 publications examined the effects of MSC administration in liver transplants [46–52]. One study explored the use of MSCs in lung transplantation [53]. No clinical studies reporting the use of MSCs in heart and pancreas transplants were found.

STUDY RESULTS

Findings from published studies indicate that both autologous and allogeneic MSCs are safe and exert a positive therapeutic effect in kidney, liver, and lung transplantation (Table). However, the extent of this effect varies among studies.

MSCs in kidney transplant

A key focus of many studies was evaluating whether immunosuppressive therapy could be safely reduced post-transplantation. For instance, Bezstarosti et al. reported that in the MSC-treated group, tacrolimus (Tac) dose was reduced by 50% during the second infusion of autologous MSCs and was completely discontinued after one week, whereas the control group continued Tac therapy. Two years post-transplant, renal function in the MSC group remained comparable to the control group, with no increase in rejection episodes [23].

Casiraghi et al. in a case report showed that infusion of autologous bone marrow-derived (BM-) MSCs in a living kidney transplant (KT) induces graft tolerance, which makes it possible to completely dispense with maintenance immunosuppressive drugs late after transplantation [28].

In a one-year follow-up of a phase I–II open-label trial involving 20 patients, Erpicum et al. demonstrated that a single infusion of allogeneic BM-MSCs after deceased-donor KT was safe, increased regulatory T cell (Treg) concentrations, and improved early allograft function. Notably, 30% of MSC-treated recipients did not require corticosteroids, compared to 40% in the control group [29]. However, long-term effects, including potential immunization against MSCs, remain to be investigated.

Dreyer et al. conducted a 12-month clinical study involving 10 kidney recipients from living (unrelated) donors. Their findings confirmed the safety of allogeneic BM-MSC infusion six months post-transplant in combination with low tacrolimus (Tac) concentrations (1.5–3.0 ng/mL). Following MSC administration, all recipients maintained stable kidney function, with no reported graft rejection or adverse effects related to cell therapy [44].

Peng et al. reported similar findings, demonstrating that allogeneic BM-MSC infusion enabled a reduction in Tac dosage from 0.077 ± 0.005 mg/kg/day to 0.045 ± 0.002 mg/kg/day in related donor kidney recipients. Importantly, this reduction was achieved without immediate or long-term toxic side effects associated with MSC administration. At 12 months of follow-up, only one acute rejection occurred in the control group, while all MSC-treated patients maintained stable kidney function with a 100% survival rate [38].

In a larger cohort, Pan et al. showed that a combination of reduced-dose Tac (0.04 ± 0.05 mg/kg/day) and allogeneic MSCs was as effective as the standard Tac regimen (0.07 ± 0.08 mg/kg/day) in maintaining graft survival for two years following living-related KT. No significant differences were observed in acute rejection rates, graft survival, serum creatinine levels, or glomerular filtration rate between the two groups [43]. These findings suggest that MSC administration may facilitate the use of lower doses of nephrotoxic calcineurin inhibitors (CNIs) post-KT.

Vanikar et al. reported a clinical case in which co-infusion of donor adipose-derived (AD-) MSCs and bone marrow-derived hematopoietic stem cells (HSCs) was administered before living-donor KT under nonmyeloablative conditioning. This approach successfully induced transplant tolerance, with stable kidney function maintained in the complete absence of immunosuppression for up to three years post-transplant [41].

Building on these findings, the authors conducted a prospective, open-blind randomized study involving 285 patients. Their results demonstrated the safety and efficacy of co-infusion of autologous AD-MSCs and bone marrow-derived HSCs into the portal circulation prior to KT. This strategy, combined with nonmyeloablative conditioning, effectively minimized the need for immunosuppression [42].

Meucci et al. demonstrated that autologous BM-MSC therapy, combined with complete Tac withdrawal, is a promising strategy for KT recipients. This approach not only effectively prevents graft rejection but also offers potential cardioprotective benefits [45]. A combination of MSC therapy with CNI withdrawal prevented progressive left atrial enlargement and dysfunction six months post-transplant [46].

In a study involving 53 patients, Wei et al. evaluated the efficacy and safety of allogeneic BM-MSC administration in kidney allograft recipients with chronic active antibody-mediated rejection. No adverse events such as fever, anaphylaxis, phlebitis, venous thrombosis, cardiovascular complications, or malignancies were observed following MSC therapy. The two-year allograft survival

rate was significantly higher in patients who received four doses of allogeneic BM-MSCs compared to the control group (87.0% *vs.* 66.7%) [26].

Reinders et al. demonstrated the feasibility, safety, and systemic immunosuppressive effects of two intravenous infusions of autologous BM-MSCs in kidney transplant recipients administered four weeks post-transplant. These recipients exhibited signs of rejection and/or increased interstitial fibrosis and tubular atrophy, highlighting the potential of MSCs in managing early post-transplant complications [39].

Similarly, Ban et al. confirmed the safety of four intravenous injections of allogeneic BM-MSCs, administered every two weeks, in two patients experiencing chronic active antibody-mediated rejection after kidney transplantation [27]. However, graft function deteriorated within six months after the final MSC dose, suggesting that MSC therapy may offer only short-term benefits in cases of prolonged antibody-mediated rejection resistant to conventional treatments.

Večerić-Haler et al. reported no positive effect of autologous MSC therapy in a patient with late antibody-mediated kidney rejection, occurring three years after transplantation. Within two months of follow-up, the patient experienced multiple complications, including nausea, vomiting, blepharitis, diarrhea, ascites, splenomegaly, arterial hypertension, proteinuria, and pancytopenia. All symptoms resolved following the removal of the damaged kidney [25]. The poor outcome was associated with parvovirus B19 infection introduced via the donor organ, underscoring the need to establish clear contraindications for MSC therapy in antibody-mediated kidney rejection.

Of particular interest is the clinical case reported by Dave et al. A patient with type I diabetes mellitus and end-stage renal disease received a combination therapy of allogeneic undifferentiated AD-MSCs, insulin-producing cells differentiated from AD-MSCs, and hematopoietic bone marrow cells one month before undergoing a living-donor KT. Remarkably, the patient maintained stable renal graft function for 13 months without signs of rejection or deterioration of diabetic status, despite continued administration of CNIs and steroids [40].

MSCs in liver transplant

Korotkov S.V. et al. reported a clinical case demonstrating the feasibility of minimizing Tac doses in cases of renal impairment associated with chronic liver transplant rejection. Their findings suggested that reducing Tac did not exacerbate immunological dysfunction and emphasized the necessity of multiple MSCs infusions to establish an adequate immunotolerant environment in the recipient [47]. Similarly, Detry et al. successfully reduced Tac doses in liver transplant recipients following allogeneic BM-MSCs infusion, without significant side effects or graft rejection, in contrast to the control group [51].

Mora et al. described a clinical case where MSCs were successfully used alongside cyclosporine and methylprednisolone to regulate the immune response in an liver transplant recipient experiencing graft-versus-host disease [49]. The authors emphasized the importance of considering individual patient factors such as disease severity, overall health status, and comorbidities. They also highlighted the necessity of continuous monitoring, including liver function assessment, infection rates, and potential complications, to enable timely adjustments in therapy.

Zhang et al. conducted a study with 82 patients diagnosed with ischemic cholangiopathy after deceased-donor liver transplant. The results showed that administering human umbilical cord-derived (UC-) MSCs to liver recipients was safe, with no significant MSC-related adverse events. UC-MSC therapy improved liver function, as indicated by decreased levels of total bilirubin, gamma-glutamyl transferase (γGT), and alkaline phosphatase at week 20 post-treatment. The need for interventional procedures (e.g., endoscopic retrograde cholangiopancreatography, stenting, percutaneous transhepatic cholangiostomy) was significantly lower in the MSC group (33.3%) compared to the control group (64.3%). Moreover, the 1- and 2-year graft survival rates were higher in the MSC-treated group than in the control group [52].

MSCs in lung transplant

Erasmus et al. found that the administration of allogeneic BM-MSCs may slow the decline in lung transplant function in recipients experiencing chronic rejection [53].

Our analysis revealed that most of the included studies (n = 23) utilized autologous or allogeneic BM-MSCs, while only five studies used AD-MSCs and one study used UC-MSCs; in two studies, the cell source was unspecified. Autologous MSCs were used in 11 studies, whereas allogeneic MSCs were used in 18 studies.

In one study, Kaundal et al. compared autologous and allogeneic BM-MSC infusion one day before and 30 days after KT from a related donor. The study found no dose-dependent toxicity from MSCs of different origins. Flow cytometric analysis showed an increase in B regulatory lymphocyte populations and nonconventional regulatory T cells (Tregs), along with a decrease in T effector lymphocyte proportions in patients receiving autologous MSCs. These preliminary findings suggest that autologous MSCs may be a safer option for reducing adverse immune responses, whereas allogeneic MSCs may trigger specific cellular and humoral immune responses against donor antigens [24].

The optimal number of MSCs required to achieve effective immunosuppression remains unknown, as do-

sage selection in studies is largely empirical and requires further investigation. The most commonly used MSC dose ranges from 1.0 to 2.0 × 10^6 cells per kg of body weight, while some studies have administered up to 5.0 × 10^6 cells per kg in a single infusion.

Of particular interest is the study by Mudrabettu et al., in which an initial lower dose of 0.21 × 10^6 cells per kg was administered to the first two patients before increasing to levels comparable to other studies. Regardless of the administered cell dose, recipients demonstrated an increase in Tregs populations and a decrease in T-cell proliferation [31].

Determining the optimal timing for MSC administration is crucial for the success of MSC therapy. In a pilot study involving two kidney recipients from a related donor, Perico et al. suggested that pre-transplant infusion of autologous BM-MSCs may be beneficial [36]. A subsequent study by the same authors demonstrated that a single pre-transplant infusion of MSCs did not negatively impact the kidney graft while maintaining therapeutic immunomodulatory effects. They also observed a correlation between Treg expansion and basiliximab induction therapy [32].

In a long-term follow-up study with a larger patient cohort, Perico et al. reported stable kidney graft function for 5–7 years after a single infusion of autologous BM-MSCs, alongside minimal maintenance immunosuppressive therapy. Importantly, their findings indicated that MSC infusion did not significantly increase susceptibility to infections or tumor development over the long term [30]. The main results of our study are summarized in Table.

Fig. 2 presents the overall screening results of scholarly publications on the use of MSCs in organ transplantation. The figure reflects the number of publications identified in the initial search, followed by the exclusion of studies focusing on conditioned media, vesicles, and exosomes, which were not within the scope of this review.

Fig. 2 highlights that the number of preclinical trials (*in vitro* and *in vivo*) significantly surpasses that of clinical trials by more than two times according to the Medline/PubMed search and over 1.5 times according to the eLIBRARY search. It should be noted that although no clinical cases of MSC use in heart transplantation have been reported, approximately 20 studies have explored this area. This suggests that MSCs in heart transplantation is an emerging field that is gradually progressing toward clinical application. Additionally, the presence of numerous literature reviews and commentaries in the search results underscores the growing interest and scientific focus on this evolving area of clinical research.

At first glance, the absence of publications on MSC use in pancreas transplantation may seem surprising. However, this can be explained by the successful application of co-transplantation of MSCs with pancreatic islets as an alternative approach to full pancreas transplantation [54–56].

Allogeneic islet transplantation is considered a viable treatment option for patients with type I diabetes mellitus who have had the disease for over five years, are aged 18 to 65 years, experience recurrent severe hypoglycemic episodes and/or glycemic instability, show lack of sensitivity to hypoglycemic states, and have undetectable C-peptide levels [57–61].

This alternative approach may explain the scarcity of clinical studies specifically investigating the use of MSCs in pancreas transplantation.

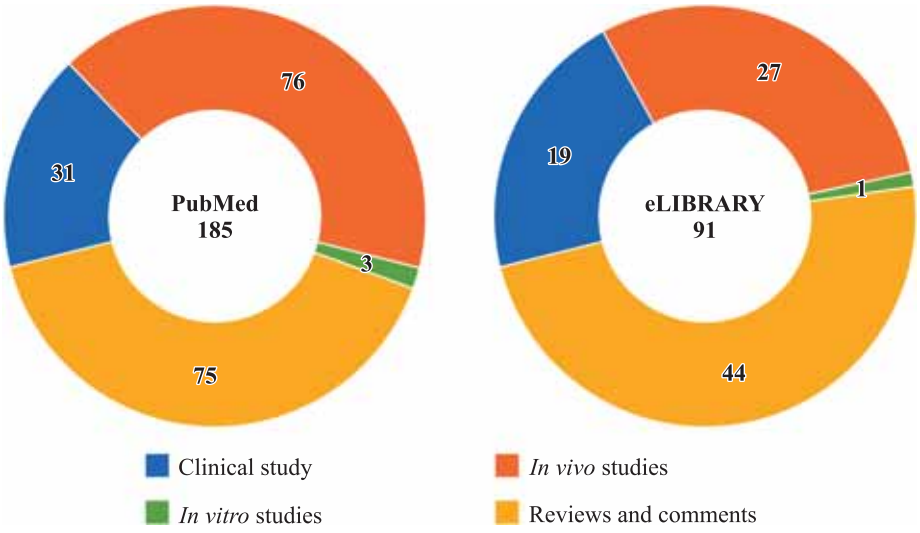

Fig. 2. Results of screening of scholarly publications covering the use of mesenchymal stems cells in organ transplantation in the electronic databases Medline/PubMed (www/ncbi.nlm.nih.gov/pubmed) and eLIBRARY/Russian Science Citation Index (https://www.elibrary.ru)

Table

General characteristics and results of studies included in this review

Publication	Patient group	Type of MSCs	Dose of MSCs	Administration route and frequency	Immunosuppressive therapy	Results
1	2	3	4	5	6	7
Kidney transplant						
Bezstarosti, 2023 [23]	70	Autologous (source not stated)	1.0–2.0 × 10^6 cells/kg body weight	IV at weeks 6 and 7 of transplantation	Tacrolimus, everolimus, prednisolone. In the MSCs group, tacrolimus dose was reduced to 50% during the second infusion of MSCs and completely withdrawn after 1 week, whereas in the control group, tacrolimus therapy was continued	MSC therapy promotes early tacrolimus withdrawal in living donor kidney transplant recipients: 45% of patients receiving MSCs were able to continue treatment without tacrolimus based on everolimus and prednisolone. The authors pointed out that more thorough research is necessary to establish precise criteria for prescribing MSCs as immunosuppressive therapy in KT
Kaundal, 2022 [24]	15	Autologous or allogeneic bone marrow-derived MSCs	1.0–1.5 × 10^6 cells/kg body weight	IV 1 day before transplantation and 30 days after transplantation	Tacrolimus, mycophenolate mofetil, prednisolone	Autologous MSC infusion was found to be safe and well tolerated by patients, and all recipients showed stable graft function following rejection episodes in a few cases. Differences in immunological responses were demonstrated regardless of the same origin, isolation, expansion conditions, and dosage of MSCs. The authors noted the need for more in-depth studies due to small sample size and lack of functional assessment data
Večerić-Haler, 2021 [25]	1	Autologous bone marrow-derived MSCs	3.0 × 10^6 cells/kg body weight	IV at 1-week intervals (1 week, 1 week, 2 weeks) 3 years after KT	Tacrolimus, mycophenolate mofetil, steroid	Lack of benefit after administration of autologous MSCs in a patient with late antibody-mediated kidney rejection. The patient was also diagnosed with parvovirus B19 acquired from donor organ
Wei, 2021 [26]	53	Allogeneic bone marrow-derived MSCs	1.0 × 10^6 cells/kg body weight	Regimen 1: 4 monthly IV Regimen 2: 4 weekly IV	Calcineurin inhibitors, mycophenolate mofetil with or without glucocorticoids, methylprednisolone	Immunosuppression combined with MSC infusion may slow down the decline in kidney allograft function in recipients with chronic active antibody-mediated rejection
Ban, 2021 [27]	2	Allogeneic bone marrow-derived MSCs	1.0 × 10^6 cells/kg body weight	4 IV every 2 weeks	Tacrolimus, mycophenolate mofetil, low-dose corticosteroid	Multiple doses of MSCs have been shown to be safe for treating chronic active antibody-mediated rejection in renal transplant recipients. Kidney function was stable during treatment with MSCs, then deteriorated within 6 months of the last MSCs infusion. The authors pointed out the need for more in-depth studies due to small sample size
Casiraghi, 2020 [28]	1	Autologous bone marrow-derived MSCs	2.0 × 10^6 cells/kg body weight	IV 1 day before transplantation	Cyclosporine, mycophenolate mofetil, methylprednisolone, prednisone	MSC infusion enabled a safe withdrawal of maintenance immunosuppressants while maintaining optimal long-term kidney allograft function

Continuation table

1	2	3	4	5	6	7
Erpicum, 2019 [29]	20	Allogeneic bone marrow-derived MSCs	2.0×10^6 cells/kg body weight	IV on 3 ± 2 days after transplantation	Cyclosporine, tacrolimus, mycophenolate mofetil, mycophenolic acid, azathioprine	One year after transplantation, 30% of MSC-treated patients did not require corticosteroids compared to 40% of the control group. It was shown that MSC infusion was safe and that early graft function improved. The authors noted the need for longer-term recipient follow-up
Perico, 2018 [30]	16	Autologous bone marrow-derived MSCs	2.0×10^6 cells/kg body weight	IV 1 day before transplantation or 7 days after	Cyclosporine, mycophenolate mofetil, prednisone	Pre-transplant infusion of MSCs in kidney transplant recipients from a related donor under low-dose maintenance immunosuppressive therapy is safe and does not cause serious side effects even with long-term follow-up
Mudrabettu, 2014 [31]	4	Autologous bone marrow-derived MSCs	First infusion: $0.35–2.1 \times 10^6$ cells/kg body weight. Second infusion: $0.21–2.26 \times 10^6$ cells/kg body weight	IV 1 day before transplantation or 30 days after	Tacrolimus, mycophenolate mofetil, prednisolone	MSCs were showed to be safe for patients who have had living-donor KT. MSC therapy expands regulatory T cells and reduces T cell proliferation. The authors emphasized the need for larger randomized studies to validate the findings
Perico, 2013 [32]	4	Autologous bone marrow-derived MSCs	2.0×10^6 cells/kg body weight	IV 1 day before transplantation	Cyclosporine, mycophenolate mofetil, prednisone	A single pre-transplant infusion of MSCs in recipients of a kidney from a related donor has no adverse effect on the graft, while providing a therapeutic immunomodulatory effect
Lee, 2013 [33]	7	Allogeneic bone marrow-derived MSCs	1.0×10^6 cells/kg body weight	Injection into the bone marrow of the right iliac bone	Calcineurin inhibitor, mycophenolate mofetil, steroids	The safety and feasibility of injecting MSCs into the iliac bone of living-donor kidney recipients was confirmed. No graft loss was detected. Three recipients experienced acute rejection
Tan, 2012 [34]	159	Autologous bone marrow-derived MSCs	$1.0–2.0 \times 10^6$ cells/kg body weight		Standard or 80% reduced dose of calcineurin inhibitors (tacrolimus, cyclosporine), mycophenolate mofetil, methylprednisolone	When compared to IL-2 receptor antibody induction therapy, the use of MSCs among related-donor kidney transplant recipients resulted in lower incidence of acute rejection, reduced risk of opportunistic infection, and improved kidney function at 1 year
Saadi, 2013 [35]	3	Allogeneic bone marrow-derived MSCs	$0.4–0.7 \times 10^6$ cells/kg body weight	2 IV with a 1-week interval	Cyclosporine, mycophenolate mofetil, prednisone	MSC therapy facilitates successful desensitization prior to a repeat KT
Perico, 2011 [36]	2	Autologous bone marrow-derived MSCs	1.7×10^6 or 2.0×10^6 cells/kg body weight	IV 7 days after transplantation	Cyclosporine, mycophenolate mofetil, prednisone	During MSC infusion, a kidney transplant from a related donor was found to be dysfunctional. The recipients were in good condition with stable graft function at 360 and 180 days after transplantation. The authors emphasized the need for more research on the undesirable side effects of MSC therapy
Vanikar, 2010 [37]	200	Allogeneic adipose-derived MSCs	–	Infusion into the omental vein 9 days before transplantation	Cyclosporine, prednisone, azathioprine	In the MSC + HSC group, 12% of recipients experienced acute rejection, 4% died, and there was no graft loss at 18 months after living-donor KT. In the HSC group, there was 18% of rejection episodes, 6% of graft loss and 9% of patients died

Continuation table

1	2	3	4	5	6	7
Peng, 2013 [38]	12	Allogeneic bone marrow-derived MSCs	First infusion: 5.0×10^6 cells/kg body weight. Second infusion: 2.0×10^6 cells/kg body weight	First infusion of MSCs directly into the renal graft artery during KT. Second infusion of MSCs IV after 1 month	Methylprednisolone, tacrolimus, mycophenolate mofetil, prednisolone	Tacrolimus dosage was lowered by 50% thanks to MSC therapy
Reinders, 2013 [39]	6	Autologous bone marrow-derived MSCs	$1.0–2.0 \times 10^6$ cells/kg body weight	Twice IV at 7-day intervals	Prednisone, tacrolimus or cyclosporine, mycophenolate mofetil	It is safe and clinically feasible to treat kidney recipients with subclinical rejection and/or interstitial fibrosis/tubule atrophy with MSCs
Dave, 2013 [40]	1	Allogeneic adipose-derived MSCs	1.1×10^4 cells/kg body weight	1 month prior to KT: infusion into the thymic bloodstream via femoral catheterization	Tacrolimus, mycophenolate sodium, prednisolone	Stable kidney graft function, no rejection, no worsening of diabetic status
Vanikar, 2013 [41]	1	Allogeneic adipose-derived MSCs	–	Portal infusion 16 days before KT	Methylprednisolone, prednisone	Achievement of graft tolerance with stable living-donor kidney graft function without immunosuppression at 6 months 3 years after transplantation
Vanikar, 2014 [42]	285	Allogeneic adipose-derived MSCs	4.6×10^4 cells/kg body weight	Infusion of cells into the omental vein 14 days before transplantation	Tacrolimus, prednisolone. The control group additionally received mycophenolate sodium	Patient survival at 7 years after living-donor KT under nonmyeloablative conditioning was 94.7% in the MSC + HSC group, 92.5% in the HSC group, and 78.4% in the control group. Graft survival rates for the same period were 94.6%, 86%, and 94.4%, respectively. The MSC + HSC group had the best outcomes, with the HSC group experiencing fewer rejection events and requiring less immunosuppression than the control group
Pan, 2016 [43]	32	Allogeneic bone marrow-derived MSCs	First infusion: 5×10^6 cells/kg body weight. Second infusion: 2×10^6 cells/kg body weight	First infusion of MSCs directly into the renal allograft artery during KT. Second infusion of MSCs intravenously 1 month later	Methylprednisolone, tacrolimus, mycophenolate mofetil, prednisolone	The combination of low-dose tacrolimus and MSC was as effective as standard-dose tacrolimus in maintaining graft survival for 2 years after transplantation
Dreyer, 2020 [44]	10	Allogeneic bone marrow-derived MSCs	$1.0–2.0 \times 10^6$ cells/kg body weight	Twice IV 6 months after transplantation	Tacrolimus, everolimus, prednisone	No acute rejection or graft loss was observed after administration of MSCs, renal function remained stable, and there were no marked changes in T- and B-cell populations or plasma cytokines. Administration of allogeneic MSCs combined with low-dose tacrolimus 6 months after transplantation is safe, at least for the first year after KT. The authors noted the need for further study of the efficacy of allogeneic MSCs in KT

Continuation table

1	2	3	4	5	6	7
Meucci, 2021 [45]	54	Autologous bone marrow-derived MSCs	1.0–2.0 × 10^6 cells/kg body weight	Twice weekly IV	Everolimus, prednisolone, tacrolimus	In KT recipients, MSC therapy combined with early tacrolimus withdrawal safely improves blood pressure control compared with standard-dose tacrolimus treatment 24 weeks after transplantation and attenuates adverse left ventricular remodeling characterized by myocardial hypertrophy and diastolic dysfunction. The authors pointed out the need for further studies to determine the impact of this promising immunosuppression regimen on long-term cardiovascular outcomes
Meucci, 2022 [46]	54	Autologous bone marrow-derived MSCs	1.0–2.0 × 10^6 cells/kg body weight	Twice weekly IV at weeks 6 and 7 post transplant	Everolimus, prednisolone, tacrolimus	A combination of MSC therapy and withdrawal of calcineurin inhibitors prevents progressive left atrial enlargement and dysfunction in the first 6 months after KT
Liver transplant						
Korotkov, 2022 [47]	1	Allogeneic adipose-derived MSCs	2.0 × 10^6 cells/kg body weight	MSCs infusion at days 392, 396, 400, 458 of transplantation	Tacrolimus, mycophenolate mofetil, medrol, certican	The efficacy of MSCs as an alternative way of immunosuppressive therapy was demonstrated, enabling to minimize tacrolimus doses in the development of renal damage against the background of chronic liver transplant rejection without running the risk of aggravating the severity of immunological dysfunction. The authors noted the need for further research on the use of MSCs in the late period after transplantation
Vandermeulen, 2021 [48]	10	Allogeneic bone marrow-derived MSCs	1.5–3.0 × 10^6 cells/kg body weight	IV at day 3 ± 2 of transplantation	Tacrolimus, mycophenolate mofetil	Infusion of MSCs did not cause infections or malignancies over 85 months of follow-up of liver recipients. No clear benefits for survival or graft function were found in the groups receiving and not receiving MSCs. The authors underlined the need for additional studies to better understand the effects of MSCs on transplanted organs
Mora, 2018 [49]	1	–	1.0 × 10^6 cells/kg body weight	MSCs infusion on day 35, 38, 42, and 47 of transplantation	Basiliximab, mycophenolate mofetil, tacrolimus, everolimus, methylprednisolone, cyclosporine	MSCs have demonstrated the potential to modulate the immune response in liver recipients against the background of graft-versus-host disease, which may lead to improved treatment outcomes and reduced the side effects of traditional immunosuppressive drugs. The authors recommended additional studies to better understand the mechanisms of action of MSCs
Casiraghi, 2020 [50]	20	Allogeneic bone marrow-derived MSCs	1.0–2.0 × 10^6 cells/kg body weight	IV during premedication	Tacrolimus, mycophenolate mofetil, methylprednisolone, prednisone	MSC infusion is safe, well-tolerated by liver recipients, does not cause infections or malignancies at 1-year follow-up, and promotes Tregs expansion. To validate the findings, the authors pointed out that a study with larger patient cohorts to confirm the results

End of table

1	2	3	4	5	6	7
Detry, 2017 [51]	20	Allogeneic bone marrow-derived MSCs	1.5–3.0 × 10^6 cells/kg body weight	IV on day 3 of LT ± 2 days	Tacrolimus, mycophenolate mofetil	No serious side effects and graft rejection were observed in liver recipients after MSC infusion in contrast to the control group. Additionally, MSCs made it possible to safely lower tacrolimus dosages
Zhang, 2016 [52]	82	Allogeneic human umbilical cord-derived MSCs	1.0 × 10^6 cells/kg body weight	IV at weeks 1, 2, 4, 8, 12, and 16 of diagnosis of ischemic cholangiopathy	Not specified	In liver recipients treated with MSCs, the need for interventional therapies reduced to 33.3% (64.3% in the control group) and graft survival increased at year 1 and 2 of follow-up
Lung transplant						
Erasmus, 2022 [53]	13	Allogeneic bone marrow-derived MSCs	0.5–1.0 × 10^6 cells/kg body weight	Single or repeated IV	Cyclosporine, mycophenolate mofetil, tacrolimus, prednisolone, azathioprine	Intravenous infusions of bone marrow-derived MSCs are well tolerated by lung transplant recipients with chronic rejection. In some patients, low doses of MSCs seem to halt the course of chronic obstructive pulmonary disease. The authors noted the need for more research to assess the efficacy of MSCs

Note: IV, intravenous infusion; MSCs, mesenchymal stem cells; KT, kidney transplant; LT, liver transplant; IL-2, interleukin-2; HSCs, hematopoietic stem cells.

Thus, the analyzed publications confirm the safety and therapeutic efficacy of MSC use in kidney, liver, and lung transplantation. MSCs exhibit regulatory potential, making them a promising tool for treating rejection reactions and inducing immune tolerance. They effectively suppress alloreactivity both before and after transplantation and may be suitable for prophylactic use during transplantation as well as for the treatment of rejection episodes post-transplant.

PROSPECTS FOR THE USE OF MESENCHYMAL STEM CELLS IN TRANSPLANTOLOGY

MSCs have shown promising potential in treating a variety of diseases including disorders of the nervous system and brain, liver cirrhosis, lung diseases, and cardiovascular diseases; they are also used in autoimmune diseases, for wound healing, in plastic surgery, etc., which has been confirmed by a large volume of preclinical and clinical trials [17, 19, 62–67]. The number of publications devoted to the use of MSCs for patient treatment is increasing. According to literature, 1426 clinical trials have been registered as of 2022, which is four times more than in 2013 [68]. The accumulated data revealed a number of potential mechanisms that explain the therapeutic effects of MSCs and the interest in them.

MSCs are multipotent cells capable of differentiating into multiple cell types, including osteoblasts (bone cells), chondrocytes (cartilage cells) and adipocytes (fat cells). In response to tissue injury signals and release of pro-inflammatory cytokines, MSCs secrete a variety of factors, including chemokines and cytokines, that promote regeneration and modulate immune responses. These include anti-apoptotic (STC-1, ECVs) and antifibrotic factors (bFGF, HGF), which help limit tissue damage and enhance healing, tissue precursor activators (TIMP-1, TIMP-2, TSP2, ECVs) and growth factors (TGF-β, VEGF, IGF1, HGF, KGF), which stimulate cell proliferation and differentiation, chemoattractants, which recruit endogenous precursors to the injury site, immune modulators (PGE2, TSG-6, ECVs), which locally regulate immune responses by selectively inhibiting immune cell proliferation (Fig. 3) [9, 69–71].

MSCs come from a variety of human tissue sources, such as bone marrow, adipose tissue, dermis, skeletal muscle, synovium, subcutaneous veins, dental pulp, umbilical cord-derived Wharton's jelly, amniotic fluid, lung and liver [8, 72]. Due to the diversity of MSCs sources, minimum criteria for identifying MSCs have been proposed by the International Society for Cell & Gene Therapy [6]: adhere to plastic when cultured under standard conditions; they must express the surface markers CD105, CD73 and CD90 and not express the surface markers CD45, CD34, CD14 or CD11b, CD79a or CD19 and HLA DR; MSCs must differentiate into osteoblasts, adipocytes and chondroblasts *in vitro*.

To use MSCs in clinical treatments, they need to be expanded in a lab to reach a large enough quantity, but this process of prolonged culturing can negatively impact

their important characteristics like phenotype, ability to differentiate into different cell types, and genetic stability, which is why careful monitoring is crucial to ensure their safety and effectiveness in therapy [73–75].

MSCs have been reported to have immunoregulatory properties, meaning they can suppress the proliferation, differentiation, maturation, and overall function of various immune cells [76–78]. MSCs have been shown to have the capability to activate regulatory T cells (Tregs) and regulatory B lymphocytes, which then function to suppress the activity of other immune cells, particularly effector and memory T cells [79]. In addition, MSCs have the capability to inhibit the development and maturation of dendritic cells (DCs), thereby significantly reducing their ability to activate T lymphocytes [80]. MSCs can induce tolerogenic DCs that produce interleukin-10 and promote Treg expansion [81]. MSCs have the ability to shift the phenotype of macrophages from a pro-inflammatory M1 state to an anti-inflammatory M2 state [82]. MSCs have also been shown to inhibit IL-2 mediated proliferation and cytotoxic activity of natural killer (NK) cells [83]. MSCs also produce significant quantities of chemokines, which attract immune cells to their location through a process called chemotaxis. Further, MSCs secrete immunosuppressive factors that act on migrating immune cells [84]. MSCs secrete a number of anti-inflammatory factors, namely, transforming growth factor (TGF-β), hepatocyte growth factor (HGF), nitric oxide, hemoxygenase-1, indoleamine-2,3-dioxygenase and express inhibitory costimulatory molecules such as, TRAIL and PD-L1 [85]. The activation of paracrine signaling pathways in the body by MSCs is of particular importance because isolated MSCs remain viable in the recipient body for a short period of time [86]. A recent study has revealed that when MSCs undergo programmed cell death (apoptosis) after being administered, this process is crucial in triggering immunosuppressive mechanisms within the body [87].

MSCs also have low immunogenicity, which allows the use of allogeneic cells. This feature of MSCs is associated with low expression of MHC class I molecules and absence of MHC class II, as well as costimulatory molecules B7-1, B7-2, CD80, CD40, CD40L and Fas ligand on the surface [88, 89].

Due to the above-mentioned properties of MSCs, their use arouses the interest of transplantologists as a means to develop a new therapeutic approach capable of improving the efficacy of treatment of solid organ recipients: MSCs possess immunomodulatory properties and can promote graft regeneration by releasing various bioactive molecules including exosomes, microvesicles, and soluble factors like growth factors, cytokines, and chemokines. There is strong evidence that MSCs have the potential to mitigate the severity of ischemic and reperfusion injury in multiple organs like heart, kidney, liver, brain, and lung [90–95].

Several key challenges complicate the clinical application of MSCs in organ transplantation. As shown

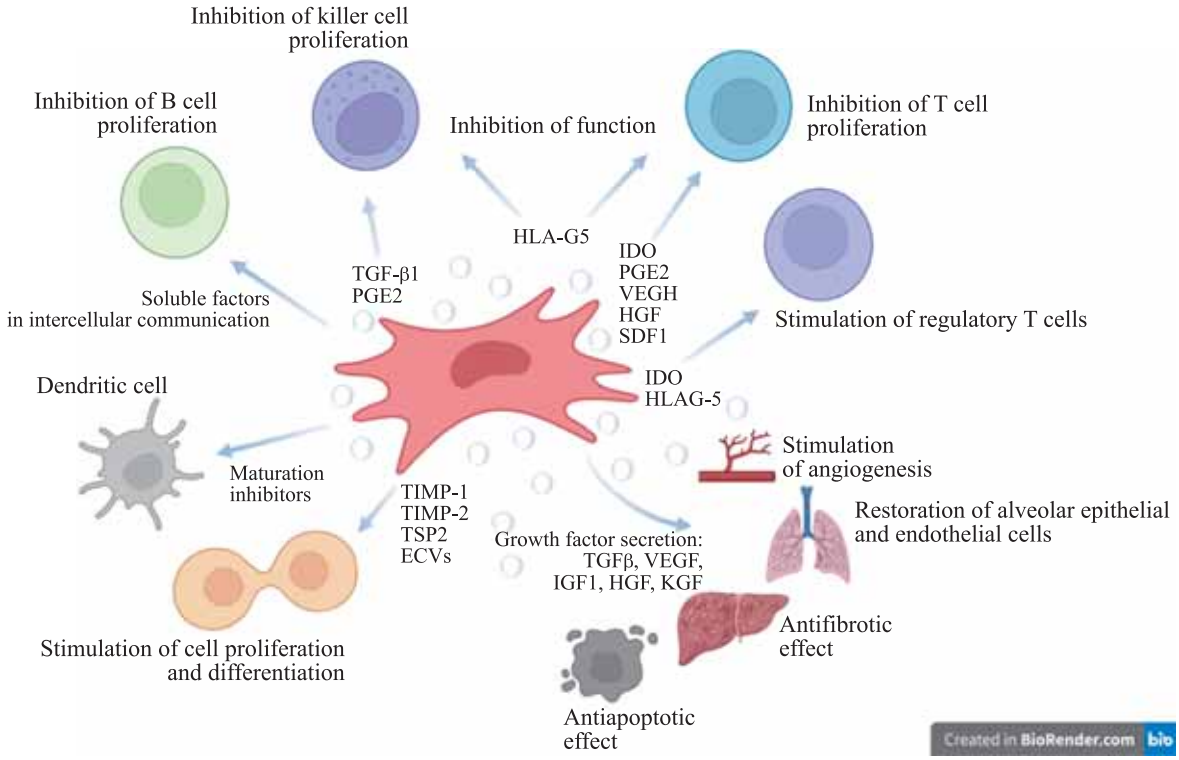

Fig. 3. Biological properties and effects of mesenchymal stem cells (MSCs). The figure was created using the BioRender.com program based on analysis of the collected database

in Table, MSCs from various sources have been used in clinical settings, yet studies indicate that their properties vary depending on their tissue of origin [96]. The heterogeneity of properties of MSCs from different donors remains an unresolved issue that may impact therapeutic outcomes [97].

The donor's age also influences MSC efficacy, as cells from older donors exhibit lower proliferative potential [98]. Furthermore, standardization of isolation and *in vitro* expansion protocols is crucial for maintaining MSC quality [99]. Current studies report significant variations in cell dose, infusion timing, and administration protocols, highlighting the need for standardized guidelines. Addressing these challenges is essential to optimizing the therapeutic efficacy of MSC therapy in transplantation.

Patients undergoing solid organ transplantation typically receive a combination of immunosuppressive drugs (ISDs) such as CNIs, corticosteroids, and mTOR inhibitors [100–102]. As discussed earlier, MSCs also exhibit immunosuppressive properties and may help mitigate the adverse effects of ISDs on the immune system [103].

Given these potential benefits, clinical trials have explored the use of MSCs as an adjunct to ISDs to enhance transplant outcomes. However, the interaction between MSCs and ISDs remains poorly understood, making it a crucial area for further research. For instance, Eggenhofer et al. demonstrated in a mouse model that different combinations of cyclosporine, everolimus, and mycophenolate mofetil with MSCs had varying effects on heart transplant survival [104].

Machine perfusion technologies have ushered in a new era in organ transplantation [105–108]. By preserving organs under near-physiological conditions, these technologies not only extend preservation time but also enable more accurate assessments of organ function [109]. Moreover, the ability to introduce drugs or cells into the perfusion solution presents an opportunity for targeted regeneration of ischemic organs.

This potential highlights the feasibility of integrating regenerative medicine approaches, particularly MSCs, into machine perfusion. MSCs offer therapeutic benefits through their ability to stimulate tissue metabolism, promote cell proliferation, and exert immunomodulatory, antiapoptotic, and antifibrotic effects. Several studies have demonstrated promising outcomes with MSC administration during machine perfusion of the kidney, liver, and lung [110–112].

As research in this field progresses, standardized protocols for MSC dosing and timing in *ex vivo* machine perfusion may be established, taking into account the organ type, size, and extent of ischemia-reperfusion injury [113].

Advancements in the use of MSC for transplantation are increasingly linked to their pre-activation strategies, one of which involves autophagy modulation [114]. Autophagy plays a crucial role in regulating MSC stemness, viability, differentiation potential, immunomodulatory properties, and pro-angiogenic activity. Enhancing MSC function through autophagy modulation before administration presents a promising approach to improving their therapeutic efficacy in organ transplantation.

By activating MSCs via autophagy modulation, their post-implantation survival can be extended, and the secretion of regulatory molecules – including growth factors, exosomes, microvesicles, lipoproteins, and miRNAs – can be enhanced. These factors accelerate tissue repair, promote angiogenesis, and mitigate apoptosis, inflammation, and fibrosis in transplanted organs [115–117].

Another method for MSC activation involves the use of scaffolds (carriers, matrices), which serve as biomimetic extracellular matrices. Scaffolds provide structural support that prolongs MSC viability and functional efficacy, ensuring an optimized microenvironment for them [118].

CONCLUSION

A review of publications in electronic databases suggests that MSC therapy holds promise for improving outcomes in kidney, liver, and lung transplantation, as well as enhancing graft quality. Studies have explored various MSC sources, dosing regimens, and immunosuppressive protocols. The scarcity of clinical trials further underscores the need for additional research to refine therapeutic protocols.

The authors declare no conflict of interest.

REFERENCES

1. *Gautier SV, Khomyakov SM*. Organ donation and transplantation in the Russian Federation in 2022. 15th Report from the Registry of the Russian Transplant Society. *Russian Journal of Transplantology and Artificial Organs*. 2023; 25 (3): 8–30. [In Russ, English abstract]. doi: 10.15825/1995-1191-2023-3-8-30.
2. *Gautier SV, Khomyakov SM*. Assessment of requirement of the population in the organ transplantation, the donor resource and planning of the effective network of the medical organizations (the centers of transplantation). *Russian Journal of Transplantology and Artificial Organs*. 2013; 15 (3): 11–24. [In Russ, English abstract]. doi: 10.15825/1995-1191-2013-3-11-24.
3. *Lewis A, Koukoura A, Tsianos GI, Gargavanis AA, Nielsen AA, Vassiliadis E*. Organ donation in the US and Europe: The supply vs demand imbalance. *Transplant Rev (Orlando)*. 2021; 35 (2): 100585. doi: 10.1016/j.trre.2020.100585. PMID: 33071161.
4. *Galeev ShR, Gautier SV*. Risks and ways of preventing kidney dysfunction in drug-induced immunosuppression in solid organ recipients. *Russian Journal of Transplantology and Artificial Organs*. 2022; 24 (4): 24–38. [In Russ, English abstract]. doi: 10.15825/1995-1191-2022-4-24-38.

5. *Parlakpinar H, Gunata M*. Transplantation and immunosuppression: a review of novel transplant-related immunosuppressant drugs. *Immunopharmacol Immunotoxicol*. 2021; 43 (6): 651–665. doi: 10.1080/08923973.2021.1966033. PMID: 34415233.
6. *Dominici M, Le Blanc K, Mueller I, Slaper-Cortenbach I, Marini F, Krause D et al*. Minimal criteria for defining multipotent mesenchymal stromal cells. The International Society for Cellular Therapy position statement. *Cytotherapy*. 2006; 8 (4): 315–317. doi: 10.1080/14653240600855905. PMID: 16923606.
7. *Wu X, Jiang J, Gu Z, Zhang J, Chen Y, Liu X*. Mesenchymal stromal cell therapies: immunomodulatory properties and clinical progress. *Stem Cell Res Ther*. 2020; 11 (1): 345. doi: 10.1186/s13287-020-01855-9. PMID: 32771052.
8. *Pittenger MF, Discher DE, Péault BM, Phinney DG, Hare JM, Caplan AI*. Mesenchymal stem cell perspective: cell biology to clinical progress. *NPJ Regen Med*. 2019; 4: 22. doi: 10.1038/s41536-019-0083-6. PMID: 31815001.
9. *Han Y, Yang J, Fang J, Zhou Y, Candi E, Wang J et al*. The secretion profile of mesenchymal stem cells and potential applications in treating human diseases. *Signal Transduct Target Ther*. 2022; 7 (1): 92. doi: 10.1038/s41392-022-00932-0. PMID: 35314676.
10. *Guo Y, Yu Y, Hu S, Chen Y, Shen Z*. The therapeutic potential of mesenchymal stem cells for cardiovascular diseases. *Cell Death Dis.* 2020; 11 (5): 349. doi: 10.1038/s41419-020-2542-9. PMID: 32393744.
11. *Poomani MS, Mariappan I, Perumal R, Regurajan R, Muthan K, Subramanian V*. Mesenchymal stem cell (MSCs) therapy for ischemic heart disease: a promising frontier. *Glob Heart*. 2022; 17 (1): 19. doi: 10.5334/gh.1098. PMID: 35342702.
12. *Li K, Li X, Shi G, Lei X, Huang Y, Bai L et al*. Effectiveness and mechanisms of adipose-derived stem cell therapy in animal models of Parkinson's disease: a systematic review and meta-analysis. *Transl Neurodegener*. 2021; 10: 14. doi: 10.1186/s40035-021-00238-1. PMID: 33926570.
13. *Carstens M, Haq I, Martinez-Cerrato J, Dos-Anjos S, Bertram K, Correa D*. Sustained clinical improvement of Parkinson's disease in two patients with facially-transplanted adipose-derived stromal vascular fraction cells. *J Clin Neurosci*. 2020; 81: 47–51. doi: 10.1016/j.jocn.2020.09.001. PMID: 33222965.
14. *Zaripova LN, Midgley A, Christmas SE, Beresford MW, Pain C, Baildam EM et al*. Mesenchymal stem cells in the pathogenesis and therapy of autoimmune and autoinflammatory diseases. *Int J Mol Sci*. 2023; 24 (22): 16040. doi: 10.3390/ijms242216040. PMID: 38003230.
15. *Jasim SA, Yumashev AV, Abdelbasset WK, Margiana R, Markov A, Suksatan W et al*. Shining the light on clinical application of mesenchymal stem cell therapy in autoimmune diseases. *Stem Cell Res Ther*. 2022; 13 (1): 101. doi: 10.1186/s13287-022-02782-7. PMID: 35255979.
16. *Cruz FF, Rocco PRM*. The potential of mesenchymal stem cell therapy for chronic lung disease. *Expert Rev Respir Med*. 2020; 14 (1): 31–39. doi: 10.1080/17476348.2020.1679628. PMID: 31608724.
17. *Han HT, Jin WL, Li X*. Mesenchymal stem cells-based therapy in liver diseases. *Mol Biomed*. 2022; 3 (1): 23. doi: 10.1186/s43556-022-00088-x. PMID: 35895169.
18. *Chen F, Chen N, Xia C, Wang H, Shao L, Zhou C et al*. Mesenchymal stem cell therapy in kidney diseases: potential and challenges. *Cell Transplant*. 2023; 32: 9636897231164251. doi: 10.1177/09636897231164251. PMID: 37013255.
19. *Deng Z, Luo F, Lin Y, Luo J, Ke D, Song C et al*. Research trends of mesenchymal stem cells application in orthopedics: a bibliometric analysis of the past 2 decades. *Front Public Health*. 2022; 10: 1021818. doi: 10.3389/fpubh.2022.1021818. PMID: 36225768.
20. *Guo BC, Wu KH, Chen CY, Lin WY, Chang YJ, Lee TA et al*. Mesenchymal stem cells in the treatment of COVID-19. *Int J Mol Sci*. 2023; 24 (19): 14800. doi: 10.3390/ijms241914800. PMID: 37834246.
21. *Li J, Peng Q, Yang R, Li K, Zhu P, Zhu Y et al*. Application of mesenchymal stem cells during machine perfusion: an emerging novel strategy for organ preservation. *Front Immunol*. 2021; 12: 713920. doi: 10.3389/fimmu.2021.713920. PMID: 35024039.
22. *Deo D, Marchioni M, Rao P*. Mesenchymal stem/stromal cells in organ transplantation. *Pharmaceutics*. 2022; 14 (4): 791. doi: 10.3390/pharmaceutics14040791. PMID: 35456625.
23. *Bezstarosti S, Meziyerh S, Reinders MEJ, Voogt-Bakker K, Groeneweg KE, Roelen DL et al*. HLA-DQ eplet mismatch load may identify kidney transplant patients eligible for tacrolimus withdrawal without donor-specific antibody formation after mesenchymal stromal cell therapy. *HLA*. 2023; 102 (1): 3–12. doi: 10.1111/tan.15008. PMID: 36841928.
24. *Kaundal U, Ramachandran R, Arora A, Kenwar DB, Sharma RR, Nada R et al*. Mesenchymal stromal cells mediate clinically unpromising but favourable immune responses in kidney transplant patients. *Stem Cells Int*. 2022; 2022: 2154544. doi: 10.1155/2022/2154544. PMID: 35211176.
25. *Večerić-Haler Ž, Kojc N, Sever M, Zver S, Švajger U, Poženel P et al*. Case report: capillary leak syndrome with kidney transplant failure following autologous mesenchymal stem cell therapy. *Front Med (Lausanne)*. 2021; 8: 708744. doi: 10.3389/fmed.2021.708744. PMID: 34368198.
26. *Wei Y, Chen X, Zhang H, Su Q, Peng Y, Fu Q et al*. Efficacy and safety of bone marrow-derived mesenchymal stem cells for chronic antibody-mediated rejection after kidney transplantation- a single-arm, two-dosing-regimen, phase I/II study. *Front Immunol*. 2021; 12: 662441. doi: 10.3389/fimmu.2021.662441. PMID: 34248942.
27. *Ban TH, Lee S, Kim HD, Ko EJ, Kim BM, Kim KW et al*. Clinical trial of allogeneic mesenchymal stem cell therapy for chronic active antibody-mediated rejection in kidney transplant recipients unresponsive to Rituximab and intravenous immunoglobulin. *Stem Cells Int*. 2021; 2021: 6672644. doi: 10.1155/2021/6672644. PMID: 33628269.

28. *Casiraghi F, Perico N, Gotti E, Todeschini M, Mister M, Cortinovis M et al*. Kidney transplant tolerance associated with remote autologous mesenchymal stromal cell administration. *Stem Cells Transl Med*. 2020; 9 (4): 427–432. doi: 10.1002/sctm.19-0185. PMID: 31872574.
29. *Erpicum P, Weekers L, Detry O, Bonvoisin C, Delbouille MH, Grégoire C et al*. Infusion of third-party mesenchymal stromal cells after kidney transplantation: a phase I–II, open-label, clinical study. *Kidney Int*. 2019; 95 (3): 693–707. doi: 10.1016/ j.kint.2018.08.046. PMID: 30528263.
30. *Perico N, Casiraghi F, Todeschini M, Cortinovis M, Gotti E, Portalupi V et al*. Long-term clinical and immunological profile of kidney transplant patients given mesenchymal stromal cell immunotherapy. *Front Immunol*. 2018; 9: 1359. doi: 10.3389/fimmu.2018.01359. PMID: 29963053.
31. *Mudrabettu C, Kumar V, Rakha A, Yadav AK, Ramachandran R, Kanwar DB et al*. Safety and efficacy of autologous mesenchymal stromal cells transplantation in patients undergoing living donor kidney transplantation: a pilot study. *Nephrology (Carlton)*. 2015; 20 (1): 25–33. doi: 10.1111/ nep.12338. PMID: 25230334.
32. *Perico N, Casiraghi F, Gotti E, Introna M, Todeschini M, Cavinato RA et al*. Mesenchymal stromal cells and kidney transplantation: pretransplant infusion protects from graft dysfunction while fostering immunoregulation. *Transpl Int*. 2013; 26 (9): 867–878. doi: 10.1111/ tri.12132. PMID: 23738760.
33. *Lee H, Park JB, Lee S, Baek S, Kim H, Kim SJ*. Intra-osseous injection of donor mesenchymal stem cell (MSC) into the bone marrow in living donor kidney transplantation; a pilot study. *J Transl Med*. 2013; 11: 96. doi: 10.1186/1479-5876-11-96. PMID: 23578110.
34. *Tan J, Wu W, Xu X, Liao L, Zheng F, Messinger S et al*. Induction therapy with autologous mesenchymal stem cells in living-related kidney transplants: a randomized controlled trial. *JAMA*. 2012; 307 (11): 1169–1177. doi: 10.1001/jama.2012.316. PMID: 22436957.
35. *Saadi G, Fadel F, El Ansary M, El-Hamid SA*. Mesenchymal stem cell transfusion for desensitization of positive lymphocyte cross-match before kidney transplantation: outcome of 3 cases. *Cell Prolif*. 2013; 46 (2): 121–126. doi: 10.1111/cpr.12012. PMID: 23510466.
36. *Perico N, Casiraghi F, Introna M, Gotti E, Todeschini M, Cavinato RA et al*. Autologous mesenchymal stromal cells and kidney transplantation: a pilot study of safety and clinical feasibility. *Clin J Am Soc Nephrol*. 2011; 6 (2): 412–422. doi: 10.2215/ CJN.04950610. PMID: 20930086.
37. *Vanikar AV, Trivedi HL, Feroze A, Kanodia KV, Dave SD, Shah PR*. Effect of co-transplantation of mesenchymal stem cells and hematopoietic stem cells as compared to hematopoietic stem cell transplantation alone in renal transplantation to achieve donor hypo-responsiveness. *Int Urol Nephrol*. 2011; 43 (1): 225–232. doi: 10.1007/ s11255-009-9659-1. PMID: 20084457.
38. *Peng Y, Ke M, Xu L, Liu L, Chen X, Xia W et al*. Donor-derived mesenchymal stem cells combined with low-dose tacrolimus prevent acute rejection after renal transplantation: a clinical pilot study [published correction appears in Transplantation. 2014 Mar 27; 97 (6): e37. Pan, Guanghui [added]]. *Transplantation*. 2013; 95 (1): 161–168. doi: 10.1097/TP.0b013e3182754c53. PMID: 23263506.
39. *Reinders ME, de Fijter JW, Roelofs H, Bajema IM, de Vries DK, Schaapherder AF et al*. Autologous bone marrow-derived mesenchymal stromal cells for the treatment of allograft rejection after renal transplantation: results of a phase I study. Ste*m Cells Transl Med*. 2013; 2 (2): 107–111. doi: 10.5966/sctm.2012-0114. PMID: 23349326.
40. *Dave SD, Vanikar AV, Trivedi HL*. Co-infusion of adipose tissue derived mesenchymal stem cell-differentiated insulin-making cells and haematopoietic cells with renal transplantation: a novel therapy for type 1 diabetes mellitus with end-stage renal disease. *BMJ Case Rep*. 2013; 2013: bcr2013009901. doi: 10.1136/bcr-2013-009901. PMID: 23709153.
41. *Vanikar AV, Trivedi HL, Gopal SC, Kumar A, Dave SD*. Pre-transplant co-infusion of donor-adipose tissue derived mesenchymal stem cells and hematopoietic stem cells may help in achieving tolerance in living donor renal transplantation. *Ren Fail*. 2014; 36 (3): 457–460. doi: 10.3109/0886022X.2013.868295. PMID: 24344734.
42. *Vanikar AV, Trivedi HL, Kumar A, Gopal SC, Patel HV, Gumber MR et al.* Co-infusion of donor adipose tissue-derived mesenchymal and hematopoietic stem cells helps safe minimization of immunosuppression in renal transplantation – single center experience. *Ren Fail*. 2014; 36 (9): 1376–1384. doi: 10.3109/0886022X.2014.950931. PMID: 25246338.
43. *Pan GH, Chen Z, Xu L, Zhu JH, Xiang P, Ma JJ et al*. Low-dose tacrolimus combined with donor-derived mesenchymal stem cells after renal transplantation: a prospective, non-randomized study. *Oncotarget*. 2016; 7 (11): 12089–12101. doi: 10.18632/oncotarget.7725. PMID: 26933811.
44. *Dreyer GJ, Groeneweg KE, Heidt S, Roelen DL, van Pel M, Roelofs H et al*. Human leukocyte antigen selected allogeneic mesenchymal stromal cell therapy in renal transplantation: The Neptune study, a phase I single-center study. *Am J Transplant*. 2020; 20 (10): 2905–2915. doi: 10.1111/ajt.15910. PMID: 32277568.
45. *Meucci MC, Reinders MEJ, Groeneweg KE, Bezstarosti S, Ajmone Marsan N, Bax JJ et al*. Cardiovascular effects of autologous bone marrow-derived mesenchymal stromal cell therapy with early tacrolimus withdrawal in renal tranplant recipients: an analysis of the randomized TRITON study. *J Am Heart Assoc*. 2021; 10 (24): e023300. doi: 10.1161/ JAHA.121.023300. PMID: 34913362.
46. *Meucci MC, Reinders MEJ, Groeneweg KE, Bezstarosti S, Marsan NA, Bax JJ et al*. Left atrial structural and functional response in kidney transplant recipients treated with mesenchymal stromal cell therapy and early tacrolimus withdrawal. *J Am Soc Echocardiogr*. 2023; 36 (2): 172–179. doi: 10.1016/j.echo.2022.10.022. PMID: 36347387.
47. *Korotkov SV, Lebed' OA, Smolnikova VV, Pikirenya II, Shcherba AE, Krivenko SI, Rummo OO*. Application of

mesenchymal stem cells for the treatment of liver graft dysfunction caused by chronic rejection. Case report. *Surgery. Eastern Europe*. 2022; 11 (2): 271–285. [In Russ, English abstract]. doi: 10.34883/PI.2022.11.2.010.
48. *Vandermeulen M, Mohamed-Wais M, Erpicum P, Delbouille MH, Lechanteur C, Briquet A et al*. Infusion of allogeneic mesenchymal stromal cells after liver transplantation: a 5-year follow-up. *Liver Transpl*. 2022; 28 (4): 636–646. doi: 10.1002/lt.26323. PMID: 34605167.
49. *Mora L, Alegre F, Rifón JJ, Marti P, Herrero JI*. Treatment of graft-versus-host disease with mesenchymal cells as a complication of a liver transplantation. *Rev Esp Enferm Dig*. 2018; 110 (11): 734–736. doi: 10.17235/reed.2018.5672/2018. PMID: 30284904.
50. *Casiraghi F, Perico N, Podestà MA, Todeschini M, Zambelli M, Colledan M et al*. Third-party bone marrow-derived mesenchymal stromal cell infusion before liver transplantation: a randomized controlled trial. *Am J Transplant*. 2021; 21 (8): 2795–2809. doi: 10.1111/ajt.16468. PMID: 33370477.
51. *Detry O, Vandermeulen M, Delbouille MH, Somja J, Bletard N, Briquet A et al*. Infusion of mesenchymal stromal cells after deceased liver transplantation: a phase I–II, open-label, clinical study. *J Hepatol*. 2017; 67 (1): 47–55. doi: 10.1016/j.jhep.2017.03.001. PMID: 28284916.
52. *Zhang YC, Liu W, Fu BS, Wang GY, Li HB, Yi HM et al*. Therapeutic potentials of umbilical cord-derived mesenchymal stromal cells for ischemic-type biliary lesions following liver transplantation. *Cytotherapy*. 2017; 19 (2): 194–199. doi: 10.1016/j.jcyt.2016.11.005. PMID: 27964826.
53. *Erasmus DB, Durand N, Alvarez FA, Narula T, Hodge DO, Zubair AC*. Feasibility and safety of low-dose mesenchymal stem cell infusion in lung transplant recipients. *Stem Cells Transl Med*. 2022; 11 (9): 891–899. doi: 10.1093/stcltm/szac051. PMID: 35881142.
54. *Mei L, Yuwei Y, Weiping L, Zhiran X, Bingzheng F, Jibing C et al*. Strategy for clinical setting of co-transplantation of mesenchymal stem cells and pancreatic islets. *Cell Transplantation*. 2024; 33: 9636897241259433. doi: 10.1177/09636897241259433. PMID: 38877672.
55. *Koehler N, Buhler L, Egger B, Gonelle-Gispert C*. Multipotent mesenchymal stromal cells interact and support islet of Langerhans viability and function. *Front Endocrinol (Lausanne)*. 2022; 13: 822191. doi: 10.3389/fendo.2022.822191. PMID: 35222280.
56. *Barachini S, Biso L, Kolachalam S, Petrini I, Maggio R, Scarselli M et al*. Mesenchymal stem cell in pancreatic islet transplantation. *Biomedicines*. 2023; 11 (5): 1426. doi: 10.3390/biomedicines11051426. PMID: 37239097.
57. *Gruessner AC*. A Decade of Pancreas Transplantation – A Registry Report. *Uro*. 2023; 3 (2): 132–150. doi: 10.3390/uro3020015.
58. *Piemonti L*. Islet transplantation. South Dartmouth (MA): MDText.com; 2020.
59. *Amer LD, Mahoney MJ, Bryant SJ*. Tissue engineering approaches to cell-based type 1 diabetes therapy. *Tissue engineering*. 2014; 20 (5): 455–467. doi: 10.1089/ten.TEB.2013.0462. PMID: 24417705.
60. *Sevastianov VI, Baranova NV, Kirsanova LA, Ponomareva AS, Basok YB, Nemets EA, Gautier SV*. Comparative analysis of the influence of extracellular matrix biomimetics on the viability and insulin-producing function of isolated pancreatic islets. *J Gene Eng Bio Res*. 2021; 3 (2): 17–25.
61. *Maffi P, Secchi* A. Islet transplantation alone versus solitary pancreas transplantation: an outcome-driven choice? *Curr Diab Rep*. 2019; 19 (5): 26. doi: 10.1007/s11892-019-1145-2. PMID: 31025188.
62. *Chen L, Qu J, Kalyani FS, Zhang Q, Fan L, Fang Y et al*. Mesenchymal stem cell-based treatments for COVID-19: status and future perspectives for clinical applications. *Cell Mol Life Sci*. 2022; 79 (3): 142. doi: 10.1007/s00018-021-04096-y. PMID: 35187617.
63. *Borow KM, Yaroshinsky A, Greenberg B, Perin EC*. Phase 3 DREAM-HF trial of mesenchymal precursor cells in chronic heart failure. *Circ Res*. 2019; 125 (3): 265–281. doi: 10.1161/CIRCRESAHA.119.314951. PMID: 31318648.
64. *Rodríguez-Fuentes DE, Fernández-Garza LE, Samia-Meza JA, Barrera-Barrera SA, Caplan AI, Barrera-Saldaña HA*. Mesenchymal stem cells current clinical applications: a systematic review. *Arch Med Res*. 2021; 52 (1): 93–101. doi: 10.1016/j.arcmed.2020.08.006. PMID: 32977984.
65. *Bonaventura G, Munafò A, Bellanca CM, La Cognata V, Iemmolo R, Attaguile GA et al*. Stem cells: innovative therapeutic options for neurodegenerative diseases? *Cells*. 2021; 10 (8): 1992. doi: 10.3390/cells10081992. PMID: 34440761.
66. *Sevastianov VI, Basok YuB, Grigoriev AM, Nemets EA, Kirillova AD, Kirsanova LA et al*. Decellularization of cartilage microparticles: Effects of temperature, supercritical carbon dioxide and ultrasound on biochemical, mechanical, and biological properties. *J Biomed Mater Res A*. 2023; 111 (4): 543–555. doi: 10.1002/jbm.a.37474. PMID: 36478378.
67. *Guillamat-Prats R*. The role of MSC in wound healing, scarring and regeneration. *Cells*. 2021; 10 (7): 1729. doi: 10.3390/cells10071729. PMID: 34359898.
68. *Hoang DM, Pham PT, Bach TQ, Ngo ATL, Nguyen QT, Phan TTK et al*. Stem cell-based therapy for human diseases. *Signal Transduct Target Ther*. 2022; 7 (1): 272. doi: 10.1038/s41392-022-01134-4. PMID: 35933430.
69. *Liu J, Gao J, Liang Z, Gao C, Niu Q, Wu F et al*. Mesenchymal stem cells and their microenvironment. *Stem Cell Res Ther*. 2022; 13 (1): 429. doi: 10.1186/s13287-022-02985-y. PMID: 35987711.
70. *Almeida-Porada G, Atala AJ, Porada CD*. Therapeutic mesenchymal stromal cells for immunotherapy and for gene and drug delivery. *Mol Ther Methods Clin Dev*. 2020; 16: 204–224. doi: 10.1016/j.omtm.2020.01.005. PMID: 32071924.
71. *Trigo CM, Rodrigues JS, Camões SP, Solá S, Miranda JP*. Mesenchymal stem cell secretome for regenerative medicine: where do we stand? *J Adv Res*. 2024; S2090-1232(24)00181-4. doi: 10.1016/j.jare.2024.05.004. PMID: 38729561.
72. *Berebichez-Fridman R, Montero-Olvera PR*. Sources and clinical applications of mesenchymal stem

cells: state-of-the-art review. *Sultan Qaboos Univ Med J*. 2018; 18 (3): e264–e277. doi: 10.18295/squmj.2018.18.03.002. PMID: 30607265.
73. *Yang YK, Ogando CR, Wang See C, Chang TY, Barabino GA*. Changes in phenotype and differentiation potential of human mesenchymal stem cells aging *in vitro*. *Stem Cell Res Ther*. 2018; 9 (1): 131. doi: 10.1186/s13287-018-0876-3. PMID: 29751774.
74. *Egorova VA, Ponomareva AS, Bogdanova NB, Abramov VJu, Sevastianov VI*. Harakteristika fenotipa mezenhimal'nyh stvolovyh kletok iz zhirovoj tkani cheloveka metodom protochnoj citometrii. *Tehnologii zhivyh sistem*. 2009; 6 (5): 40–46. [In Russ].
75. *Hladik D, Höfig I, Oestreicher U, Beckers J, Matjanovski M, Bao X et al*. Long-term culture of mesenchymal stem cells impairs ATM-dependent recognition of DNA breaks and increases genetic instability. *Stem Cell Res Ther. 2019;* 10 (1): 218. doi: 10.1186/s13287-019-1334-6. PMID: 31358047.
76. *Deng W, Han Q, Liao L, You S, Deng H, Zhao RC*. Effects of allogeneic bone marrow-derived mesenchymal stem cells on T and B lymphocytes from BXSB mice. *DNA Cell Biol.* 2005; 24 (7): 458–463. doi: 10.1089/dna.2005.24.458. PMID: 16008514.
77. *Aggarwal S, Pittenger MF*. Human mesenchymal stem cells modulate allogeneic immune cell responses. *Blood*. 2005; 105 (4): 1815–1822. doi: 10.1182/blood-2004-04-1559. PMID: 15494428.
78. *Rasmusson I, Ringden O, Sundberg B, Le Blanc K*. Mesenchymal stem cells inhibit lymphocyte proliferation by mitogens and alloantigens by different mechanisms. *Exp Cell Res.* 2005; 305 (1): 33–41. doi: 10.1016/j.yexcr.2004.12.013. PMID: 15777785.
79. *Ma OK, Chan KH*. Immunomodulation by mesenchymal stem cells: interplay between mesenchymal stem cells and regulatory lymphocytes. *World J Stem Cells*. 2016; 8 (9): 268–278. doi: 10.4252/wjsc.v8.i9.268. PMID: 27679683.
80. *Zhao Z-G, Xu W, Sun L, You Y, Li F, Li Q-B et al*. Immunomodulatory function of regulatory dendritic cells induced by mesenchymal stem cells. *Immunol Invest*. 2012; 41 (2): 183–198. doi: 10.3109/08820139.2011.607877. PMID: 21936678.
81. *Rutz S, Janke M, Kassner N, Hohnstein T, Krueger M, Scheffold A*. Notch regulates IL-10 production by T helper 1 cells. *Proc Natl Acad Sci USA*. 2008; 105 (9): 3497–3502. doi: 10.1073/pnas.0712102105. PMID: 18292228.
82. *Cho D-I, Kim MR, Jeong H-Y, Jeong HC, Jeong MH, Yoon SH et al*. Mesenchymal stem cells reciprocally regulate the M1/M2 balance in mouse bone marrow-derived macrophages. *Exp Mol Med.* 2014; 46 (1): e70. doi: 10.1038/emm.2013.135. PMID: 24406319.
83. *Sotiropoulou PA, Perez SA, Gritzapis AD, Baxevanis CN, Papamichail M*. Interactions between human mesenchymal stem cells and natural killer cells. *Stem Cells.* 2006; 24 (1): 74–85. doi: 10.1634/stemcells.2004-0359. PMID: 16099998.
84. *Ren G, Zhang L, Zhao X, Xu G, Zhang Y, Roberts AI et al*. Mesenchymal stem cell-mediated immunosuppression occurs via concerted action of chemokines and nitric oxide. *Cell Stem Cell.* 2008; 2 (2): 141–150. doi: 10.1016/j.stem.2007.11.014. PMID: 18371435.
85. *Kyurkchiev D, Bochev I, Ivanova-Todorova E, Mourdjeva M, Oreshkova T, Belemezova K et al*. Secretion of immunoregulatory cytokines by mesenchymal stem cells. *World J Stem Cells.* 2014; 6 (5): 552–570. doi: 10.4252/wjsc.v6.i5.552. PMID: 25426252.
86. *Gotherstrom C, Lundqvist A, Duprez IR, Childs R, Berg L, le Blanc K*. Fetal and adult multipotent mesenchymal stromal cells are killed by different pathways. *Cytotherapy.* 2011; 13 (3): 269–278. doi: 10.3109/14653249.2010.523077. PMID: 20942778.
87. *Galleu A, Riffo-Vasquez Y, Trento C, Lomas C, Dolcetti L, Cheung TS et al*. Apoptosis in mesenchymal stromal cells induces *in vivo* recipient-mediated immunomodulation. *Sci Transl Med.* 2017; 9 (416): eaam7828. doi: 10.1126/scitranslmed.aam7828. PMID: 29141887.
88. *Chen W, Lv L, Chen N, Cui E*. Immunogenicity of mesenchymal stromal/stem cells. *Scand J Immunol*. 2023; 97 (6): e13267. doi: 10.1111/sji.13267. PMID: 39007962.
89. *Borovkova NV, Khubutiya MSh, Rzhevskaya ON, Pinchuk AV, Vasil'chenkov DA*. Multipotent mesenchymal stem cells in renal transplantation. *Transplantologiya. The Russian Journal of Transplantation*. 2019; 11 (1): 21–36. [In Russ, English abstract]. doi: 10.23873/2074-0506-2019-11-1-21-36.
90. *Preda MB, Rønningen T, Burlacu A, Simionescu M, Moskaug JØ, Valen G*. Remote transplantation of mesenchymal stem cells protects the heart against ischemia-reperfusion injury. *Stem Cells*. 2014; 32 (8): 2123–2134. doi: 10.1002/stem.1687. PMID: 24578312.
91. *Shi W, Zhou X, Li X, Peng X, Chen G, Li Y et al*. Human umbilical cord mesenchymal stem cells protect against renal ischemia-reperfusion injury by secreting extracellular vesicles loaded with miR-148b-3p that target pyruvate dehydrogenase kinase 4 to inhibit endoplasmic reticulum stress at the reperfusion stages. *Int J Mol Sci*. 2023; 24 (10): 8899. doi: 10.3390/ijms24108899. PMID: 37240246.
92. *Saidi RF, Rajeshkumar B, Shariftabrizi A, Bogdanov AA, Zheng S, Dresser K et al*. Human adipose-derived mesenchymal stem cells attenuate liver ischemia-reperfusion injury and promote liver regeneration. *Surgery*. 2014; 156 (5): 1225–1231. doi: 10.1016/j.surg.2014.05.008. PMID: 25262218.
93. *Qiao LY, Huang FJ, Zhao M, Xie JH, Shi J, Wang J et al*. A two-year follow-up study of cotransplantation with neural stem/progenitor cells and mesenchymal stromal cells in ischemic stroke patients. *Cell Transplant*. 2014; 23 Suppl 1: S65–S72. doi: 10.3727/096368914X684961. PMID: 25333752.
94. *Gorman E, Millar J, McAuley D, O'Kane C*. Mesenchymal stromal cells for acute respiratory distress syndrome (ARDS), sepsis, and COVID-19 infection: optimizing the therapeutic potential. *Expert Rev Respir Med*. 2021; 15 (3): 301–324. doi: 10.1080/17476348.2021.1848555. PMID: 33172313.
95. *Miceli V, Bulati M, Gallo A, Iannolo G, Busà R, Conaldi PG et al*. Role of mesenchymal stem/stromal cells in modulating ischemia/reperfusion injury: current state of

the art and future perspectives. *Biomedicines*. 2023; 11 (3): 689. doi: 10.3390/biomedicines11030689. PMID: 36979668.

96. *Giai Via A, Frizziero A, Oliva F*. Biological properties of mesenchymal stem cells from different sources. *Muscles Ligaments Tendons J*. 2012; 2 (3): 154–162. PMID: 23738292.
97. *Jones E, Schäfer R*. Where is the common ground between bone marrow mesenchymal stem/stromal cells from different donors and species? *Stem Cell Res Ther.* 2015; 6 (1): 143. doi: 10.1186/s13287-015-0144-8. PMID: 26282627.
98. *Ganguly P, El-Jawhari JJ, Giannoudis PV, Burska AN, Ponchel F, Jones EA*. Age related changes in bone marrow mesenchymal stromal cells: a potential impact on osteoporosis and osteoarthritis development. *Cell Transpl.* 2017; 26 (9): 1520–1529. doi: 10.1177/0963689717721201. PMID: 29113463.
99. *Kaundal U, Bagai U, Rakha A*. Immunomodulatory plasticity of mesenchymal stem cells: a potential key to successful solid organ transplantation. *J Transl Med*. 2018; 16 (1): 31. doi: 10.1186/s12967-018-1403-0. PMID: 29448956.
100. *Halloran PF*. Immunosuppressive drugs for kidney transplantation. *N Engl J Med.* 2004; 351 (26): 2715–2729. doi: 10.1056/NEJMra033540. PMID: 15616206.
101. *Pilch NA, Bowman LJ, Taber DJ*. Immunosuppression trends in solid organ transplantation: the future of individualization, monitoring, and management. *Pharmacotherapy*. 2021; 41 (1): 119–131. doi: 10.1002/phar.2481. PMID: 33131123.
102. *Gautier SV*. Immunosupressija pri transplantacii solidnyh organov. M.–Tver': Triada, 2011; 472.
103. *Hajkova M, Hermankova B, Javorkova E, Bohacova P, Zajicova A, Holan V et al*. Mesenchymal stem cells attenuate the adverse effects of immunosuppressive drugs on distinct T cell subopulations. *Stem Cell Rev Rep*. 2017; 13 (1): 104–115. doi: 10.1007/s12015-016-9703-3. PMID: 27866327.
104. *Eggenhofer E, Renner P, Soeder Y, Popp FC, Hoogduijn MJ, Geissler EK et al*. Features of synergism between mesenchymal stem cells and immunosuppressive drugs in a murine heart transplantation model. *Transpl Immunol*. 2011; 25 (2–3): 141–147. doi: 10.1016/j.trim.2011.06.002. PMID: 21704160.
105. *Tatum R, O'Malley TJ, Bodzin AS, Tchantchaleishvili V*. Machine perfusion of donor organs for transplantation. *Artif Organs*. 2021; 45 (7): 682–695. doi: 10.1111/aor.13894. PMID: 33349946.
106. *Weissenbacher A, Vrakas G, Nasralla D, Ceresa CDL*. The future of organ perfusion and re-conditioning. *Transpl Int*. 2019; 32 (6): 586–597. doi: 10.1111/tri.13441. PMID: 30980772.
107. *Gautier SV, Tsirulnikova OM, Pashkov IV, Oleshkevich DO, Filatov IA, Bogdanov VK et al*. Normothermic *ex vivo* perfusion of isolated lungs in an experiment using a russian-made perfusion system. *Russian Journal of Transplantology and Artificial Organs*. 2022; 24 (2): 94–101. [In Russ, English abstract]. doi: 10.15825/1995-1191-2022-2-94-101.
108. *Almeida S, Snyder W, Shah M, Fisher J, Marsh C, Hawkes A et al*. Revolutionizing deceased donor transplantation: how new approaches to machine perfusion broadens the horizon for organ donation. *Transplantation Reports*. 2024; 9 (3): 100160. doi: 10.1016/j.tpr.2024.100160.
109. *Iske J, Schroeter A, Knoedler S, Nazari-Shafti TZ, Wert L, Roesel MJ et al*. Pushing the boundaries of innovation: the potential of *ex vivo* organ perfusion from an interdisciplinary point of view. *Front Cardiovasc Med*. 2023; 10: 1272945. doi: 10.3389/fcvm.2023.1272945. PMID: 37900569.
110. *Brasile L, Henry N, Orlando G, Stubenitsky B*. Potentiating renal regeneration using mesenchymal stem cells. *Transplantation*. 2019; 103 (2): 307–313. doi: 10.1097/TP.0000000000002455. PMID: 30234788.
111. *Sun D, Yang L, Zheng W, Cao H, Wu L, Song H*. Protective effects of bone marrow mesenchymal stem cells (BMMSCS) combined with normothermic machine perfusion on liver grafts donated after circulatory death via reducing the ferroptosis of hepatocytes. *Med Sci Monit*. 2021; 27: e930258. doi: 10.12659/MSM.930258. PMID: 34112750.
112. *Nakajima D, Watanabe Y, Ohsumi A, Pipkin M, Chen M, Mordant P et al*. Mesenchymal stromal cell therapy during *ex vivo* lung perfusion ameliorates ischemia-reperfusion injury in lung transplantation. *J Heart Lung Transplant*. 2019; 38 (11): 1214–1223. doi: 10.1016/j.healun.2019.07.006. PMID: 31474491.
113. *Bogensperger C, Hofmann J, Messner F, Resch T, Meszaros A, Cardini B et al*. *Ex vivo* mesenchymal stem cell therapy to regenerate machine perfused organs. *Int J Mol Sci*. 2021; 22 (10): 5233. doi: 10.3390/ijms22105233. PMID: 34063399.
114. *Shravage BV, Turksen K*. Autophagy in stem cell maintenance and differentiation. 1st ed. Cham, Switzerland: Springer; 2022.
115. *Sbrana FV, Cortini M, Avnet S, Perut F, Columbaro M, De Milito A et al*. The role of autophagy in the maintenance of stemness and differentiation of mesenchymal stem cells. *Stem Cell Rev Rep*. 2016; 12: 621–633. doi: 10.1007/s12015-016-9690-4. PMID: 27696271.
116. *Hou J, Han ZP, Jing YY, Yang X, Zhang SS, Sun K et al*. Autophagy prevents irradiation injury and maintains stemness through decreasing ROS generation in mesenchymal stem cells. *Cell Death Dis*. 2013; 4 (10): e844. doi: 10.1038/cddis.2013.338. PMID: 24113178.
117. *El Nashar EM, Alghamdi MA, Alasmari WA, Hussein MMA, Hamza E, Taha RI et al*. Autophagy promotes the survival of adipose mesenchymal stem/stromal cells and enhances their therapeutic effects in cisplatin-induced liver injury via modulating TGF-β1/Smad and PI3K/AKT signaling pathways. *Cells*. 2021; 10 (9): 2475. doi: 10.3390/cells10092475. PMID: 34572126.
118. *Sevastianov VI, Basok YuB*. Biomimetics of extracellular matrices for cell and tissue engineered medical products. Newcastle upon Tyne, UK: Cambridge Scholars Publishing; 2023.

The article was submitted to the journal on 9.09.2024

DOI: 10.15825/1995-1191-2025-1-135-144

INVESTIGATION OF THE HISTOARCHITECTURE OF BOVINE PERICARDIUM AS THE PRIMARY MATERIAL USED IN RECONSTRUCTIVE SURGERY AND BIOPROSTHESIS

A.I. Zvyagina[1], K.V. Pyatina[1], V.V. Minaiychev[1], M.I. Kobyakova[1], Ya.V. Lomovskaya[1], A.S. Senotov[1], A.Yu. Teterina[2], I.S. Fadeeva[1]

[1] Institute of Theoretical and Experimental Biophysics, Moscow, Russian Federation
[2] Baikov Institute of Metallurgy and Materials Science, Moscow, Russian Federation

Objective: to study the composition and topology of the extracellular matrix (ECM) of bovine pericardium and to identify the best tissue areas suitable for the fabrication of bioprosthetic heart valves (BHVs). **Materials and methods.** The pericardium samples of healthy sexually mature bulls were studied; the native pericardium was divided into three experimental groups: core tissue (BP-CT group), heart base (BP-HB) and connective ligament base (BP-CL). Scanning electron microscopy was used to examine the structure of the pericardial surfaces (*p. serosum* and *p. fibrosum*), while differential histochemical analysis was used to study the topology of various pericardial regions, with identification and quantification of the main constituents of the extracellular matrix (ECM) (collagen, elastin, lipids, and glycosaminoglycans). Quantification was performed by bioimaging and digital analysis of histological images using the ImageJ software. **Results.** The BP-CT group had the lowest cellular density and, consequently, DNA content (369.75 ± 23.12 ng/mg), in addition to having the most homogeneous, predominantly collagenous (95.6 ± 2.9%) matrix composition with minimal lipid (2.6 ± 1.5%), glycosaminoglycan (0.68 ± 0.7%) and elastin (3 ± 2.4%) content. The BP-CL group had the highest levels of elastin and glycosaminoglycans (27.8 ± 3% and 17.5 ± 0.6%, respectively), while the BP-HB group had the highest lipid content (21.2 ± 2.7%.). On the *p. serosum* side, the ECM composition was noticeably homogeneous, while elastin fibers, glycosaminoglycans, and lipid clusters were predominantly found on the *p. fibrisum* side, indicating the natural polarity of the material, which should be considered when fabricating biomaterials. **Conclusion.** The findings in this study revealed that bovine pericardial topology varied depending on the tissue area. Only the main pericardial tissue can be used to create BHVs, as evidenced by the comparative homogeneity of ECM composition and relatively low cellular density. The high content of elastin, glycosaminoglycans and lipids in specific pericardial tissue areas (the BP-HB and BP-CL groups) suggests that either this layer needs to be removed more thoroughly during implant fabrication (e.g., by selective purification techniques) or these pericardial tissue areas should be used where heterogeneity of the composition is desired (e.g., in maxillofacial and orthopedic surgery).

Keywords: bovine xenopericardium, pericardial topology, extracellular matrix, bioprosthetic heart valves, calcification.

INTRODUCTION

Xenogeneic serous membranes are increasingly used as a base for developing a wide range of implantable biomaterials [1]. Among them, bovine xenopericardium (BP) – which undergoes fixation, decellularization, and delipidization – is one of the most commonly used biomaterials in modern cardiovascular surgery [2].

BP serves as the primary material for various bioprostheses and auxiliary cardiovascular implants, including bioprosthetic heart valves (BHVs), venous and arterial conduits, cardiovascular patches, and sutures [1, 3, 4]. However, a major challenge with BP-based biomaterials is their susceptibility to calcification within the recipient's body, significantly limiting implant longevity. Addressing this issue remains a critical priority in reconstructive cardiovascular surgery [5–7].

At the same time, it is known that the composition of the pericardial extracellular matrix (ECM) can influence the body's general tissue and cellular response to an implanted material [8, 9]. For example, it has been shown that pericardial basal membrane proteins positively influence human aortic endothelial cell migration, adhesion, proliferation, inflammatory response, and laminin production, which in turn contributes to one of the most important indicators of BHV biointegration – reendothelization. Moreover, emerging data suggest that the propensity of BHVs to calcification may also be influenced by the composition of the pericardial ECM. Elastin fibers, for instance, are well-known biomaterial

Corresponding author: Alena Zvyagina. Address: 3, Institutskaya str., Pushchino, 142290, Russian Federation. Phone: (960) 600-93-00. E-mail: alennazvyagina@gmail.com

calcification sites [10, 11]. Elastin is a key structural protein that forms the framework of blood vessel walls (primarily arteries), the dermis, and interalveolar septa of the lungs. When damaged, it has been shown to accumulate calcium salts, becoming a site for medial calcification in several pathological conditions, including hyperphosphatemia (linked to kidney and endocrine disorders), diabetes and atherosclerosis, pseudoxanthoma elasticum, beta-thalassemia, monckeberg calcification, rheumatoid arthritis, Singleton–Merten syndrome, secondary hyperparathyroidism, Kawasaki disease, vitamin K deficiency (including warfarin-associated variant) and vitamin D metabolic disorders [10, 12]. A number of studies have also shown that degradation and fragmentation of elastin fibers in heart and vascular valve grafts are major contributors to aseptic calcification after implantation in the recipient's body [10–14].

Damaged (primarily sulfated) glycosaminoglycans (GAGs) play a crucial role in biomaterial calcification by acting as nucleation sites for calcium deposition in biomaterials [12]. Furthermore, the destruction of proteoglycans – which contain up to 95% GAGs and play a crucial role in collagen fiber stabilization – leads to the exposure of gap zones (H-zones) on collagen fibrils, facilitating the deposition of calcium phosphates directly within the ECM of biomaterials [15].

The significant role of these matrix components in BHV calcification is underscored by the ongoing development of anticalcification treatments aimed at stabilizing elastin and GAGs. Numerous studies have demonstrated that preserving GAGs and elastin effectively reduces BHV calcification, highlighting their potential as therapeutic targets [16–19].

In addition, cellular density is a key factor in donor tissue selection for biomaterial manufacturing, as cell membranes carry the primary antigens responsible for implant rejection [20]. This is particularly critical for BHVs, where, beyond immunological rejection, residual lipids from cell membranes can trigger passive aseptic calcification [21, 22].

Despite years of research into decellularization and delipidization techniques, complete lipid removal remains challenging. Achieving an optimal balance between effective lipid extraction and preservation of the biomaterial's structural and mechanical integrity is crucial [23].

Moreover, nuclear DNA, being one of the most resilient biomolecules, poses additional challenges in complete tissue clearance during decellularization. Residual DNA not only remains difficult to degrade but also serves as a phosphate source, further contributing to calcification [24].

Currently, there is an ongoing search for the optimal pericardial sites best suited for biomaterial production [2]. Studies have shown that BHV calcification patterns depend significantly on the type of donor tissue used in prosthesis fabrication [25]. In this context, it is essential to consider key donor tissue parameters – such as elastin, GAG content, lipid composition, and cellular density – when selecting pericardial tissue for BHV manufacturing. However, no such data currently exist for BP, with most guidelines focusing primarily on physical properties, such as biomechanical strength and elasticity, which are influenced by anisotropy and fiber orientation.

Given the lack of scientific literature detailing the histoarchitecture and biochemical composition of BP using differential histochemistry methods, this study conducted a comprehensive histochemical analysis of native BP. The goal was to identify tissue regions with the most homogeneous collagen composition, minimal elastin, GAG, and lipid content, and the greatest potential for use in BHV fabrication.

MATERIALS AND METHODS

Object of study

Pericardial samples were obtained from sexually mature, healthy bulls through the slaughterhouse of the Kaluga Niva APK meat processing plant (Torkotino village, Kaluga Oblast). All collected tissue was immediately placed in sterile 0.9% sodium chloride solution containing gentamicin (400 μg/mL) and fluconazole (50 μg/mL) within 30 minutes post-slaughter and transported to the laboratory in a thermocontainer maintained at 2–8 °C.

Upon arrival at the laboratory – no later than 4 hours post-slaughter and extraction – the pericardium was mechanically cleaned of adipose tissue and rinsed in 0.9% NaCl solution containing 5000 ED/100 mL heparin (Moscow Endocrine Plant, Russia) to remove blood residues.

After cleansing and rinsing the pericardial fragments free of heparin using sterile cold 0.9% sodium chloride solution, the samples were divided into three study groups based on tissue region (Fig. 1): the core tissue (BP-CT group), the heart base (BP-HB group), and the connective ligament base (BP-CL group).

Scanning electron microscopy

The surface structure of lyophilized BP fragments (1 cm^2) was then examined using scanning electron microscopy (SEM) (VEGA III, Tescan, Czech Republic). To ensure optimal surface preservation and prevent matrix component degradation, a matrix-preserving lyophi-

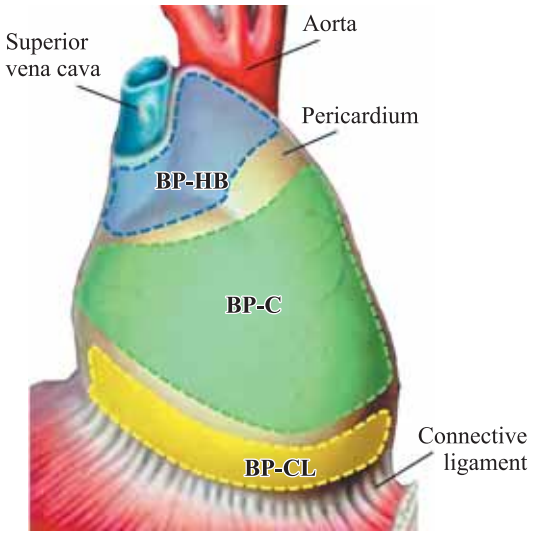

Fig. 1. Sampling areas of the studied fragments of the native pericardium. BP-HB, vessel base zone; BP-CT, main part of tissue; BP-CL, ligament base zone

lization process was employed. This included rapid deep freezing of tissue fragments in a Kelvenator laboratory freezer at –80 °C, reaching the conditional eutectic point of –57 °C, and lyophilization for 24 hours in freeze-drying flasks (FreeZone 2.5 Liter Benchtop Freeze Dry System, Labconco, Canada) while keeping samples suspended to prevent direct contact with flask surfaces.

After lyophilization, a conductive coating was applied to the surface of the studied fragments by sputtering gold particles using a vacuum atomizer Q150R ES (Quorum Technologies, England). For all examined fragments, the microrelief of both the serous (*p. serosum*) and fibrous (*p. fibrosum*) surfaces was analyzed.

DNA quantification

To determine DNA content, 20 mg BP fragments were selected ($n \geq 5$ per study group). Genomic DNA was isolated using the DNA-EXTRAN-2 kit (Syntol, Russia) following the manufacturer's instructions. The DNA concentration in the extracted solutions was measured using a NanoVue Plus spectrophotometer (Biochrom, USA) at a wavelength of 260 nm.

Differential histologic analysis

To preserve the native structure of the BP extracellular matrix, cryotomy was employed to prepare histologic sections, preventing lipid washout, tissue shrinkage from dehydration, and structural matrix alterations. For this purpose: BP fragments were fixed in 10% buffered neutral formalin at 22 ± 2 °C for at least 24 hours, excess phosphates were removed by washing with running water, samples were embedded in cryopreservation medium (O.C.T. Compound Tissue Tek, Sakura, Japan). Sections 9 μm thick were obtained using an MEV cryotome (SLEE Medical GmbH, Germany).

Histological preparations were stained using a combination of histological and differential histochemical stains, including: hematoxylin-eosin, Sudan III (lipid identification), Lilly trichrome (collagen detection), Verhoeff–Van-Gieson (elastin identification), and periodic acid-Schiff (PAS) & alcian blue (GAG detection) [26].

Micrographs and overview histotopograms of the stained preparations were captured using a Nikon Eclipse Ti-E microscopy station (Nikon, Tokyo, Japan).

Histomorphometric analysis

Inverted microscope system Nikon Eclipse Ti-E (Nikon, Tokyo, Japan) was used in combination with the splicing method to generate high-resolution histotopograms of stained histological specimens. These images were processed using NIS Elements AR4.13.05 software (build 933, Nikon, Tokyo, Japan).

Histomorphometric analysis was conducted using ImageJ software (version 1.54h, NIH, Bethesda, MD, USA). Each group included a minimum of four histotopograms, with each histotopogram representing an average splice of 35 ± 15 standard ×4 magnified images.

Bioimaging of micrographs was performed by superimposing color masks onto the images and calculating the area of the mask relative to the total sample slice within the field of view (2000×2000 μm). The proportion of collagen, elastin, lipids, and GAGs in each sample was quantified as a percentage of the total evaluated slice area.

Statistical analysis

The study results are expressed as mean ± standard deviation (M ± SD). Each experiment was conducted with at least four repetitions ($n \geq 4$), and 16 fields of view per group ($n = 16$) were analyzed for microscopic images. Statistical significance was assessed using one-way analysis of variance (ANOVA), followed by the Holm–Sidak multiple comparison test, with a significance threshold of $p < 0.05$. Data processing was performed using Python 3 (ver. 3.10.10) in the Spyder development environment (v. 5.4.1), utilizing the Pandas (v. 1.5.2), NumPy (v. 1.24.2), SciPy (v. 1.5.2) and SciPy (v. 1.10.0) libraries. Graphical representation of results was done using Seaborn (v. 0.12.2) and Matplotlib (v. 3.7.0).

RESULTS AND DISCUSSION

For all groups, the microrelief of the *p. serosum* and *p. fibrosum* surfaces – critical structures of bioprosthetic

tissue that absorb the hydraulic shock of systemic blood flow – was thoroughly examined.

Thanks to the use of gentle lyophilization and cryotomy methods, a delicate, syrup-like GAG layer was observed on the surface of the collagen matrix in all study groups (Fig. 2). Comparative analysis revealed that on the *p. serosum* side, this layer was denser and smoother in the BP-HB and BP-CL groups than in the BP-CT group.

The presence of an intact GAG layer, which envelops collagen and elastin fibers susceptible to platelet aggregation and calcification, is a crucial factor in enhancing the durability and thromboresistance of BHVs.

No additional structural differences were observed among the studied groups using SEM.

Histochemical analysis of BP-CT group samples revealed that the primary pericardial matrix predominantly comprised wave-like collagen fibers (Fig. 3, a). The overall matrix architecture exhibited a porous structure with numerous cavities, which play a vital physiological role in maintaining biomechanical strength and turgor, allowing for physiological hypertrophy of cardiac tissue during exercise.

Notably, the medial ECM region featured a collagen matrix layer forming particularly large cavities, where localized lipid inclusions were observed (Fig. 3, b). The entire pericardial matrix was uniformly saturated with a small amount of neutral glycosaminoglycans (GAGs). However, acidic GAGs were detected exclusively within the basal membrane structure on the *p. serosum* side of the native pericardium (Fig. 3, c).

Differential elastin staining revealed a small number of elastin fibrils penetrating the entire tissue thickness, with the highest concentration observed on the *p. fibrosum* side (Fig. 3, d).

The ECM of BP-HB group samples exhibited a denser and more compact arrangement of collagen fibers compared to other groups (Fig. 3, a). Notably, extensive fatty inclusions were identified primarily on the *p. fibrosum* side of the tissue (Fig. 3, b).

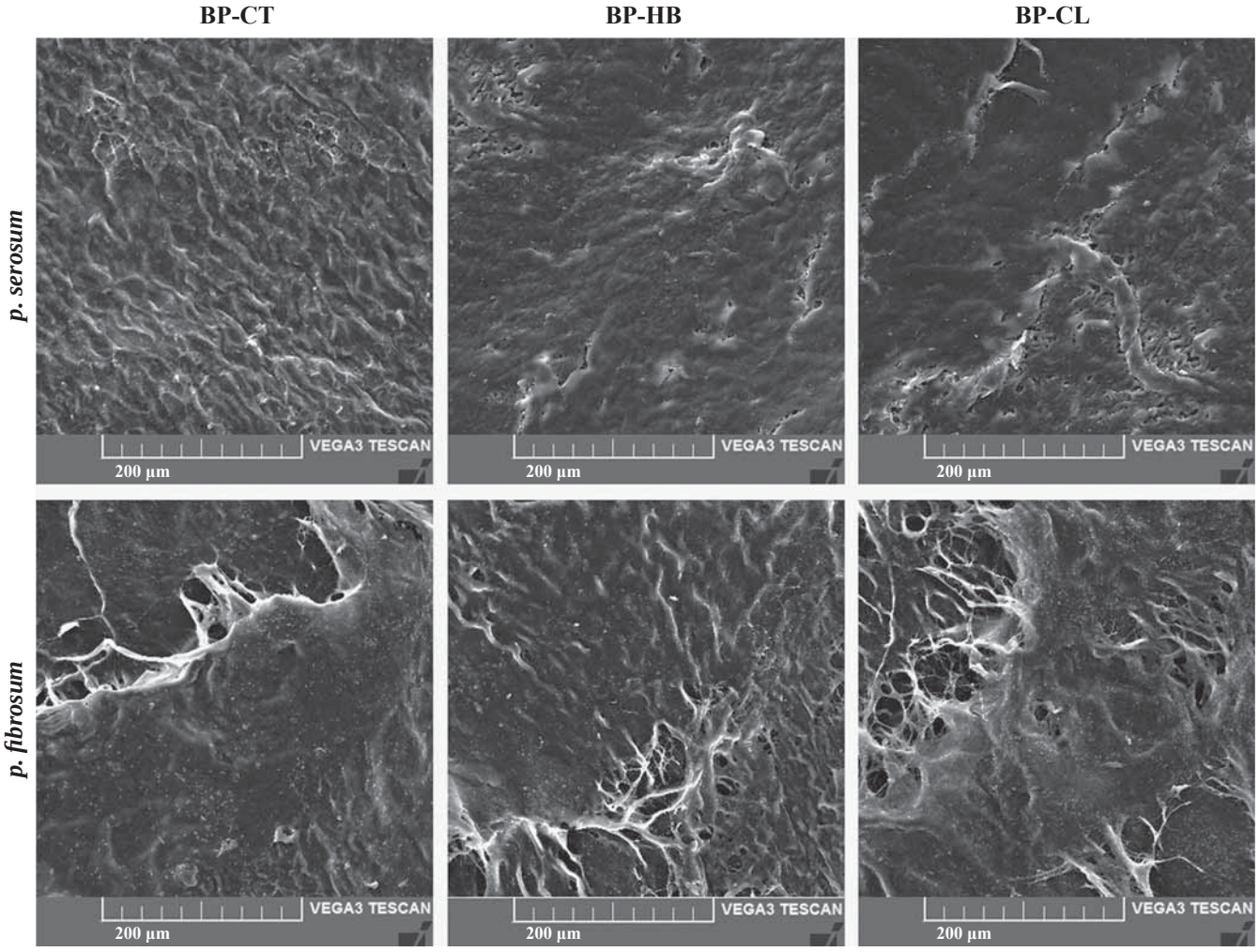

Fig. 2. Surface structure of the *p. serosum* and *p. fibrosum* of bovine pericardium in different tissue areas: core tissue area (BP-CT group), pericardial region at the heart base (BP-HB group) and at the connective ligament base (BP-CL group). Scanning electron microscopy

In addition, the fibrous side showed a higher elastin content, with elastin forming dense strands interwoven between collagen fibers. Furthermore, neutral GAGs were observed in close association with these elastin fibrils (Fig. 3, c, d).

The BP-CL group exhibited a significantly higher content of non-collagenous ECM components. A large number of elastin structures were detected, primarily on the fibrous side, where they were co-localized with neutral GAGs (Fig. 3, c, d). These samples contained abundant lipids within the tissue itself, along with large lipid deposits observed on the surface of the *p. fibrosum* (Fig. 3, b).

Histomorphometric analysis revealed that the BP-CT zone had the most homogeneous and predominantly collagenous composition, with a collagen content of 95.6 ± 2.9% (Fig. 4).

The highest elastin and GAG content was observed in the BP-CL group, at 27.8 ± 3% and 17.5 ± 0.6%, respectively, while the BP-HB group exhibited the highest lipid content, reaching 21.2 ± 2.7%.

The lowest cellular density was found in the BP-CT group (Fig. 5, a). DNA quantification further confirmed this, with BP-CT tissue containing 369.75 ± 23.12 ng/mg DNA, which was 1.5 times lower than in the BP-HB group and 2.5 times lower than in the BP-CL group (Fig. 5, b).

Based on these findings, the main pericardial tissue (BP-CT group) is the most suitable for decellularization techniques, as it has the lowest cell and DNA content, allowing for effective immunogenicity suppression while preserving the ECM structure. In addition, the BP-CT group exhibits the most homogeneous ECM compositi-

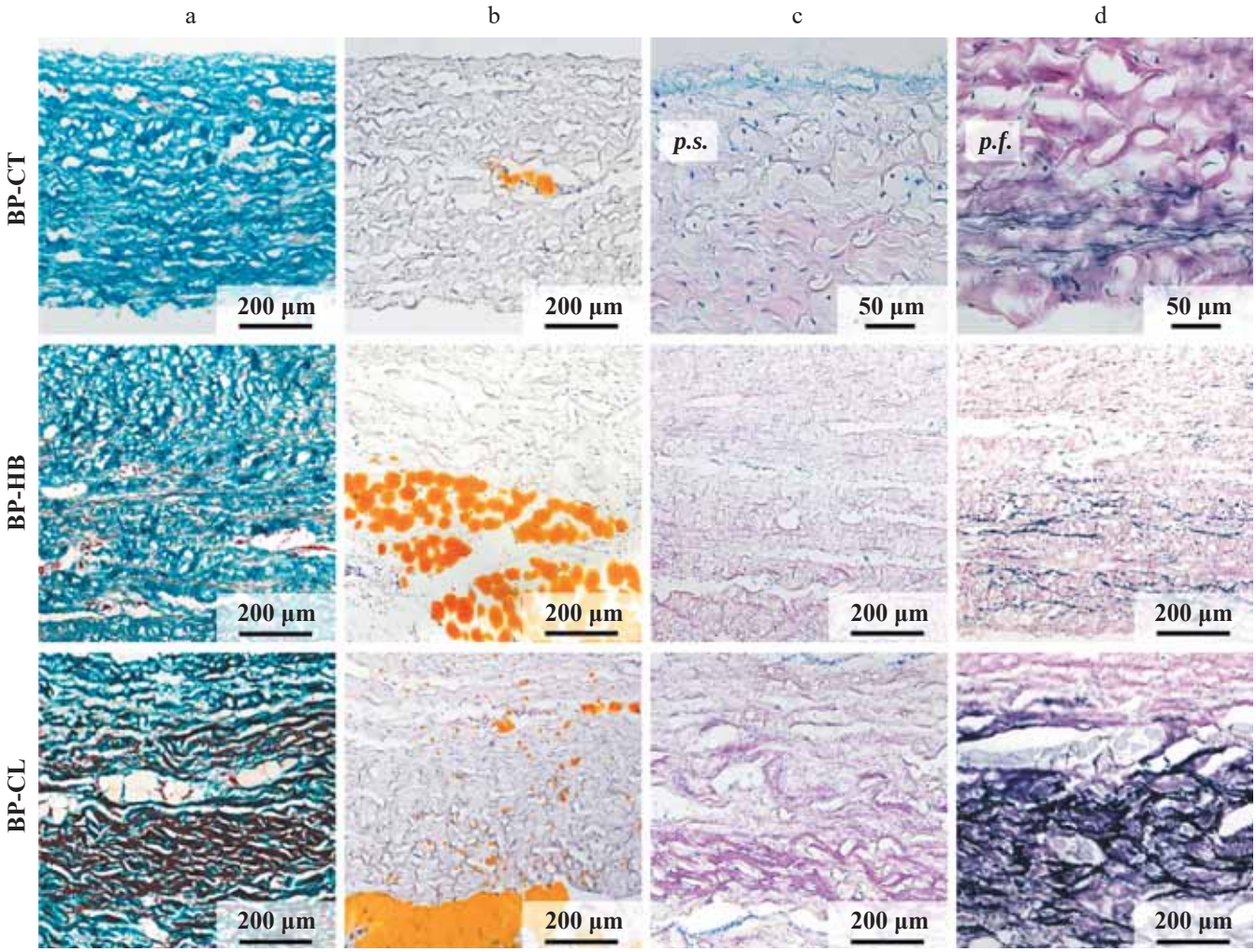

Fig. 3. Structure and composition of bovine pericardium matrix in different tissue areas: core tissue area (BP-CT group), heart base area (BP-HB) and connective ligament base (BP-CL). Light microscopy: a, Lillie's trichrome (collagen – green, non-collagen components – red-brown); b, Sudan III (lipids – yellow-orange); c, Periodic Acid Schiff-Alcian Blue (acidic GAGs – blue, neutral GAGs – pink); d, Verhoeff–Van Gieson (elastin – black, background – pink). Due to low cellular density and the lowest elastin content in the ECM structure of preparations in the BP-CT group, enlarged fragments are presented for easy perception

on, predominantly collagenous, with low lipid, elastin, and GAG content. This is crucial, as damage to these components during preimplantation processing can trigger calcification and inflammatory responses.

Therefore, the main pericardial tissue (the BP-CT region) is the preferred and safest biomaterial source for manufacturing BHVs and other auxiliary cardiovascular materials, ensuring resistance to calcification and

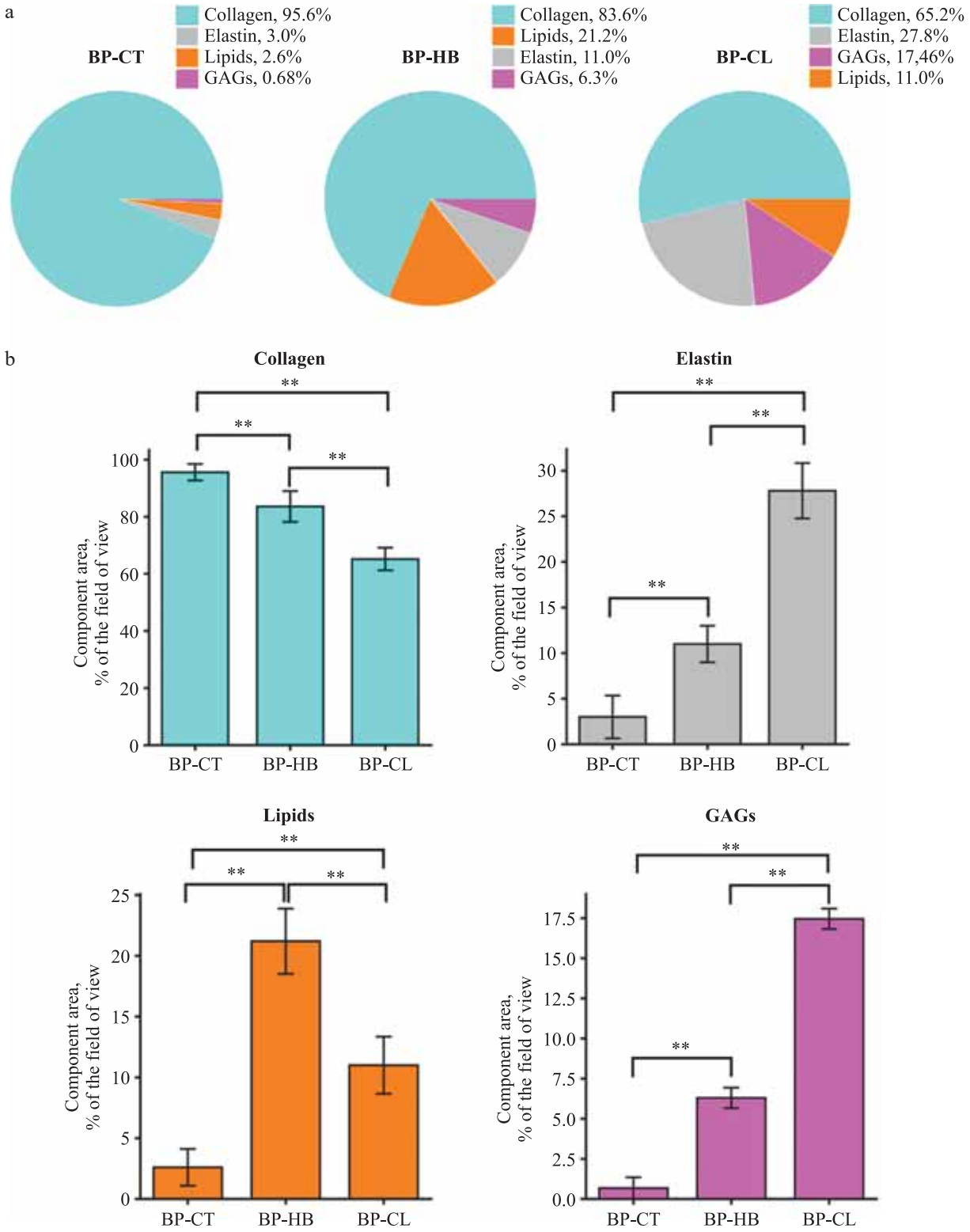

Fig. 4. Results of bioimaging and quantification of histological images of bovine xenopericardium in different topographic areas: core tissue area (BP-CT group), pericardial area at the heart base (BP-HB), connective ligament base area (BP-CL): a, diagrams demonstrating tissue composition; the total percentage of quantified ECM components exceeds 100% owing to the overlap in the color mask areas of co-localized components; b, graphs demonstrating the ratio of components, n = 16, $p < 0.01$ (Holm–Sidak test)

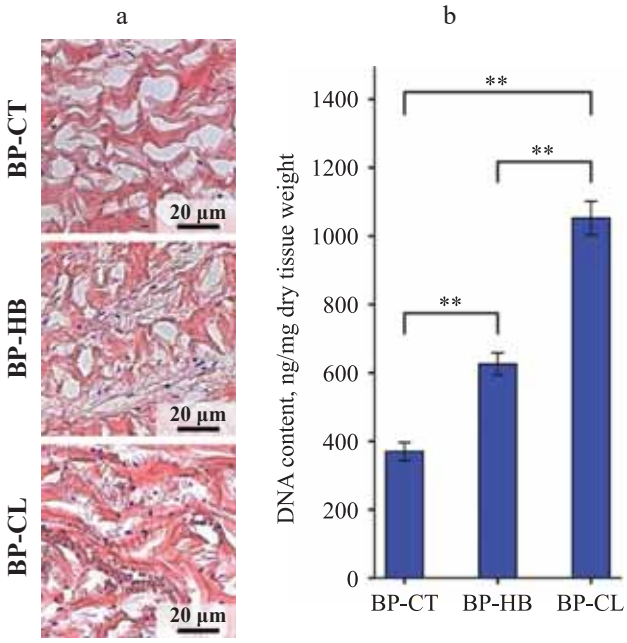

Fig. 5. Cellular composition of bovine pericardium in different tissue areas: core tissue area (BP-CT group), pericardial area at the heart base (BP-HB), connective ligament base area (BP-CL): a, histological images, light microscopy, H&E stain (cell nuclei – purple, matrix components – pink); b, graph showing quantitative DNA content, $n \geq 5$, $p < 0.01$ (Holm–Sidak test)

degeneration. Meanwhile, the heart base (BP-HB) and connective ligament base (BP-CL), due to their heterogeneity and mineralization potential, are better suited for manufacture of resorbable implants.

CONCLUSION

The study results highlight the heterogeneous topology of BP across different tissue regions. The high elastin, GAG, and lipid content in certain regions of the pericardium (BP-HB and BP-CL groups) emphasizes the importance of careful tissue selection for biomaterial fabrication, especially for BHVs, which require immunogenic neutrality, calcification resistance, thromboresistance, biostability, biomechanical strength, and re-endothelialization potential.

Given its high ECM homogeneity, stable microarchitecture, minimal immunogenic and proinflammatory components (cells, lipid fractions, and debris), and well-preserved basal lamina (*p. serosum*) – which enhances thromboresistance and re-endothelialization – the xenopericardial core tissue (BP-CT) region is the preferred choice for fabricating BHVs and all other biomaterials in contact with blood and high pressure of systemic blood flow.

Meanwhile, elastin-rich pericardial regions can be repurposed for other reconstructive applications, such as traumatology, orthopedics, and maxillofacial surgery, where their thin, strong, and elastic properties make them ideal for barrier membranes. Additionally, their calcification potential could be leveraged for osteogenesis induction in peri-implant beds.

The publication of this work was supported by the Russian Science Foundation, Project No. 24-73-10208 "Development of Injectable Calcium Phosphate Hydrated Pastes for Minimally Invasive Administration and Polar Remineralized Composite Barrier Membranes for the Purpose of Targeted Tissue Regeneration in Traumatology and Maxillofacial Surgery".

This paper does not describe any research using humans and animals as subjects.

The authors declare no conflict of interest.

REFERENCES

1. *Shklover J, McMasters J, Alfonso-Garcia A, Higuita ML, Panitch A, Marcu L, Griffiths L.* Bovine pericardial extracellular matrix niche modulates human aortic endothelial cell phenotype and function. *Sci Rep*. 2019; 9 (1): 16688. doi: 10.1038/s41598-019-53230-1. PMID: 31723198.
2. *Stieglmeier F, Grab M, König F, Büch J, Hagl C, Thierfelder N.* Mapping of bovine pericardium to enable a standardized acquirement of material for medical implants. *J Mech Behav Biomed Mater*. 2021; 118 (3): 104432. doi: 10.1016/j.jmbbm.2021.104432. PMID: 33853036.
3. *Texakalidis P, Giannopoulos S, Charisis N, Giannopoulos S, Karasavvidis T, Koullias G, Jabbour P.* A meta-analysis of randomized trials comparing bovine

pericardium and other patch materials for carotid endarterectomy. *J Vasc Surg*. 2018; 68 (4): 1241–1256.e1. doi: 10.1016/j.jvs.2018.07.023. PMID: 30244928.

4. *Morales MM, Anacleto A, Ferreira Leal JC, Greque VG, Souza AS Jr, Wolosker N.* Saccular Superior Vena Cava Aneurysm: Case Report and Comprehensive Review. *Ann Vasc Surg*. 2021; 72: 666.e23–666.e32. doi: 10.1016/j.avsg.2020.10.033. PMID: 33333194.
5. *Bogdanov LA, Osyaev NYu, Bogdanova YuD, Mukhamadiyarov RA, Shabaev AR, Evtushenko AV, Kutikhin AG.* Elemental analysis of valvular and atherosclerotic calcification. *Complex Issues of Cardiovascular Diseases*. 2021; 10 (3): 26–33. (In Russ.). doi: 10.17802/2306-1278-2021-10-3-26-33.
6. *Kostyunin AE, Glushkova TV, Lobov AA, Ovcharenko EA, Zainullina BR, Bogdanov LA et al*. Proteolytic Degradation Is a Major Contributor to Bioprosthetic Heart Valve Failure. *J Am Heart Assoc*. 2023; 12 (1): e028215. doi: 10.1161/JAHA.122.028215.
7. *Koziarz A, Makhdoum A, Butany J, Ouzounian M, Chung J.* Modes of bioprosthetic valve failure: a narrative review. *Curr Opin Cardiol*. 2020; 35 (2): 123–132. doi: 10.1097/HCO.0000000000000711. PMID: 31972604.
8. *Wong ML, Griffiths LG*. Immunogenicity in xenogeneic scaffold generation: antigen removal vs decellularization. *Acta Biomater*. 2014; 10: 1806–1816. doi: 10.1016/j.actbio.2014.01.028.
9. *Liu ZZ, Wong ML, Griffiths LG.* Effect of bovine pericardial extracellular matrix scaffold niche on seeded human mesenchymal stem cell function. *Sci Rep*. 2016; 6: 37089. doi: 10.1038/srep37089.
10. *Fadeeva IS.* The role of recipient cells and tissue matrix structure disorders in the mechanism of calcification of vascular and heart valve transplants: diss. … Cand. of Biological Sciences. Pushchino, 2013; 158.
11. *Bailey MT, Pillarisetti S, Xiao H, Vyavahare NR*. Role of elastin in pathologic calcification of xenograft heart valves. *J Biomed Mater Res A*. 2003; 66 (1): 93–102. doi: 10.1002/jbm.a.10543. PMID: 12833435.
12. *Millán Á, Lanzer P, Sorribas V*. The Thermodynamics of Medial Vascular Calcification. *Front Cell Dev Biol*. 2021; 9: 633465. doi: 10.3389/fcell.2021.633465. PMID: 33937234; PMCID: PMC8080379.
13. *Simionescu DT, Lovekamp JJ, Vyavahare NR*. Extracellular matrix degrading enzymes are active in porcine stentless aortic bioprosthetic heart valves. *J Biomed Mater Res A*. 2003; 66 (4): 755–763. doi: 10.1002/jbm.a.10066. PMID: 12926026.
14. *Wang X, Zhai W, Wu C, Ma B, Zhang J, Zhang H et al*. Procyanidins-crosslinked aortic elastin scaffolds with distinctive anti-calcification and biological properties. *Acta Biomater*. 2015; 16: 81–93. doi: 10.1016/j.actbio.2015.01.028. PMID: 25641644.
15. *Wen S, Zhou Y, Yim WY, Wang S, Xu L, Shi J et al*. Mechanisms and Drug Therapies of Bioprosthetic Heart Valve Calcification. *Front Pharmacol*. 2022; 13: 909801. doi: 10.3389/fphar.2022.909801. PMID: 35721165; PMCID: PMC9204043.
16. *Ohri R, Hahn SK, Hoffman AS, Stayton PS, Giachelli CM*. Hyaluronic acid grafting mitigates calcification of glutaraldehyde-fixed bovine pericardium. *J Biomed Mater Res A*. 2004; 70 (2): 328–334. doi: 10.1002/jbm.a.30088. PMID: 15227678.
17. *Raghavan D, Simionescu DT, Vyavahare NR.* Neomycin prevents enzyme-mediated glycosaminoglycan degradation in bioprosthetic heart valves. *Biomaterials*. 2007; 28 (18): 2861–2868. doi: 10.1016/j.biomaterials.2007.02.017. PMID: 17353047; PMCID: PMC2262162.
18. *Leong J, Munnelly A, Liberio B, Cochrane L, Vyavahare N*. Neomycin and carbodiimide crosslinking as an alternative to glutaraldehyde for enhanced durability of bioprosthetic heart valves. *J Biomater Appl*. 2013; 27 (8): 948–960. doi: 10.1177/0885328211430542. PMID: 22207605.
19. *Lei Y, Ning Q, Xia Y, Wang Y*. Enzyme-oxidative-polymerization method for improving glycosaminoglycans stability and reducing calcification in bioprosthetic heart valves. *Biomed Mater*. 2019; 14 (2): 025012. doi: 10.1088/1748-605X/aafd7c. PMID: 30630147.
20. *Cravedi P, Farouk S, Angeletti A, Edgar L, Tamburrini R, Duisit J et al*. Regenerative immunology: the immunological reaction to biomaterials. *Transpl Int*. 2017; 30 (12): 1199–1208. doi: 10.1111/tri.13068. PMID: 28892571; PMCID: PMC6697146.
21. *Ghadially FN.* As you like it, Part 3: A critique and historical review of calcification as seen with the electron microscope. *Ultrastruct Pathol*. 2001; 25 (3): 243–267. doi: 10.1080/019131201300343874. PMID: 11465480.
22. *Boskey AL, Posner AS.* Extraction of a calcium-phospholipid-phosphate complex from bone. *Calcif Tissue Res*. 1976; 19 (4): 273–283. doi: 10.1007/BF02564010. PMID: 3268.
23. *Neishabouri A, Khaboushan AS, Daghigh F, Kajbafzadeh AM, Zolbin MM.* Decellularization in Tissue Engineering and Regenerative Medicine: Evaluation, Modification, and Application Methods. *Front Bioeng Biotechnol*. 2022; 10: 805299. doi: 10.3389/fbioe.2022.805299.
24. *Coscas R, Bensussan M, Jacob MP, Louedec L, Massy Z, Sadoine J et al.* Free DNA precipitates calcium phosphate apatite crystals in the arterial wall *in vivo*. *Atherosclerosis*. 2017; 259: 60–67. doi: 10.1016/j.atherosclerosis.2017.03.005.
25. *Glushkova TV, Kostyunin AE*. Calcification of bioprosthetic heart valves treated with ethylene glycol diglycidyl ether. *Complex Issues of Cardiovascular Diseases*. 2021; 10 (2): 16–24. (In Russ.). doi: 10.17802/2306-1278-2021-10-2-16-24.
26. *Lilly RD.* Pathohistological technique and practical histochemistry. Moscow: MIR, 1969; 645.

The article was submitted to the journal on 20.01.2025

DOI: 10.15825/1995-1191-2025-1-145-159

LAPAROSCOPIC AND ROBOTIC HEPATECTOMY IN LIVING LIVER DONORS. CURRENT STATE AND PROSPECTS

K.O. Semash

National Children's Medical Center, Tashkent, Republic of Uzbekistan

Minimally invasive living-donor hepatectomy is a relatively new surgical technique that can improve donor safety and expedite donor rehabilitation. Following an early stage of research where donor safety was not adequately established, the minimally invasive approach nowadays yields better outcomes when carried out by experienced surgeons. Important factors include donor selection criteria, hospital equipment, and surgeon's learning curve. This review describes the current status of laparoscopic and robotic living-donor hepatectomy, along with the challenges facing the advancement of these surgical techniques.

Key words: liver transplantation, living donation, laparoscopic liver resection, robotic liver resection.

INTRODUCTION

Living-donor liver transplantation (LDLT) became a viable alternative to deceased-donor liver transplantation (DDLT) due to a series of surgical innovations developed in the late 20th century. This was prompted by the rapidly increasing number of liver transplant (LT) candidates in cases of severe organ shortage. In children with end-stage liver disease, especially in their first years of life, reduced cadaveric grafts and split LT are not always feasible due to organ size and technical challenges. In some countries, including the Russian Federation, there are no specific legal prerequisites or well-defined regulations for using children as deceased organ donors [1–2]. Liver grafts from living donors provide comparable or even superior outcomes in terms of graft function and long-term survival, particularly in pediatric recipients, when compared to whole or split LT from deceased donors [3–5]. LDLT offers significant advantages over DDLT, primarily due to the predictable quality of the liver parenchyma by selection and preparation of related donors, and the ability to plan the surgery under optimal conditions. Advancements in hepatobiliary surgery and organ preservation techniques have significantly improved the quality of LDLT grafts, minimizing ischemic and mechanical injury [6–7]. More than 50% of pediatric LT worldwide are performed using LDLT, with relatives being the primary donors [8].

Donor safety during liver donation surgery, specifically hepatectomy, is a significant concern, with complications like biliary problems (bile duct damage, leaks), infections, and vascular issues (bleeding) contributing to donor morbidity. Other factors such as adhesive intestinal obstruction, postoperative hernias and prolonged stay in the operating room may also contribute to donor morbidity [9].

Minimally invasive donor hepatectomy (MIDH) has emerged as a promising technique to reduce donor morbidity. Potential advantages inherent in the minimally invasive technique are better cosmetic results, less postoperative pain, faster recovery, and earlier return to daily activities [10]. MIDH was first described in France by Daniel Cherqui and colleagues, who performed a laparoscopic left lateral sectorectomy on a 27-year-old female donor for transplantation into her child. This pioneering case paved the way for its widespread adoption.

The purpose of this review is to describe the current status of laparoscopic and robotic donor hepatectomy and to identify the barriers to the spread of these surgical techniques.

CURRENT CHALLENGES

In the United States, LDLT peaked in 2001, when it accounted for approximately 10% of all LT [12]. However, following reports of donor complications, the number of LDLT procedures dropped by nearly 40% in subsequent years [12, 13]. As a result, in 2021, when a record 9,234 LT were performed in the United States, only 6.2% of recipients received a graft from a living donor. Most of these were right-lobe grafts [14]. These data contrast with the figures cited for kidney donation. For example, in 2021, related kidney donations accounted for 31.1% of all living-donor kidney transplants in the United States [15].

According to the International Registry of Organ Donation and Transplantation, in Asian countries such as South Korea, Turkey, and Saudi Arabia, living-donor organ transplantation significantly exceeds deceased-donor transplantation. Meanwhile, there is no difference by donated organ [16].

Several meta-analyses and randomized controlled trials have confirmed that minimally invasive laparoscopic

Corresponding author: Konstantin Semash. Address: 294, Parkentskaya str., Yashnobod District, Tashkent, Uzbekistan. Phone: +998 (94) 090-89-05. E-mail: mail@doctorsemash.com

donor nephrectomy offers lower risks of complications, less postoperative pain, faster rehabilitation, and consequently lower treatment costs [17–19]. Living-donor nephrectomy (LDN) is generally not considered a particularly technically challenging procedure, primarily because the kidney is removed intact, including its capsule, vascular pedicle, and ureter, without needing to transect the parenchyma. On the other hand, MIDH is more technically demanding than living-donor nephrectomy (LDN) because it requires parenchymal transection, and also liver resection is associated with individual anatomical features of each donor [20]. These factors, especially the anatomical complexity and the size (thickness) of the parenchyma, have slowed down progress in the development of this surgical field [21].

Donor safety and rapid postoperative rehabilitation are the two main goals of minimally invasive living-donor graft retrieval [22]. The risk of mortality and morbidity after living-donor liver resection is influenced by three key parameters: physiological status (e.g., comorbidities), volume of liver parenchyma removed, which is directly related to the risk of postoperative liver failure, and intraoperative blood loss and subsequent transfusion need [23]. As a result, in order to minimize the number of complications, surgical teams performing these operations should focus on high-quality donor selection and refinement of surgical techniques. According to the 2021 International Consensus on Minimally Invasive Donor Liver Resection, there is still debate over whether laparoscopic and robotic techniques can fully achieve these goals [21, 23].

However, systematic reviews on laparoscopic graft retrieval in LDLT have provided growing evidence that this technique is safe and effective, particularly when performed by experienced surgeons. The reviews conclude that laparoscopic donor hepatectomy is associated with fewer postoperative complications, lead to less intraoperative bleeding and ensures faster return to normal activities compared to open hepatectomy [24–26]. However, it should be noted that LDLT is fundamentally different from traditional hepatectomy because the vascular pedicles of the resected part must be preserved as carefully as possible throughout [11].

The 2008 International Consensus Conference on Laparoscopic Liver Resection in Louisville highlighted significant concerns about MIDH, particularly regarding donor safety and reproducibility [27]. At the Second International Consensus Conference on Laparoscopic Liver Resections held in Morioka in 2015, it was argued that while MIDH was no longer inferior to open surgery in terms of donor safety, it was not recommended as a standard procedure due to insufficient long-term data on postoperative complications [28]. After publications and reports of positive outcomes, an expert consensus was held in Seoul to make clear guideline for the safe widespread implementation of this minimally invasive technique in living liver donors [29]. The results showed that MIDH yields superior outcomes compared to the open approach when performed in high-volume transplant centers by surgical teams with extensive experience in both transplantation and laparoscopy. Moreover, data from the United States show that donors are more willing to accept surgery when offered a minimally invasive procedure [30].

LAPAROSCOPIC LATERAL SECTIONECTOMY

While minimally invasive liver resection has evolved with different options (hand-assisted laparoscopic surgery, laparoscopic-assisted surgery, pure laparoscopic laparoscopic hepatectomy), the procedure to remove the left lateral sector (LLS) from a living donor was initially demonstrated exclusively as a fully laparoscopic technique. All stages of the operation (mobilization, vascular isolation, parenchymal transection) were performed laparoscopically without manual assistance, and the graft was retrieved through a small suprapubic incision (according to Pfannenstiel) [11]. According to French surgeon Daniel Cherqui, LLS is an ideal structure for fully laparoscopic resection because of its convenient location in the abdominal cavity, high mobility relative to the rest of the liver and few anatomical variations [31]. Following the first successful demonstrations of the feasibility of laparoscopic left lateral sectionectomy (LLLS) in France, Belgium and South Korea, the safety and reproducibility of the procedure were validated by Olivier Scatton [11, 32–35]. In their paper, Scatton et al. analyzed 70 LLLS and noted that after overcoming the learning curve, the median hospital stay gradually decreased, blood loss on average remained around 50 mL, and Clavien–Dindo grade II or higher complications were less frequent. However, it was emphasized that this procedure requires at least two experienced surgeons to complete the necessary learning curve [35]. Soubrane et al. compared not only surgical outcomes but also economic outcomes and concluded that mini-invasive left lateral sectionectomy provides at least equal short-term outcomes compared to laparoscopic nephrectomy [32].

In the Russian Federation, the LLLS program was launched in 2016 at the Shumakov National Medical Research Center of Transplantology and Artificial Organs (“Shumakov Center”) in Moscow. Gautier et al. reported less blood loss and shorter hospital stay, but longer surgery time with fully LLLS compared to the open approach at the program formation stage [36]. However, as this field developed, the operation time decreased significantly, complications became less in comparison with open surgery, and LLLS gradually became the gold standard method for left lateral sectionectomy [37–43]. Similar results have been reported by other authors worldwide [44–46].

LAPAROSCOPIC LEFT HEMIHEPATECTOMY

With regard to laparoscopic left hemihepatectomy (LLH), no serious complications have been reported at present, however, with limited experience in such surgical procedures, since the left lobe is a very specific graft from the point of view of transplantation in adults, and is used more in pediatric practice [26, 41, 47]. However, Japanese researchers have reported series of left lobe transplants in adults [48–49]. The authors note a lower donor morbidity after these operations, which they attribute mainly to fewer biliary and pulmonary complications. They also believe that the left lobe graft may be a choice for adult patients where the graft-to-recipient weight ratio (GRWR) is greater than 0.8% or between 0.6% and 0.8%, provided that the recipient's MELD (Model for End-Stage Liver Disease) score is less than 15. The main risk of these operations is small-for-size syndrome, which ultimately leads to graft dysfunction in the recipient. However, no high risks have been described specifically for donors.

Similar results have been reported in a multinational multicenter study (France, Japan, South Korea, Spain, USA, Italy), where the authors compared the results of minimally invasive right and left hemihepatectomies [50]. No statistically significant difference in complications and outcomes between right and left lobe donors was reported.

LAPAROSCOPIC RIGHT HEMIHEPATECTOMY

Fully laparoscopic right hemihepatectomy (LRH) in a living donor was first performed in 2010 in South Korea by Korean surgeon Han, but the outcomes were not reported until 2014. This delay in publication led to the general belief that the first documented LRH was performed by French surgeon Olivier Soubrane in 2013 [23]. Nevertheless, LRH in living donors has been successfully developed and implemented primarily in Asian countries like Japan and South Korea, where LDLT is more common than DDLT [26, 51, 52]. However, despite its success, there is significant variation in surgical techniques between hospitals, particularly in trocar placement and the sequence of surgical steps [53, 54].

Although the right lobe of the liver provides an adequate parenchyma volume for the recipient, this approach raises serious concerns about donor safety. Abecassis et al. reported postoperative complication rates of up to 40% [9]. The laparoscopic approach has been advocated in many transplant centers to minimize these complications. Minimally invasive right lobe resection is technically more demanding than left lobe resection due to the deep subdiaphragmatic location of the right lobe and the need for extensive mobilization. [55]. These technical difficulties have slowed the development and widespread adoption of fully LRH for living donors. In its infancy, hybrid techniques (with manual assistance) were used [26, 27, 53]. Even now, experienced surgeons recommend for many centers to use hybrid approaches before moving to fully laparoscopic right lobe resection [27]. Importantly, if the anatomic integrity of the graft is jeopardized, the most appropriate decision is to go for the open option (conversion).

Nevertheless, in Asia, especially in South Korea, performing laparascopic hemihepatectomies in donors is quite common. For example, in 2018, a paper was published reporting the outcomes of 172 right lobe resections in living donors performed in hospitals in South Korea between 2013 and 2017 [56]. In 2021, an article was published reporting 255 completely laparoscopic right lobe resections in a single center [57]. At the same time, the studies compared open and laparoscopic liver resections and demonstrated the high efficiency of minimally invasive techniques in terms of postoperative complications, intraoperative blood loss and length of postoperative hospital stay.

In Russia, Voskanyan et al. were the first to report on the performance of such a surgical operation [54], with the greatest cumulative experience of donor right hemihepatectomies accumulated at Shumakov Center. As of 2022, Monakhov et al. reported 276 laparoscopic donor liver hepatectomies, including 11 cases of completely laparoscopic right lobe resections [41].

DONOR SELECTION

Careful donor selection is considered to be of utmost importance in preparation for MIDH. Preoperative evaluation includes a thorough physical examination. Of particular importance are any concomitant cardiovascular, renal, pulmonary, coagulation-related disorders, and infectious diseases. Many centers exclude patients with arterial hypertension and psychiatric disorders despite the possibility of conservative correction [7, 58, 59]. In addition, standard liver function tests, serologic tests for hepatitis B and C, and chest and abdominal examinations are always used. A contrast-enhanced triple-phase liver CT scan is a critical part of preoperative evaluation for MIDH. It provides essential information for volumetric analysis and vascular assessment of the donor liver.

Magnetic resonance cholangiopancreatography (MRCPG) provides a non-invasive, high-resolution view of the biliary tree, helping to identify anatomical variations and determine the optimal bile duct division point (see Table 1). Misinterpretation of biliary anatomy may require intraoperative cholangiography, but it requires experience, additional costs, and prolongs operative time [60].

Nevertheless, in recent years, indocyanine green fluorescence imaging has been actively used. It helps to visualize bile ducts in more detail when performing laparoscopic liver resection [26, 61]. Methods of using methylene blue to control bile flow have also been reported [46].

Surgeons from different centers define different anatomical criteria for selecting a potential liver donor. For example, Kim et al. considered only donors who had one long right hepatic duct, one artery, and standard portal vein anatomy (Table 1) [62]. They also excluded donors whose right lobe mass exceeded 650 g. Gautier et al. considered the separation of the 2nd and 3rd segment veins as a contraindication for LLS retrieval, as it could cause difficulties during suturing and lead to intraoperative bleeding; however, this ceased to be a contraindication with the accumulation of experience [36, 39]. Rotellar et al. believe that the right lobe graft should have one artery, one portal vein and one bile duct, but, at the same time, variations are acceptable, and each donor should be assessed individually [63].

Anatomical variations of the portal vein (Table 1) were once considered a contraindication for MIDH. However, recent reports suggest that experienced surgical teams can achieve safe and successful outcomes, even in donors with portal vein anomalies [57, 64].

BLOOD LOSS

A strong obstacle in the development of the minimally invasive approach in donor liver surgery has been the difficulty and limitations in approaches when intraoperative bleeding develops. With improvement in technology and surgical technique in the last three decades, it has been possible to significantly reduce blood loss and decrease the frequency of blood transfusion during laparoscopic liver hepatectomies [22, 74, 75].

Gentle parenchymal transection and the pneumoperitoneum effect (i.e., the tamponade effect on the dissected surface due to increased intra-abdominal pressure) play a critical role in reducing blood loss during MIDH.

Table 1

Anatomical variation of the bile ducts and portal vein

Anatomical variation of the bile ducts	
A	Standard bifurcation (57%)
B	Trifurcation (12%)
C	Right anterior (C1, 16%) or right posterior (C2, 4%) ducts draining into the common hepatic duct
D	Right posterior (D1, 5%) or right anterior (D2, 1%) duct draining into the left hepatic duct
E	No hepatic duct confluence (3%)
F	Right posterior duct draining into the cystic duct (2%)
Anatomical variation of the portal vein	
I	Standard bifurcation
II	Trifurcation
III	Right posterior branch as the first branch of the main portal vein
IV	Segment VII branch arising as a separate branch from the right portal vein
V	Segment VI branch arising as a separate branch from the right portal vein

These factors help mitigate venous backflow, which is the primary source of intraoperative bleeding [35]. For instance, Olivier Scatton suggests temporarily increasing the pneumoperitoneum pressure to 14–16 mmHg in order to control and minimize bleeding [35]. The greatest risk of intraoperative bleeding occurs during parenchymal transection. In the minimally invasive approach, this step is performed very precisely and under magnification. Transecting the hepatic vein is also crucial because slippage of the vascular clamp or a defect in the vascular stapler can lead to massive bleeding [39, 76].

Comparative studies have consistently shown that MIDH results in lower [36, 45, 71, 77] or equal [30, 57, 64, 69] blood loss compared to the traditional open approach. However, the studies emphasized that the lack of a statistically significant difference in blood loss was due to small sample sizes [30]. Hence, another advantage of the minimally invasive method can be considered less blood loss compared to the traditional approach.

CONVERSIONS

Any incident that may jeopardize donor safety or graft integrity is an indication for conversion to open surgery. Conversion itself is not a complication but implies that some adverse event occurred during the procedure. The most frequently described reasons for conversion to open access were difficulty in differentiating the anatomy of the bile ducts or porta hepatis and vascular injury resulting in significant bleeding. Also, cases of poor visualization in overweight donors were reported, which also required conversion [50].

Scatton et al. reported 4 conversions (6%) out of 70 operations, of which 69 were LLS retrieval and 1 was left lobe retrieval. The reasons for conversion were injury to the left branch of the portal vein, poor exposure, and uncertainty about biliary tract anatomy. None of the conversions was associated with acute or uncontrolled bleeding or the need for blood transfusion, and all donors recovered without complications [35]. Monakhov et al. reported two conversions (1.2%) out of 164 LLS retrieval surgeries; the conversion cases were associated with occlusion of the left branch of the portal vein by a clip and longitudinal rupture of the left hepatic vein; all donors were also discharged without complications. The outcomes in the recipients were also uneventful [39].

Choi et al. reported a 6.7% conversion rate (4 out of 60 cases) when performing hand-assisted right lobe resections in living liver donors. The primary reasons for conversion were right hepatic vein injury and adrenal vein injury [65].

Soubrane et al. reported a conversion rate of 4.1% (17 out of 412 cases) in MIDH. The primary reasons for conversion were portal vein injury, difficulty mobilizing the porta hepatis and identifying structures in the hepatoduodenal ligament [50].

Rhu reported a 5.0% conversion due to portal vein injury, donor liver steatosis detected during intraoperative biopsy and inferior vena cava injury [57].

LEARNING CURVE AND OPERATIVE TIME

The major obstacle to the global spread of the laparoscopic technique in liver donation is that, apart from technical equipment, it requires considerable experience in both liver surgery and laparoscopic surgery. A multinational study showed that 65.6% of surgeons had performed >50 non-donor laparoscopic hepatectomies and 43.8% had performed >50 open donor hepatectomies before their first minimally invasive donor liver resection [29]. The learning curve for MIDH is primarily influenced by a surgeon's ability to carefully divide liver parenchyma and control intraoperative bleeding. It is also believed that the surgeon spends the most time learning to dissect and mobilize vascular structures [59]. Several reports have emphasized that a minimum of 15–60 procedures are required to achieve optimal outcomes, depending on the liver fragment to be resected [39, 86]. For example, Scatton et al. showed that at least 20 procedures are required to achieve optimal hemostasis and shorten operative time [35]. A similar result was demonstrated by Monakhov et al. in their study [39].

MIDH tends to take longer, especially during the training period of surgeons [39, 45, 62, 69]. Baker et al. found an association between higher body mass index and longer operative time, while Rhu et al. emphasized that after the first 100 operations, surgical time decreased regardless of donor body weight [30, 77].

However, it should be noted that defining a learning criterion for a single surgeon is not possible because experience and outcomes vary between different surgical teams. Rhu et al. reported no change in surgical time from the first to the second quartile over time, but reported a significant decrease from the second to the third quartile and from the third to the fourth quartile. His team was able to meaningfully reduce surgical time after 50 laparoscopic surgeries [77]. To determine the learning curve, Korean surgeon Lee used two variables – intraoperative blood loss and operative time. The learning period was determined based on when these two factors reached a plateau, indicating surgeons had gained proficiency. Significant improvement in surgical outcomes (less blood loss, reduced operative time) was observed after the 15th operation, marking the transition into the "experience accumulation phase" [87].

COMPLICATIONS

As mentioned above, donor safety is the main criterion for living-donor hepatectomies. According to a study conducted at Oxford University, a 30-day postoperative outpatient follow-up is not sufficient; such follow-up underestimates the morbidity of donors after liver resection. A 90-day outpatient follow-up is recommended for donors [66].

The Clavien–Dindo classification, although widely used, tends to consider only the most severe complications and does not consider other less severe complications in the same patient [67]. The new Comprehensive Complication Index method developed on the basis of the Clavien–Dindo classification summarizes all postoperative complications and is the most sensitive tool for assessing the real severity of postoperative complications [68].

The incidence of complications in minimally invasive living-donor hepatectomies ranges from 0 to 40%, with most studies reporting it in the range of 10–26% [50, 57, 69, 70]. The most common complications are wound complications, pleural effusion, biliary effusion or biliary stricture (Table 2).

Most studies comparing MIDH with open hepatectomy found no statistically significant difference in complication rates. However, this lack of statistical significance is likely due to small sample sizes in many studies. Rhu et al. noted an interesting finding that complications were significantly higher in the first quartile of surgeries, suggesting surgeon inexperience during early cases contributes to more complications [57]. Broering also reported that the complication rate decreased from 26.7% to 9.7% after developing appropriate surgical skill [45]. The complication rates did not differ significantly between right and left lobe donors [50]. Also, the complication rate in donors was comparable when comparing surgical outcomes in donors with variant and standard portal vein anatomy [57].

Biliary complications are among the most serious complications following MIDH. Takahara et al. reported three cases of bile leaks even though each bile duct stump was clipped twice and at the end of the operation looked quite normal and there were no signs of biliary leak [71]. The authors suggest that the clips fell off due to necrosis of the bile duct stump with subsequent development of bile leak.

Table 2

Reported complications of minimally invasive living donor hepatectomy (Clavien–Dindo classification)

I	Fever, gastroenteritis, gastric ulcer, occipital alopecia, pneumothorax without drainage, wound infection, suprapubic hematoma, ileus, arm neuropraxia, atelectasis, transient neutropenia
II	Gastroparesis, pulmonary infection, segment IV infarction, bile duct stenosis, pancreatitis, cystitis, incisional port-size hernia
IIIa	Biliary leakage, fluid collection, bladder injury, portal vein thrombosis or stenosis
IIIb	Abdominal abscess, intra-abdominal bleeding

Regarding wound complications, open resection (especially right lobe resection) in the donor requires a large incision with extensive muscle incision, resulting in pain for several days and discomfort for several weeks [11]. During this incision, sensitive nerve endings (ventral branches of intercostal nerves T8 and T9) are transected, which may result in loss of sensation of the anterior abdominal wall. In contrast, suprapubic incisions are usually well tolerated without sequelae, and postoperative hernias are rare. In addition, they are virtually inconspicuous if located low enough in the pubic hair region [11]. Care must be taken when suturing the abdominal wall closure, as bladder injury may occur [20]. MIDH involves small incisions for trocar placement, which can lead to local ischemia and wound infections. However, these complications occur less frequently in MIDH compared to the open approach [72].

Theoretically, there is a risk of gas embolism due to pneumoperitoneum. However, pneumoperitoneum is created by insufflation of carbon dioxide, a gas with a higher solubility than nitrogen. Several experimental studies have established that absorption of carbon dioxide into systemic circulation is not associated with hemodynamic instability [27].

PAIN SYNDROME

In their works separate and joint studies, Monakhov et. al. and Syomash used an analog scale for pain assessment in donors after open and laparoscopic hepatectomies and reported lower pain syndrome in donors who underwent laparoscopic graft retrieval [26, 39] Kurosaki et al. used less additional analgesia in donors operated mini-invasively compared to patients who underwent open hepatectomy [78]. Reduced dosage or shorter duration of analgesic use has also been shown in a series of studies in donors who underwent minimally invasive hepatectomy [45, 62, 65, 69].

LENGTH OF HOSPITAL STAY AND COST OF TREATMENT

The length of postoperative stay depends largely on the policies of the institution and the health care system. In eastern countries such as Japan and South Korea, the policy is for donors to be hospitalized until they can return to normal daily activities [59]. In addition, some eastern national health care systems do not require patients to be discharged even after they have recovered from surgery [57, 76, 79]. Western countries seem to have an extended recovery protocol. Several reports show no statistically significant decrease in length of stay between the minimally invasive and open approach [30, 80]. However, in most centers, the length of stay was shorter in the minimally invasive graft retrieval group [39, 45, 57].

In terms of treatment costs, the material costs of performing an MIDH were higher. Baker reports that despite the high costs of the surgery itself, these costs were offset by lower costs associated with length of hospital stay [30]. Chinese colleagues report opposite results. In their observational series, MIDH was significantly more expensive than the open procedure [69].

OUTCOMES IN RECIPIENTS

It should be noted that surgical outcomes in donors should not be assessed separately from those in recipients. For example, Troppmann et al. found that laparoscopic donor nephrectomy was associated with delayed graft function and increased acute rejection rates. The reasons for this finding are unclear, but hemodynamic compromise in the renal vasculature due to pneumoperitoneum pressure may be a possible factor [73]. On the other hand, in almost all studies comparing laparoscopic graft retrieval with open donor resection, the authors found no difference between the minimally invasive and conventional approach in terms of vascular and biliary complications, graft survival, and overall recipient survival [26, 36, 39, 45, 46, 63, 94]. The minimally invasive technique did not increase the risks to the recipient even in cases of variant portal vein anatomy [57]. Hong et al. were the only team that observed a higher rate of biliary complications in recipients of grafts from MIDH procedures. The authors believe that most likely this was due to longer warm ischemia time and multiple bile ducts in the graft [64].

ROBOTIC HEPATECTOMY IN LIVING LIVER DONORS

Robotic hepatectomy in living donors is much less common than laparoscopic hepatectomy, but it is considered safe and feasible in the hands of experienced professionals. The first robotic graft retrieval was performed by Italian surgeon Giulianotti and colleagues in 2012. The operation was performed using the da Vinci Robotic Surgical System on a 53-year-old man, from whom the right liver lobe was removed for subsequent transplantation to his 61-year-old brother [26, 81].

Compared to the laparoscopic approach, evolution of the robotic approach has been slow. Potential advantages include an expanded and more stable view as well as better precision of movements. The Da Vinci surgical system can rotate in all directions, allowing a wider range of motion compared to the human hand. This allows manipulation and suturing in the subhepatic space at angles that are not possible with conventional instruments. On the downside, the surgeon has no haptic feedback. Also, the success of the operation depends on the level of training of the assistant who changes the robotic instruments during parenchymal transection [82].

Recent studies have shown that robotic liver resection is feasible and produces similar short-term outcomes as the laparoscopic procedure, but with higher costs, as health insurance does not usually cover such high-

tech surgeries [70]. Another obstacle to the spread of this technique is the need for high specialization of the medical center and surgical instruments, since only ultrasonic scalpels, hem-o-lok clips and staplers can be used during robotic liver surgery; cavitron ultrasonic surgical aspirators cannot be used [83]. Nevertheless, not only robot-assisted donor resection but also robot-assisted graft implantation has been reported [91].

Two studies comparing robotic living-donor hepatectomy with open hepatectomy found the robot-assisted approach to be just as effective in terms of complications and intraoperative blood loss [83, 84].

Currently, there are no data to suggest that the robotic technique is superior to the open or laparoscopic approach. Troisi et al. did not find any superior outcome to justify the higher cost of the robotic approach compared

Table 3

Results of laparoscopic hepatectomy at different transplant centers

Author	Number of operations (n)	Retrieved liver fragment	Operation time (minutes, range)	Blood loss (milliliters)	Conversions (n, %)	Learning curve (number of operations)	Complications (C–D, number)	Hospital stay (days, range)
Soubrane et al., 2006 [32]	16	LLS	320 ± 67	18.7 ± 44.2	1 (6.25%)	not assessed	I – 2 IIIb – 1	11.0 ± 2.7
Kim et al., 2011 [34]	11	LLS	330 ± 68	396 ± 72	0	not assessed	0	6.9 ± 0.3
Yu et al., 2012 [88]	15	LLS	331.3 ± 63	410.0 ± 71.2	0	not assessed	0	7.1 ± 0.8
Scatton et al., 2015 [35]	70	LLS – 69 LL – 1	308 (180–555)	50 (10–500)	4 (6%)	20	I – 9 II – 2 IIIa – 4 IIIb – 1	4
Soubrane et al., 2015 [20]	124	LLS	308 (180–555)	50 (10–500)	4 (3.2%)	faster operation time	I – 6 II – 15 IIIa – 6	6.3 (2–18)
Broering et al., 2018 [45]	72	LLS	293 (192–420)	100 (50–600)	3 (4.8%)	15	I and II – 3 IIIa – 1	4.1 ± 1.33
Gautier et al., 2018 [37]	37	LLS	277.9 ± 16.3	96.8 ± 16.5	0	faster operation time	IIIb – 1	4 ± 0.4
Semash [26]	100	LLS	262 ± 60	85 ± 68	1 (1%)	faster operation time	II – 1 IIIa – 1 IIIb – 1	4.5 ± 1.6
Monakhov et al., 2021 [39]	164	LLS	227.5 (140–400)	50 (20–400)	2 (1.2%)	37	II – 2 IIIa – 2 IIIb – 1	5 (2–14)
Kwon et al., 2018 [56]	54	RL – 41 ERL – 10 LL – 3	436 (294–684)	300 (10–850)	4 (7.4%)	20	I and II – 9 IIIa – 6 IIIb – 3	10 (7–27)
Takahara et al., 2017 [71]	54	RL	454.93 ± 85	81.07 ± 52.78	1 (1.9%)	40	I and II – 6 IIIa – 4	8.43 ± 1.65
Park et l, 2019 [89]	91	RL	345 ± 225	300 ± 200	5 (5.5%)	30	I and II – 2 IIIa – 11 IIIb – 3	10 ± 3
Rhu et al., 2021 [57]	255	RL	261 (230–325)	200 (150–300)	5 (2%)	not assessed	I – 7 II – 20 IIIa – 11 IIIb – 4	8.87 ± 3.00
Soubrane et al., 2022 [50]	412	LL – 164 RL – 248	424 (240–850)	410 (10–3550)	17 (4.1%)	faster operation time	I and II – 70 III and IV – 38	10 (2–50)
Seo et al., 2022 [90]	376	RL	260.9 ± 66.1	257.8 ± 194.6	not described	faster operation time	I and II – 10 IIIa and IIIb – 19	7.2 ± 2.4

Note: LLS, left lateral sector; LL, left lobe; RL, right lobe; ERL, extended right lobe; C–D, Clavien–Dindo classification.

Table 4

Results of robot-assisted living-donor hepatectomy at different transplant centers

Author	Number of operations (n)	Retrieved liver fragment	Operation time (minutes, range)	Blood loss (milliliters)	Conversions (n, %)	Learning curve (number of operations)	Complications (C–D, number)	Hospital stay (days, range)
Chen et al., 2016 [92]	16	RL	596 (353–753)	169 (50–500)	0	15	IIIa – 1	7 (6–8)
Broering et al., 2020 [83]	35	RL	504 ± 73.5	250 (100–800)	0	15	I and II – 2	5.3 (3–12)
Binoj et al., 2020 [93]	51	RL	536.8 ± 73.4	530.39 ± 222.72	0	not described	not described	8.27 ± 3.0
Rho et al., 2020	52	RL	493.6	109.8	2 (3.8%)	faster operation time	I and II – 8 IIIa and IIIb – 2	
Broering et al., 2020 [95]	175	LLS – 61 LL – 34 RL – 80	424 (177–693)	138.1 (20–1000)	2 (1.14%)	not assessed	I and II – 12	4.3 (2–22)
Troisi et al., 2021 [85]	25	LLS	290	100	0	15	0	3 ± 0.3

Note: LLS, left lateral sector; LL, left lobe; RL, right lobe; ERL, extended right lobe; C–D, Clavien–Dindo classification.

with the laparoscopic method [85]. They also emphasized that conversion in robotic resection takes longer than in the laparoscopic approach. Therefore, it is crucial to apply all laparoscopic techniques to stop unexpected bleeding before conversion.

Regarding the learning curve in robotic donor surgery, Broering et al. argue that robotic hemihepatectomy takes a short learning curve, with the mastery phase reached in 15 procedures [83]. Chen et al. took a more measured approach to learning and divided the learning curve into three phases – novice surgeon (1–15 procedures), trained surgeon (15–25 procedures), and experienced surgeon (25–52 procedures). The effect of training was demonstrated by a reduction in surgery time and donor hospital stay after phase 1 of training. Blood loss decreased after phase 2 of training. The authors also note that the presence of dual robot control consoles offers a safe form of training, as the supervisor (instructor) can assist the surgeon during surgery and take over control if necessary [84, 92].

The most extensive experience with robot-assisted living-donor hepatectomy is currently available at the King Faisal Specialist Hospital & Research Centre (KFSHRC) in Saudi Arabia. Surgeons at this hospital reported retrieval of 61 LLS, 34 left lobes and 80 right lobes [95]. The cumulative worldwide experience is summarized in Table 4.

In any case, the robotic method is still very limited in geographic distribution and requires much more experience than laparoscopy. The upcoming introduction of new robotic systems that support haptic feedback or cavitron ultrasound-guided surgical dissectors will facilitate further spread of robotic living-donor hepatectomy.

PROSPECTS FOR FURTHER DEVELOPMENT

The main obstacles to the development and widespread adoption of minimally invasive living-donor surgery include lack of material and technical resorces at hospitals, surgical skill gap and institutional barriers and resistance. Also, there is no uniform and standardized surgical protocol, each transplant center follows a different approach [53]. Establishing an international registry for minimally invasive living-donor hepatectomies and implementing standardized surgical techniques will help in training surgeons worldwide.

Also, new techniques are constantly being introduced into medicine. One of the new technologies that are already beginning to be applied in laparoscopic surgery, including hepatobiliary surgery, is augmented reality (AR) technology. The surgeon, using special AR spectacles, can see in the monitor not only the operating field, but also vascular structures that are loaded using multislice CT scan data and virtual reality technology. Prototypes already exist and are being tested [96–98].

CONCLUSION

Living donation contributes significantly to the expansion of the organ donor pool. Minimally invasive hepatectomies have the potential to increase the number of transplants from living donors due to a number of advantages. These advantages include lower intraoperative blood loss, less pain, faster rehabilitation, and minimized complications. In the hands of experienced surgeons, this approach is safe not only for donors, but also for recipients, as graft quality does not become worse after the procedure. This direction is promising, but not all transplant centers can perform such operations. The main obstacles to the development of minimally invasive living-donor hepatectomies are lack of advanced

equipment and resources, as well as conservatism among surgeons. When launching a minimally invasive hepatectomy program, ensuring surgeon expertise and proper mentorship is critical for safety and success.

The authors declare no conflict of interest.

REFERENCES

1. *Gautier SV, Monakhov AR, Tsirulnikova OM, Latypov RA, Dzhanbekov TA, Mescheryakov SV et al*. Split liver transplantation: a single center experience. *Almanac of Clinical Medicine*. 2020; 48 (3): 162–170. https://doi.org/10.18786/2072-0505-2020-48-031.
2. *Ghobrial RM, Amersi F, Busuttil RW.* Surgical advances in liver transplantation. Living related and split donors. *Clin Liver Dis*. 2000; 4 (3): 553–565. https://doi.org/10.1016/s1089-3261(05)70126-4.
3. *Austin MT, Feurer ID, Chari RS, Gorden DL, Wright JK, Pinson CW*. Survival after pediatric liver transplantation: why does living donation offer an advantage? *Arch Surg*. 2005; 140 (5): 465–470; discussion 470–471. https://doi.org/10.1001/archsurg.140.5.465.
4. *Bourdeaux C, Darwish A, Jamart J, Tri TT, Janssen M, Lerut J et al*. Living-related versus deceased donor pediatric liver transplantation: a multivariate analysis of technical and immunological complications in 235 recipients. *Am J Transplant*. 2007; 7 (2): 440–447. https://doi.org/10.1111/j.1600-6143.2006.01626.x.
5. *Kasahara M, Umeshita K, Inomata Y, Uemoto S; Japanese Liver Transplantation Society.* Long-term outcomes of pediatric living donor liver transplantation in Japan: an analysis of more than 2200 cases listed in the registry of the Japanese Liver Transplantation Society. *Am J Transplant*. 2013; 13 (7): 1830–1839. https://doi.org/10.1111/ajt.12276.
6. *Semash K, Janbekov T, Akbarov M, Usmonov A, Gaibullaev T.* Stages of preparation and examination of related liver donors and their perioperative management. *Coloproc.* 2023; (1): 41–54. https://doi.org/10.56121/2181-4260-2023-1-41-54.
7. *Semash KO, Dzhanbekov TA, Akbarov MM, Usmanov AA, Povlonniezov KhG.* Prizhiznennoe donorstvo fragmentov pecheni. Rekomendatsii po selektsii i obsledovaniyu rodstvennykh donorov fragmenta pecheni. Tashkent, 2023; 24. https://search.rads-doi.org/project/10145/index (date of access: 13.02.2024). https://doi.org/10.61726/4427.2024.11.78.001.
8. *Quirino L, Jan PL.* Living-Related Liver Transplantation. Progress, Pitfalls, and Promise. *Regen Med Appl Organ Transplant*. 2014: 283–298. https://doi.org/10.1016/B978-0-12-398523-1.00021-5.
9. *Abecassis MM, Fisher RA, Olthoff KM, Freise CE, Rodrigo DR, Samstein B et al.* A2ALL Study Group. Complications of living donor hepatic lobectomy – a comprehensive report. *Am J Transplant*. 2012; 12 (5): 1208–1217. https://doi.org/10.1111/j.1600-6143.2011.03972.x.
10. *Novitsky YW, Litwin DE, Callery MP.* The net immunologic advantage of laparoscopic surgery. *Surg Endosc*. 2004 Oct; 18 (10): 1411–1419. https://doi.org/10.1007/s00464-003-8275-x.
11. *Cherqui D, Soubrane O, Husson E, Barshasz E, Vignaux O, Ghimouz M et al*. Laparoscopic living donor hepatectomy for liver transplantation in children. *Lancet*. 2002 Feb 2; 359 (9304): 392–396. https://doi.org/10.1016/S0140-6736(02)07598-0.
12. Organ Procurement and Transplantation network [Internet]. Liver Donors Recovered in the U.S. by Donor Type. (date of access: 13.02.2024). https://optn.transplant.hrsa.gov/data/view-data-reports/national-data/.
13. *Ghobrial RM, Freise CE, Trotter JF, Tong L, Ojo AO, Fair JH et al.* A2ALL Study Group. Donor morbidity after living donation for liver transplantation. *Gastroenterology*. 2008 Aug; 135 (2): 468–476. https://doi.org/10.1053/j.gastro.2008.04.018.
14. *Kwong AJ, Ebel NH, Kim WR, Lake JR, Smith JM, Schladt DP et al*. OPTN/SRTR 2021 Annual Data Report: Liver. *Am J Transplant*. 2023 Feb; 23 (2 Suppl 1): S178–S263. https://doi.org/10.1016/j.ajt.2023.02.006.
15. *Lentine KL, Smith JM, Miller JM, Bradbrook K, Larkin L, Weiss S et al*. OPTN/SRTR 2021 Annual Data Report: Kidney. *Am J Transplant.* 2023; 23 (2 Suppl 1): S21–S120. https://doi.org/10.1016/j.ajt.2023.02.004.
16. International Registry in Organ Donation and Transplantation [Internet]. Final Numbers in 2022. (date of access: 13.02.2024) https://www.irodat.org.
17. *Nanidis TG, Antcliffe D, Kokkinos C, Borysiewicz CA, Darzi AW, Tekkis PP, Papalois VE.* Laparoscopic versus open live donor nephrectomy in renal transplantation: a meta-analysis. *Ann Surg*. 2008 Jan; 247 (1): 58–70. https://doi.org/10.1097/SLA.0b013e318153fd13.
18. *Yuan H, Liu L, Zheng S, Yang L, Pu C, Wei Q, Han P.* The safety and efficacy of laparoscopic donor nephrectomy for renal transplantation: an updated meta-analysis. *Transplant Proc*. 2013 Jan-Feb; 45 (1): 65–76. https://doi.org/10.1016/j.transproceed.2012.07.152.
19. *Nicholson ML, Kaushik M, Lewis GR, Brook NR, Bagul A, Kay MD et al*. Randomized clinical trial of laparoscopic versus open donor nephrectomy. *Br J Surg*. 2010 Jan; 97 (1): 21–28. https://doi.org/10.1002/bjs.6803.
20. *Soubrane O, de Rougemont O, Kim KH, Samstein B, Mamode N, Boillot O et al*. Laparoscopic Living Donor Left Lateral Sectionectomy: A New Standard Practice for Donor Hepatectomy. *Ann Surg*. 2015 Nov; 262 (5): 757–761; discussion 761–763. https://doi.org/10.1097/SLA.0000000000001485.
21. *Cherqui D, Ciria R, Kwon CHD, Kim KH, Broering D, Wakabayashi G et al*. Expert Consensus Guidelines on Minimally Invasive Donor Hepatectomy for Living Donor Liver Transplantation From Innovation to Implementation: A Joint Initiative From the International Laparoscopic Liver Society (ILLS) and the Asian-Pacific Hepato-Pancreato-Biliary Association (A-PHPBA). *Ann Surg*. 2021 Jan 1; 273 (1): 96–108. https://doi.org/10.1097/SLA.0000000000004475.
22. *Semash KO, Dzhanbekov TA, Akbarov MM, Usmanov AA, Povlonniezov KhG.* Prizhiznennoe donorstvo fragmentov pecheni. Taktika vedeniya rodstvennykh donorov fragmenta pecheni v usloviyakh statsionara, a takzhe

ambulatorno posle rezektsii pecheni. Tashkent, 2023; 21. https://search.rads-doi.org/project/10146/index (date of access: 15.02.2024). https://doi.org/10.61726/7507.2024.31.90.001.
23. *Soubrane O, Perdigao Cotta F, Scatton O.* Pure laparoscopic right hepatectomy in a living donor. *Am J Transplant*. 2013 Sep; 13 (9): 2467–2471. https://doi.org/10.1111/ajt.12361.
24. *Nguyen KT, Marsh JW, Tsung A, Steel JJ, Gamblin TC, Geller DA.* Comparative benefits of laparoscopic vs open hepatic resection: a critical appraisal. *Arch Surg*. 2011 Mar; 146 (3): 348–356. https://doi.org/10.1001/archsurg.2010.248.
25. *Ciria R, Cherqui D, Geller DA, Briceno J, Wakabayashi G.* Comparative Short-term Benefits of Laparoscopic Liver Resection: 9000 Cases and Climbing. *Ann Surg*. 2016 Apr; 263 (4): 761–777. https://doi.org/10.1097/SLA.0000000000001413.
26. *Semash KO.* Laparoskopicheskoe iz''yatie levogo lateral'nogo sektora pecheni u prizhiznennogo donora: dis. … kand. med. nauk. M., 2020; 113. https://doi.org/0.61726/5567.2024.63.97.001.
27. *Buell JF, Cherqui D, Geller DA, O'Rourke N, Iannitti D, Dagher I et al*. World Consensus Conference on Laparoscopic Surgery. The international position on laparoscopic liver surgery: The Louisville Statement, 2008. *Ann Surg*. 2009 Nov; 250 (5): 825–830. https://doi.org/10.1097/sla.0b013e3181b3b2d8.
28. *Wakabayashi G, Cherqui D, Geller DA, Buell JF, Kaneko H, Han HS et al*. Recommendations for laparoscopic liver resection: a report from the second international consensus conference held in Morioka. *Ann Surg*. 2015 Apr; 261 (4): 619–629. https://doi.org/10.1097/SLA.0000000000001184.
29. *Rotellar F, Ciria R, Wakabayashi G, Suh KS, Cherqui D*. On behalf of the WS-MIDH collaborative group. World Survey on Minimally Invasive Donor Hepatectomy: A Global Snapshot of Current Practices in 2370 Cases. *Transplantation*. 2022 Jan 1; 106 (1): 96–105. https://doi.org/10.1097/TP.0000000000003680.
30. *Baker TB, Jay CL, Ladner DP, Preczewski LB, Clark L, Holl J, Abecassis MM.* Laparoscopy-assisted and open living donor right hepatectomy: a comparative study of outcomes. *Surgery*. 2009 Oct; 146 (4): 817–823; discussion 823–825. https://doi.org/10.1016/j.surg.2009.05.022.
31. *Cherqui D.* Laparoscopic liver resection. *Br J Surg*. 2003 Jun; 90 (6): 644–646. https://doi.org/10.1002/bjs.4197.
32. *Soubrane O, Cherqui D, Scatton O, Stenard F, Bernard D, Branchereau S et al*. Laparoscopic left lateral sectionectomy in living donors: safety and reproducibility of the technique in a single center. *Ann Surg*. 2006 Nov; 244 (5): 815–820. https://doi.org/10.1097/01.sla.0000218059.31231.b6.
33. *Troisi R, Debruyne R, Rogiers X*. Laparoscopic living donor hepatectomy for pediatric liver transplantation. *Acta Chir Belg*. 2009 Jul-Aug; 109 (4): 559–562. https://doi.org/ 10.1080/00015458.2009.11680486.
34. *Kim KH, Jung DH, Park KM, Lee YJ, Kim DY, Kim KM, Lee SG.* Comparison of open and laparoscopic live donor left lateral sectionectomy. *Br J Surg*. 2011 Sep; 98 (9): 1302–1308. https://doi.org/10.1002/bjs.7601.
35. *Scatton O, Katsanos G, Boillot O, Goumard C, Bernard D, Stenard F et al*. Pure laparoscopic left lateral sectionectomy in living donors: from innovation to development in France. *Ann Surg*. 2015 Mar; 261 (3): 506–512. https://doi.org/10.1097/SLA.0000000000000642.
36. *Gautier S, Monakhov A, Gallyamov E, Tsirulnikova O, Zagaynov E, Dzhanbekov T et al*. Laparoscopic left lateral section procurement in living liver donors: A single center propensity score-matched study. *Clin Transplant*. 2018 Sep; 32 (9): e13374. https://doi.org/10.1111/ctr.13374.
37. *Monakhov A, Semash K, Tsiroulnikova O, Djanbekov T, Khizroev K, Kurtak N, Gautier S*. Laparoscopic left lateral sectionectomy in living liver donors: from the first experience to routine usage. *Transplantation.* 2020 Sep; 104 (S3): S241. https://doi.org/10.1097/01.tp.0000699664.06418.8f.
38. *Gautier SV, Monakhov AR, Gallyamov EA, Zagaynov EV, Tsirulnikova OM, Semash KO et al*. Laparoscopic Approach in Liver Harvesting from Living Donors for Transplantation in Children. *Annaly khirurgicheskoy gepatologii = Annals of HPB Surgery*. 2018; 23 (1): 13–18. (In Russ.). https://doi.org/10.16931/1995-5464.2018-1-13-18.
39. *Monakhov A, Gautier S, Tsiroulnikova O, Semash O, Latypov R, Dzhanbekov T et al*. Living donor left lateral sectionectomy: Should the procedure still be performed open? *Journal of Liver Transplantation*. 2021; 1: 100001. https://doi.org/10.1016/j.liver.2020.100001.
40. *Monakhov A, Semash K, Khizroev K, Tsiroulnikova O, Voskanov M, Gallyamov E et al*. Laparoscopic living donor hepatectomy: a new standard for left-sided grafts? *Transplantation.* 2022; 106 (8S): 139–139.
41. *Monakhov A, Semash K, Boldyrev M, Mescheryakov S, Gautier S.* Laparoscopic donor hepatectomy in settings of pediatric living donor liver transplantation: single center experience. *Korean J Transplant*. 2022; 36 (Supple 1): S354. http://doi.org/10.4285/ATW2022.F-4979.
42. *Monakhov A, Gautier S, Tsiroulnikova O, Semash K, Khizroev K, Gallamov E et al*. 332.3: Laparoscopic hepatectomy in living liver donors for transplantation in children: From implementation to routine use. *Transplantation.* 2019; 103 (11S): S82. https://doi.org/10.1097/01.tp.0000612032.55662.25.
43. *Gautier SV, Gallyamov EA, Monakhov AR, Khizroev HM, Zagainov EV, Semash KO*. Laparoscopic removal of liver fragments from a living donor for transplantation to children. *Russian Journal of Transplantology and Artificial Organs*. 2017; 19 (S): 90–91.
44. *Samstein B, Griesemer A, Halazun K, Kato T, Guarrera JV, Cherqui D, Emond JC.* Pure Laparoscopic Donor Hepatectomies: Ready for Widespread Adoption? *Ann Surg*. 2018 Oct; 268 (4): 602–609. https://doi.org/10.1097/SLA.0000000000002959.
45. *Broering DC, Elsheikh Y, Shagrani M, Abaalkhail F, Troisi RI.* Pure Laparoscopic Living Donor Left Lateral Sectionectomy in Pediatric Transplantation: A Propensity Score Analysis on 220 Consecutive Patients.

Liver Transpl. 2018 Aug; 24 (8): 1019–1030. https://doi.org/10.1002/lt.25043.

46. *Kim WJ, Kim KH, Cho HD, Namgoong JM, Hwang S, Park JI, Lee SG.* Long-Term Safety and Efficacy of Pure Laparoscopic Donor Hepatectomy in Pediatric Living Donor Liver Transplantation. *Liver Transpl*. 2021 Apr; 27 (4): 513–524. https://doi.org/10.1002/lt.25910.
47. *Semash KO, Monakhov AR, Khizroev HM, Dzhanbekov TA, Meshcheryakov SV, Boldyrev MA et al.* Laparoscopic hemihepatectomy in a living liver donor. *Russian Journal of Transplantology and Artificial Organs*. 2021; 23 (S): 65.
48. *Taketomi A, Kayashima H, Soejima Y, Yoshizumi T, Uchiyama H, Ikegami T et al*. Donor risk in adult-to-adult living donor liver transplantation: impact of left lobe graft. *Transplantation*. 2009 Feb 15; 87 (3): 445–450. https://doi.org/10.1097/TP.0b013e3181943d46.
49. *Iida T, Ogura Y, Oike F, Hatano E, Kaido T, Egawa H et al*. Surgery-related morbidity in living donors for liver transplantation. *Transplantation*. 2010 May 27; 89 (10): 1276–1282. https://doi.org/10.1097/TP.0b013e3181d66c55.
50. *Soubrane O, Eguchi S, Uemoto S, Kwon CHD, Wakabayashi G, Han HS et al*. Minimally Invasive Donor Hepatectomy for Adult Living Donor Liver Transplantation: An International, Multi-institutional Evaluation of Safety, Efficacy and Early Outcomes. *Ann Surg*. 2022 Jan 1; 275 (1): 166–174. https://doi.org/10.1097/SLA.0000000000003852.
51. *Han HS, Cho JY, Yoon YS, Hwang DW, Kim YK, Shin HK, Lee W.* Total laparoscopic living donor right hepatectomy. *Surg Endosc*. 2015 Jan; 29 (1): 184. https://doi.org/10.1007/s00464-014-3649-9.
52. *Lin NC, Nitta H, Wakabayashi G.* Laparoscopic major hepatectomy: a systematic literature review and comparison of 3 techniques. *Ann Surg*. 2013 Feb; 257 (2): 205–213. https://doi.org/10.1097/SLA.0b013e31827da7fe.
53. *Semash KO, Gautier SV*. Review of surgical techniques for performing laparoscopic donor hepatectomy. *Russian Journal of Transplantology and Artificial Organs*. 2020; 22 (4): 149–153. https://doi.org/10.15825/1995-1191-2020-4-149-153.
54. *Voskanyan SAe, Artem'ev AI, Zabezhinskiyi DA, Shabalin MV, Bashkov AN*. Laparoscopic donor right hemihepatectomy (first experience in Russia). *Endoscopic Surgery*. 2017; 23 (3): 37–40. (In Russ.). doi: 10.17116/endoskop201723337-40.
55. *Suh KS, Yi NJ, Kim T, Kim J, Shin WY, Lee HW et al*. Laparoscopy-assisted donor right hepatectomy using a hand port system preserving the middle hepatic vein branches. *World J Surg*. 2009 Mar; 33 (3): 526–533. https://doi.org/10.1007/s00268-008-9842-z.
56. *Kwon CHD, Choi GS, Kim JM, Cho CW, Rhu J, Soo Kim G et al*. Laparoscopic Donor Hepatectomy for Adult Living Donor Liver Transplantation Recipients. *Liver Transpl*. 2018 Nov; 24 (11): 1545–1553. https://doi.org/10.1002/lt.25307.
57. *Rhu J, Kim MS, Choi GS, Kim JM, Kwon CHD, Joh JW.* Laparoscopic Living Donor Right Hepatectomy Regarding the Anatomical Variation of the Portal Vein: A Propensity Score-Matched Analysis. *Liver Transpl*. 2021 Jul; 27 (7): 984–996. https://doi.org/10.1002/lt.26050.
58. *Gautier SV, Monakhov AR*. Evaluation, selection and preparation of living donor for partial liver transplantation in children. *Russian Journal of Transplantology and Artificial Organs*. 2015; 17 (1): 134–146. (In Russ.). https://doi.org/10.15825/1995-1191-2015-1-134-146.
59. *Marubashi S, Wada H, Kawamoto K, Kobayashi S, Eguchi H, Doki Y et al*. Laparoscopy-assisted hybrid left-side donor hepatectomy. *World J Surg*. 2013 Sep; 37 (9): 2202–2210. https://doi.org/10.1007/s00268-013-2117-3.
60. *Ausania F, Holmes LR, Ausania F, Iype S, Ricci P, White SA.* Intraoperative cholangiography in the laparoscopic cholecystectomy era: why are we still debating? *Surg Endosc*. 2012 May; 26 (5): 1193–1200. https://doi.org/10.1007/s00464-012-2241-4. Epub 2012 Mar 22.
61. *Kim YS, Choi SH.* Pure Laparoscopic Living Donor Right Hepatectomy Using Real-Time Indocyanine Green Fluorescence Imaging. *J Gastrointest Surg*. 2019 Aug; 23 (8): 1711–1712. https://doi.org/10.1007/s11605-019-04217-w.
62. *Kim KH, Kang SH, Jung DH, Yoon YI, Kim WJ, Shin MH, Lee SG.* Initial Outcomes of Pure Laparoscopic Living Donor Right Hepatectomy in an Experienced Adult Living Donor Liver Transplant Center. *Transplantation*. 2017 May; 101 (5): 1106–1110. https://doi.org/10.1097/TP.0000000000001637.
63. *Rotellar F, Pardo F, Benito A, Zozaya G, Martí-Cruchaga P, Hidalgo F et al*. Totally Laparoscopic Right Hepatectomy for Living Donor Liver Transplantation: Analysis of a Preliminary Experience on 5 Consecutive Cases. *Transplantation*. 2017 Mar; 101 (3): 548–554. https://doi.org/10.1097/TP.0000000000001532.
64. *Hong SK, Tan MY, Worakitti L, Lee JM, Cho JH, Yi NJ et al*. Pure Laparoscopic Versus Open Right Hepatectomy in Live Liver Donors: A Propensity Score-matched Analysis. *Ann Surg*. 2022 Jan 1; 275 (1): e206–e212. https://doi.org/10.1097/SLA.0000000000003914.
65. *Choi HJ, You YK, Na GH, Hong TH, Shetty GS, Kim DG.* Single-port laparoscopy-assisted donor right hepatectomy in living donor liver transplantation: sensible approach or unnecessary hindrance? *Transplant Proc*. 2012 Mar; 44 (2): 347–352. https://doi.org/10.1016/j.transproceed.2012.01.018.
66. *Egger ME, Ohlendorf JM, Scoggins CR, McMasters KM, Martin RC 2nd.* Assessment of the reporting of quality and outcome measures in hepatic resections: a call for 90-day reporting in all hepatectomy series. *HPB (Oxford)*. 2015 Sep; 17 (9): 839–845. https://doi.org/10.1111/hpb.12470.
67. *Clavien PA, Barkun J, de Oliveira ML, Vauthey JN, Dindo D, Schulick RD et al*. The Clavien–Dindo classification of surgical complications: five-year experience. *Ann Surg*. 2009 Aug; 250 (2): 187–196. https://doi.org/10.1097/SLA.0b013e3181b13ca2.
68. *Slankamenac K, Graf R, Barkun J, Puhan MA, Clavien PA.* The comprehensive complication index: a novel continuous scale to measure surgical morbidity. *Ann Surg*. 2013 Jul; 258 (1): 1–7. https://doi.org/10.1097/SLA.0b013e318296c732.

69. *Zhang X, Yang J, Yan L, Li B, Wen T, Xu M et al*. Comparison of laparoscopy-assisted and open donor right hepatectomy: a prospective case-matched study from china. *J Gastrointest Surg*. 2014 Apr; 18 (4): 744–750. https://doi.org/10.1007/s11605-013-2425-9.
70. *Lei HJ, Lin NC, Chen CY, Chou SC, Chung MH, Shyr BU et al*. Safe Strategy to Initiate Total Laparoscopic Donor Right Hepatectomy: A Stepwise Approach From a Laparoscopy-Assisted Method. *World J Surg*. 2020 Sep; 44 (9): 3108–3118. https://doi.org/10.1007/s00268-020-05572-5.
71. *Takahara T, Wakabayashi G, Nitta H, Hasegawa Y, Katagiri H, Umemura A et al*. The First Comparative Study of the Perioperative Outcomes Between Pure Laparoscopic Donor Hepatectomy and Laparoscopy-Assisted Donor Hepatectomy in a Single Institution. *Transplantation*. 2017 Jul; 101 (7): 1628–1636. https://doi.org/10.1097/TP.0000000000001675.
72. *Makki K, Chorasiya VK, Sood G, Srivastava PK, Dargan P, Vij V.* Laparoscopy-assisted hepatectomy versus conventional (open) hepatectomy for living donors: when you know better, you do better. *Liver Transpl*. 2014 Oct; 20 (10): 1229–1236. https://doi.org/10.1002/lt.23940.
73. *Troppmann C, Ormond DB, Perez RV.* Laparoscopic (vs open) live donor nephrectomy: a UNOS database analysis of early graft function and survival. *Am J Transplant*. 2003 Oct; 3 (10): 1295–1301. https://doi.org/10.1046/j.1600-6143.2003.00216.x.
74. *Fancellu A, Rosman AS, Sanna V, Nigri GR, Zorcolo L, Pisano M, Melis M.* Meta-analysis of trials comparing minimally-invasive and open liver resections for hepatocellular carcinoma. *J Surg Res*. 2011 Nov; 171 (1): e33–e45. https://doi.org/10.1016/j.jss.2011.07.008.
75. *Xiong JJ, Altaf K, Javed MA, Huang W, Mukherjee R, Mai G et al*. Meta-analysis of laparoscopic vs open liver resection for hepatocellular carcinoma. *World J Gastroenterol*. 2012 Dec 7; 18 (45): 6657–6668. https://doi.org/10.3748/wjg.v18.i45.6657.
76. *Kitajima T, Kaido T, Iida T, Seo S, Taura K, Fujimoto Y et al*. Short-term outcomes of laparoscopy-assisted hybrid living donor hepatectomy: a comparison with the conventional open procedure. *Surg Endosc*. 2017 Dec; 31 (12): 5101–5110. https://doi.org/10.1007/s00464-017-5575-0.
77. *Rhu J, Choi GS, Kwon CHD, Kim JM, Joh JW.* Learning curve of laparoscopic living donor right hepatectomy. *Br J Surg*. 2020 Feb; 107 (3): 278–288. https://doi.org/10.1002/bjs.11350. Epub 2019 Oct 25.
78. *Kurosaki I, Yamamoto S, Kitami C, Yokoyama N, Nakatsuka H, Kobayashi T et al*. Video-assisted living donor hemihepatectomy through a 12-cm incision for adult-to-adult liver transplantation. *Surgery*. 2006 May; 139 (5): 695–703. https://doi.org/10.1016/j.surg.2005.12.002.
79. *Song JL, Yang J, Wu H, Yan LN, Wen TF, Wei YG, Yang JY.* Pure laparoscopic right hepatectomy of living donor is feasible and safe: a preliminary comparative study in China. *Surg Endosc*. 2018 Nov; 32 (11): 4614–4623. https://doi.org/10.1007/s00464-018-6214-0.
80. *Rotellar F, Pardo F, Martí-Cruchaga P, Zozaya G, Valentí V, Bellver M et al*. Liver mobilization and liver hanging for totally laparoscopic right hepatectomy: an easy way to do it. *Langenbecks Arch Surg*. 2017 Feb; 402 (1): 181–185. https://doi.org/10.1007/s00423-016-1473-5.
81. *Giulianotti PC, Tzvetanov I, Jeon H, Bianco F, Spaggiari M, Oberholzer J, Benedetti E.* Robot-assisted right lobe donor hepatectomy. *Transpl Int*. 2012 Jan; 25 (1): e5–e9. https://doi.org/10.1111/j.1432-2277.2011.01373.x.
82. *Salloum C, Lim C, Lahat E, Gavara CG, Levesque E, Compagnon P, Azoulay D.* Robotic-Assisted Versus Laparoscopic Left Lateral Sectionectomy: Analysis of Surgical Outcomes and Costs by a Propensity Score Matched Cohort Study. *World J Surg*. 2017 Feb; 41 (2): 516–524. https://doi.org/10.1007/s00268-016-3736-2.
83. *Broering DC, Elsheikh Y, Alnemary Y, Zidan A, Elsarawy A, Saleh Y et al*. Robotic Versus Open Right Lobe Donor Hepatectomy for Adult Living Donor Liver Transplantation: A Propensity Score-Matched Analysis. *Liver Transpl*. 2020 Nov; 26 (11): 1455–1464. https://doi.org/10.1002/lt.25820.
84. *Chen PD, Wu CY, Hu RH, Chen CN, Yuan RH, Liang JT et al*. Robotic major hepatectomy: Is there a learning curve? *Surgery*. 2017 Mar; 161 (3): 642–649. https://doi.org/ 10.1016/j.surg.2016.09.025.
85. *Troisi RI, Elsheikh Y, Alnemary Y, Zidan A, Sturdevant M, Alabbad S et al*. Safety and Feasibility Report of Robotic-assisted Left Lateral Sectionectomy for Pediatric Living Donor Liver Transplantation: A Comparative Analysis of Learning Curves and Mastery Achieved With the Laparoscopic Approach. *Transplantation*. 20211; 105 (5): 1044–1051. https://doi.org/10.1097/TP.0000000000003332.
86. *Cai X, Li Z, Zhang Y, Yu H, Liang X, Jin R, Luo F.* Laparoscopic liver resection and the learning curve: a 14-year, single-center experience. *Surg Endosc*. 2014 Apr; 28 (4): 1334–1341. https://doi.org/10.1007/s00464-013-3333-5.
87. *Lee B, Choi Y, Han HS, Yoon YS, Cho JY, Kim S et al*. Comparison of pure laparoscopic and open living donor right hepatectomy after a learning curve. *Clin Transplant*. 2019 Oct; 33 (10): e13683. https://doi.org/10.1111/ctr.13683.
88. *Yu YD, Kim KH, Jung DH, Lee SG, Kim YG, Hwang GS.* Laparoscopic live donor left lateral sectionectomy is safe and feasible for pediatric living donor liver transplantation. *Hepatogastroenterology*. 2012; 59 (120): 2445–2449. https://doi.org/10.5754/hge12134.
89. *Park J, Kwon DCH, Choi GS, Kim SJ, Lee SK, Kim JM et al*. Safety and Risk Factors of Pure Laparoscopic Living Donor Right Hepatectomy: Comparison to Open Technique in Propensity Score-matched Analysis. *Transplantation*. 2019 Oct; 103 (10): e308–e316. https://doi.org/10.1097/TP.0000000000002834.
90. *Seo J, Hong SK, Lee S, Hong SY, Choi Y, Yi NJ et al*. Pure Laparoscopic Versus Open Right Hepatectomy in Living Liver Donors: Graft Weight Discrepancy. *Ann Transplant*. 2022 Dec 2; 27: e938274. https://doi.org/10.12659/AOT.938274.

91. *Lee KW, Choi Y, Hong SK, Lee S, Hong SY, Suh S et al*. Laparoscopic donor and recipient hepatectomy followed by robot-assisted liver graft implantation in living donor liver transplantation. *Am J Transplant*. 2022 Apr; 22 (4): 1230–1235. https://doi.org/10.1111/ajt.16943.
92. *Chen PD, Wu CY, Hu RH, Ho CM, Lee PH, Lai HS et al*. Robotic liver donor right hepatectomy: A pure, minimally invasive approach. *Liver Transpl*. 2016 Nov; 22 (11): 1509–1518. https://doi.org/10.1002/lt.24522.
93. *Binoj ST, Mathew JS, Nair K, Mallick S, Chandran B, Menon R et al*. 260 Robotic Donor Right Hepatectomy: Is It Just Flaunting the Scar? *Gastroenterology.* 2020; 158: S-1263. https://doi.org/10.1016/S0016-5085(20)33815-4.
94. *Semash KO, Dzhanbekov TA, Akbarov MM*. Vascular complications after liver transplantation: contemporary approaches to detection and treatment. A literature review. *Russian Journal of Transplantology and Artificial Organs*. 2023; 25 (4): 46–72. https://doi.org/10.15825/1995-1191-2023-4-46-72.
95. *Broering DC, Zidan A*. Advancements in Robotic Living Donor Hepatectomy, Review of Literature and Single-Center Experience. *Curr Transpl Rep.* 2020; 7: 324–331. https://doi.org/10.1007/s40472-020-00311-0.
96. *Li D, Wang M.* A 3D Image Registration Method for Laparoscopic Liver Surgery Navigation. *Electronics*. 2022; 11 (11): 1670. https://doi.org/10.3390/electronics11111670.
97. *Golse N, Petit A, Lewin M, Vibert E, Cotin S*. Augmented Reality during Open Liver Surgery Using a Markerless Non-rigid Registration System. *J Gastrointest Surg*. 2021; 25 (3): 662–671. https://doi.org/10.1007/s11605-020-04519-4.
98. *Naito S, Kajiwara M, Nakashima R, Sasaki T, Hasegawa S.* Application of Extended Reality (Virtual Reality and Mixed Reality) Technology in Laparoscopic Liver Resections. *Cureus.* 2023 Sep 1; 15 (9): e44520. https://doi.org/10.7759/cureus.44520.

The article was submitted to the journal on 15.02.2024

DOI: 10.15825/1995-1191-2025-1-160-171

PRIMARY ARTERIOVENOUS FISTULA FAILURE IN PATIENTS ON MAINTENANCE HEMODIALYSIS: PREVALENCE, RISK FACTORS, AND IMPACT ON LONG-TERM OUTCOMES

A.B. Zulkarnaev, K.V. Bylov, V.A. Stepanov

Vladimirsky Moscow Regional Research and Clinical Institute, Moscow, Russian Federation

Objective: to assess the prevalence of primary arteriovenous fistula (AVF) failure in patients commencing chronic hemodialysis, to evaluate the relationship between primary failure and long-term outcomes, and to identify risk factors for its development. **Materials and methods.** This retrospective cohort study reports the outcomes of 1595 adult patients starting chronic hemodialysis treatment for the first time. **Results.** Primary failure was noted in 369 patients (23.1%), whereas in 1,226 patients (76.9%), the AVF matured normally and was accessible to puncture without additional interventions. Follow-up by a nephrologist, preoperative evaluation by a surgeon, and ultrasound were linked to a lower risk of primary failure: RR = 0.624 [95% CI 0.523; 0.746], $p < 0.001$; 0.648 [0.469; 0.894], $p = 0.005$; and 0.606 [0.471; 0.78], $p < 0.001$ (when ultrasound was performed by or in the presence of a surgeon 0.372 [0.24; 0.577], $p < 0.001$), respectively. The risk of primary failure increased if AVF was created in two weeks and one week before, and during the first and second weeks after hemodialysis initiation. In single-factor analysis, primary failure was linked to a higher risk of all-cause mortality (HR = 1.54 [1.20; 1.97], $p < 0.001$), but not after adjustment for age and comorbidity (HR = 1.11 [0.85; 1.44], $p = 0.761$). Primary failure was associated with poorer secondary patency (HR = 1.79 [1.28; 2.51] $p < 0.001$) and increased need for reconstructive interventions (IRR = 2.199 [1.985; 2.434], $p < 0.001$). **Conclusion.** Risk reduction factors for primary failure include follow-up by a nephrologist, preliminary examination by a surgeon, supplemented by ultrasound scan. Primary failure is not linked to decreased patient survival (after adjustment for comorbid background and age), but to decreased secondary patency of vascular access.

Keywords: arteriovenous fistula, hemodialysis, failure, synthetic vascular graft, primary patency, secondary patency.

INTRODUCTION

Arteriovenous fistula (AVF) is widely considered the optimal type of vascular access for patients on chronic hemodialysis (HD) [1]. For obvious reasons, after AVF creation, time is needed for its maturation, during which volumetric blood flow rate increases in order to ensure a reliable required blood flow into the extracorporeal circuit. In this case, the diameter of the vein and artery increases, the vein wall is transformed, etc. [2] An AVF should typically be ready for successful routine punctures within 4–6 weeks [3] and remain functional for at least 6 months after creation [4]. If it does not mature within this timeframe, it is considered dysfunctional or slow-maturing. Approximately 20% [5] to 30% [6] of patients have primary AVF dysfunction.

Primary dysfunction of an AVF, i.e., issues arising during its maturation process before it can be used for dialysis, often leads to complications like requiring a central venous catheter (CVC) for access, which can result in increased hospital stays and higher treatment costs.

However, the impact of primary dysfunction on long-term outcomes has not been determined. The fact that primary AVF failure is associated with worse long-term outcomes may be due to other reasons, namely the fact that patients with poorer overall health are more likely to experience primary dysfunction, which determines long-term outcome.

Objective: To assess the prevalence of primary AVF failure in patients commencing chronic HD for the first time, to evaluate the relationship between PF and long-term outcomes, and to identify risk factors for its development.

MATERIALS AND METHODS

Study Design

This retrospective cohort study analyzed treatment outcomes in 1,595 patients who underwent AVF creation between June 2018 and February 2024. Inclusion criteria included age over 18 years, initiation of renal replacement therapy (RRT) for the first time, and availability of

Corresponding author: Alexey Zulkarnaev; Address: 61/2, Shchepkina str., Moscow, 129110, Russian Federation. Phone: (916) 705-98-99. E-mail: 7059899@gmail.com

comprehensive medical history (to the required extent) and follow-up data.

Primary dysfunction (failure) was defined as either thrombosis before the first use of the AVF or unsuccessful puncture three months post-creation (delayed maturation).

Our approach prioritized the formation of native AVFs on the lower third of the forearm of the non-dominant upper limb. When native vessels were unsuitable, a synthetic vascular graft (SVG) was used. In the absence of ultrasound data, the access type was selected based on clinical examination. The use of SVG as an alternative to native AVF was intended to improve the likelihood of establishing functional vascular access or shorten maturation time.

The study considered the type of vascular access (native AVF or SVG), the level of creation (lower third of the forearm or other), and the outcomes of only the first intervention for permanent vascular access formation.

Ethical approval was obtained from the independent local ethics committee at Vladimirsky Moscow Regional Research and Clinical Institute under protocol No. 5, dated May 25, 2018.

Data source

The database was compiled using systematized information from the Medical Information System Everest, the Unified Medical Information and Analytical System of the Moscow Oblast, and data from outpatient dialysis centers.

Statistical analysis

Quantile plots and frequency diagrams were used to visually assess whether the quantitative characteristics (and residuals of regression models) followed a normal distribution. Since the distributions showed no significant deviations from normality, data are presented as mean and standard deviation (reported in parentheses). Qualitative variables are described using absolute numbers and percentages.

For comparisons between quantitative variables and binary qualitative factors, Student's or Welch's t-test was applied. When qualitative factors had more than two levels, one-way analysis of variance (ANOVA) was used as an omnibus test, followed by Tukey's criterion for post-hoc pairwise comparisons. For the joint distribution of qualitative variables, Fisher's exact test was applied for 2×2 tables, while the Fisher–Freeman–Halton exact test was used for larger contingency tables. Effect sizes were expressed as risk ratio (RR) and odds ratio (OR) with 95% confidence intervals (95% CI), reported in square brackets.

The association between primary dysfunction and the frequency of CVC use over time was quantified using the incidence rate ratio (IRR), interpreted as relative risk.

Unadjusted patient survival and secondary AVF patency were assessed using the Kaplan–Meier method, with survival curves plotted and asymmetric 95% CI calculated. Differences in survival were evaluated using the log-rank test. Type I right-censoring was applied in survival analysis. Effect size was expressed as hazard ratio (HR) with 95% CI.

Adjusted survival analysis was conducted using the Cox proportional hazards regression model with the adjustedCurves::adjustedsurv() package. The proportional hazards assumption was verified through Schoenfeld residuals analysis, while the linearity between predictors and the log-risk function was examined using martingale residuals. These residual plots were also analyzed for influential observations, supplemented by DFBETAs analysis to identify influential observations. Predictor multicollinearity was assessed using the correlation matrix and variance inflation factor.

Sample size was not pre-calculated but was determined by the available data. Statistical analysis was conducted using R 4.4.1 within the RStudio Desktop 2024.04.2 environment, along with relevant libraries. All tests were two-tailed, and p-values less than 0.05 were considered statistically significant.

RESULTS

Prevalence

Primary failure was observed in 369 patients (23.1% of 1,595), while AVF maturation occurred successfully in 1,226 patients (76.9%) without the need for repeat surgical interventions.

Among patients with primary AVF failure, 127 (34.4% of 369; 8.0% of 1,595) had delayed AVF maturation, while 242 (65.6% of 369; 15.2% of 1,595) developed thrombosis.

A summary of patient characteristics is presented in Table 1.

Despite all efforts, a functional AVF could not be formed in 41 patients (2.6% of 1,595, 11.1% of 369), and there was a conversion of vascular access to CVC (14 patients, 34.1% of 41) or RRT modality from hemodialysis to peritoneal dialysis (27 patients, 65.9% of 41). Among these patients, PF presented as delayed maturation in 7 cases (17.1% of 41) and thrombosis in 34 cases (82.9% of 41). None of these patients underwent a single HD session using AVF.

As shown in Fig. 1, the proportion of patients who required conversion of vascular access or RRT modality remained relatively consistent across all stages. This observation is further supported by the absence of significant differences in the mean number of days between AVF creation and HD initiation among patients who underwent access or modality conversion versus those without dysfunction: –63.5 (52) days (range: –183 to 49) and –67.7 (55.5) days (range: –201 to 125), respectively (P = 0.881).

Additionally, in patients with dysfunction, AVF was generally created closer to the time of HD initiation (–53.4 [53.9] days, range: –194 to 101) compared to those without dysfunction (P < 0.001).

Risk factors

Potential risk factors for primary AVF dysfunction, along with descriptive statistics for the entire cohort, are summarized in Tables 1 and 2. Patients with dysfunction were more likely to be female and had a higher mean age compared to those without dysfunction. Additionally, while small, statistically significant differences were observed in body mass index (BMI), with slightly higher mean values in patients with dysfunction. However, as shown in Table 1, despite formal statistical significance,

Table 1

Potential risk factors for primary AVF failure: demographics and comorbid background. Fisher's exact test (also called the Fisher–Freeman–Halton test) and Student's t-test (Welch's t-test) were used

Characteristics	Total, n = 1595	Primary failure		P value
		Yes, n = 369	No, n = 1226	
Age, years	49.1 (8.6)	54.3 (8.6)	47.5 (8.0)	**<0.001**
Female	720 (45.1%)	204 (55.3%)	516 (42.1%)	**<0.001**
Body mass index, kg/m^2	28.4 (3.7)	28.8 (4.0)	28.3 (3.5)	**0.029**
Persistent hypotension	99 (6.2%)	45 (12.2%)	54 (4.4%)	**<0.001**
Diabetes mellitus	342 (21.4%)	103 (27.9%)	239 (19.5%)	**<0.001**
Polycystic kidney disease	133 (8.3%)	85 (23.0%)	48 (3.9%)	**<0.001**
Systemic processes[1]	53 (3.3%)	41 (11.1%)	12 (1.0%)	**<0.001**
Body weight:				
Malnutrition	11 (0.7%)	3 (0.8%)	8 (0.7%)	
Undernutrition	10 (0.6%)	3 (0.8%)	7 (0.6%)	
Normal	377 (23.6%)	79 (21.4%)	298 (24.3%)	
High nutrition	315 (19.7%)	67 (18.2%)	248 (20.2%)	**0.048**
Grade I obesity	467 (29.3%)	98 (26.6%)	369 (30.1%)	
Grade II obesity	388 (24.3%)	108 (29.3%)	280 (22.8%)	
Grade III obesity	27 (1.7%)	11 (3.0%)	16 (1.3%)	
Nature of deviation of body mass index				
Underweight	21 (1.3%)	6 (1.6%)	15 (1.2%)	
Normal body weight	377 (23.6%)	79 (21.4%)	298 (24.3%)	0.420
Overweight	1197 (75.0%)	284 (77.0%)	913 (74.5%)	

Note: [1] Vasculitis, myeloma, HIV-associated nephropathy, kidney tumors, history of drug abuse/addiction, etc.

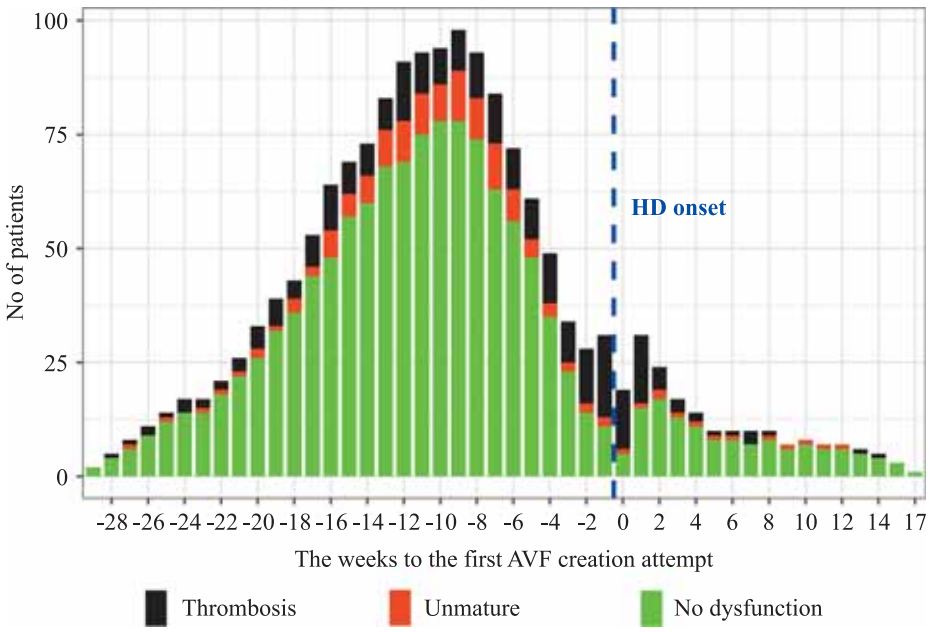

Fig. 1. Frequency of primary AVF failure

the distribution of patients across BMI categories remained relatively uniform.

Although most patients had at least one nephrology consultation six months or more before HD initiation, fewer than 10% were evaluated by a surgeon before AVF creation (excluding the day of the procedure). Preoperative ultrasound was performed in approximately one in five patients, while Doppler ultrasound was conducted in about one in seven. Notably, patients without dysfunction were more likely to have been seen by a nephrologist and/or surgeon before AVF creation and had undergone preoperative ultrasound (with or without Doppler ultrasound); see Table 2.

Among patients who underwent a preoperative surgical evaluation, the interval between consultation and AVF creation, as well as between AVF creation and HD initiation, was shorter in patients with dysfunction compared to those without. Additionally, patients with dysfunction were significantly less likely to have undergone preoperative ultrasound performed by or in the presence of the operating surgeon.

While all quantitative risk factors in Table 1 showed statistically significant associations with primary AVF failure, their clinical relevance varied. For example, the mean age difference between patients with and without dysfunction was 6.8 [95% CI 5.8, 7.7] years, whereas the mean BMI difference was only 0.47 [95% CI 0.02, 0.93] kg/m^2 with higher values in PF patients. Similarly, the mean time between surgical consultation and AVF creation was 10.3 [95%DI –16.4; –4.1] days shorter in patients with dysfunction.

Since these indicators are measured in different units, Fig. 2 presents standardized mean differences to facilitate comparison of their relative impact on primary AVF dysfunction.

When evaluating the association between primary AVF dysfunction and qualitative factors, systemic processes and polycystic kidney disease emerged as the most significant contributors (Table 3). However, no statistically significant association was found between primary AVF dysfunction and abnormal BMI (either decreased or increased relative to normal).

Regarding the impact of preoperative follow-up factors, all analyzed variables were linked to a reduced risk of primary AVF failure (Table 4).

As demonstrated above, the proportion of patients experiencing primary AVF failure increased significantly

Table 2

Potential common risk factors for primary AVF failure: features of preoperative follow-up. Fisher's exact test (also called the Fisher–Freeman–Halton test) and Student's t-test (Welch's t-test) were used

Characteristics	Total, n = 1595	Primary failure		P value
		Yes, n = 369	No, n = 1226	
Follow-up by a nephrologist[1]	1106 (69.3%[3])	216 (58.5%[3])	890 (72.6%[3])	**<0.001**
Follow-up by a surgeon[2]	203 (12.7%[3])	19 (5.1%[3])	184 (15.0%[3])	**0.005**
Time between surgeon's visit and AVF creation, days[4]	28.4 (12.2)	19.6 (11.7)	29.8 (11.6)	**0.001**
Ultrasound before AVF creation	387 (24.3%[3])	60 (16.3%[3])	327 (26.7%[3])	**<0.001**
Doppler ultrasound before AVF creation	264 (16.6%[3])	42 (11.4%[3])	222 (18.1%[3])	**0.002**
Ultrasound performed by or in the presence of an operating surgeon	203 (12.7%[3], 44.4%[5])	19 (5.1%[3], 50.0%[5])	184 (15.0%[3], 72.7%[5])	**<0.001**
Time between AVF creation and the beginning of HD, days	–64.6 (55.3)	–54.5 (53.7)	–67.7 (55.5)	**<0.001**

Note: [1] At least one visit to a nephrologist 6 months or more before starting HD; [2] At least one visit to a surgeon before AVF creation; [3] Percentage of total patient count in this category; [4] Only among patients who were examined by a surgeon prior to AVF creation (not on the day of formation); [5] Percentage of patients who underwent preoperative ultrasound scanning.

Table 3

Strength of association of the risk of primary AVF failure with qualitative attributes: demographics and comorbid background

Characteristics	RR [95% CI]	OR [95% CI]
Female	1.503 [1.255; 1.799]	1.701 [1.346; 2.151]
Persistent hypotension	2.099 [1.657; 2.658]	3.014 [1.992; 4.562]
Diabetes mellitus	1.419 [1.169; 1.722]	1.599 [1.223; 2.09]
Polycystic kidney disease	3.29 [2.79; 3.88]	7.345 [5.039; 10.71]
Systemic processes[1]	3.637 [3.055; 4.33]	12.65 [6.57; 24.34]
Low body mass index[2]	1.363 [0.674; 2.757]	1.529 [0.522; 3.937]
High body mass index[3]	1.132 [0.908; 1.412]	1.172 [0.888; 1.561]

Note: [1] Vasculitis, myeloma, HIV-associated nephropathy, kidney tumors, history of drug abuse/addiction; [2] Relative to normal, P = 0.415; [3] Relative to normal, P = 0.266.

when AVF was created closer to the onset of HD (see Fig. 1).

As shown in Fig. 3, the relative risk of primary dysfunction was statistically significantly increased in the case where AVF was created two and one week before HD onset (RR = 2.44 [95% CI 1.66; 3.59], P < 0.001 and RR = 3.06 [95% CI 2.31; 4.05], P < 0.001, respectively), and in the case of AVF creation during the first and second weeks after HD onset (RR = 2.78 [95% CI 1.93; 4.02], P < 0.001 and RR = 2.47 [95% CI 1.55; 3.96], P = 0.001, respectively).

Impact on long-term outcomes

In the univariate analysis, we identified statistically significant differences in patient survival based on primary AVF failure; see Fig. 4.

The starting time point for survival analysis was the onset of chronic HD.

Censoring criteria: Patients were censored in cases of conversion to another RRT modality or death. Thus, survival among PF-free patients was 95.4% [95% CI 94.1; 96.6], 87.0% [95% CI 84.9; 89.2], 78.4% [95% CI 75.7; 81.3], and among PF patients, 92.7% [95% CI 90.1; 95.4], 80.3% [95% CI 76.1; 84.7], 68.1% [95% CI 62.9; 73.8] at 12, 36, and 60 months, respectively. HR = 1.54 [95% CI 1.20; 1.97], P < 0.001.

As expected, the risk of primary dysfunction was associated with several factors that were also linked to mortality risk. However, after adjusting for comorbidities and age, the association between primary AVF dysfunction and mortality risk was no longer statistically significant (Fig. 5). Adjusted survival among patients without primary dysfunction was 95.0% [95% CI 93.8; 96.2], 85.5% [95% CI 83.4; 87.6], 76.8% [95% CI 74.0; 79.7], and among patients with primary dysfunction was 94.5% [95% CI 93.0; 96.0], 84.1% [95% CI 80.7; 87.5], 74.7% [95% CI 69.9; 79.6] at 12, 36, and 60 months, respectively. HR = 1.11 [95% CI 0.85; 1.44], P = 0.761.

In cases where a functional AVF was achieved in a patient, PF was associated with decreased secondary patency. In patients with primary AVF failure, secondary patency at 12, 36, and 60 months was 91.7% [95% CI

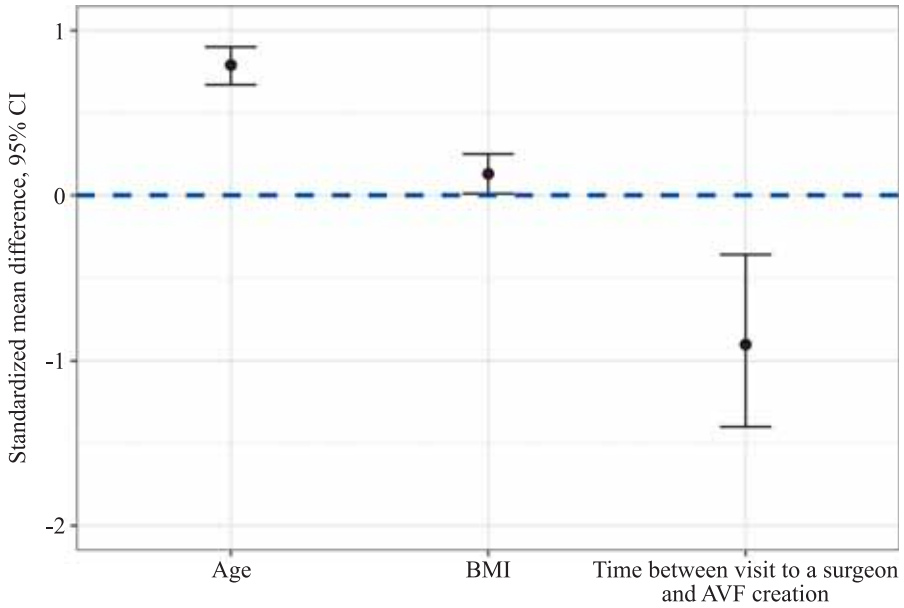

Fig. 2. Standardized difference of quantitative mean scores. Value in patients with primary AVF failure – value in patients without failure

Table 4

Strength of association of the risk of primary AVF failure with qualitative attributes: preoperative follow-up features

Characteristics	RR [95% CI]	OR [95% CI]
Follow-up by a nephrologist[1]	0.624 [0.523; 0.746]	0.533 [0.418; 0.679]
Follow-up by a surgeon[2]	0.648 [0.469; 0.894]	0.582 [0.396; 0.857]
Ultrasound before AVF creation	0.606 [0.471; 0.78]	0.534 [0.394; 0.724]
Doppler ultrasound before AVF creation	0.648 [0.483; 0.868]	0.581 [0.408; 0.826]
Ultrasound performed by or in the presence of an operating surgeon	0.372 [0.24; 0.577]	0.307 [0.189; 0.501]

Note: [1] At least one visit to a nephrologist 6 months or more before starting HD; [2] At least one visit to a surgeon before the day of AVF creation.

88.7; 94.9], 79.7% [95% CI 73.8; 86.1], and 64.7% [95% CI 54.9; 76.2], respectively; in PF-free patients, it was 95.8% [95% CI 94.6; 97.1], 88.4% [95% CI 85.8; 91.1], and 82.9% [95% CI 79.1; 87.0], respectively. Thus, primary AVF failure was associated with a greater than 1.5-fold increase in total loss of function (analyzed period, 60 months after the start of AVF use): HR = 1.79 [95% CI 1.28, 2.51], P < 0.001.

Moreover, primary patency was slightly greater in patients in whom we observed PF: 89.3% [95% CI 85.9; 92.8], 67.5% [95% CI 60.9; 74.8] and 51.4% [95% CI 42.6; 62.1] at 12, 36, and 60 months, respectively; in PF-free patients, 85.9% [95% CI 83.7; 88.2], 60.0% [95% CI 55.8; 64.6] and 44.6% [95% CI 39.1; 50.9], respectively, HR = 0.76 [95% CI 0.60, 0.97], P = 0.029. These paradoxical differences can be explained by the fact that in PF cases, the subsequent vascular access used for HD was typically formed more proximally compared to patients whose initial access matured successfully.

In patients without dysfunction, the first vascular access became functional within the first three months after its formation. The type and localization of these accesses are detailed in Table 5.

Notably, at the time of formation, the distribution of vascular access types and their localization differed significantly between patients with and without PF. Spe-

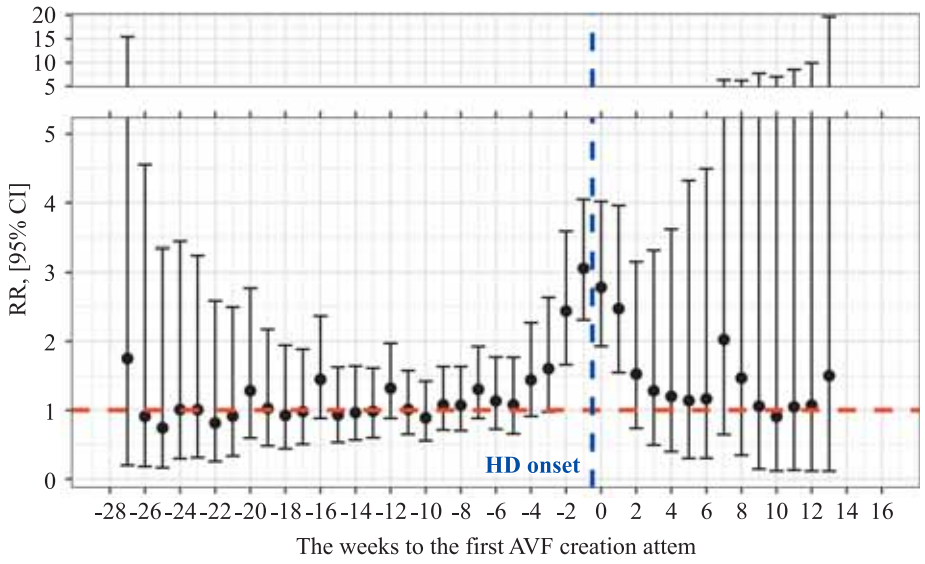

Fig. 3. Relative risk of primary AVF failure depending on the timing of creation and HD onset. When computing estimates, the number of patients at each stage was correlated with the number of patients at earlier (for cases where AVF was created before HD onset) or – later (for cases where AVF was created after HD onset) stages

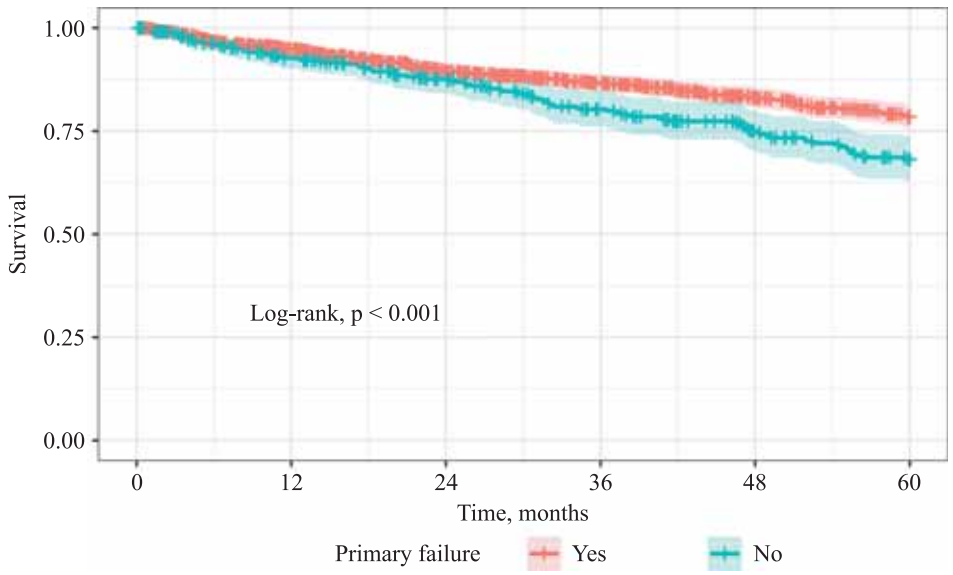

Fig. 4. Unadjusted patient survival (patients who died within 90 days of HD onset were excluded). Kaplan–Meier estimates. Fill indicates 95% CI limits, + – censoring. HD onset served as the baseline time point. In case of HD conversion to other RRT modalities or death, the patient was censored

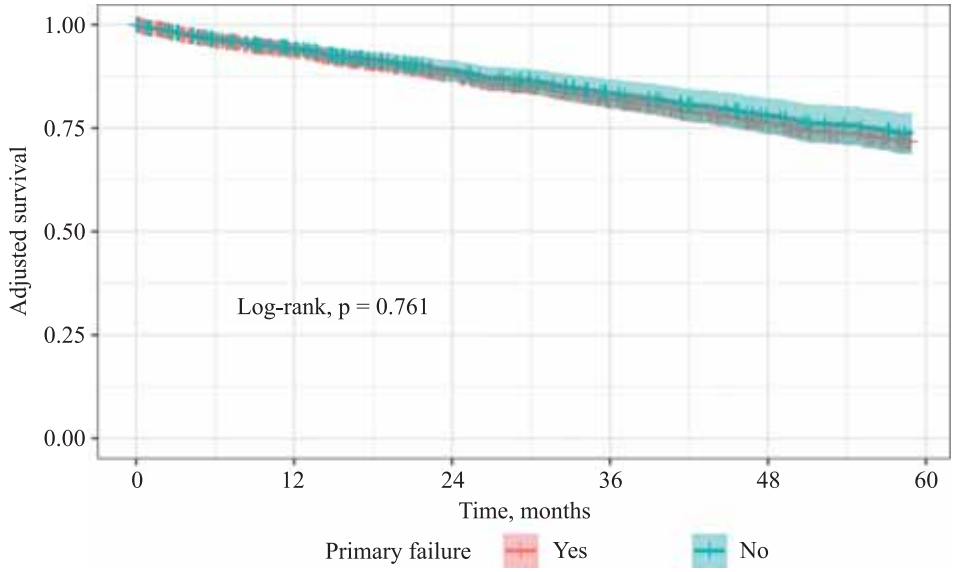

Fig. 5. Comorbidity-adjusted (CCI score) and age-adjusted patient survival at the time of first AVF creation (patients who died within 90 days of HD onset were excluded). Cox proportional hazards regression model. Fill indicates 95% CI limits, + – censoring. HD onset served as the baseline time point. In case of HD conversion to other renal replacement therapy modalities or death, the patient was censored

Table 5

Type and localization of vascular access in the groups at the time of creation and at the time of first puncture

Access type	No primary failure, n = 1226	Primary failure	
		At the time of first creation, n = 328	At the time of first puncture on HD, n = 328
Native AVF, lower third of the forearm	1064 (86.8%)	308 (93.9%)	0
Native AVF of other localization	98 (8.0%)	13 (4.0%)	239 (79.0%)
Synthetic vascular graft	64 (5.2%)	7 (2.1%)	69 (21.0%)

cifically, in PF patients, the proportion of SVG and AVF created outside the lower third of the forearm was approximately half that observed in PF-free patients (P < 0.001).

PF patients underwent one to six reconstructive surgeries. PF was associated with an increased need for reconstructive interventions (excluding the first attempt at AVF creation): IRR = 2.199 [95% CI 1.985; 2.434], P < 0.001 (1.740 [95% CI 1.609; 1.879] per 10 patient-months / 0.791 [95% CI 0.741; 0.845]).

As a result, as shown in Table 5, at the time of the first puncture, 21% of patients had a vascular access formed as an SVG or AVF proximal to the lower third of the forearm (including operations with vein transposition).

Also, primary AVF dysfunction was associated with a significant increase in the need for CVC implantation: IRR = 2.151 [95% CI 1.911; 2.419], P < 0.001 (1.302 [95% CI 1.189; 1.424] per 10 patient-months / 0.606 [95% CI 0.561; 0.652]).

The mean duration of catheterization in PF patients was 13.7 catheter-days [95% CI 12.5; 14.9] per 100 patient-months of follow-up, and in PF-free patients it was 5.2 catheter-days [95% CI 4.8; 5.7] per 100 patient-months of follow-up, IRR = 2.615 [95% CI 2.319; 2.947], P < 0.001. The greater need for CVC use in PF patients naturally resulted in a higher incidence of central vein stenosis (CVS) compared to PF-free patients: HR = 3.706 [95% CI 1.571; 8.739], P = 0.003 (actual incidence of CVS at 60 months 7.3% [95% CI 2.3; 12.0] / 2.1% [95% CI 0.5; 3.7]). In total, CVS developed in 21 patients (11 PF patients and 10 PF-free patients). In case of subclavian, brachiocephalic, or superior vena cava vein lesions, endovascular intervention was performed.

DISCUSSION

Currently, there is no universally accepted timeframe after which a AVF is considered primarily dysfunctional. The European Society for Vascular Surgery (ESVS) Clinical Practice Guidelines [7], recommend assessing AVF readiness for needle puncture 4–6 weeks post-creation. If successful puncture is not possible, further diagnostic and therapeutic interventions should be considered to restore AVF function. The European Society of Nephrology holds a similar opinion [3].

The National Kidney Foundation Kidney Disease Outcomes Quality Initiative (NKF KDOQI) guidelines [4] define primary AVF dysfunction as an access that remains non-functional for dialysis within 6 months of creation, despite radiologic or surgical interventions (endovascular or open surgical procedures).

For this study, we adopted a three-month threshold, as it aligns more closely with domestic clinical practices, particularly regarding preoperative follow-up and patient routing. This timeframe was chosen based on the observation that the mean time between AVF creation and HD onset was just over two months (see Table 2).

Studies assessing the prevalence and risk factors of primary AVF dysfunction, as well as the time required to establish a stable functional access, often focus primarily on delayed maturation, without considering AVF thrombosis.

From our perspective, when planning a patient's long-term vascular access strategy – including the timing and type of initial access formation and possibly even the choice of RRT modality – it is more appropriate to assess PF as a whole, rather than differentiating between thrombosis and delayed maturation.

However, such differentiation remains relevant in the context of evaluating the efficacy of therapeutic or surgical interventions aimed at preventing specific types of PF, a topic that falls outside the scope of this study.

The risk factors for primary AVF dysfunction (PF) presented in Table 3 are well-documented in the literature, reinforcing their significance and aligning with findings from other studies [8–11]. Given that an increased risk of PF is associated with a longer time required to establish a stable vascular access, it is reasonable to suggest that vascular access formation should be planned earlier in patients with these risk factors.

However, in current clinical practice, this is not routinely implemented. Patients with high PF risk typically undergo vascular access formation following the same standard protocol as the general population initiating chronic HD.

In our sample, only 69% of patients had seen a nephrologist at least six months before starting HD and only 13.5% had a preoperative consultation with a surgeon before the day of AVF creation.

This highlights the need for improved CKD screening in high-risk groups and modifications to patient routing protocols to enhance vascular access planning and reduce PF incidence. In addition, as shown in Table 4, preoperative ultrasound performed by or in the presence of the operating surgeon plays a crucial role in improving AVF outcomes.

A previous study with a smaller sample size [12] reported that primary AVF dysfunction was associated with an increased risk of all-cause mortality. However, our analysis yielded a different result: after adjusting for comorbid background (using the Charlson Comorbidity Index) and age, the association became statistically insignificant.

The difference in findings can be attributed to several key factors: the previous study assessed individual comorbid conditions, whereas we employed an integrated assessment of comorbidity; we excluded patients who died within 90 days of HD onset, as mortality during this period is more likely influenced by acute clinical factors unrelated to PF, and this we believe is the major cause of the main difference in findings.

This suggests that while an association between PF and mortality may exist, it is unlikely to be causal – rather, it reflects the complex interplay of multiple health factors affecting patient survival.

The association between PF and both increased primary obstruction (functional vascular access) and decreased secondary obstruction can be attributed to two key factors. First, as shown in Table 5, a significantly higher proportion of PF patients had AVFs created more proximally to the lower third of the forearm (compared to PF-free patients). Proximal AVF location is linked to greater primary patency [5, 13, 14]. However, repeated dysfunctions and reconstructions in these patients exhaust vascular resources, leading to faster complete access failure. Furthermore, primary dysfunction was associated with a significantly increased need for SVG, which may contribute to poorer secondary patency compared to native AVF [15]. While proximal AVFs and SVGs demonstrate a lower incidence of primary dysfunction [16, 17], we recommend considering these options only for patients with risk factors for AVF dysfunction in the lower third of the forearm.

Based on our findings, all patients should undergo a comprehensive preoperative evaluation, including a mandatory surgical consultation before vascular access formation, complemented by ultrasound assessment.

The prevalence of PF in our study (23.1%) aligns with estimates from earlier research [5, 6]. A 2004 meta-analysis [18] reported a PF incidence of 15.3% (95% CI: 12.7–18.3%) with a 95% range of 6–34%, while a 2014 meta-analysis [13] found an incidence of 23% (18–28%). Despite numerous proposed initiatives [19], PF rates have not significantly declined – and may have even slightly increased – over the past two decades.

Most studies identify similar sets of significant risk factors, yet the persistent incidence of PF suggests that improving vascular access outcomes in chronic HD patients requires not just repeated hypothesis testing, but the effective application of existing knowledge, tailored to local clinical practices and systemic organizational changes.

Limitations of the study. This study is retrospective, which comes with inherent methodological limitations.

We did not account for the surgeon's experience or the number of procedures performed per year. However, evidence suggests that surgeon expertise may sig-

nificantly influence vascular access outcomes [20, 21]. In our setting, we believe this factor can be reasonably disregarded, as all participating surgeons had over eight years of experience and performed more than 200 procedures annually.

Additionally, we did not incorporate ultrasound findings in our analysis. This aspect warrants a dedicated investigation, which we plan to publish separately.

CONCLUSION

Factors that reduce PF risk include nephrologist follow-up within six months before HD, preoperative evaluation by a surgeon, and ultrasound examination. While PF is not linked to decreased patient survival after adjusting for comorbid background and age, it is associated with poorer secondary patency of vascular access.

The authors declare no conflict of interest.

REFERENCES

1. *Ravani P, Palmer SC, Oliver MJ, Quinn RR, MacRae JM, Tai DJ et al*. Associations between hemodialysis access type and clinical outcomes: a systematic review. *J Am Soc Nephrol*. 2013; 24 (3): 465–473. doi: 10.1681/ASN.2012070643.
2. *Remuzzi A, Bozzetto M*. Biological and Physical Factors Involved in the Maturation of Arteriovenous Fistula for Hemodialysis. *Cardiovasc Eng Technol*. 2017; 8 (3): 273–279. doi: 10.1007/s13239-017-0323-0.
3. *Gallieni M, Hollenbeck M, Inston N, Kumwenda M, Powell S, Tordoir J et al*. Clinical practice guideline on peri- and postoperative care of arteriovenous fistulas and grafts for haemodialysis in adults. *Nephrol Dial Transplant*. 2019; 34 (Suppl 2): ii1–ii42. doi: 10.1093/ndt/gfz072.
4. *Lok CE, Huber TS, Lee T, Shenoy S, Yevzlin AS, Abreo K et al*. KDOQI Clinical Practice Guideline for Vascular Access: 2019 Update. *Am J Kidney Dis*. 2020; 75 (4 Suppl 2): S1–S164. doi: 10.1053/j.ajkd.2019.12.001.
5. *Voorzaat BM, van der Bogt KEA, Janmaat CJ, van Schaik J, Dekker FW, Rotmans JI et al*. Arteriovenous Fistula Maturation Failure in a Large Cohort of Hemodialysis Patients in the Netherlands. *World J Surg*. 2018; 42 (6): 1895–1903. doi: 10.1007/s00268-017-4382-z.
6. *Huber TS, Berceli SA, Scali ST, Neal D, Anderson EM, Allon M et al*. Arteriovenous Fistula Maturation, Functional Patency, and Intervention Rates. *JAMA Surg*. 2021; 156 (12): 1111–1118. doi: 10.1001/jamasurg.2021.4527.
7. *Schmidli J, Widmer MK, Basile C, de Donato G, Gallieni M, Gibbons CP et al*. Editor's Choice – Vascular Access: 2018 Clinical Practice Guidelines of the European Society for Vascular Surgery (ESVS). *Eur J Vasc Endovasc Surg*. 2018; 55 (6): 757–818. doi: 10.1016/j.ejvs.2018.02.001.
8. *Woodside KJ, Bell S, Mukhopadhyay P, Repeck KJ, Robinson IT, Eckard AR et al*. Arteriovenous Fistula Maturation in Prevalent Hemodialysis Patients in the United States: A National Study. *Am J Kidney Dis*. 2018; 71 (6): 793–801. doi: 10.1053/j.ajkd.2017.11.020.
9. *Farrington CA, Robbin ML, Lee T, Barker-Finkel J, Allon M*. Early Predictors of Arteriovenous Fistula Maturation: A Novel Perspective on an Enduring Problem. *J Am Soc Nephrol*. 2020; 31 (7): 1617–1627. doi: 10.1681/ASN.2019080848.
10. *Copeland T, Lawrence P, Woo K*. Outcomes of initial hemodialysis vascular access in patients initiating dialysis with a tunneled catheter. *J Vasc Surg*. 2019; 70 (4): 1235–1241. doi: 10.1016/j.jvs.2019.02.036.
11. *Yan Y, Ye D, Yang L, Ye W, Zhan D, Zhang L et al*. A meta-analysis of the association between diabetic patients and AVF failure in dialysis. *Ren Fail*. 2018; 40 (1): 379–383. doi: 10.1080/0886022X.2018.1456464.
12. *Yap Y-S, Chi W-C, Lin C-H, Liu Y-C, Wu Y-W*. Association of early failure of arteriovenous fistula with mortality in hemodialysis patients. *Sci Rep*. 2021; 11 (1): 5699. doi: 10.1038/s41598-021-85267-6.
13. *Al-Jaishi AA, Oliver MJ, Thomas SM, Lok CE, Zhang JC, Garg AX et al*. Patency rates of the arteriovenous fistula for hemodialysis: a systematic review and meta-analysis. *Am J Kidney Dis*. 2014; 63 (3): 464–478. doi: 10.1053/j.ajkd.2013.08.023.
14. *Bylsma LC, Gage SM, Reichert H, Dahl SLM, Lawson JH*. Arteriovenous Fistulae for Haemodialysis: A Systematic Review and Meta-analysis of Efficacy and Safety Outcomes. *Eur J Vasc Endovasc Surg*. 2017; 54 (4): 513–522. doi: 10.1016/j.ejvs.2017.06.024.
15. *Hajibandeh S, Burton H, Gleed P, Hajibandeh S, Wilmink T*. Impact of arteriovenous fistulas versus arteriovenous grafts on vascular access performance in haemodialysis patients: A systematic review and meta-analysis. *Vascular*. 2022; 30 (6): 1021–1033. doi: 10.1177/17085381211041473.
16. *Wu CC, Jiang H, Cheng J, Zhao LF, Sheng KX, Chen JH*. The outcome of the proximal radial artery arteriovenous fistula. *J Vasc Surg*. 2015; 61 (3): 802–808. doi: 10.1016/j.jvs.2014.08.112.
17. *Jennings WC, Mallios A, Mushtaq N.* Proximal radial artery arteriovenous fistula for hemodialysis vascular access. *J Vasc Surg*. 2018; 67 (1): 244–253. doi: 10.1016/j.jvs.2017.06.114.
18. *Rooijens PP, Tordoir JH, Stijnen T, Burgmans JP, Smet de AA, Yo TI*. Radiocephalic wrist arteriovenous fistula for hemodialysis: meta-analysis indicates a high primary failure rate. *Eur J Vasc Endovasc Surg.* 2004; 28 (6): 583–589. doi: 10.1016/j.ejvs.2004.08.014.
19. *Lee T*. Fistula First Initiative: Historical Impact on Vascular Access Practice Patterns and Influence on Future Vascular Access Care. *Cardiovasc Eng Technol*. 2017; 8 (3): 244–254. doi: 10.1007/s13239-017-0319-9.
20. *Shahinian VB, Zhang X, Tilea AM, He K, Schaubel DE, Wu W et al*. Surgeon Characteristics and Dialysis Vascular Access Outcomes in the United States: A Retrospective Cohort Study. *Am J Kidney Dis*. 2020; 75 (2): 158–166. doi: 10.1053/j.ajkd.2019.08.001.
21. *Regus S, Almási-Sperling V, Rother U, Meyer A, Lang W*. Surgeon experience affects outcome of forearm arteriovenous fistulae more than outcomes of upper-arm fistulae. *J Vasc Access*. 2017; 18 (2): 120–125. doi: 10.5301/jva.5000639.

The article was submitted to the journal on 16.09.2024

DOI: 10.15825/1995-1191-2025-1-172-182

FEATURES OF POLYURETHANE AND XENOPERICARDIAL PATCH REMODELING USING A LARGE ANIMAL MODEL AS AN EXAMPLE

E.A. Senokosova, E.S. Prokudina, R.A. Mukhamadiyarov, E.A. Velikanova, E.O. Krivkina, A.V. Mironov, E.S. Sardin, L.V. Antonova

Research Institute for Complex Issues of Cardiovascular Diseases, Kemerovo, Russian Federation

Objective: to compare the remodeling features of polyurethane (PU) and bovine pericardium (BP) patches that have been implanted in a sheep carotid artery for 6 months. **Materials and methods.** Synthetic matrices were fabricated from a 12% PU solution in chloroform by electrospinning on a Nanon-01A machine (MECC, Japan). Biological matrices made from commercially produced PU (Kem-Periplas Neo, CJSC Neocor, Russia) were used for comparison. The matrices were implanted as vascular patches into sheep carotid arteries (n = 3). Implantation period was 6 months. Via ultrasound scan, the patency of arteries bearing the implanted vascular prostheses was evaluated. After removal, the matrix samples were studied by histological examination, scanning electron microscopy and confocal microscopy. Prior to this, they had been stained with specific fluorescently labeled antibodies. The GraphPad Prism 8 application was used to process statistical data. **Results.** The sheep carotid artery wall was completely patent, with no aneurysmal dilatations, significant stenoses, and hematomas six months after the PU and BP matrices were implanted. The PU matrix was distinguished by a less pronounced connective-tissue capsule and no neointima hyperplasia; the thickness of the remodeled PU wall was 731.2 (711.5; 751.3) μm. At the same time, there was BP neointimal hyperplasia with a thickness of 627 (538; 817) μm and a remodeled wall thickness of 1723 (1693; 1772) μm. In comparison to BP, the PU matrix exhibited greater endothelialization and structural integrity. **Conclusion.** An *in vivo* study on sheep demonstrated the potential of PU matrix, a novel and effective material for vascular reconstruction, to maintain harmonious remodeling, bioinertness and structural integrity when in contact with blood. Due to its excellent elastic qualities and durability, PU is interesting both as a monocomponent and as a component of a composite material that can be used to create products for the needs of cardiovascular surgery.

Keywords: polyurethane, arterial patch, vascular prosthesis, xenopericardium, electrospinning, carotid artery.

INTRODUCTION

Cardiovascular diseases are the leading cause of death globally, and they also cause significant disability [1]. Atherosclerosis is a common disease that can affect the carotid arteries, leading to carotid artery stenosis of different degrees [2–5]. Angioplasty is the gold standard surgical treatment for hemodynamically significant carotid artery stenosis. It involves excision of the vessel area with atherosclerotic plaque and closure of the incision with primary sutures or a vascular patch. Autologous vessels and commercial flaps, such as decellularized bovine pericardium, porcine small intestinal submucosa (SIS), polytetrafluoroethylene (PTFE), and polyethylene terephthalate (Dacron), are commonly used as patches. However, these materials have several drawbacks, often failing to provide a long-term solution and necessitating repeated surgeries for patch replacement.

Autologous vessels, such as the great saphenous vein and superior thyroid artery, are considered the optimal material for patches due to their complete biocompatibility, absence of immune response, and resistance to thrombosis and restenosis. However, their use requires additional surgical intervention and may be restricted by vascular diseases or the limited availability of suitable implantation sites [6, 7].

Despite the widespread use of xenopericardial flaps, they have a significant drawback – the use of cytotoxic glutaraldehyde as a stabilizing cross-linking agent during material processing. Even with extensive washing protocols, complete removal of this toxic substance cannot be guaranteed. Additionally, glutaraldehyde has been linked to increased calcification, further compromising long-term graft viability [8].

As a result, various methods for processing and preserving xenomaterials are being developed to improve their safety and effectiveness [9–10]. Clinical trials of SIS as a patch have demonstrated minimal bleeding during implantation. However, pseudoaneurysm formation

Corresponding author: Evgeniya Senokosova. Address: 6, Bul'var Barbarasha, Kemerovo, 650002, Russian Federation. Phone: (951) 611-60-76. E-mail: sergeewa.ew@yandex.ru

was observed after six months, suggesting an imbalance between patch degradation and newly formed tissue synthesis, which could unpredictably affect SIS integrity [11].

Polymeric patches offer several advantages. Expanded PTFE has a porous structure, low thrombogenicity, and the ability to support endothelialization. Dacron is known for its high strength and resistance to overstretching [7]. However, PTFE implantation has been associated with prolonged hemostasis time, and long-term studies have reported cases of hemodynamically significant complications and ipsilateral strokes [12, 13]. Similarly, the use of Dacron patches carries risks of inflammatory reactions, infections, perioperative strokes, transient ischemic attacks, and restenosis [14–16].

The development of a novel material for angioplasty that ensures long-term patency of reconstructed blood vessels while minimizing the risks of restenosis, aneurysms, destructive changes, and inflammatory reactions remains a critical challenge. Tissue engineering approaches enable the creation of biomimetic materials using both natural and synthetic components.

For this purpose, we selected medical-grade polyurethane (PU) (TecoFlex) as the base material. PU exhibits several properties essential for vascular applications, including high tensile strength, elasticity, wear resistance, a small bend radius for tubular structures, and resistance to microbial attack and hydrolysis. Additionally, PU is biocompatible and hemocompatible, making it suitable for implantation [17].

PU has already been widely used in the manufacture of medical device components and implantable products [18, 19]. *In vitro* and *in vivo* studies have demonstrated its stability, showing no signs of biodegradation [20–22]. This resistance to degradation is expected to provide structural stability to the PU matrix during vascular remodeling, reducing the likelihood of aneurysm formation and ensuring long-term functionality within the vascular system.

According to the literature, sheep are considered the optimal large animal model for preclinical testing of tissue-engineered products for cardiovascular surgery, as they allow for the evaluation of key parameters such as patency, endothelialization, thromboresistance, and aneurysm formation at the implantation site [23].

In this study, a 3D porous non-woven matrix based on 12% PU was implanted into the carotid artery of sheep as a long-term vascular patch. The study duration was six months, during which the patency and remodeling of the PU matrix were assessed. As a comparison, a commercial bovine pericardial (BP) flap, routinely used in angioplasty at our medical center, was included in the evaluation.

This study will help to establish the suitability of PU for cardiovascular surgical products.

The study **aims** to assess the remodeling characteristics of synthetic PU vascular patches and compare them with BP patches following implantation in a sheep carotid artery over a six-month period.

MATERIALS AND METHODS

Fabrication of matrices

Synthetic PU matrices were fabricated using a 12% solution of Tecoflex EG-80A (Lubrizol Advanced Materials, USA) in chloroform (Vecton, Russia) via electrospinning on a Nanon-01A apparatus (MECC, Japan). The electrospinning parameters were set as follows: voltage 20 kV, manifold rotation speed 200 rpm, solution feed rate 0.5 mL/hour, and needle cleaning time 30 seconds. For comparison, biological matrices were obtained from commercially produced BP (Kem-Periplas Neo, CJSC "Neocor", Russia).

Matrix implantation into a sheep carotid artery

Surgical implantation of synthetic and biological matrices as vascular patches was performed on female Edilbay sheep, each weighing approximately 42–45 kg. The procedures were conducted sequentially in compliance with regulatory guidelines, including Order No. 1179 of the USSR Ministry of Health (October 10, 1993) and Order No. 267 of the Russian Ministry of Health (June 19, 2003), which outline the "Rules for conducting work using experimental animals". The study also adhered to the principles of the European Convention (Strasbourg, 1986) and the Helsinki Declaration of the World Medical Association (1996) on the humane treatment of animals. Ethical approval for the study was granted by the local ethics committee of the Research Institute for Complex Issues of Cardiovascular Diseases (protocol No. 6, dated May 4, 2023).

PU and BP matrices were implanted into a sheep carotid artery for a period of 6 months (n = 3, one sample for each patch type). The implanted patches measured 4×40 mm.

The surgical procedures were performed under general anesthesia, with anesthesia, intraoperative drug management, and postoperative drug support following previously established protocols [24]. Throughout the intervention, vital parameters were continuously monitored, including blood pressure, heart rate, and SpO_2. Mechanical ventilation was maintained with a respiratory rate of 12–15 breaths per minute, positive end-expiratory pressure (PEEP) of 7–9 mbar, tidal volume of 6–8 mL/kg, and an inspired oxygen fraction (FiO_2) of 40–60%.

The implantation procedure involved gaining access to the carotid artery, followed by systemic administration of 5000 U of heparin intravenously. The carotid artery was then clamped, and a longitudinal arteriotomy of up to 40.0 mm in length was performed.

Matrices measuring 40.0×4.0 mm were sutured into the arteriotomy defect using interrupted sutures with Prolene 6/0 thread (Ethicon, USA). Blood flow was restored according to the standard air embolism prevention protocol. The surgical wound was closed with Vicryl 2.0 thread (Ethicon, USA) and treated with BF glue. Additionally, 4000 anti-Xa IU/0.4 mL of enoxaparin sodium was administered subcutaneously, and the animal was subsequently extubated.

Assessment of patency of vessels with implanted matrices

The patency of carotid arteries with implanted matrices in sheep was assessed using ultrasound scanning with a portable, premium-class color Doppler system (M7, Mindray, China). Evaluations were conducted on postoperative days 1 and 5, followed by bi-monthly assessments until the planned endpoint of the study at 6 months.

Scanning electron microscopy

The explanted PU and BP matrix specimens, along with adjacent carotid artery sections, were fixed in 10% aqueous formalin (pH 7.4, BioVitrum, Russia). Post-fixation, dehydration with alcohols, and staining with uranyl acetate were performed as per a previously described technique [25]. The stained patch samples were embedded in Epon epoxy resin (Electron Microscopy Science, USA). The epoxy blocks were then ground and polished using a TegraPol-11 machine (Struers, USA), followed by contrast staining with Reynolds lead citrate. A carbon layer (10–15 nm) was sputtered using a vacuum sputtering system (EM ACE200, Leica). The surface structure of the samples was examined in backscattered electron mode using a Hitachi-S-3400N scanning electron microscope (Hitachi, Japan) in BSECOMP mode at an accelerating voltage of 10 kV.

Histological examination of samples

The preparation of explanted PU and BP matrix samples for histological examination followed a previously described procedure [26]. After deparaffinization, selected sections were stained with Harris hematoxylin (BioVitrum, Russia, Novosibirsk) and eosin (BioVitrum, Russia, Novosibirsk), followed by washing in running water, fixation in 96% alcohol, and clarification in o-xylene. Collagenization of the samples was assessed using Van Gieson stain, which involved sequential staining with Weigert's hematoxylin (BioVitrum, Russia, Novosibirsk) and picrofuchsin (BioVitrum, Russia, Novosibirsk). Calcium presence was identified using alizarin red S (Khimservice, Russia) and DAPI nuclear dye (Sigma-Aldrich, USA). The stained sections were mounted with Vitrogel (BioVitrum, Russia, Novosibirsk) and examined under an AXIO Imager A1 microscope (Carl Zeiss, Germany) at 100× and 200× magnification.

Confocal microscopy

For immunofluorescence analysis, slices were prepared from frozen explanted specimens using a cryotome (Microm HM 525, Thermo Scientific). These slices were fixed in 4% paraformaldehyde for 10 minutes and permeabilized with Triton-X100 solution (Sigma-Aldrich, USA) for 15 minutes. The sections were then stained with specific primary antibodies: rabbit anti-CD31 (Abcam, UK), mouse anti-alpha-smooth muscle actin (ACTA2) (Abcam, UK), rabbit anti-von Willebrand Factor (vWF, Abcam, UK), rabbit anti-collagen IV (Abcam, UK), mouse anti-collagen I (Abcam, UK), and rabbit anti-collagen III (Novus Biologicals, USA).

Following overnight incubation at 4 °C with the primary antibodies, the sections were treated with secondary antibodies for 1 hour at room temperature: donkey anti-rabbit IgG conjugated with Alexa Fluor 488 (Thermo Fisher Scientific, USA) and donkey anti-mouse IgG conjugated with Alexa Fluor 555 (Thermo Fisher Scientific, USA). At all staining stages, phosphate-buffered saline supplemented with 0.1% Tween (Sigma-Aldrich, USA) was used for washing. Autofluorescence was eliminated using an Autofluorescence Eliminator Reagent (Millipore, USA) according to the manufacturer's instructions. Cell nuclei were stained with DAPI (10 μg/mL, Sigma-Aldrich, USA) for 30 minutes.

The prepared samples were examined using a confocal laser scanning microscope LSM 700 (Carl Zeiss, Germany).

Statistical data analysis

Statistical data analysis was conducted using GraphPad Prism 8 software (GraphPad Software, USA). The distribution of the data was assessed using the Kolmogorov–Smirnov test. Results were presented as median (Me) with interquartile range (Q1; Q3). To compare differences between two independent groups, the Mann–Whitney U test was applied. Differences were considered statistically significant at a significance level of $p < 0.05$.

RESULTS

Results of PU matrix implantation in a sheep carotid artery

Ultrasound results at 6 months post-implantation of the PU matrix showed complete patency of the carotid artery. No significant aneurysmal dilatations, stenoses, or hematomas were detected (Fig. 1, a, b). Blood flow velocity in the patched vessel was measured at 75 cm/s (Fig. 1, b).

Upon visual inspection during access to the sheep carotid artery, the implanted PU matrix appeared consistent with ultrasound findings. The implantation site was moderately surrounded by a connective tissue capsule without signs of inflammation (Fig. 1, a). The PU patch exhibited no significant structural changes or aneurys-

mal dilations. Macroscopically, the PU matrix closely resembled the native carotid artery wall due to complete integration and remodeling (Fig. 1, a–c). The explant was soft and elastic.

In the transverse section of the carotid artery with the implanted patch, the PU matrix maintained a circular lumen alongside the vascular wall (Fig. 1, d). The matrix wall showed no neointimal hyperplasia and matched the thickness of the carotid artery wall (Fig. 1, d).

Histological examination revealed that the PU matrix maintained its structural integrity without signs of inflammation or calcification, both within the patch and in the surrounding tissues, indicating a low resorption rate and high biocompatibility (Fig. 2, a–d).

The PU matrix had a thickness of 343.3 (331.3; 361.2) μm. A neointima formed on the inner surface of the vessel at the site of the implanted patch, measuring 191.4 (164.3; 289.2) μm in thickness. Externally, the patch was

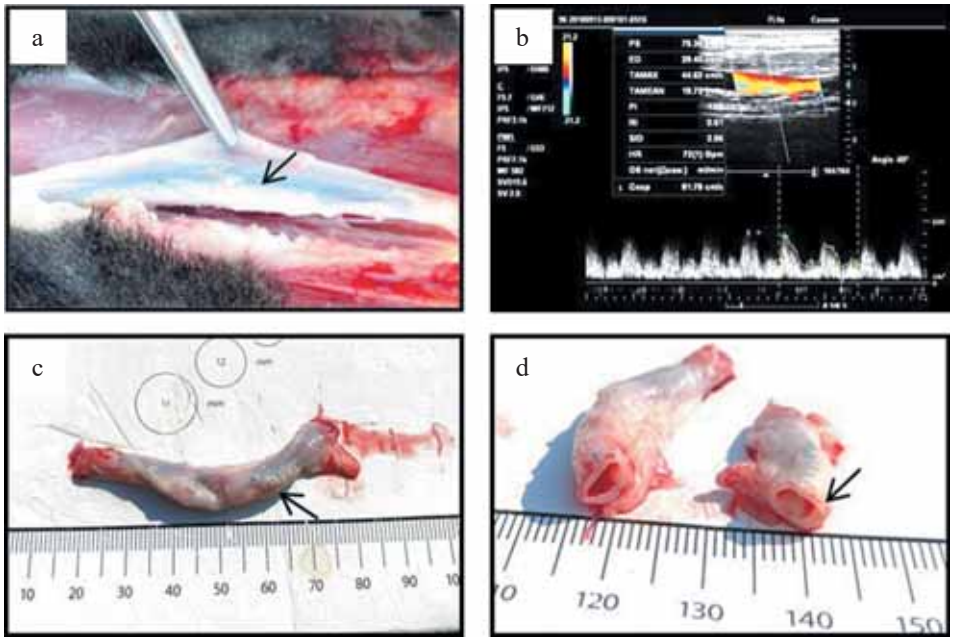

Fig. 1. PU matrix: a, view of the PU matrix 6 months after implantation in a sheep carotid artery; b, ultrasound scan image of the carotid artery 6 months after PU matrix implantation; c, explanted PU matrix with neighboring sections of the sheep carotid artery; d, cross section of the carotid artery with the implanted PU matrix

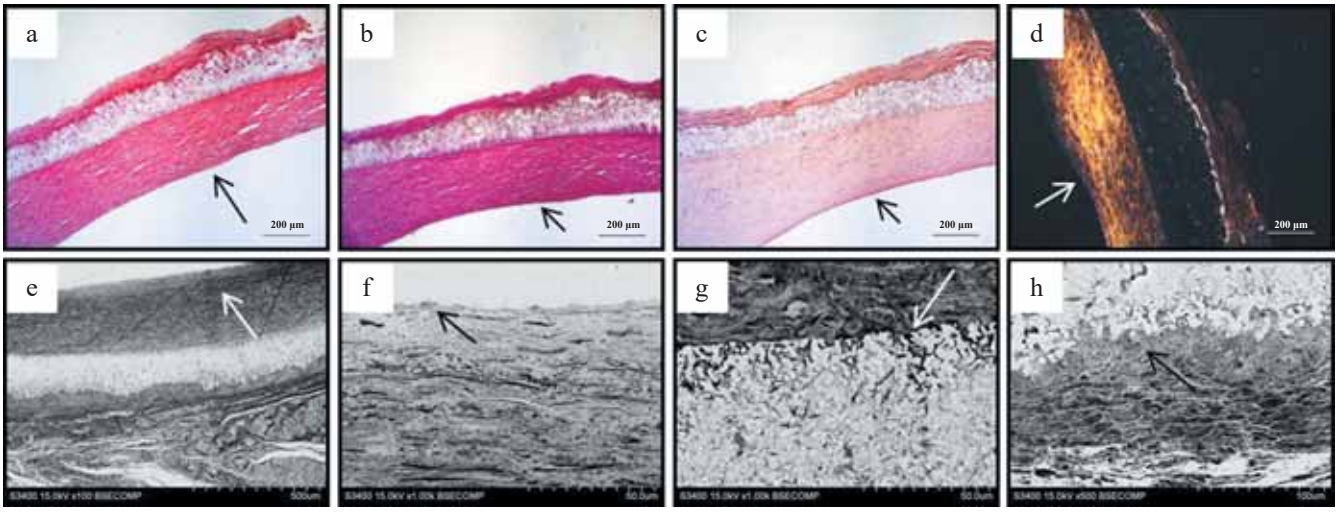

Fig. 2. Results of histological examination and scanning electron microscopy of the PU matrix 6 months after implantation into a sheep carotid artery (white and black arrows indicate neointima of the vessel): a, general view of the explanted PU matrix, H&E stain, ×50 magnification; b, general view of the PU matrix, Van Gieson's stain, ×50 magnification; c, general view of the PU matrix, alizarin red S stain, ×50 magnification; d, general view of the PU matrix, DAPI-stained fluorescence image, ×50 magnification; e, general view of the matrix, ×100 magnification; f, neointima, ×1000 magnification; g, area of junction between vessel neointima and PU matrix, ×1000 magnification; h, single foreign-body giant cells with PU fibers in the cytoplasm in the area of contact between the neoadventitia and the matrix, ×500 magnification

covered by newly formed adventitia with a thickness of 192.2 (164.0; 289.2) μm.

For comparison, the native sheep carotid artery had the following parameters: intima (20.14 (16.32; 22.70) μm; medial 530.1 (517.2; 547.7) μm; adventitia 202.6 (190.6; 212.7) μm).

Thus, remodeling of the implanted PU matrix under blood flow conditions led to the formation of both neointima and neoadventitia. The total thickness of the patched vascular wall after 6 months of implantation was 731.2 (711.5; 751.3) μm, which did not significantly differ from the native wall thickness of the sheep carotid artery (766.8 (740.4; 791.2) μm).

SEM analysis of the explanted PU matrix corroborated the histological findings, revealing no evidence of neointimal hyperplasia, inflammation, or calcification (Fig. 2, e–h). The inner vascular surface of the implanted patch was covered by a continuous layer of endothelium-like cells (Fig. 2, f). At the neointima-patch interface, macrophages were observed, with some demonstrating the ability to migrate into the matrix (Fig. 2, g).

The outer surface of the matrix was enveloped by neoadventitia, which contained histological elements characteristic of the carotid adventitial sheath, including newly formed vasa vasorum (Fig. 2, a, h). Signs of partial bioresorption were observed on the side of the implanted patch facing the neoadventitia, where the matrix was surrounded by clusters of multinucleated foreign-body giant cells (FBGCs) with isolated PU fibers detected within their cytoplasm (Fig. 2, h). Overall, monocytic-macrophage cells and multinucleated FBGCs were primarily localized in the superficial layers of the patch, while only a sparse number of cellular elements were present within the deeper regions of the PU matrix (Fig. 2, g, h).

Immunofluorescence analysis followed by confocal microscopy confirmed the presence of α-actin-producing smooth muscle-like cells within the neointima (Fig. 3, a). The inner vascular surface of the implanted PU matrix was lined by a monolayer of mature endothelial cells actively synthesizing von Willebrand factor (Fig. 3, b). Collagen III and IV were detected throughout all layers of the examined sections, including the PU matrix, neointima, and neoadventitia. However, the most intense fluorescence of these proteins was observed in the endothelial layer (Fig. 3, c, d). Cellular infiltration within the PU matrix remained low.

Consequently, the remodeling of the PU matrix implanted into a sheep carotid artery over a 6-month period led to the development of a three-layer structure resembling the native vascular wall. The absence of premature material degradation, calcification, inflammation, aneurysmal formation, or stenotic changes highlights the high biocompatibility of PU as a vascular patch material.

Results of BP matrix implantation in a sheep carotid artery

Ultrasound evaluation at 6 months post-implantation of the BP matrix in a sheep carotid artery confirmed vessel patency, with no evidence of aneurysmal dilatation, stenosis, or significant hematomas. The blood flow velocity at the site of the implanted patch averaged 67 cm/s (Fig. 4, a, b).

Upon visual inspection during access to the sheep carotid artery, no significant structural changes, aneurysmal dilatations, or hematomas were observed at the BP matrix implantation site (Fig. 4, a). A vascularized connective tissue capsule uniformly enveloped the implanted BP matrix (Fig. 4, a, c). The explant remained elastic with a dense structure.

A transverse section of the carotid artery confirmed that the BP matrix maintained a circular lumen in combination with the vascular wall (Fig. 4, d). However, the implanted patch site appeared thicker than the native carotid artery wall, which may indicate neointimal hyperplasia (Fig. 4, d).

Histological analysis of the explanted BP matrix confirmed that its structural integrity was largely preserved after 6 months of implantation (Fig. 5, a–d). However, minor areas of delamination were observed within the

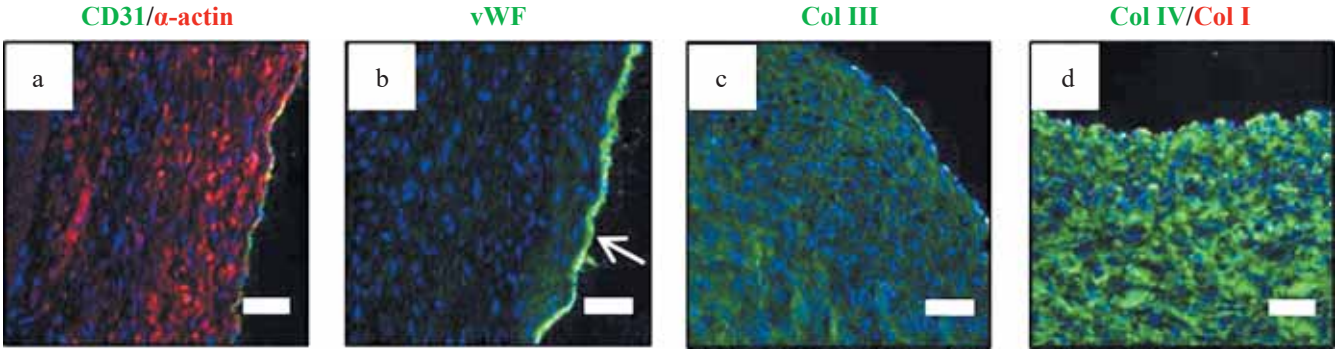

Fig. 3. Results of immunofluorescence study of PU matrix 6 months after implantation in a sheep carotid artery, ×200 magnification, scale bar 50 μm: a, endothelium on the inner surface (CD31, green glow), alpha actin-containing cells (red glow); b, von Willebrand factor (vWF, green glow); c, collagen type III (Col III, green glow); d, collagen type IV (Col IV, green glow), collagen type I (Col I, red glow), DAPI-stained cell nuclei (blue glow)

patch, though these did not significantly affect its overall architecture (Fig. 5, a–d). No signs of calcification or inflammation were detected.

By the end of the 6-month implantation period, remodeling of the BP matrix led to the formation of a neointima with a thickness of 627 (538; 817) μm and a neoadventitia with an average thickness of 540 (504; 540) μm. The total vascular wall thickness at the implantation site measured 1723 (1693; 1772) μm, nearly twice the thickness of the intact carotid artery wall (869 (833; 875) μm), indicating the presence of neointimal hyperplasia in the patched region.

A detailed examination of the explanted BP matrix confirmed the absence of inflammation and calcification (Fig. 5, e–h). The inner vascular surface was lined with a loose layer of endothelial-like cells (Fig. 5, e–g). Single areas of delamination were observed at the BP matrix implantation site, but these did not compromise the overall structural integrity of the patch (Fig. 5, e–f). The neointima exhibited a tendency to thicken, both centrally and

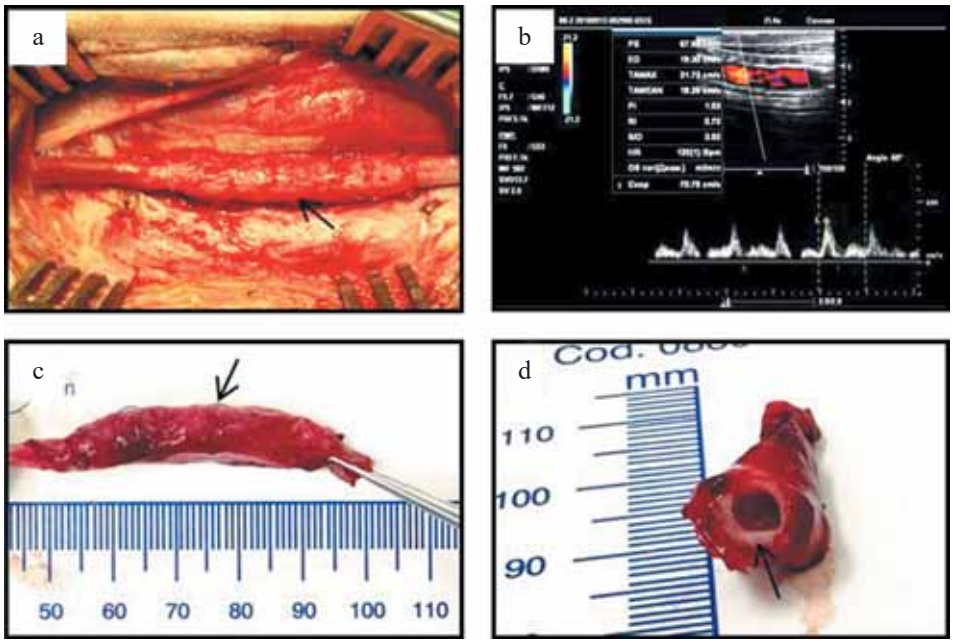

Fig. 4. BP matrix: a, view of the BP matrix 6 months after implantation in a sheep carotid artery; b, ultrasound scan of the carotid artery 6 months after implantation of the BP matrix; c, explanted section of the carotid artery with the implanted BP matrix; d, cross section of the carotid artery with the implanted BP matrix

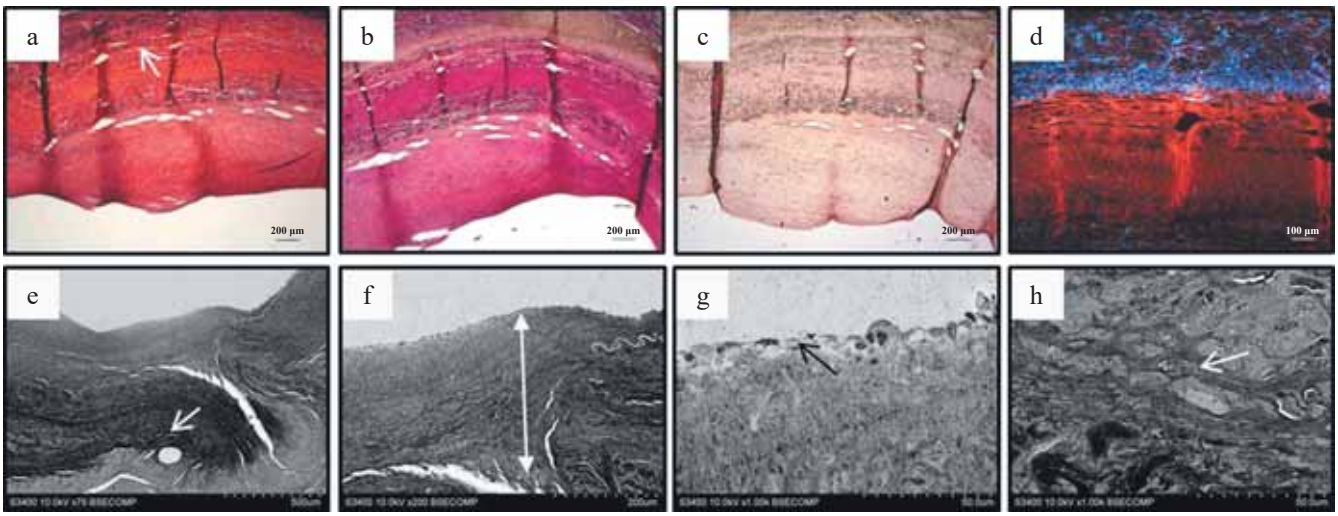

Fig. 5. Results of histologic examination and scanning electron microscopy of the BP matrix 6 months after implantation into a sheep carotid artery: a, general view of the BP matrix, H&E stain, ×50 magnification; b, general view of the BP matrix, Van Gieson's stain, ×50 magnification; c, general view of the BP matrix, alizarin red C color, ×50 magnification; d, general view of the BP matrix, DAPI-stained fluorescence image, ×100 magnification; e, general view of the matrix, ×75 magnification; f, area of anastomosis, ×200 magnification; g, vessel neointima, magnification ×1000; h, single foreign-body giant cells in the area of contact between the neoadventitia and the matrix, ×1000 magnification

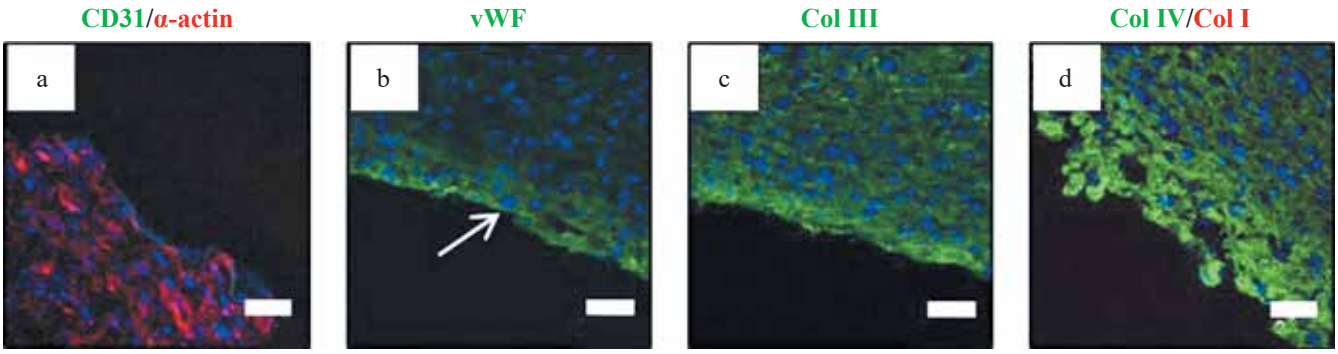

Fig. 6. Results of immunofluorescence study of the BP matrix 6 months after implantation in a sheep carotid artery, ×200 magnification, scale bar 50 μm: a, endothelium on the inner surface (CD31, green glow), alpha actin-containing cells (red glow); b, von Willebrand factor (vWF, green glow); c, collagen type III (Col III, green glow); d, collagen type IV (Col IV, green glow), collagen type I (Col I, red glow), DAPI-stained cell nuclei (blue glow)

in the anastomotic regions (Fig. 5, e–f). The implanted xenopericardial flap retained the fibrous structure characteristic of bovine pericardium (Fig. 5, e). While the cellularity of the patch was low, single multinucleated foreign-body giant cells (FBGCs) were detected at the interface with the neoadventitia (Fig. 5, h).

Immunofluorescence analysis of the explanted BP matrix revealed the presence of squamous alpha-actin-producing cells within the neointima (Fig. 6, a). The endothelial layer lining the inner vascular surface appeared loose and discontinuous, with weak expression of von Willebrand factor (Fig. 6, b). Collagen III fibers were detected throughout all layers of the sample, including the neointima, matrix, and neoadventitia (Fig. 6, c). Collagen IV was present in all layers, with individual brightly stained secreting cells scattered throughout (Fig. 6, d).

Thus, remodeling of the BP matrix implanted in a sheep carotid artery followed the process of forming a tissue analog of the vascular wall, comprising both neointima and neoadventitia. A key distinguishing feature of the biological patch was the presence of localized delamination, indicative of material degradation. Additionally, the pronounced neointimal hyperplasia observed after six months of implantation highlights structural and functional differences between the implanted BP matrix and the native carotid artery wall.

DISCUSSION

Commercial grafts used for vascular reconstruction present several unresolved challenges, including thrombosis, calcification, neointimal hyperplasia, and aneurysm formation [27, 28]. Beyond these issues, xenopericardial grafts are particularly susceptible to structural degeneration, especially in younger individuals [29, 30]. Materials such as PTFE and Dacron have also been associated with calcium deposition, not only within the graft itself but also in adjacent vascular structures, including the adventitia, media, and intima [31].

Neointimal hyperplasia remains a critical concern in vascular surgery, as it significantly impacts the long-term success of both surgical and endovascular procedures [32]. In our previous *in vitro* studies, we demonstrated that a PU material exhibited favorable physical and mechanical properties, with the potential to mitigate neointimal hyperplasia. Notably, PU showed lower stiffness compared to xenopericardium [33].

Our in-house study on a novel vascular patch material composed of 12% electrospun PU in a long-term sheep carotid artery implantation model demonstrated several advantages over commercial BP.

A key distinction between the two materials was observed visually at the time of explantation. The connective tissue capsule surrounding the BP patch was denser compared to PU. Cross-sectional analysis further revealed a seamless integration of PU with the arterial wall, whereas BP exhibited pronounced thickening, indicating structural disparity.

Secondly, histological evaluation confirmed the absence of neointimal hyperplasia in the PU matrix and a closer resemblance to the native artery. The total thickness of the remodeled PU vascular wall was 731.2 (711.5; 751.3) μm, aligning well with the native carotid artery. In contrast, BP demonstrated significant neointimal hyperplasia (627 (538; 817) μm thick), resulting in an overall vascular wall thickness of 1723 (1693; 1772) μm after six months of implantation.

Thirdly, the endothelial lining on the PU matrix was more continuous and functionally active compared to the less-developed endothelialization observed in BP.

Fourthly, the structural integrity of PU was higher than that of BP. While multinucleated FBGCs were present at the neoadventitia border in both materials, the location of these cells in BP was the same, but the material was stratified.

Despite both materials supporting 100% patency of the reconstructed carotid arteries and maintaining physiological blood flow over the six-month implantation period without aneurysm formation, the PU-based matrix demonstrated superior remodeling capabilities under hemodynamic conditions. Given these advantages, PU

shows strong potential for use as a standalone component or as part of a composite structure to enhance elasticity and durability in vascular reconstruction applications.

CONCLUSION

The implantation of a PU matrix as a vascular patch demonstrated harmonious remodeling and preservation of the polymer framework under physiological blood flow conditions in a sheep model. Its high elasticity and durability make PU a promising material for cardiovascular surgical applications, either as a standalone component or as part of a composite structure designed to enhance vascular reconstruction outcomes.

This research was conducted as part of the fundamental theme of the Research Institute for Complex Issues of Cardiovascular Diseases, No. 0419-2022-0001: "Molecular, cellular, and biomechanical mechanisms of the pathogenesis of cardiovascular diseases in the development of new treatment methods for cardiovascular diseases based on personalized pharmacotherapy, minimally invasive medical devices, biomaterials, and tissue-engineered implants".

The authors declare no conflict of interest.

REFERENCES

1. *Virani SS, Alonso A, Benjamin EJ, Bittencourt MS, Callaway CW, Carson AP et al*. Heart Disease and Stroke Statistics-2020 Update: A Report From the American Heart Association. *Circulation*. 2020; 141 (9): e139–e596. doi: 10.1161/CIR.0000000000000757.
2. *Feigin VL, Brainin M, Norrving B, Martins S, Sacco RL, Hacke W et al.* World Stroke Organization (WSO): Global Stroke Fact Sheet 2022. *Int J Stroke.* 2022; 17 (1): 18–29. doi: 10.1177/17474930211065917.
3. *Pashneh-Tala S., MacNeil S., Claeyssens F.* The Tissue-Engineered Vascular Graft-Past, Present, and Future. *Tissue Eng Part B Rev.* 2016; 22 (1): 68–100. doi: 10.1089/ten.teb.2015.0100.
4. *Benjamin EJ, Muntner P, Alonso A, Bittencourt MS, Callaway CW, Carson AP et al.* Heart Disease and Stroke Statistics-2019 Update: A Report From the American Heart Association. *Circulation.* 2019; 139 (10): 56–528. doi: 10.1161/CIR.0000000000000659.
5. *Roth GA, Mensah GA, Johnson CO, Addolorato G, Ammirati E, Baddour LM et al.* Global Burden of Cardiovascular Diseases and Risk Factors, 1990–2019: Update From the GBD 2019 Study. *J Am Coll Cardiol*. 2020; 76 (25): 2982–3021. doi: 10.1016/j.jacc.2020.11.010.
6. *Yarikov AV, Balyabin AV, Yashin KS, Mukhin AS.* Surgical Treatment Modalities of Carotid Artery Stenosis (Review). *Modern Technologies in Medicine*. 2015; 7 (4): 189–200. doi: 10.17691/stm2015.7.4.25.
7. *Muto A, Nishibe T, Dardik H, Dardik A.* Patches for carotid artery endarterectomy: current materials and prospects. *J Vasc Surg.* 2009; 50 (1): 206–213. doi: 10.1016/j.jvs.2009.01.062.
8. *Chernyavskiy AM, Larionov PM, Stolyarov MS, Starodubtsev VB.* Structural transformation of xenopericardium after implantation into the carotid artery (prospective study). *Pathology of blood circulation and cardiac surgery*. 2007; 4: 37–40.
9. *Kudryavtseva Yu.A.* Bioprosthetic heart valves. From idea to clinical use. *Complex Issues of Cardiovascular Diseases*. 2015; (4): 6–16. (In Russ.). doi: 10.17802/2306-1278-2015-4-6-16.
10. *Rezvova MA, Ovcharenko EA, Glushkova TV, Kudryavtseva YuA, Barbarash LS.* Evaluation of calcification resistance of xenopericardium treated with polyhydroxy compounds. *Russian Journal of Transplantology and Artificial Organs*. 2021; 23 (1): 75–83. doi: 10.15825/1995-1191-2021-1-75-83.
11. *Weber SS, Annenberg AJ, Wright CB, Braverman TS, Mesh CL.* Early pseudoaneurysm degeneration in biologic extracellular matrix patch for carotid repair. *J Vasc Surg.* 2014; 59 (4): 1116–1118. doi: 10.1016/j.jvs.2013.05.012.
12. *Fokin AA, Kuvatov AV.* Remote results of carotid artery reconstructions using a patch. *Journal of Experimental and Clinical Surgery*. 2013; 6 (2): 239–243.
13. *Ren S, Li X, Wen J, Zhang W, Liu P.* Systematic review of randomized controlled trials of different types of patch materials during carotid endarterectomy. *PLoS One.* 2013; 8 (1): e55050. doi: 10.1371/journal.pone.0055050.
14. *Alawy M, Tawfick W, ElKassaby M, Shalaby A, Zaki M, Hynes N, Sultan S.* Late Dacron Patch Inflammatory Reaction after Carotid Endarterectomy. *Eur J Vasc Endovasc Surg.* 2017; 54 (4): 423–429. doi: 10.1016/j.ejvs.2017.06.015.
15. *Xu JH, Altaf N, Tosenovsky P, Mwipatayi BP.* Management challenges of late presentation Dacron patch infection after carotid endarterectomy. *BMJ Case Rep.* 2017; 2017: bcr2017221541. doi: 10.1136/bcr-2017-221541.
16. *Rerkasem K, Rothwell PM.* Systematic review of randomized controlled trials of patch angioplasty versus primary closure and different types of patch materials during carotid endarterectomy. *Asian J Surg.* 2011; 34 (1): 32–40. doi: 10.1016/S1015-9584(11)60016-X.
17. *Kucinska-Lipka J, Gubanska I, Janik H, Sienkiewicz M.* Fabrication of polyurethane and polyurethane based composite fibres by the electrospinning technique for soft tissue engineering of cardiovascular system. *Mater Sci Eng C Mater Biol Appl.* 2015; 46: 166–176. doi: 10.1016/j.msec.2014.10.027.
18. *LaPorte RJ.* Hydrophilic polymer coatings for medical devices. *Routledge.* 2017; 11–16. doi: 10.1201/9780203751381.
19. *Kheradvar A, Groves EM, Dasi LP, Alavi SH, Tranquillo R, Grande-Allen KJ et al.* Emerging trends in heart valve engineering: Part I. Solutions for future. *Ann Biomed Eng*. 2015; 43 (4): 833–843. doi: 10.1007/s10439-014-1209-z.
20. *Bergmeister H, Grasl C, Walter I, Plasenzotti R, Stoiber M, Schreiber C et al.* Electrospun small-diameter polyurethane vascular grafts: ingrowth and differentiation of vascular-specific host cells. *Artif Organs.* 2012; 36 (1): 54–61. doi: 10.1111/j.1525-1594.2011.01297.x.

21. *Grasl C, Bergmeister H, Stoiber M, Schima H, Weigel G.* Electrospun polyurethane vascular grafts: *in vitro* mechanical behavior and endothelial adhesion molecule expression. *J Biomed Mater Res A.* 2010; 93 (2): 716–723. doi: 10.1002/jbm.a.32584.
22. *Bergmeister H, Schreiber C, Grasl C, Walter I, Plasenzotti R, Stoiber M et al.* Healing characteristics of electrospun polyurethane grafts with various porosities. *Acta Biomater*. 2013; 9 (4): 6032–6040. doi: 10.1016/j.actbio.2012.12.009.
23. *Schleimer K, Jalaie H, Afify M, Woitok A, Barbati ME, Hoeft K et al.* Sheep models for evaluation of novel patch and prosthesis material in vascular surgery: tips and tricks to avoid possible pitfalls. *Acta Vet Scand*. 2018; 60 (1): 42. doi: 10.1186/s13028-018-0397-1.
24. *Antonova LV, Mironov AV, Yuzhalin AE, Krivkina EO, Shabaev AR, Rezvova MA et al.* A Brief Report on an Implantation of Small-Caliber Biodegradable Vascular Grafts in a Carotid Artery of the Sheep. *Pharmaceuticals (Basel).* 2020 May 21; 13 (5): 101. doi: 10.3390/ph13050101.
25. *Antonova L, Kutikhin A, Sevostianova V, Lobov A, Repkin E, Krivkina E et al.* Controlled and Synchronised Vascular Regeneration upon the Implantation of Iloprost- and Cationic Amphiphilic Drugs-Conjugated Tissue-Engineered Vascular Grafts into the Ovine Carotid Artery: A Proteomics-Empowered Study. *Polymers (Basel).* 2022 Nov 26; 14 (23): 5149. doi: 10.3390/polym14235149.
26. *Antonova L, Kutikhin A, Sevostianova V, Velikanova E, Matveeva V, Glushkova T et al.* bFGF and SDF-1α Improve *In Vivo* Performance of VEGF-Incorporating Small-Diameter Vascular Grafts. *Pharmaceuticals (Basel)*. 2021 Mar 28; 14 (4): 302. doi: 10.3390/ph14040302.
27. *Terakawa K, Yamauchi H, Lee Y, Ono M.* A Novel Knitted Polytetrafluoroethylene Patch for Cardiovascular Surgery. *Int Heart J.* 2022; 63 (1): 122–130. doi: 10.1536/ihj.21-564.
28. *Liesker DJ, Gareb B, Looman RS, Donners SJA, de Borst GJ, Zeebregts CJ, Saleem BR.* Patch angioplasty during carotid endarterectomy using different materials has similar clinical outcomes. *J Vasc Surg.* 2023; 77 (2): 559–566.e1. doi: 10.1016/j.jvs.2022.09.027.
29. *Aguiari P, Fiorese M, Iop L, Gerosa G, Bagno A.* Mechanical testing of pericardium for manufacturing prosthetic heart valves. *Interact Cardiovasc Thorac Surg*. 2016; 22 (1): 72–84. doi: 10.1093/icvts/ivv282.
30. *Fadeeva IS, Sorkomov MN, Zvyagina AI, Britikov DV, Sachkov AS, Evstratova YaV et al.* Study of Biointegration and Elastic-Strength Properties of a New Xenopericardium-Based Biomaterial for Reconstructive Cardiovascular Surgery. *Bull Exp Biol Med.* 2019; 167 (4): 496–499. doi: 10.1007/s10517-019-04558-1.
31. *Lejay A, Bratu B, Kuntz S, Neumann N, Heim F, Chakfé N.* Calcification of Synthetic Vascular Grafts: A Systematic Review. *EJVES Vasc Forum.* 2023; 29 (60): 1–7. doi: 10.1016/j.ejvsvf.2023.05.013.
32. *Collins MJ, Li X, Lv W, Yang C, Protack CD, Muto A et al.* Therapeutic strategies to combat neointimal hyperplasia in vascular grafts. *Expert Rev Cardiovasc Ther.* 2012; 10 (5): 635–647. doi: 10.1586/erc.12.33.
33. *Senokosova EA, Prokudina ES, Matveeva VG, Velikanova EA, Glushkova TV, Koshelev VA et al.* Tissue engineering matrix based on polyurethane: *in vitro* research. *Complex Issues of Cardiovascular Diseases.* 2023; 12 (4S): 120–130. [In Russ.]. doi: 10.17802/2306-1278-2023-12-4S-120-130.

The article was submitted to the journal on 19.03.2024

DOI: 10.15825/1995-1191-2025-1-183-187

PATHOMORPHOLOGICAL AND MICROBIOLOGICAL ANALYSIS OF AN EPOXY-TREATED BIOPROSTHETIC HEART VALVE FUNCTIONING FOR 25 YEARS IN A PATIENT WITH RHEUMATIC HEART DISEASE: A CASE REPORT

A.E. Kostyunin, T.V. Glushkova, T.N. Akentyeva, E.A. Ovcharenko
Research Institute for Complex Issues of Cardiovascular Diseases, Kemerovo, Russian Federation

Bioprosthetic heart valves (BHVs) rarely last longer than 20 years due to the development of degenerative changes in their leaflets. We present a detailed pathomorphological description of KemCor, an epoxy-treated BHV that was removed from the mitral position 25 years after implantation. Literature review shows that this is the longest recorded lifespan of an epoxy-treated implant.

Keywords: bioprosthetic heart valves, structural valve degeneration, histology, clinical case.

INTRODUCTION

Limited lifespan is a major drawback of bioprosthetic heart valves (BHVs). On average, these medical devices function for 10–15 years before requiring replacement due to structural degeneration (SD) of their biological component [1]. Morphologically and histologically, SD is an irreversible process of fatigue-induced destruction and calcification of the collagen base of the leaflet apparatus of BHVs [1]. Degenerative changes in the leaflets become the cause of hemodynamic dysfunction of BHVs, leading to valve stenosis and/or insufficiency [1].

Several papers have described in detail the histopathological pattern of SD, characteristic of foreign BHVs [2, 3]. It is important to note that the latter differ from some Russian-made models by the method of treatment: in their manufacture they use animal biomaterial treated with glutaraldehyde (GA), whereas in Russia a unique technology of biotissue stabilization with diglycidyl ether of ethylene glycol is widespread [4]. The durability of BHVs treated with diepoxy compounds is similar to that of foreign BHVs [4]; however, the histopathological features of SD are poorly studied for this type of implants [5, 6].

In the present article, we present a morphological and histological description of a KemCor BHV (NeoCor, Russia), which was removed 25 years after implantation due to dysfunction. Our hospital records and literature review show that the studied sample is the longest recorded lifespan of an epoxy-treated BHV.

CLINICAL CASE DESCRIPTION AND CHARACTERISTICS OF THE EXPLANTED BIOPROSTHETIC HEART VALVE

A man born in 1960, suffering from rheumatic heart disease and mitral valve stenosis, was implanted with KemCor BHV (NeoCor, Russia) in 1995. The valve was replaced in 2020 (after 25 years) due to grade IV prosthetic valve dysfunction. No history of hypertension, diabetes mellitus, dyslipidemia or kidney failure was noted in the patient's history.

The BHV retrieved during prosthetic replacement was sent to the laboratory for study. Macroscopic analysis revealed the presence of numerous perforations in the dome of the leaflets (Fig. 1, a). Two leaflets were characterized by extensive intraleaflet hemorrhages, while the leaflet apparatus retained elasticity and had no visible calcifications. There were no vegetations on the surface of the leaflets, the frame struts were covered with connective tissue without signs of calcification. Pannus was present on the BHV on the exit site, but it was poorly developed: connective tissue slightly fixed the leaflets adjacent to each other in the commissure zone on one frame strut.

For microscopic analysis, BHV leaflets were separated from the framework and cryosections were prepared on an HM525 microtome cryostat (Thermo Fisher Scientific, USA) using Neg-50 rapid tissue freezing medium (6502, Thermo Fisher Scientific, USA). Examination of slices stained with hematoxylin (05-06004, Bio-Optica, Italy) and eosin (HK-EV-A500, Biovitrum, Russia) showed pronounced stratification and fragmentation of

Corresponding author: Alexander Kostyunin. Address: 6, Bul'var Barbarasha, Kemerovo, 650002, Russian Federation. Phone: (900) 108-10-97. E-mail: rhabdophis_tigrina@mail.ru

the biomaterial. Due to significant tissue damage, the slices were often not monolithic, but were arranged as separate fragments on a glass slide (Fig. 1, b). Alizarin red S staining (ab142980, Abcam, UK) showed the presence of single small (up to 1 mm) calcifications (Fig. 1, c), while Gram staining (ab150672, Abcam, UK) revealed bacterial colonies at the free edge of one of the leaflets (Fig. 1, d). Histological examination of the microorganisms showed Gram-positive cocci and Gram-negative bacilliform bacteria (Fig. 2, a), however, attempts at taxonomic identification of bacteria by PCR using OneStep test systems (Litech, Russia) did not yield results (we used kits for detection of the main pathogens of infective endocarditis (IE) from the genera: *Enterobacter*, *Enterococcus*, *Escherichia*, *Proteus*, *Serratia*, *Staphylococcus* and *Streptococcus*).

Among other things, the leaflet apparatus of the BHV in question was characterized by moderate cell infiltration. The cells were located singly or formed small clusters (not more than 30 cells) localized on the surface of the leaflets, in the thickness of loosened areas of the biomaterial and near calcifications. Cell typing was performed by immunohistochemical reaction using a commercial kit Novolink Polymer Detection Systems (RE7150-CE, Leica Biosystems, USA) and antibodies to pan-leukocyte marker CD45 (ab10558, Abcam, UK), macrophage marker CD68 (ab955, Abcam, UK), T cell marker CD3 (ab16669, Abcam, UK), B-lymphocyte CD19 (MA5-32544, Invitrogen, USA) and neutrophil marker MPO (ab208670, Abcam, UK). Examination of the cellular infiltrates showed that they consisted exclusively of leukocytes (CD45+), represented predominantly by macrophages (CD68+), and single T cells (CD3+) and neutrophils (MPO+) (Fig. 2, b). Oil Red O staining of slices allowed to reveal accumulations of foam cells and large lipid droplets in the biomaterial (Fig. 2, b, c).

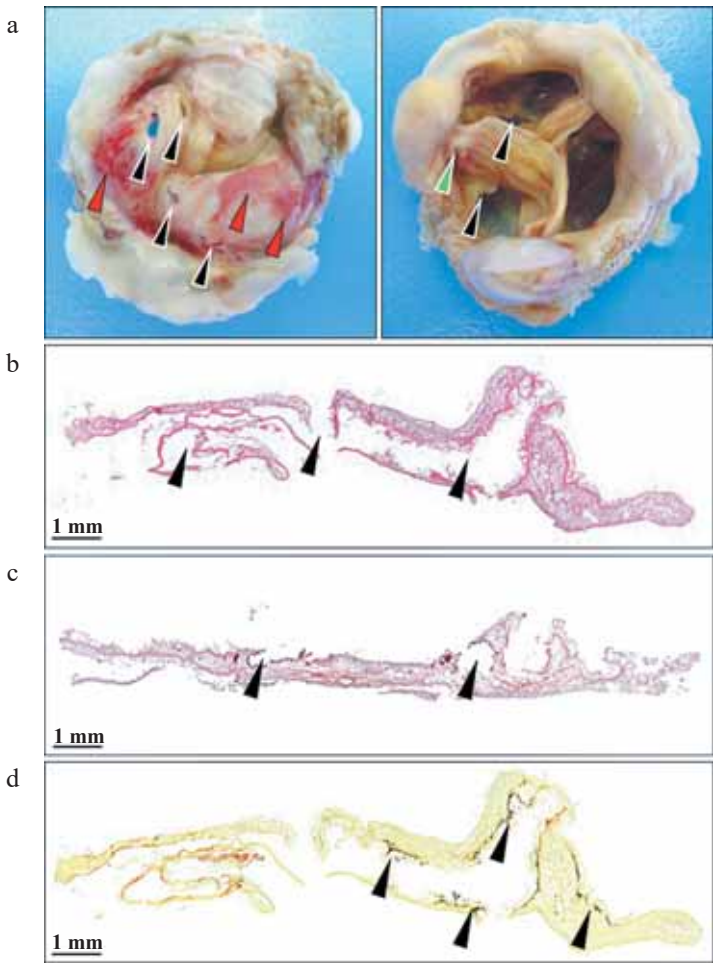

Fig. 1. Results of macro- and microscopic analysis of the studied bioprosthetic heart valve: a, an image of the sample, (left and right – inflow and outflow sections, respectively; black arrows indicate leaflet perforations, red indicate intravalvular hemorrhages, green shows pannus buildup areas); b, histological slice of the leaflet stained with hematoxylin and eosin (arrows indicate areas of delamination and ruptures of extracellular matrix); c, slice stained with alizarin red S (arrows indicate microcalcifications); d, slice stained by Gram staining (arrows indicate colonies of microorganisms)

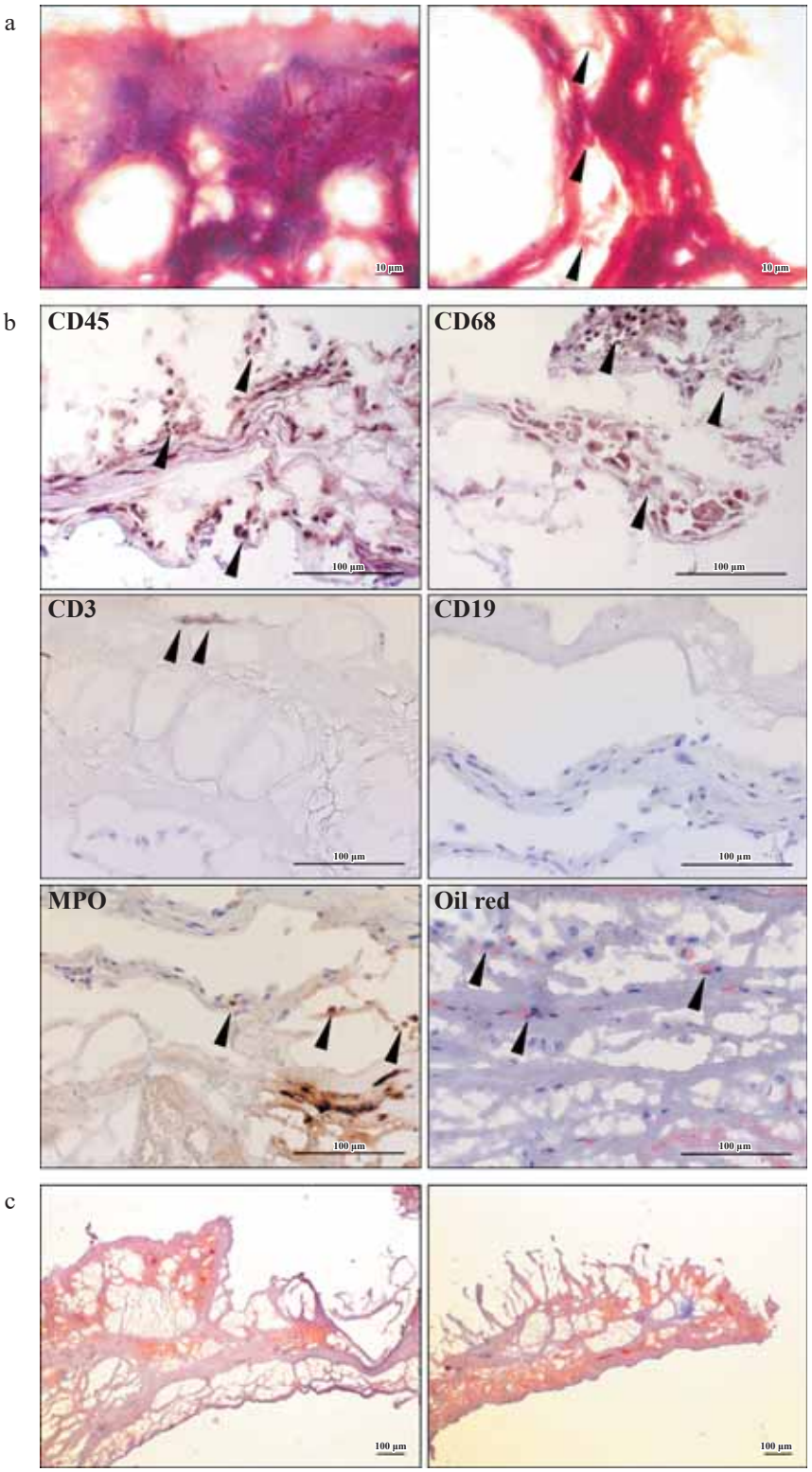

Fig. 2. Results of histological and immunohistochemical staining of the bioprosthetic valve leaflets: a, Gram-stained bacterial colonies composed of Gram-positive cocci and Gram-negative bacilli (arrows indicate recipient cells colocalized with microorganisms); b, cell typing results (arrows indicate positively stained cells; immunohistochemistry and oil red O staining); c, visualization of lipid droplets in the bioprosthetic valve leaflet (on the left is the leaflet dome, on the right is the free edge of the leaflet; oil red O staining)

DISCUSSION

BHVs with a functional lifespan exceeding 20 years are rarely available for histopathological examination. This situation is related to both the relatively short (10–15 years on average) durability of these medical devices and the use of BHVs mainly in patients older than 65 years of age [7]. In the latter case, failed BHVs are usually unavailable for study due to natural death of recipients

or impossibility of retrieval due to transcatheter valve-to-valve replacement method [7]. Consequently, there is little data on BHVs that functioned 20–25 years after implantation [8, 9].

The biomaterial of the leaflets of the BHV in question was characterized by extreme stratification and fragmentation of collagen fibers, which is obviously associated with the duration of exposure of the valve to cyclic loads (over 25 years, the BHV performed about 1 billion cycles of opening and closing). At the same time, calcification of the BHV was negligible. This picture differs from the known cases of long-term (>20 years) functioning of GA-treated BHVs, which are characterized by pronounced calcification of the leaflet apparatus [8, 9]. The obtained data indirectly confirm the opinion of experts, according to which epoxy-treated BHVs are considered to be more resistant to calcification than the GA-treated ones [4]. However, due to lack of a sample, it is still impossible to make a final conclusion about the influence of the tissue preservation method on the nature of degenerative changes in BHVs during their extremely long-term functioning.

Detection of microorganisms in the biomaterial of the BHV was unexpected, although the results of macroscopic analysis, blood cultures and patient intake did not reveal any signs of infective endocarditis (IE) in the patient. It is important to emphasize that the pattern of localization of bacterial agents was not characteristic of classical IE, in the development of which bacteria populate microthrombi on the surface of the flaps with subsequent formation of vegetations. In the case under consideration, bacterial clusters were located in the thickness of the leaflet apparatus in the areas with severe tissue damage. Apparently, the observed picture is due to the entrapment of microorganisms from blood by the network of loosened collagen fibers that form the basis of the biomaterial of the leaflet.

In addition to bacterial agents, the BHV was infiltrated by different types of leukocytes penetrating the thickness of the biomaterial. Apparently, like bacterial contamination, cellular invasion of the flaps is associated with trapping of circulating immune cells from the bloodstream by the loosened tissue. The predominance of macrophages and foam cells in the infiltrates indicates chronic inflammation, which is consistent with the results of previous studies [2, 3, 6]. At the same time, the presence of single T cells and neutrophils may be due to the development of latent IE.

CONCLUSION

In this paper, we reported an epoxy-treated BHV that was removed 25 years after mitral valve replacement. Literature review showed that this is the longest reported lifespan of a BHV treated with ethylene glycol diglycidyl ether. Identification and description of similar cases in the future will help to study the mechanisms of structural degeneration of these medical devices in more detail (in particular, to assess the resistance of an epoxy-treated biomaterial to calcification in a recipient's body compared to a GA-stabilized biomaterial in long-term BHV functioning).

The study was carried out within the framework of the fundamental theme of the Research Institute for Complex Issues of Cardiovascular Diseases, No. 0419-2022-0001 "Molecular, Cellular and Biomechanical Mechanisms of the Pathogenesis of Cardiovascular Diseases in the Development of New Methods of Treatment of Cardiovascular Diseases based on Personalized Pharmacotherapy, Introduction of Minimally Invasive Medical Devices, Biomaterials and Tissue-engineered Implants".

The study was conducted in accordance with the principles of the Good Clinical Practice and Declaration of Helsinki of the World Medical Association, and was approved by the local ethics committee of the Research Institute for Complex Issues of Cardiovascular Diseases (report #19 dated November 6, 2018). The patient signed a written informed consent.

The authors declare no conflict of interest.

REFERENCES

1. *Head SJ, Çelik M, Kappetein AP.* Mechanical versus bioprosthetic aortic valve replacement. *Eur Heart J*. 2017; 38 (28): 2183–2191. doi: 10.1093/eurheartj/ehx141.
2. *Shetty R, Pibarot P, Audet A, Janvier R, Dagenais F, Perron J et al.* Lipid-mediated inflammation and degeneration of bioprosthetic heart valves. *Eur J Clin Invest*. 2009; 39 (6): 471–480. doi: 10.1111/j.1365-2362.2009.02132.x.
3. *Sakaue T, Koyama T, Nakamura Y, Okamoto K, Kawashima T, Umeno T et al.* Bioprosthetic valve deterioration: accumulation of circulating proteins and macrophages in the valve interstitium. *JACC Basic Transl Sci*. 2023; 8 (7): 862–880. doi: 10.1016/j.jacbts.2023.01.003.
4. *Barbarash LS, Zhuravleva IYu.* Bioprosthetic heart valve evolution: two decades of advances and challenges. *Complex Issues of Cardiovascular Diseases*. 2012; 1: 4–11. (in Russ.). doi: 10.17802/2306-1278-2012-1-4-11.
5. *Mukhamadiyarov RA, Rutkovskaia NV, Milto IV, Sidopova OD, Kudryavtseva YuA, Barbarash LS.* Investigation of the structure of a functionally intact xenopericardial bioconduit after long-term implantation. *Arkhiv Patolo-*

gii. 2017; 79 (5): 25–33. (In Russ.). doi: 10.17116/patol201779525-33.

6. *Mukhamadiyarov RA, Rutkovskaya NV, Sidorova OD, Barbarash LS.* Cellular composition of calcified bioprostheti c heart valves. *Annals of the Russian Academy of Medical Sciences*. 2015; 70 (6): 662–668. (In Russ.). doi: 10.15690/vramn560.
7. *Otto CM, Nishimura RA, Bonow RO, Carabello BA, Erwin JP, Gentile F et al.* 2020 ACC/AHA guideline for the management of patients with valvular heart disease: a report of the American College of Cardiology/American Heart Association Joint Committee on clinical practice guidelines. *Circulation*. 2021; 143 (5): e72–e227. doi: 10.1161/CIR.0000000000000923.
8. *Kubota S, Wakasa S, Ooka T, Tachibana T, Shiiya N, Matsui Y.* A case of Carpentier-Edwards pericardial bioprosthesis in mitral position explanted 22 years after implantation. *J Artif Organs*. 2010; 13 (1): 48–50. doi: 10.1007/s10047-010-0483-2.
9. *Koizumi S, Fukunaga N, Ikeda T, Koyama T.* A case of an explanted 26-year-old Carpentier-Edwards supra-annular valve in the tricuspid position. *J Cardiol Cases*. 2016; 15 (1): 36–38. doi: 10.1016/j.jccase.2016.10.003.

The article was submitted to the journal on 13.05.2024

DOI: 10.15825/1995-1191-2025-1-188-197

TRANSCUTANEOUS PERMEATION ENHANCER COMPLEX FOR POLYMER-BASED TRANSDERMAL PATCHES

E.G. Kuznetsova[1], L.A. Salomatina[1], O.M. Kuryleva[1], Yu.B. Basok[1], V.I. Sevastianov[1, 2]

[1] Shumakov National Medical Research Center of Transplantology and Artificial Organs, Moscow, Russian Federation

[2] Institute of Biomedical Research and Technology, Moscow, Russian Federation

Selecting a permeation enhancer complex (PEC) for inclusion in a matrix-type transdermal patch (TP) is a primary task in creating a new dosage form with percutaneous administration. **Objective:** to develop a biologically safe PEC capable of regulating percutaneous diffusion of low-molecular-weight drugs from the polyacrylate matrix of a TP and without causing adverse skin reactions. **Materials and methods.** The PEC contained apricot kernel oil, dioctyl sodium sulfosuccinate, dihydroquercetin and alpha-tocopherol acetate – substances that have a good impact on the functional properties of polymer-based TPs. Low-molecular alcohol-soluble drugs (chlorpropamide, caffeine and sodium benzoate and lidocaine hydrochloride) used to treat diseases of various etiologies were used as active ingredients. *In vitro* studies of percutaneous drug delivery were carried out on male Chinchilla rabbits in Franz glass diffusion cells using a drug diffusion analyzer. Using spectrophotometry and high-performance liquid chromatography, concentrations of drugs in aqueous solutions and in the blood plasma of the laboratory animals were measured. The irritant effect of the lidocaine-loaded transdermal polymeric matrix was tested on sexually mature young male New Zealand White rabbits. **Results.** When PEC was introduced into the polymer matrix film, percutaneous diffusion of the drugs increased significantly from 2.1 ± 0.4 to 9.2 ± 1.4 mg over 24 hours of experiment for the chlorpropamide-loaded TP and from 9.2 ± 1.2 to 35.2 ± 7.5 mg for the caffeine-loaded TP. Additionally, there was a 1.7- and 2.9-fold decrease and a 2.3- and 2.7-fold increase in the time to reach a constant drug concentration in blood for the chlorpropamide- and caffeine-containing TPs, respectively. Using the lidocaine- and chlorpropamide-loaded TPs, it was shown that the presence of PEC in the polymer matrix film causes no skin irritation and that the shelf life of the transdermal form increases from 1 to 3 years. **Conclusion.** Introduction of the proposed PEC into the polymeric matrixes of TPs enhanced percutaneous diffusion of the drugs, reduced skin irritation from the TP components, and increased the shelf life of the finished dosage forms.

Keywords: transdermal patches, polymer matrix film, transcutaneous permeation enhancers, chlorpropamide, caffeine and sodium benzoate, lidocaine hydrochloride.

INTRODUCTION

Transdermal patches (TPs) are an external dosage form designed for the controlled delivery of active substances into the systemic circulation by passive diffusion through intact skin [1]. They are widely used in modern medicine, particularly for managing chronic conditions. Their ease of application and the straightforward manufacturing process of polymeric matrix systems – especially the drug-in-adhesive subtype – make them a preferred choice for both manufacturers and consumers [2].

The composition of a TP is carefully designed to maintain a therapeutic drug concentration in the bloodstream throughout its duration of action [3–5]. Most commercially available TPs utilize polymeric adhesive matrices, which not only ensure skin contact but also serve as a reservoir for the active drug and excipients. The polymer matrix must be biocompatible, avoiding local irritation or allergic reactions. The most suitable adhesives include polysiloxane polymers, polyisobutylene, and acrylic polymers [3]. Among acrylic adhesives, DURO-TAK and GELVA, manufactured by Henkel (Germany) [6], are the most widely used.

In addition to form-forming components, permeation enhancers are incorporated into the TP matrix to facilitate drug penetration through the skin. These enhancers include various chemical compounds such as alcohols, monoterpenes, sulfoxides, phospholipids, fatty acids and their esters, surfactants [7–9]. All excipients used in a TP must be carefully selected to minimize the risk of toxicity, irritation, allergic reactions, or interactions with the active drug.

When developing TP formulations, multiple excipients are often combined to enhance and complement each other's effects. This approach helps maintain the stability and functionality of the active drug over extended storage periods while also reducing potential skin irritation caused by the TP components [8].

This study aimed to develop a biologically safe permeation enhancer complex (PEC) that effectively regu-

Corresponding author: Evgeniya Kuznetsova. Address: 1, Shchukinskaya str., Moscow, 123182, Russian Federation. Phone: (499) 196-26-61. E-mail: kuzeugenia@yandex.ru

lates percutaneous diffusion of low-molecular-weight drugs from the polyacrylate matrix of a TP while minimizing the risk of adverse skin reactions.

MATERIALS AND METHODS

Materials

The following drug substances were used as active substances in the TP: hypoglycemic agent chlorpropamide (MM 276.74) (Dipharma Francis, Spain), psychostimulant caffeine and sodium benzoate (MM 338.29) (Shandong Xinhua Pharmaceutical Co. Ltd., China), and local anesthetic lidocaine hydrochloride (MM 234.34) (Peptek, Russia).

For the manufacture of laboratory samples of TPs, we used the acrylic adhesive Duro-Tak 87-4287 (Henkel Chemical Company, Germany). This adhesive forms a strong bond with the skin, facilitates drug release, and can be easily removed after application. Its low shear resistance eliminates the need for plasticizers, and it has a viscosity of 8000 mPa·s [10].

To enhance the functional properties of the polymeric TP, a complex of excipients was incorporated into the polymer matrix, including apricot kernel oil (Desert Whale Jojoba Company Ltd., USA), alpha-tocopherol acetate (BASF SE, Germany), dihydroquercetin (Research and Production Company 'FLAVIT'), and dioctyl sodium sulfosuccinate (Sigma, USA).

Table 1 shows the ranges of variation of the content of permeation enhancers in the polymer matrix film of TP.

Drug substances intended for incorporation into the polymer matrix film were pre-dissolved in 95% ethyl alcohol (RFK, Russia) to ensure uniform distribution. Laboratory samples of TPs loaded with chlorpropamide, caffeine, and lidocaine were fabricated using high-quality film materials: Cotran 9715 film (3M, USA) as the substrate and Scotchpack 1022 PET film (3M, USA) as the protective layer. For primary packaging, sachets from Proflex (Russia) were utilized.

Table 1

Composition of the polymer matrix film of transdermal patches

S/N	Matrix components	Mass, %
1	Alpha-tocopherol acetate	0.02–0.1
2	Dihydroquercetin	0.04–0.14
3	Dioctyl sodium sulfosuccinate	0.06–0.14
4	Apricot kernel oil	4.0–9.6
5	Acrylic adhesive	≤100%

Equipment

Quantification of drug concentrations in aqueous solutions and blood plasma of laboratory animals was performed using spectrophotometric analysis (UV-2600 spectrophotometer, Shimadzu, Japan) and high-performance liquid chromatography (HPLC) on an Agilent 1260 Infinity chromatograph (Agilent Technologies, USA). The HPLC system was equipped with a G1311A pump, a G1314B diode array detector, a column thermostat, and ChemStation software (Agilent, USA).

Drug diffusion studies were conducted using a HDT 1000 diffusion analyzer (Copley Scientific Ltd., UK). Additional laboratory equipment included an Elmasonic S 60 H ultrasonic bath (Elma, Germany), GH-200 analytical scales (AND, Japan), a Rotina 38R centrifuge (Hettich, Germany), and a Simplicity water purification system (Millipore, Germany).

Research algorithm

The paper presents and experimentally validates an algorithm for developing safe and effective polymeric TPs incorporating a complex of low-molecular-weight drug permeation enhancers (Fig.). The proposed algo-

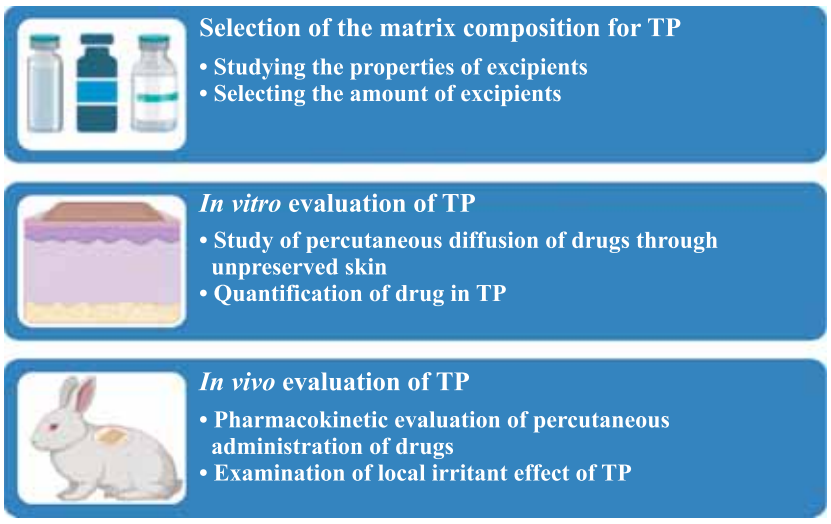

Fig. Algorithm for creating transdermal patches with a permeation enhancer complex. TP, transdermal patch

rithm consists of three key stages: theoretical analysis, *in vitro* studies, and *in vivo* evaluations. A comprehensive laboratory study was conducted for each drug substance.

Laboratory animals

The studies were conducted on male Chinchilla rabbits (3.5–4.0 kg) and New Zealand White rabbits (2.0–3.7 kg), obtained from the laboratory animal nursery of KrolInfo LLC. The producer provided a veterinary certificate confirming the animals' health status. All experimental animals were specifically bred for research purposes and had not previously participated in any studies.

All procedures were designed to minimize discomfort and adhered to ethical guidelines, including the European Convention for the Protection of Vertebrate Animals Used for Experimental and Other Scientific Purposes (ETS 123, Strasbourg, 1986). The study was also conducted in compliance with Russian regulations: GOST 33215-2014 (Guidelines for the Maintenance and Care of Laboratory Animals, Rules for Equipping Premises and Organizing Procedures) and GOST 33216-2014 (Guidelines for Housing and Care of Laboratory Animals, Rules for the Maintenance and Care of Laboratory Rodents and Rabbits).

In vitro studies of transdermal drug delivery

The diffusion of drugs through unpreserved rabbit skin from a TP with a polymer matrix containing a PEC and a control TP without enhancers was studied using glass Franz diffusion cells and a drug diffusion analyzer. The receiving chamber of the diffusion cells was filled with degassed 0.9% sodium chloride solution, which was prepared using an ultrasonic bath. After 24 hours of incubation at 32 °C, samples were collected from the receiving chamber and analyzed.

Quantification of chlorpropamide in aqueous solutions was performed using HPLC under the following conditions: column NF28948 (150 mm length, 4.6 mm inner diameter 5 μm grain size), mobile phase acetonitrile : water : trifluoroacetic acid 250 : 750 : 1, isocratic elution mode, mobile phase flow rate 0.8 mL/min, column thermostat temperature 25 °C, sample volume 5 μL, detection wavelength 240 nm, retention time 2.3 min.

The optical density of aqueous caffeine solutions was determined using spectrophotometric analysis at a wavelength of 273 ± 2 nm, corresponding to the maximum absorption of the substance.

Quantification of lidocaine in aqueous solutions was performed using HPLC under the following conditions: Column: Hypersil BDS-C18 (length 150 mm, inner diameter 4.6 mm, grain size 5 μm), mobile phase: acetonitrile : (water + 0.05 M KH_2PO_4 + trifluoroacetic acid) 30 : 70, isocratic elution mode, mobile phase flow rate 1 mL/min, column thermostat temperature 25 °C, sample volume 20 μL, detection wavelength: 254 nm, retention time 3.8 min.

Determination of drug concentration in blood plasma of laboratory animals in transdermal administration *in vivo*

The concentration of drugs released from the TP into blood plasma was evaluated in male Chinchilla rabbits. The animals were divided into two groups of three each. The first group received a PEC-containing TP applied to a shaved area on the back near the neck for 24 hours, while the second group received a PEC-free TP under the same conditions.

Blood samples were collected from the marginal ear vein into tubes containing 3.8% sodium citrate solution (RENAM, Russia) before TP application and at specific time points: 1, 2, 4, 6, 12, 15, 18, 20, and 24 hours after application. Blood plasma was obtained by centrifugation at 1500 rpm for 10 minutes. Before chromatographic analysis, the samples were filtered through a polytetrafluoroethylene membrane with a 0.45 μm pore size (Supelco, USA).

Drug concentrations in rabbit blood plasma were determined using HPLC.

Quantitative analysis of chlorpropamide in plasma was performed under the following conditions: a Diabond C16T column (Elsico, Russia) was used, with a mobile phase consisting of acetonitrile (Merck, Germany) and a 0.03% aqueous phosphoric acid solution (Merck, Germany) in a gradient elution mode. The mobile phase flow rate was set at 1 mL/min, with the column thermostat maintained at 25 °C. The injection volume was 5 μL, and detection was carried out at a wavelength of 240 nm. The retention time for chlorpropamide was 2.3 minutes.

Quantification of caffeine and sodium benzoate (CSB) in rabbit blood plasma during TP application was performed using HPLC under the following conditions: a Hypersil ODS C18 column (Elsico, Russia) was used with a mobile phase consisting of acetonitrile (Merck, Germany) and a 0.03% aqueous phosphoric acid solution (Merck, Germany) in a gradient elution mode. The mobile phase flow rate was set at 1 mL/min, and the column thermostat was maintained at 25 °C. The injection volume was 5 μL, with detection carried out at a wavelength of 254 nm.

Assessment of local irritant effect when using a transdermal patch

The local irritant effect of a lidocaine-loaded TP was assessed in accordance with GOST ISO 1099-10-2011 Medical Devices – Evaluation of the Biological Action of Medical Devices, Part 10: Studies of Irritant and Sensitizing Effects.

Rabbits were divided into two groups of three animals each. A lidocaine-loaded TP (2.5 × 4.0 cm^2) with a po-

lymer matrix was applied to a shaved skin area on both sides of the back and secured with a bandage. The first group received a PEC-containing TP, while the second received a PEC-free TP. After 24 hours, the patches were removed, and skin condition was evaluated at 1, 24, 48, and 72 hours post-exposure.

Quantification of drug content in laboratory samples of transdermal patches

To determine the chlorpropamide content in the dosage form, TP samples (without protective and covering layers) were placed in a conical flask containing 200 mL of 0.01 N hydrochloric acid solution. The flask was maintained in a boiling water bath for 1 hour. The resulting solution was then filtered through a paper filter into a 2000 mL volumetric flask. This extraction process was repeated four additional times under the same conditions.

Chlorpropamide concentration was quantified using spectrophotometric analysis by measuring the optical density of the solution at a wavelength of 231 ± 2 nm. A 0.01 N hydrochloric acid solution served as the reference.

The content of chlorpropamide in TP in grams (X) was calculated according to the formula:

$$X = \frac{D_x \cdot m \cdot 2000 \cdot 5}{D_0 \cdot 100 \cdot 50} = \frac{2D_x \cdot m}{D_0},$$

where D_x is the optical density of the test solution; D_0 is optical density of chlorpropamide standard sample solution; m is the weight (in grams) of chlorpropamide taken for preparation of the standard sample solution.

The experiment was repeated six times, and the average result calculated.

Statistical data processing

Significance of differences was determined using Student's t-test (standard software package Microsoft Excel 2010). Differences were considered statistically significant at $p < 0.05$.

RESULTS AND DISCUSSION

Characteristics of substances included in the permeation enhancer complex

The developed polymer matrix for the TP consisted of an acrylic adhesive combined with a PEC containing apricot kernel oil, dioctyl sodium sulfosuccinate, dihydroquercetin, and alpha-tocopherol acetate [11]. The PEC composition was carefully selected based on an analysis of the individual properties of each excipient incorporated into the matrix.

Alpha-tocopherol acetate and dihydroquercetin, key components of the PEC, are well known for their potent antioxidant properties [12, 13]. These substances possess unique characteristics that mitigate potential adverse effects of the polymer composition on the skin during TP application. Alpha-tocopherol acetate (vitamin E), for instance, enhances the skin's water-binding capacity when applied topically. It optimizes nutrient delivery to the dermis and epidermis, facilitates detoxification, promotes tissue healing and regeneration, and improves microcirculation in the skin [14].

Dihydroquercetin exhibits a range of beneficial effects, including angioprotective, regenerative, detoxifying, anti-edematous, antibiotic, radioprotective, and immunomodulatory properties [13].

In the PEC formulation, alpha-tocopherol acetate and apricot kernel oil interact synergistically to preserve each other's functional properties while providing protection against oxidation. Vegetable oils play a crucial role in replenishing lost epidermal lipids, restoring the skin's barrier function, and stimulating lipid metabolism [15]. Due to its high oleic acid content, apricot kernel oil is readily absorbed into the skin, facilitating the penetration of other active ingredients and enhancing their bioavailability [16].

Dioctyl sodium sulfosuccinate (DSS) is a synthetic surfactant with both lipophilic and hydrophilic properties, making it structurally similar to phospholipids. This anionic surfactant readily forms micelles in aqueous and organic media, adapting its spatial orientation based on solvent polarity [17]. The ability of micelles to transport drugs through the stratum corneum is attributed to their hydrophobic outer surface, which facilitates penetration. As micelles diffuse through the hydrophilic dermis, sodium docusate molecules gradually reorient their hydrophilic groups toward the surrounding environment, enabling the controlled release of drugs, which then diffuse into the bloodstream through capillary walls [17]. Previous studies have demonstrated that DSS significantly enhances the percutaneous diffusion of bromocaine in emulsion-based TPs [18]. Subsequent research has explored its use in microemulsions for transdermal delivery of essential amino acids [19, 20]. In this study, DSS was incorporated into the PEC to improve drug diffusion from the polymer matrix.

Study of transdermal diffusion of drugs through unpreserved skin *in vitro* from polymer matrices of different compositions

In preliminary studies, the optimal composition of the PEC for chlorpropamide-loaded, caffeine-loaded, and lidocaine-loaded TPs was determined to achieve the desired transdermal diffusion rate for a dosage form with an area of 10 cm^2.

Tables 2 and 3 present the *in vitro* results of the 24-hour transdermal diffusion study of chlorpropamide and caffeine from TPs. PEC components are indicated with an asterisk (*).

Tables 2 and 3 demonstrate a significant enhancement ($p < 0.05$) in transdermal drug diffusion from a TP in-

corporating a PEC-containing polymer matrix. Diffusion of chlorpropamide increased from 2.1 ± 0.4 mg to 9.2 ± 1.4 mg, while caffeine diffusion rose from 9.2 ± 1.2 mg to 35.2 ± 7.5 mg over 24 hours.

A similar improvement in drug diffusion through unpreserved rabbit skin *in vitro* was observed for lidocaine-loaded TPs with a PEC-containing polymer matrix, as shown in Table 4.

It is important to note that when developing a TP for a specific drug, the ratio of PEC components must be carefully optimized based on the drug's properties and the target therapeutic concentration in the blood.

Effect of the permeation enhancer complex on drug concentration in blood during transdermal administration to laboratory animals

Table 5 presents the *in vivo* results of PEC's effect on drug concentration in rabbit blood during for chlorpropamide-loaded TP (15 mg drug, 10 cm^2). PEC components are indicated with *.

Table 6 summarizes the time required to achieve a steady-state blood concentration of caffeine and sodium benzoate (CSB), as well as the duration for which this concentration was maintained, during application of both PEC-containing and PEC-free TPs (50 mg drug, 10 cm^2). PEC components are indicated with *.

As shown in Tables 5 and 6, incorporating PEC into the polymeric TP reduces the time required to reach a steady-state drug concentration in the blood – by 1.7 times for chlorpropamide-loaded TP and 2.9 times for caffeine-loaded TP – while also increasing the achieved concentration – by 2.3 times for chlorpropamide TP and 2.7 times for caffeine TP.

Calculations indicate that to achieve the target drug concentration in rabbit blood, a PEC-free chlorpropamide-loaded TP would require a contact area of 23 cm^2 – 2.3 times larger than the PEC-containing formulation. Similarly, a PEC-free caffeine-loaded TP would require

Table 2

Effect of the permeation enhancer complex on percutaneous diffusion of chlorpropamide from the transdermal patch (15 mg, 10 cm^2)

S/N	Polymer matrix composition	Quantity in the matrix, mass %	Quantity in the TP, g	Mass of the drug that passed through the skin, mg, n = 20	Release of drug from TP, %
1	Acrylic adhesive	95.88	0.155	9.2 ± 1.4	61.3
	Apricot kernel oil*	4.0			
	Alpha-tocopherol acetate*	0.02			
	Dioctyl sodium sulfosuccinate*	0.06			
	Dihydroquercetin*	0.04			
	Ethanol		0.100		
	Chlorpropamide		0.015		
2	Acrylic adhesive	100	0.155	2.1 ± 0.4	14.0
	Ethanol		0.100		
	Chlorpropamide		0.015		

Note: TP, transdermal patch.

Table 3

Effect of the permeation enhancer complex on percutaneous diffusion of caffeine from the transdermal patch (50 mg, 10 cm^2)

S/N	Polymer matrix composition	Quantity in the matrix, mass %	Quantity in the TP, g	Mass of the drug that passed through the skin, mg, n = 15	Release of drug from TP, %
1	Acrylic adhesive	90.02	0.12	35.2 ± 7.5	70.4
	Apricot kernel oil*	9.6			
	Alpha-tocopherol acetate*	0.10			
	Dioctyl sodium sulfosuccinate*	0.14			
	Dihydroquercetin*	0.14			
	Ethanol		0.10		
	Caffeine		0.05		
2	Acrylic adhesive	100	0.12	9.2 ± 1.2	18.4
	Ethanol		0.10		
	Caffeine		0.05		

Note: TP, transdermal patch.

a 27 cm^2 contact area, which is 2.7 times larger than its PEC-containing counterpart. These findings highlight the effectiveness of PEC in significantly reducing the required TP contact area.

Pharmacokinetic studies of the lidocaine-containing TP revealed that drug concentrations in the blood of laboratory animals were near the HPLC detection limit, consistent with the characteristics of topical formulations.

Table 4

Effect of the permeation enhancer complex on percutaneous diffusion of lidocaine from the transdermal patch (50 mg, 10 cm^2)

S/N	Polymer matrix composition	Quantity in the matrix, mass %	Quantity in the TP, g	Mass of the drug that passed through the skin, mg, n = 15	Release of drug from TP, %
1	Acrylic adhesive	94.76	0.12	21.8 ± 3.0	43.6
	Apricot kernel oil*	5.0			
	Alpha-tocopherol acetate*	0.1			
	Dioctyl sodium sulfosuccinate*	0.06			
	Dihydroquercetin*	0.08			
	Ethanol		0.10		
	Lidocaine		0.05		
2	Acrylic adhesive	100	0.12	9.1 ± 0.2	18.2
	Ethanol		0.10		
	Lidocaine		0.05		

Note: TP, transdermal patch.

Table 5

Results of the study of chlorpropamide content in the blood of laboratory animals *in vivo*

S/N	Polymer matrix composition	Quantity in the matrix, mass %	Quantity in the TP, g	Time (h) to reach a constant concentration, n = 3	Constant concentration (μg/mL) in blood, n = 3
1	Acrylic adhesive	95.88	0.155	4.4 ± 0.5	1.73 ± 0.16
	Apricot kernel oil*	4.0			
	Alpha-tocopherol acetate*	0.02			
	Dioctyl sodium sulfosuccinate*	0.06			
	Dihydroquercetin*	0.04			
	Ethanol		0.100		
	Chlorpropamide		0.015		
2	Acrylic adhesive	100	0.155	7.3 ± 0.3	0.75 ± 0.11
	Ethanol		0.100		
	Chlorpropamide		0.015		

Note: TP, transdermal patch.

Table 6

Results of the study of caffeine and sodium benzoate content in the blood of laboratory animals *in vivo*

S/N	Polymer matrix composition	Quantity in the matrix, mass %	Quantity in the TP, g	Time (h) to reach a constant concentration, n = 3	Constant concentration (μg/mL) in blood, n = 3
1	Acrylic adhesive	90.02	0.12	2.2 ± 0.4	2.63 ± 0.15
	Apricot kernel oil*	9.6			
	Alpha-tocopherol acetate*	0.10			
	Dioctyl sodium sulfosuccinate*	0.14			
	Dihydroquercetin*	0.14			
	Ethanol		0.10		
	Caffeine and sodium benzoate		0.05		
2	Acrylic adhesive	100	0.12	6.3 ± 0.9	0.96 ± 0.10
	Ethanol		0.10		
	Caffeine and sodium benzoate		0.05		

Note: TP, transdermal patch.

Table 7

Extent of skin reaction in rabbits to the lidocaine-containing transdermal patch

TP composition	Rabbit no.	Time after detachment of TP							
		1 hr		24 hr		48 hr		72 hr	
Polymer matrix with PEC: – Apricot kernel oil, 5.0% – Alpha-tocopherol acetate, 0.1% – Dioctyl sodium sulfosuccinate, 0.06% – Dihydroquercetin, 0.08%	1	0	0	0	0	0	0	0	0
	2	0	0	0	0	0	0	0	0
	3	0	0	0	0	0	0	0	0
Polymer matrix without PEC	1	1	1	0	0	0	0	0	0
	2	1	1	1	1	0	0	0	0
	3	1	1	1	1	0	0	0	0

Note: 0, no irritation; 1, faint erythema; TP, transdermal patch; PEC, permeation enhancer complex.

Table 8

Quantity of chlorpropamide in the transdermal patch at different storage periods

TP composition	Quantity of chlorpropamide in the TP, g			
	Immediately after production, g (n = 6)	After 1 year, g (n = 6)	After 2 years, g (n = 6)	After 3 years, g (n = 6)
Polymer matrix with PEC: – Apricot kernel oil, 5.0% – Alpha-tocopherol acetate, 0.1% – Dioctyl sodium sulfosuccinate, 0.06% – Dihydroquercetin, 0.08%	0.0151 ± 0.0006	0.0148 ± 0.0009	0.0148 ± 0.0006	0.0146 ± 0.0003
Polymer matrix without PEC	0.0150 ± 0.0010	0.0148 ± 0.0006	0.0142 ± 0.0003	0.0120 ± 0.0008

Note: TP, transdermal patch; PEC, permeation enhancer complex.

Effect of introducing the permeation enhancer complex in the matrix on the possibility of local irritant effect of a transdermal patch

An assessment of the possibility of skin irritation from polymeric TPs was conducted using laboratory samples of lidocaine-loaded TP (50 mg, 10 cm^2) as a topical agent. The extent of skin reaction in rabbits following TP application is summarized in Table 7.

Table 6 indicates that in all three rabbits from the second group, mild erythema was observed at both application sites one hour after removing the lidocaine-loaded TP with a PEC-free polymer matrix. This erythema persisted for 24 hours in two rabbits but resolved completely within the next 24 hours. In contrast, no signs of irritation were observed at the application site in the group of animals that received the lidocaine-loaded TP with a PEC-containing polymer matrix throughout the study period. Similar findings of reduced local irritation were noted in the studies of caffeine-loaded and chlorpropamide-loaded TP.

Effect of the permeation enhancer complex in the polymer matrix on the shelf life of transdermal patches

To demonstrate the effect of PEC in the polymer matrix composition on the shelf life of the TP, Table 8 presents the results of a three-year study on the quantitative content of chlorpropamide in the TP.

According to the 15th edition of the State Pharmacopoeia of the Russian Federation, deviation in the active substance content of a TP should not exceed 15% [1]. Therefore, chlorpropamide content in a single TP must not be lower than 0.0150 ± 0.00225 g. The study results indicate that the shelf life of a chlorpropamide-loaded TP with a PEC-containing polymer matrix extends up to three years, whereas a similar TP without PEC has a shelf life of only one year.

Similar studies have demonstrated that incorporating PEC into caffeine-loaded and lidocaine-loaded TPs also enhances their shelf life.

CONCLUSION

The findings of this study demonstrate that incorporating the proposed PEC – comprising of apricot kernel oil, dioctyl sodium sulfosuccinate, dihydroquercetin, and alpha-tocopherol acetate – into polyacrylate TP matrices significantly enhances the functional properties of these dosage forms. Specifically, the PEC:

– Increases transdermal drug diffusion, enabling a substantial reduction in the required contact area of the dosage form.
– Shortens the time needed to reach a stable equilibrium drug concentration in the bloodstream compared to PEC-free formulations.

– Reduces the risk of skin irritation at the application site.
– Extends the shelf life of the dosage form.

The authors declare no conflict of interest.

REFERENCES

1. General Pharmacopoeia Article "Transdermal Patches" OFS.1.4.1.0016 State Pharmacopoeia of the Russian Federation XV edition.
2. *Losenkova SO, Tunina ED, Pavluchenkova NA, Losenkov PV, Emelyanov AA, Machotina MV*. Modern range of transdermal dosage forms in the pharmaceutical market of russia. *Vestnik of the Smolensk State Medical Academy*. 2022; 21 (1): 152–159. [In Russ, English abstract]. doi: 10.37903/vsgma.2022.1.20.
3. *Basok YuB, Kuznetsova EG, Kuryleva OM, Perova NV, Ryzhikova VA, Salomatina LA et al.* Transdermal therapeutic systems / Ed. V.I. Sevastyanov, E.G. Kuznetsova. SPb.: Science-intensive technologies, 2023; 276. [In Rus].
4. *Phatale V, Vaiphei KK, Jha S, Patil D, Agrawal M, Alexander A*. Overcoming skin barriers through advanced transdermal drug delivery approaches. *J Control Releas*. 2022; 351: 361–380. doi: 10.1016/j.jconrel.2022.09.025. PMID: 36169040.
5. *Sevastyanov VI, Salomatina LA, Kuznetsova EG, Seregina MV, Basok YuB.* Transdermal dosage form of acyzol – carbon monoxide antidote. *Perspective materials*. 2008; 6: 55–59. [In Rus].
6. *Maciejewski B, Dłabiszewska J, Mikolaszek B, Sznitowska M.* The Impact of Liquid Components on Alteration of the Adhesion of Polyacrylate and Silicone Patches. *Polymers (Basel)*. 2023; 15 (22): 4355. doi: 10.3390/polym15224355. PMID: 38006080. PMCID: PMC10674843.
7. *Kuznetsova EG, Ryzhikova VA, Salomatina LA, Sevastianov VI.* Transdermal drug delivery and methods to enhance it. *Russian Journal of Transplantology and Artificial Organs.* 2016; 18 (2): 152–162. [In Russ, English abstract]. doi: 10.15825/1995-1191-2016-2-152-162.
8. *Kováčik A, Kopečná M, Vávrová K*. Permeation enhancers in transdermal drug delivery: benefits and limitations. *Expert Opin Drug Deliv.* 2020; 17 (2): 145–155. doi: 10.1080/17425247.2020.1713087. PMID: 31910342.
9. *Vasyuchenko EP, Orekhov PS, Armeev GA, Bozdaganyan ME*. CPE-DB: An Open Database of Chemical Penetration Enhancers. *Pharmaceutics*. 2021; 13 (1): 66. doi: 10.3390/pharmaceutics13010066. PMID: 33430205. PMCID: PMC7825720.
10. Henkel-adhesives.com [Internet]. Product selection guid. Henkel. DURO-TAK and GELVA Transdermal Pressure Sensitive Adhesives [cited 2022 March 21]. Available from: https://www.henkel-adhesives.com/content/dam/uai/AIH/master/images/drug-delivery-polymers/duro-tak-gelva-production-guide-US-4pager-160920.pdf.
11. *Sevastyanov VI, Kuznetsova EG, Salomatina LA, Kuryleva OM, Basok YuB, Gautier SV*. Patent RU2812184C1. Matrix based on acrylic adhesive with complex of transdermal transfer activators for transdermal therapeutic systems. Published 24.01.2024.
12. *Gavrilov AS.* Pharmaceutical technology. Manufacturing of medicinal products (study guide). Chapter 5. Excipients / Ed. A.S. Gavrilov. Moscow: GEOTAR-Media, 2010; 624. [In Rus].
13. *Tutelyan VA, Kravchenko LV, Avrenyeva LI, Morozov SV.* Evaluation of antioxidant and antitoxic efficiency of natural flavonoid dihydroquercetin. *Toxicological Bulletin*. 2005; 1: 14–20. [In Rus].
14. *Tsoureli-Nikita E, Hercogova J, Lotti T, Menchini G.* Evaluation of dietary intake of vitamin E in the treatment of atopic dermatitis: a study of the clinical course and evaluation of the immunoglobulin E serum levels. *Int J Dermatol*. 2002; 41 (3): 146–150. doi: 10.1046/j.1365-4362.2002.01423.x. PMID: 12010339.
15. *Bykova SF, Davidenko EK, Efimenko SG.* Prospects for the development of the raw material base for the production of new types of edible vegetable oils. *Oils and fats.* 2014; 1: 20–24. [In Rus].
16. *Lin T-K, Zhong L, Santiago JL.* Anti-Inflammatory and Skin Barrier Repair Effects of Topical Application of Some Plant Oils. *Int J Mol Sci.* 2017; 19 (1): 70. doi: 10.3390/ijms19010070. PMID: 29280987.
17. *Sevastianov VI.* Biomaterials, drug delivery systems, and bioengineering. *Russian Journal of Transplantology and Artificial Organs.* 2009; 11 (3): 69–80. [In Russ, English abstract]. https://doi.org/10.15825/1995-1191-2009-3-69-80.
18. *Ryzhikova VA, Tikhobayeva AA, Salomatina LA, Kursakov SV, Kuznetsova EG, Kuryleva OM, Sevastianov VI.* Effect of the Transfer Activator on Functional Properties of the Bromocain Matrix Transdermal Therapeutic Systems. *Inorganic Materials: Applied Research.* 2014; 5 (5): 498–503. doi: 10.1134/S2075113314050177.
19. *Sautina NV, Rybakova AI, Gubaidullin AT, Galyametdinov YuG*. Liquid crystal mesophase of the water / AOT / isopropylmiristat system in the processes of transdermal delivery of amino acids. *Liquid crystals and their application*. 2020; 20 (2): 91–99. doi: 10.18083/LCAppl.2020.2.91. [In Russ, English abstract].
20. *Sautina NV, Rybakova AI, Galyametdinov YuG*. Kinetics of l-lysine mass transfer in reverse microemulsions, stabilized by AOT. *Liquid crystals and their application*. 2019; 19 (1): 26–32. doi: 10.18083/LCAppl.2019.1.26. [In Russ, English abstract].

The article was submitted to the journal on 27.08.2024

DOI: 10.15825/1995-1191-2025-1-198-208

EFFECT OF MEDIASTINAL RADIOTHERAPY ON 30-DAY MORTALITY AFTER CARDIAC SURGERY

M.N. Sorkomov, S.I. Babenko, D.A. Titov, A.S. Sachkov, M.I. Terekhov, R.A. Serov, R.M. Muratov

Bakulev National Medical Research Center for Cardiovascular Surgery, Moscow, Russian Federation

Late complications affecting the cardiovascular system depend on the extent of the capture of cardiac structures in the radiation field and the cumulative dose of exposure. They are characterized by polymorphism in clinical manifestations. **Objective:** to identify the predictors influencing in-hospital mortality (IHM) in order to optimize the treatment of patients with radiation-induced heart disease. **Materials and methods.** This is a single-patient cohort study that was retrospective from 2004 to 2018 and prospective from 2018. Death after 30 days following heart valve surgery (HVS) under artificial circulation was taken as the end point of the study. The study included 86 patients (mean age 59 ± 13 years, 81.4% female) who underwent HVS. They were split into 2 groups (extensive, tangential) depending on the cause of cancer. **Results.** In the postoperative period, the group with extensive irradiation had statistically significant differences in the need for prolonged ventilation, OR 5.17 (CI 95% 1.7–15.7), more frequent exudative pleurisy OR 3.4 (CI 95% 1.1–10.8), and acute renal failure OR 1.2 (CI 95% 1.05–1.37). Regardless of postoperative complications, the length of hospital stay did not differ statistically across the groups, with a median of 10.5 (CI 7.25:16.75) *vs.* 11 (CI 9:15.25) days, respectively. Overall IHM was 14 (16.27%) patients. Multiple organ failure (MOF) was the cause of death in 9 cases. Multivariate analysis revealed that extensive irradiation for lymphogranulomatosis increased IHM risk by 5.099 times, and an increase in the EuroSCORE II score by every "1" increased IHM risk by 1.19 times. **Conclusion.** Patients with post-radiation damage to heart valves and coronary arteries with a history of tangential irradiation can be successfully operated on. Extensive irradiation in anamnesis is associated with a high risk of heart failure and MOF in the early postoperative period.

Keywords: radiation therapy, cardiac surgery, in-hospital mortality.

INTRODUCTION

Radiation therapy (RT) is widely used in the treatment of chest tumors, but its late cardiovascular complications depend on the extent of cardiac exposure and the cumulative radiation dose. These complications exhibit polymorphic clinical manifestations, with their development following a time-dependent pattern [1–3].

The earliest manifestation of radiation-induced cardiac damage is often coronary heart disease, which can become as significant as cancer itself within the first five years post-RT [4]. In contrast, radiation-induced valvular disease emerges later and follows a linear-quadratic progression model [5, 6]. Over time, radiation-induced heart injury advances and frequently presents as a complex syndrome, involving multiple cardiac structures alongside extracardiac complications.

Objective: to identify the predictors influencing in-hospital mortality (IHM) in order to optimize the treatment of patients with radiation-induced heart disease.

MATERIAL AND METHODS

Place and time of study

The study included patients treated at the Department of Emergency Surgery for Acquired Heart Defects, Bakulev National Medical Research Center for Cardiovascular Surgery in Moscow (Department headed by Prof. R.M. Muratov from 2002 to 2023, and by D.A. Titov from 2023 to the present), and it covered the period from June 2004 to May 2023.

Study population

The main inclusion criteria for the study were a documented history of RT, a minimum interval of 9 years from RT to the development of cardiac pathology, presence of valvular disease requiring surgical intervention, and clinical group 3 status (complete cancer remission) at the time of hospitalization for valvular surgery. Based on these criteria, the study included 86 patients who had previously undergone RT for breast cancer (tangential field) or Hodgkin's lymphoma (extensive field exposure).

Study Design

This single-cohort study was conducted retrospectively from 2004 to 2018 and prospectively from 2018 onward. The primary objective was to identify predictors of IHM in patients with radiation-induced cardiac lesions.

Corresponding author: Maxim Sorkomov. Address: 135, Rublevskoe Shosse, Moscow, 121552.
Phone: (495) 414-78-49. E-mail: sorcommn@gmail.com

The study endpoint was mortality within 30 days following cardiopulmonary bypass surgery for radiation-induced valvular disease.

Methods

All patients underwent clinical, laboratory, and instrumental examinations following standard cardiac surgical care protocols. The diagnostic criteria for stenosis and regurgitation were based on the 2021 guidelines of the European Society of Cardiology (ESC) and the European Association for Cardio-Thoracic Surgery (EACTS) for managing valvular heart disease [7].

To assess mitral stenosis severity, echocardiographic evaluation included leaflet mobility, leaflet thickness, degree of subvalvular structure involvement, and annulus fibrosus calcification. Each parameter was scored from 1 to 4, with a maximum Wilkins score of 16 [8]. For patients with echocardiographic signs of mitral annular calcification, the severity was further evaluated using Rajesh Movva et al.'s criteria [9], with annulus fibrosus scoring and summation.

Coronary angiography was performed following the ESC/EACTS guidelines for myocardial revascularization [10]. For patients with extensive radiation exposure, diagnostic coronary angiography was conducted more broadly in the presence of clinical signs of coronary heart disease. To objectively assess the complexity of coronary artery lesions, the study used the SYNTAX Score (Synergy Between PCI With Taxus and Cardiac Surgery), a widely accepted anatomic classification system [11].

A chest CT scan was performed to assess the severity of calcification in cardiac structures and the presence of pneumofibrosis. Calcium deposits in the aortic valve, ascending aorta, and coronary arteries were measured using the Agatston method (1990) [12]. For Agatston score calculation, a 130 HU attenuation threshold was applied (130–199 corresponds to 1 point, 200–299 to 2 points, 300–399 to 3 points, 400 and above to 4 points). Each calcified area was assigned a score based on its attenuation value, then multiplied by the lesion area, with all values summed. The final total calcium score was calculated for the mitral annulus fibrosus, coronary arteries, and ascending aorta.

Pneumofibrosis was assessed using a semi-quantitative method, modifying the radiologic criteria for pneumofibrosis on a 0–3 scale for each lung lobe, where 0 = absent, 1 = linear streaks, 2 = moderate fibrosis, and 3 = severe fibrosis with bronchiectasis. The total pneumofibrosis score was obtained by summing the scores across all lung lobes [13].

For risk stratification based on the nature of surgery, the following logistic scoring systems were used to estimate 30-day mortality: EuroSCORE, EuroSCORE II, and STS PROM.

Statistical analysis

Normality of distribution was tested using the Kolmogorov–Smirnov test. Quantitative variables with normal distribution were processed using descriptive statistics, calculating mean ± standard deviation. On the contrary, variables with other type of distribution were evaluated by calculating the median and interquartile range (1st and 3rd quartiles). Qualitative variables were presented as absolute frequencies and percentages. When comparing groups with normal distribution, the data were analyzed using a parametric method (Student's t-test for independent samples), the rest of the data were analyzed using a non-parametric method (Mann–Whitney U test). A binary logistic regression model was used to identify IHM predictors (outcome: dead/alive). Previous preoperative RT, clinical and instrumental data were used as independent variables. A significance level of 0.05 was adopted for all statistical results.

Clinical material

The mean age of patients included in the study was 58.85 ± 12.71 years. The most widely represented age group were old patients from 60 to 74 years old; they made up 42 (48.84%) patients. Middle-aged patients (45–59 years old) were 15 in number (17.44%), while young patients (18–44 years old) were 23 (26.74%). The smallest group was the very old group according to the WHO classification (75–90 years), represented by 6 (6.98%) patients. Females prevailed over males, accounting for 70 (81.4%) patients. According to the etiology of the oncological disease, the patients were distributed as follows: Hodgkin's lymphoma (HL), 41 (46.67%) patients, and breast cancer (BC), 45 (53.33%) (Fig. 1).

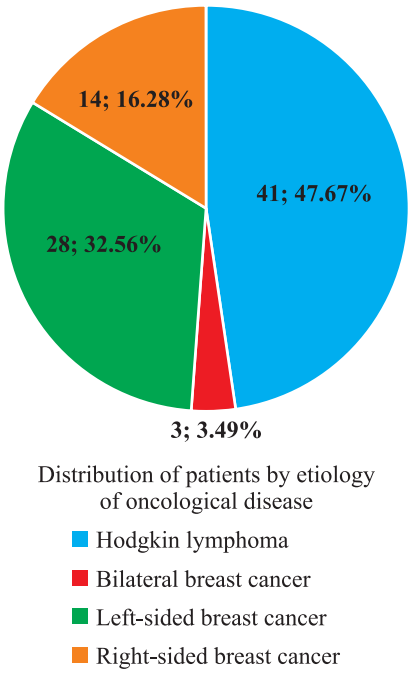

Fig. 1. Structure of oncological diseases

To evaluate demographic indicators, risk factors of cardiovascular diseases, comorbid pathology, combined diseases reflecting the severity of cardiovascular conditions and symptoms of circulatory failure and functional status depending on tumor type and direction of ionizing radiation in relation to the mediastinum, patients were divided into two conditional groups: extensive irradiation and tangential irradiation (Table 1).

RESULTS

Analysis of preoperative data revealed significant differences between the groups. The extensive irradiation group was notably younger. While the absolute values of coronary artery lesions were comparable, the number of combined lesions was significantly higher in this group. Additionally, coronary artery lesions in the extensive irradiation group were predominantly proximal.

Pearson's correlation analysis showed a significant inverse relationship between the year of RT and the time of cardiac pathology occurrence ($r = –0.897$, $p < 0.001$).

As shown in Table 2, hemodynamic parameters did not differ significantly. Most patients had aortic stenosis, with an average peak gradient of 80 ± 28 mmHg. The primary differences between the groups were in the morphofunctional parameters of the left ventricle. Indexed myocardial mass was significantly lower in the extensive irradiation group compared to the tangentially irradiated group (122 *vs.* 156 g/m^2, respectively). Additionally, a significantly higher proportion of patients in the extensive irradiation group had concentric hypertrophy (84.1% *vs.* 46.5%, $p < 0.001$). This phenomenon, known as 'immobilizing interstitial myocardial fibrosis,' is characterized by disruption of the endomysium and perimysium structure, leading to gradual mechanical compression and immobilization of the myocardium. Analysis of the mean fiber shortening fraction revealed a slight decrease in the tangential irradiation group, while the fraction remained preserved in the extensive irradiation group, possibly due to the high proportion of patients with arterial hypertension.

An integrated assessment of global longitudinal left ventricular (LV) strain parameters showed a significant decrease in the extensive irradiation cohort (11.1 ± 9%) and a moderate decrease in the tangential irradiation group (14.5 ± 3.2%). Despite volume overload in patients with mitral and aortic regurgitation, the proportion of those with eccentric hypertrophy remained low – 13.6% in the tangential irradiation group and 18.2% in the extensive irradiation group. These findings suggest that the observed changes can be interpreted in the context

Table 1

Clinical characteristics of patients

	Tangential (n = 45)	Extensive (n = 41)	General (n = 86)	P value
Age (years)	67 ± 7	49 ± 11	59 ± 13	**0.000**
BMI (kg/m^2)	29 ± 5.06	26.33 ± 4.56	27.8 ± 5	**0.07**
BSA (m^2)	1.87 ± 0.15	1.87 ± 0.22	1.87 ± 0.19	0.910
Interval between RT and surgical treatment of cardiac pathology (years)	23 ± 9	27 ± 9	25 ± 9	**0.044**
Age at the time of RT (years)	44.67 ± 9.29	22.37 ± 9.8	34.03 ± 14.63	**0.000**
Female	45 (100)	26 (60.9)	70 (81.4)	**0.000**
Combination chemotherapy, n (%)	27 (61.4)	36 (87.8)	63 (74.1)	**0.005**
NYHA functional class III and IV, n (%)	44 (53)	39 (47)	82 (95.34)	0.503
Pacemaker, n (%)	1 (25)	3 (75)	4 (4.6)	0.262
Arterial hypertension, n (%)	37 (62)	23 (38)	60	**0.08**
Atrial fibrillation, n (%)	6 (60)	4 (40)	10 (11.83)	0.605
CHD, n (%)	5 (26)	14 (74)	19 (22.09)	**0.010**
Diabetes mellitus, n (%)	13 (93)	1 (7)	14 (16.27)	**0.001**
COPD FEV_1 <50–80% FEV_1 <49–39%	11 2 36.6 40	19 3 63.4 60	30 5 34.88 5.8	**0.006**
SYNTAX Score	12 [8–16]	10 [3–16.5]	10.5 [4.7–16.2]	0.218
EuroSCORE I	6.35 [3.5–8.4]	3.89 [2.1–6.9]	4.9 [3.2–7.8]	**0.008**
EuroSCORE II	2.3 [1.6–4.9]	2.4 [1.5–4.4]	2.4 [1.6–4.7]	0.619
STS PROM	4.9 [3.4–6.2]	4.2 [1.9–6.8]	4.7 [2.5–6.9]	0.308
Creatinine clearance (CKD-EPI)	67 [54–78]	82 [66–104]	72 [57–89]	**0.001**

Note: BMI, body mass index; BSA, body surface area; RT, radiation therapy; NYHA, New York Heart Association; CHD, coronary heart disease; COPD, chronic obstructive pulmonary disease; FEV_1, forced expiratory volume in 1 second; SYNTAX Score, Synergy Between PCI With TAXUS and Cardiac Surgery Systematic Coronary Risk Evaluation; EuroSCORE I and EuroSCORE II, European System for Cardiac Operative Risk Evaluation; STS, Society of Thoracic Surgeons.

of myocardial fibrosis resulting from radiation exposure to the LV myocardium.

Echocardiographic assessment (Table 2) revealed a high incidence of mitral annular calcification in patients who RT for breast cancer. However, a semiquantitative analysis of calcification using Movva's criteria showed no significant differences between the groups.

While calcium deposition in cardiac structures was prevalent, there was no statistically significant variation between groups. Notably, extensive irradiation resulted in significant lung tissue exposure, leading to widespread pulmonary parenchymal fibrosis, which was markedly more severe in the extensive irradiation group (Table 2).

All patients underwent surgery with artificial circulation (Table 3). Although median cardiopulmonary bypass time differed between groups – 137 minutes (105–205) in the tangential group *vs.* 177 minutes (130–220) in the extensive group ($p = 0.084$) – the difference was not statistically significant. However, aortic clamping time was significantly longer in the extensive irradiation group (103 minutes [77–124] *vs.* 78 minutes [63–109], $p < 0.018$), likely due to the greater surgical volume. In most cases, the procedure was limited to a single-valve intervention, with aortic valve replacement performed in 51.7% of patients.

Due to post-RT skin changes preventing median sternotomy (Fig. 2), alternative surgical access was used in 20.98% of cases (n = 18), including J-shaped ministernotomy along the 4th intercostal space and, in one case, bipleural access.

Prolonged ventilation (PV) was required in 22 patients (25.58%), most commonly due to heart failure, which developed in 17 patients. Intra-aortic balloon counterpulsation was used in 7 patients, while extracorporeal membrane oxygenation (ECMO) was required in 4 cases. Acute renal failure developed in 5 patients (Fig. 3).

In the postoperative period, there were statistically significant differences in the need for PV (OR 5.17, CI 95% 1.7–15.7), more frequent exudative pleurisy (OR 3.4, CI 95% 1.1–10.8), and acute renal failure (OR 1.2, CI 95% 1.05–1.37) in the extensive radiation group. Re-

Table 2

Findings from instrumental diagnostic methods

	Tangential	Extensive	P value
Electrocardiographic parameters			
Preoperative HR (beats/min)	78.5 ± 13.4	84.39 ± 11.1	**0.033**
QT interval (sec)	0.397 ± 0.05	0.404 ± 0.05	0.547
QRS (sec)	0.1 [0.09–0.12]	0.108 [0.008–0.120]	0.336
Echocardiographic findings			
Left atrium, cm	5.1 ± 1	4.2 ± 0.809	0.118
LV end-diastolic volume (cm)	122 ± 35.1	127 ± 41.4	0.522
LV ejection fraction (%)	64 ± 10.3	62 ± 11.5	0.425
LV fractional shortening (%)	36 ± 8.05	34 ± 8.03	0.473
LV relative wall thickness	0.55 ± 0.13	0.47 ± 0.2	**0.016**
Mean circumferential fiber shortening fraction, %	12.5 ± 3.16	14.29 ± 3.1	**0.019**
Indexed myocardial mass, gr/	156 ± 67.1	122 ± 64.2	**0.006**
Mitral stenosis (n)	9	10	0.374
Peak diastolic gradient across MV, mmHg.	10 [7.5–13]	11 [9.7–13.5]	0.787
Annular calcification (n)	29	12	**0.024**
Calcification total score	7.38 [6.31–8.47]	6.7 [5.15–8.39]	0.802
Wilkins score	8.9 [7–10.7]	8.37 [7–9.7]	0.454
MV regurgitation > grade 2 (n)	13	22	**0.020**
Aortic stenosis >40 mmHg (n)	36	27	0.716
Aortic valve annulus size, mm	21.91 ± 2.44	21.7 ± 2.08	0.695
Aortic valve peak gradient, mmHg.	83 [73–93]	75 [65–85]	0.266
AV regurgitation > grade 2 (n)	8	8	0.916
LV systolic pressure, mmHg	38 ± 23	46 ± 17.2	0.189
Computer tomography			
Coronary artery calcification	681 [204–1158]	857 [442–1273]	0.334
Ascending aorta calcification	3018 [1649–4387]	2136 [1113–3159]	0.785
Aortic valve calcification	3945 [2227–5663]	2802 [1473–4132]	0.895
Mitral annular calcification	3872 [1596–6148]	2974 [881–5067]	0.9
Pulmonary fibrosis level	3.35 [2.45–4.25]	7.15 [5.9–8.41]	**0.0001**

Note: HR, heart rate; LV, left ventricular; MV, mitral valve; AV, aortic valve.

gardless of postoperative complications, the length of hospital stay was not statistically different between the groups, with a median of 10.5 (CI 7.25:16.75) *vs.* 11 (CI 9:15.25) days, respectively.

Overall, IHM was 16.27% (n = 14). Multiple organ dysfunction syndrome (MODS) was the leading cause of death in 9 cases. Among these, MODS resulted from acute cerebrovascular insufficiency in one case, respiratory failure in two cases, and acute heart failure in four cases during the postperfusion period. In these four cases, ECMO was required due to the ineffectiveness of intra-aortic balloon pump (IABP) in stabilizing hemodynamics. In two additional cases, IABP was initiated in the intensive care unit due to worsening heart failure.

In five cases, the immediate cause of death was acute heart failure. In two patients, heart failure resulted from ventricular fibrillation – one occurring on day 3 post-aortic prosthesis and mammary-coronary artery bypass of the anterior interventricular artery, and the other on day 9 after aortic valve replacement and coronary artery bypass grafting (CABG) in a patient with multivessel coronary artery disease, poor peripheral circulation, and aortic stenosis. Additionally, one case involved iatrogenic injury to the left coronary artery trunk due to massive arterial

Table 3

Scope of surgical intervention

	Tangential	Extensive	Σ
Single-valve intervention (n = 47)			
AV replacement	30 (66.7%)	14 (34.14%)	44
MV repair	1 (2.2%)	0	1
MV replacement	0	2 (4.9%)	2
Two-valve intervention (n = 26)			
MV and TV repair	1 (2.2%)	0	1
AV replacement and TV repair	1 (2.2%)	0	1
AV and MV replacement	3 (6.7%)	8 (19.5%)	11
MV and TV replacement	1 (2.2%)	0	1
AV replacement and MV repair	2 (4.4%)	3 (7.3%)	5
MV replacement and TV repair	1 (2.2%)	6 (14.6%)	7
Three-valve intervention (n = 13)			
AV, MV and TV replacement	0	1 (2.2%)	1
AV and MV replacement, and TV repair	4 (8.9%)	5 (12.2%)	9
AV replacement and atrioventricular valve repair	1 (2.2%)	2 (4.9%)	3
Additional procedures			
Jatene ventriculoplasty	0	1	1
Myocardial revascularization	5	14	19
Annulus fibrosus decalcification with repair	3	2	5
AV annulus fibrosus boring	0	1	1
Reoperation	2	1	3
Pericardiectomy	0	2	2

Note: AV, aortic valve; MV, mitral valve; TV, tricuspid valve.

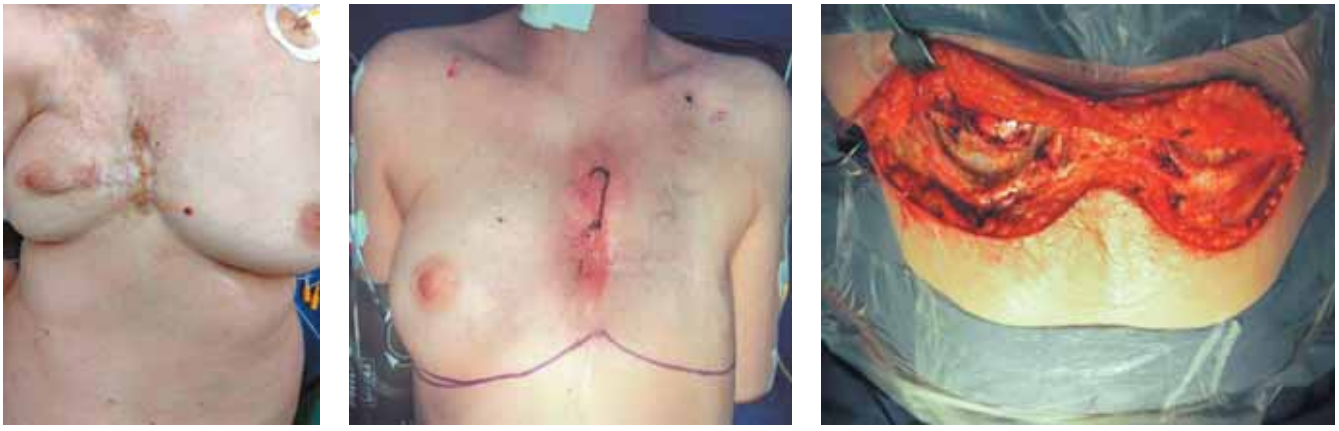

Fig. 2. Radiation injury to the chest skin

calcification. In one case, early prosthetic endocarditis developed on day 16 after two-valve replacement, necessitating repeat surgery. However, this was complicated by acute heart failure in the postperfusion period. Another case of acute heart failure occurred during cardiac recovery following aortic and mitral valve replacement, tricuspid valve repair, and CABG of the anterior interventricular artery. Intra-aortic balloon counterpulsation failed to stabilize hemodynamics, and ECMO could not be initiated due to a high risk of bleeding.

Pathological and morphological examinations were performed on 11 patients. Histological analysis of the heart revealed interstitial and perivascular spaces replaced by collagen fibers (Fig. 4). Qualitative assessment of the micropreparations showed that cardiomyocyte replacement by collagen fibers averaged 33.1 ± 5.6%. Among patients who underwent mantle irradiation, interstitial fibrosis measured 32 ± 3.09%, while in the tangential irradiation group, it was 37 ± 7%.

Table 4

Multivariate analysis results

	Beta regression coefficient	P value	OR	95% confidence interval for OR	
				Lower	Upper
Extensive RT	1.510	0.033	4.526	1.130	18.129
EuroScore II	0.170	0.016	1.185	1.032	1.361
Constant	–3.282	0.000	0.038		

Note: OR, odds ratio; RT, radiation therapy; EuroSCORE II, European System for Cardiac Operative Risk Evaluation II.

Multivariate analysis using the stepwise exclusion method identified a predictive model with two significant factors influencing IHM (Table 4). Extensive chest irradiation for lymphogranulomatosis increased the risk of IHM by 5.099 times, while each 1-point increase in the EuroSCORE II scale raised the risk by 1.19 times. This model demonstrated satisfactory predictive accuracy, with an AUC of 75% (CI: 63–87%) (Fig. 5).

DISCUSSION

Advances in anticancer therapy have significantly reduced mortality for certain types of cancer. However, in the long term, treatment-related side effects and subsequent development of cardiovascular complications remain critical concerns for early detection and management. To mitigate these risks, baseline risk assessment for cardiac toxicity (Class I, Level of Evidence B) is recommended before initiating cancer treatment.

Stratifying risk levels for late complications can help identify patients at higher risk for unfavorable cardiovascular outcomes. However, many quality-of-care improvements, including guideline recommendations, were not introduced until the early 21st century. As a result, the ESC guidelines on cardio-oncology – developed in collaboration with the European Hematology Association (EHA), the European Society for Radiotherapy and Oncology (ESTRO), and the International Cardio-Oncology Society (ICOS) – were only published on August 26, 2022.

Treatment standards for this patient population have not yet been established, as no randomized trials exist

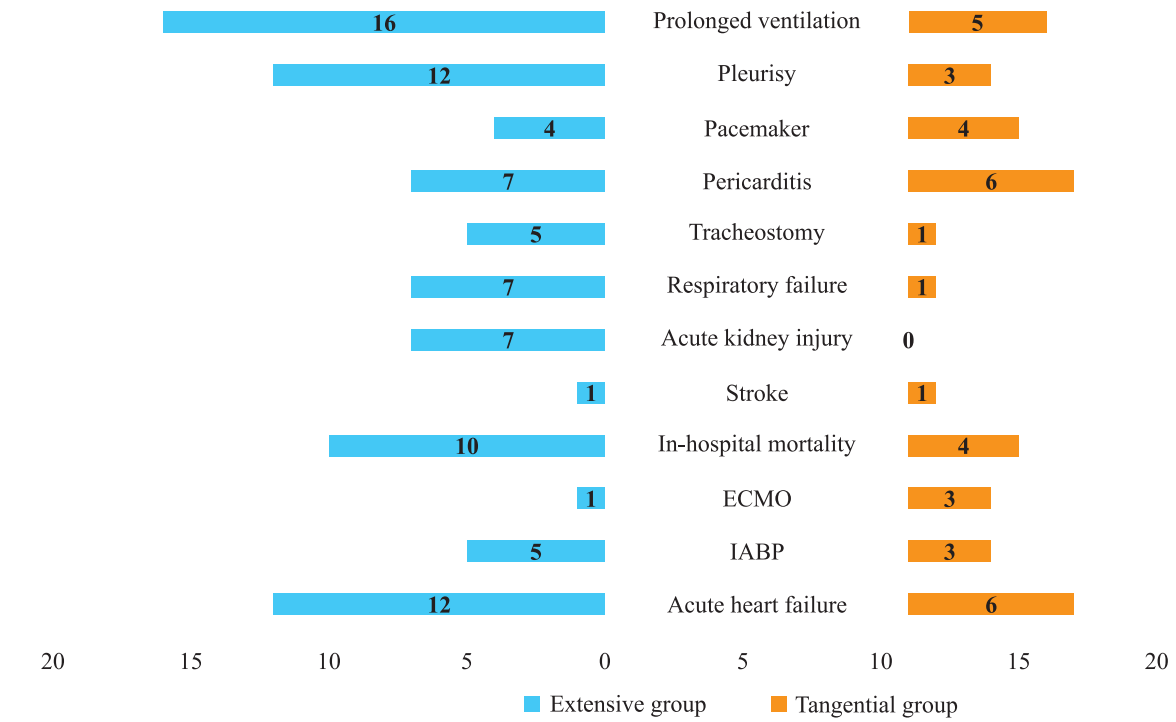

Fig. 3. Postoperative complications and in-hospital mortality. ECMO, extracorporeal membrane oxygenation; IABP, intra-aortic balloon counterpulsation

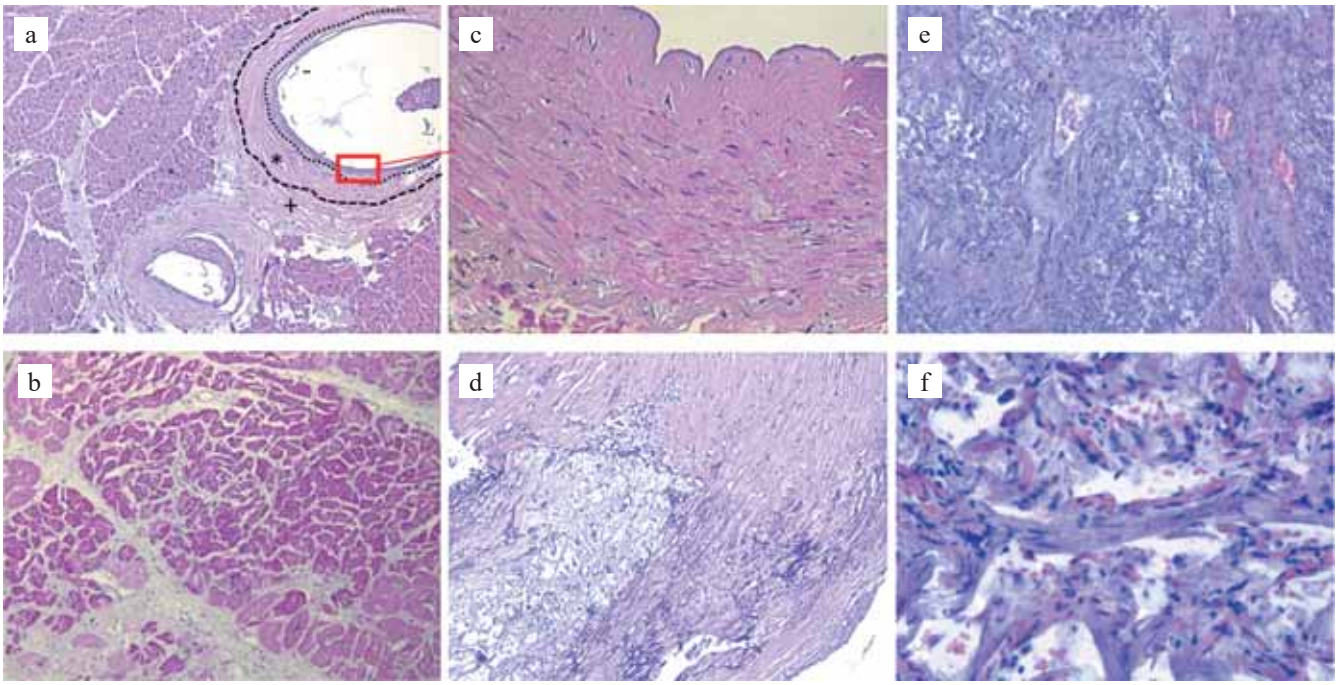

Fig. 4. Image 1 a, sclerosis and hyalinosis of all layers of intramural coronary arteries; +, adventitia, *, media, intima lens 10, eyepiece 10; b, left ventricular myocardial fibrosis. Myocardial fibrosis of the perivascular and interstitial space 42%. lens 20, eyepiece 10; c, diffuse thickening and fibrosis of the vessel intima lens 40, eyepiece 10; d, coronary artery wall calcification lens 20, eyepiece 10; e and f, pulmonary fibrosis

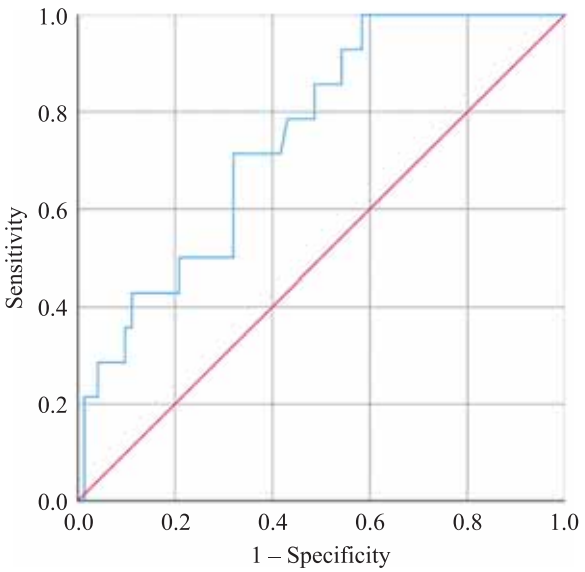

Fig. 5. ROC curve of the predictive model for the development of in-hospital mortality

due to the limited number of cases (competing secondary malignancies) and the unclear effects of prior treatments. Therefore, a multidisciplinary team approach is recommended to evaluate and determine surgical treatment options (Class I, Level of Evidence C).

The treatment principles for cardiac pathology in patients with prior radiotherapy (RT) generally align with conventional methods. However, the correction of valvular disease due to radiation exposure presents unique challenges. The 2017 ESC/EACTS guidelines provide limited guidance on RT-related valvular dysfunction, primarily recommending against conventional surgical treatment for aortic stenosis (Class I) in favor of transcatheter aortic valve replacement (TAVR), based on the heart team's discretion. The latest guidelines do not offer clear recommendations regarding RT-related valvular disease. However, the 2022 ESC cardio-oncology guidelines suggest that for patients at intermediate risk of complications, an alternative to TAVR (Class IIa, Level B) may be considered if severe aortic stenosis has resolved following radiotherapy [14].

Correlation analysis revealed an inverse relationship ($r = –0.897$, $p < 0.001$) between the year of RT and the interval before the development of cardiac pathology. However, this correlation is purely statistical and not a direct causal link to modern RT techniques. Instead, it reflects multiple contributing factors, particularly improved post-cancer therapy surveillance in high-risk survivors. For patients who underwent high-risk cancer therapy in childhood, echocardiographic screening is recommended every two years (Class IIa, Level B). In adults, annual risk stratification (class I, level B) is advised, with echocardiography at 1, 3, and 5 years after treatment (Class IIa, Level C).

With growing attention to cancer treatment-related complications, current guidelines emphasize risk stratification for late effects. In our study, we specifically analyzed a cohort with extensive irradiation. The evidence linking RT to heart failure is dose-dependent and follows

a linear model for late complication development. A multicenter, retrospective case-control study demonstrated a high risk of heart failure in individuals exposed to high mean doses of left ventricular irradiation [15].

An EBCTCG study examined estimated cardiac radiation doses and their association with adverse cardiovascular events in 30,000 women over a 20-year follow-up. The analysis revealed a 3% increase in the risk of death from heart disease per Gy of average cardiac dose [16].

Additionally, Brown et al. compared extensive and tangential exposure groups, demonstrating that patients with tangential or minimal exposure had a lower risk of death compared to those with extensive irradiation (OR 0.6, 95% CI: 0.35–1.02, p = 0.060) [17].

Our meta-analysis demonstrated a 4.98-fold (95% CI 1.86–13.12; p < 0.001) increase in IHM risk in patients with a history of RT compared to a control group without RT [18].

The study also found that the extensive irradiation group was significantly younger, aligning with the findings of Chang et al., where the mean age in the tangential and extensive groups was 72 ± 8.8 *vs.* 51 ± 13 years, respectively (p < 0.001) [19]. Despite their younger age, patients in the extensive irradiation group experienced severe circulatory disorders due to the combined nature of the lesions and concomitant diseases.

Our data indirectly confirm that high-dose irradiation induces significant changes in all cardiac structures and is a key factor in the development of in-hospital mortality (IHM). In our study, IHM was 16.4%, whereas Ejifor reported rates of 3.8% for primary interventions and 17.4% for repeat procedures.

A potential explanation for this elevated IHM could be the extensive radiation exposure, leading to a high cumulative left ventricular radiation dose. However, these findings should be interpreted with caution. One major limitation is that the exact radiation dose to mediastinal structures was only available for a subset of patients due to the long history of prior radiotherapy.

Our data indirectly confirm that high-dose irradiation induces significant changes in all cardiac structures and is a key factor in the development of IHM. In our study, IHM was 16.4%, whereas Ejifor reported rates of 3.8% for primary interventions and 17.4% for repeat procedures [20]. A potential explanation for this elevated IHM could be the extensive radiation exposure, leading to a high cumulative left ventricular radiation dose. However, these findings should be interpreted with caution. One major limitation is that the exact radiation dose to mediastinal structures was only available for a subset of patients due to the long history of prior RT.

Secondly, during the treatment of breast cancer in the 1970s–1980s, RT targeting the internal mammary lymph node chain was commonly used to improve tumor control in internal quadrant lesions. Indirect signs of such irradiation, such as skin manifestations, can be observed in Fig. 2. This historical treatment approach likely explains the absence of significant differences in calcification of cardiac and ascending aortic structures. However, our findings highlight the critical role of myocardial interstitial fibrosis as a key predictor of IHM.

CONCLUSION

The degree of calcification in cardiac structures, the presence of pulmonary fibrosis, and the extent of cardiac surgery were not significant factors influencing IHM. Patients with post-radiation damage to heart valves and coronary arteries following tangential irradiation can successfully undergo surgery with artificial circulation. However, a history of extensive irradiation is associated with a high risk of cardiac and multiple organ failure in the early postoperative period. To reduce IHM, a more comprehensive assessment of both cardiac and non-cardiac complications from prior RT is essential.

The authors declare no conflict of interest.

REFERENCES

1. *Cutter DJ, Schaapveld M, Darby SC, Hauptmann M, van Nimwegen FA, Krol AD et al*. Risk of valvular heart disease after treatment for Hodgkin lymphoma. *J Natl Cancer Inst*. 2015 Feb 23; 107 (4): djv008. https://doi.org/10.1093/jnci/djv008.
2. *Van Nimwegen FA, Schaapveld M, Cutter DJ, Janus CP, Krol AD, Hauptmann M et al*. Radiation Dose-Response Relationship for Risk of Coronary Heart Disease in Survivors of Hodgkin Lymphoma. *J Clin Oncol.* 2016 Jan 20; 34 (3): 235–243. https://doi.org/10.1200/JCO.2015.63.4444.
3. *Van Nimwegen FA, Ntentas G, Darby SC, Schaapveld M, Hauptmann M, Lugtenburg PJ et al*. Risk of heart failure in survivors of Hodgkin lymphoma: effects of cardiac exposure to radiation and anthracyclines. *Blood*. 2017 Apr 20; 129 (16): 2257–2265. https://doi.org/10.1182/blood-2016-09-740332.
4. *Atkins KM, Rawal B, Chaunzwa TL, Lamba N, Bitterman DS, Williams CL et al*. Cardiac Radiation Dose, Cardiac Disease, and Mortality in Patients With Lung Cancer. *J Am Coll Cardiol*. 2019 Jun 18; 73 (23): 2976–2987. doi: 10.1016/j.jacc.2019.03.500.
5. *Machann W, Beer M, Breunig M, Störk S, Angermann C, Seufert I et al*. Cardiac magnetic resonance imaging findings in 20-year survivors of mediastinal radiotherapy for Hodgkin's disease. *Int J Radiat Oncol Biol Phys*. 2011 Mar 15; 79 (4): 1117–1123. doi: 10.1016/j.ijrobp.2009.12.054. Epub 2010 Apr 10. PMID: 20385449.
6. *Adams MJ, Lipsitz SR, Colan SD, Tarbell NJ, Treves ST, Diller L et al*. Cardiovascular status in long-term survivors of Hodgkin's disease treated with chest radiotherapy. *J Clin Oncol*. 2004 Aug 1; 22 (15): 3139–3148. doi: 10.1200/JCO.2004.09.109. PMID: 15284266.
7. *Vahanian A, Beyersdorf F, Praz F, Milojevic M, Baldus S, Bauersachs J et al.* ESC/EACTS Scientific Document

Group. 2021 ESC/EACTS Guidelines for the management of valvular heart disease. *Eur Heart J*. 2022 Feb 12; 43 (7): 561–632. doi: 10.1093/eurheartj/ehab395. Erratum in: *Eur Heart J*. 2022 Feb 18. PMID: 34453165.

8. *Wilkins GT, Weyman AE, Abascal VM, Block PC, Palacios IF.* Percutaneous balloon dilatation of the mitral valve: an analysis of echocardiographic variables related to outcome and the mechanism of dilatation. *Br Heart J*. 1988 Oct; 60 (4): 299–308. https://doi.org/10.1136/hrt.60.4.299.
9. *Movva R, Murthy K, Romero-Corral A, Seetha Rammohan HR, Fumo P, Pressman GS*. Calcification of the mitral valve and annulus: systematic evaluation of effects on valve anatomy and function. *J Am Soc Echocardiogr*. 2013 Oct; 26 (10): 1135–1142. https://doi.org/10.1016/j.echo.2013.06.014.
10. *Neumann FJ, Sousa-Uva M, Ahlsson A, Alfonso F, Banning AP, Benedetto U et al.* ESC Scientific Document Group. 2018 ESC/EACTS Guidelines on myocardial revascularization. *Eur Heart J*. 2019 Jan 7; 40 (2): 87–165. https://doi.org/10.1093/eurheartj/ehy394.
11. *Sianos G, Morel MA, Kappetein AP, Morice MC, Colombo A, Dawkins K et al.* The SYNTAX Score: an angiographic tool grading the complexity of coronary artery disease. *EuroIntervention*. 2005 Aug; 1 (2): 219–227.
12. *Agatston AS, Janowitz WR, Hildner FJ, Zusmer NR, Viamonte M Jr, Detrano R.* Quantification of coronary artery calcium using ultrafast computed tomography. *J Am Coll Cardiol*. 1990 Mar 15; 15 (4): 827–832. doi: 10.1016/0735-1097(90)90282-t. PMID: 2407762.
13. *Arriagada R, de Guevara JC, Mouriesse H, Hanzen C, Couanet D, Ruffie P et al*. Limited small cell lung cancer treated by combined radiotherapy and chemotherapy: evaluation of a grading system of lung fibrosis. *Radiother Oncol*. 1989 Jan; 14 (1): 1–8. https://doi.org/10.1016/0167-8140(89)90002-9.
14. *Lyon AR, López-Fernández T, Couch LS, Asteggiano R, Aznar MC, Bergler-Klein J et al*. ESC Scientific Document Group. 2022 ESC Guidelines on cardio-oncology developed in collaboration with the European Hematology Association (EHA), the European Society for Therapeutic Radiology and Oncology (ESTRO) and the International Cardio-Oncology Society (IC-OS). *Eur Heart J*. 2022 Nov 1; 43 (41): 4229–4361. https://doi.org/10.1093/eurheartj/ehac244.
15. *Van Nimwegen FA, Ntentas G, Darby SC, Schaapveld M, Hauptmann M, Lugtenburg PJ et al*. Risk of heart failure in survivors of Hodgkin lymphoma: effects of cardiac exposure to radiation and anthracyclines. *Blood*. 2017 Apr 20; 129 (16): 2257–2265. https://doi.org/10.1182/blood-2016-09-740332.
16. Early Breast Cancer Trialists' Collaborative Group. Long term toxicity of radiation therapy. 2006 Update of the Early Breast Cancer Trialists' Collaborative group overview of radiation therapy for early breast cancer; 2007 American Society of Clinical Oncology Annual Meeting; June 1–5 2007; Chicago.
17. *Brown JA, Aranda-Michel E, Kilic A, Serna-Gallegos D, Bianco V, Thoma FW, Sultan I.* Impact of Thoracic Radiation on Patients Undergoing Cardiac Surgery. *Semin Thorac Cardiovasc Surg*. 2022 Spring; 34 (1): 136–143. https://doi.org/10.1053/j.semtcvs.2021.01.008.
18. *Muratov RM, Babenko SI, Sorkomov MN, Sachkov AS*. Meta-analysis of surgical treatment of valvular pathology after radiotherapy for cancer of the mediastinal organs. *Creative cardiology*. 2023; 17 (4): 453–463. doi: 10.24022/1997-3187-2023-17-4-453-463.
19. *Chang AS, Smedira NG, Chang CL, Benavides MM, Myhre U, Feng J et al*. Cardiac surgery after mediastinal radiation: extent of exposure influences outcome. *J Thorac Cardiovasc Surg*. 2007 Feb; 133 (2): 404–413. https://doi.org/10.1016/j.jtcvs.2006.09.041.
20. *Ejiofor JI, Ramirez-Del Val F, Nohria A, Norman A, McGurk S, Aranki SF et al*. The risk of reoperative cardiac surgery in radiation-induced valvular disease. *J Thorac Cardiovasc Surg*. 2017 Dec; 154 (6): 1883–1895. doi: 10.1016/j.jtcvs.2017.07.033. Epub 2017 Jul 29. PMID: 28870399.

The article was submitted to the journal on 9.07.2024

INSTRUCTIONS TO AUTHORS

Articles should contain original information that has not been previously published and is not considered for publication in other editions. Fee for publication of manuscripts will not be charged.

The manuscript should be presented in Microsoft Word format A4, 1.5 spacing, and Times New Roman font size 12. Submit your article to the online submission system in accordance with the instructions on the journal's website https://journal.transpl.ru.

Structure of the article

The Title page should include:

– Initials (first name and patronymic) of the authors of the article should be specified before their respective last names.
– Author names (list the author's initials before listing his or her last name as when registering for ORCID, or Open Researcher and Contributor ID – a non-proprietary alphanumeric code that uniquely identifies scientific authors).
– Full official name of the institution, city and country.
– If authors from different institutions participated in writing of the manuscript, it is necessary to correlate those with the names of the authors by adding a digital index uppercase after last name, and right before the name of the institution.

Information about the authors

For each author fully specify the last and the first name, patronymic and position in the relevant department/institution.

For correspondence

Fully specify the last and the first name, patronymic of the author, who will be holding correspondence, address (including postal code), telephone, fax number, e-mail.

Abstract

Each article must be accompanied by an abstract. The amount of text for the abstract of the original article should be of no more than 300 words, for a literature review, clinical observation – no more than 200 words. The abstract must fully comply with the content of the work. The abstract should not use abbreviations without prior expansion.

Abstract of ***the original article*** should contain the following sections: ***Objective***, ***Materials and methods***, ***Results***, ***Conclusion***. The abstract should present the most important results of the research.

Do not write: "*A comparative analysis of the sensitivity and specificity was conducted …*"

Should write: "*The sensitivity was ... % and ...%, p = , specificity, respectively ...% and ...%, p =* ".

Keywords

At the end of the abstract keywords must be given. To select the keywords a thesaurus of U.S. National Library of Medicine should be used – Medical Subject Headings (MeSH) at http://www.ncbi.nlm.nih.gov/mesh.

Conflict of interest

The author should inform the editor about the factual or potential conflict of interest have included the information about such conflict into the respective section of an article.

If there is no conflict of interest, the author should say so in the form like the following: "Author declares unawareness of the conflict of interest".

This information is supposed to be placed before the article text.

Text of article

Original article should include the following sections:

- Introduction
- Materials and methods
- Results
- Discussion
- Conclusion
- References

Review article should include an analysis of the literature with the presentation of modern sources (mainly in the last 5 years).

Clinical observation should be well illustrated (to reflect the essence of the problem) and include discussion with the use of literature data.

References in the text are indicated by number in square brackets: [1], [2, 5], [14–18] and ***in the references section are presented in order of their appearance in the text.*** All values given in the article should be expressed or duplicated in **SI** units.

References

The author is solely responsible for the accuracy of the data included in the references section of the article. References to unpublished papers or papers in print works are not allowed.

References are presented on a separate page.

The names of journals can be contracted in accordance with an embodiment of reduction adopted by the specific journal.

If the article quoted has DOI (a digital object identifier) or/and PMID (Pub Med identifier) they must be specified after the description of the article. To compile descriptions in References section NLM bibliographic reference citation standard is used – U.S. National Library of Medicine (http://www.nlm.nih.gov/bsd/uniform_requirements.html). If the number of authors does not exceed 6, the bibliographic description includes all the authors. If the number of authors is more, only the first six authors should be indicated and then add et al.

Requirements for tables and figures

Tables should be placed into the text; they should have numbered heading and clearly labeled graphs, convenient and simple to read. Table's data must comply with the numbers in the text, but should not duplicate the information therein. Table references in the text are required.

Illustrations and drawings should be submitted in electronic format (JPEG or TIFF format with a resolution of at least 300 dpi and no smaller than 6 × 9 cm), in a volume of close to 1 MB. Drawings must include all copyright symbols – arrows, numbers, signs, etc. Figure captions should be submitted in a separate file with the extension *.doc. First, the name is given, then all arithmetic and alphabetical symbols (lettering) are explained.

Articles should be addressed
to the Russian Journal of Transplantology and Artificial Organs website:
https://journal.transpl.ru/vtio
E-mail: vestniktranspl@gmail.com

Издание зарегистрировано в Госкомпечати РФ, № 018616 от 23.03.99 г.

Подписано к печати 21.03.25.

Тираж 1000 экз.

ООО «Издательство «Триада».
ИД № 06059 от 16.10.01 г.
170034, г. Тверь, пр. Чайковского, 9, оф. 514,
тел.: +7 (915) 730-10-37, +7 (910) 647-49-85
E-mail: triadatver@yandex.ru
http://www.triada.tver.ru

Заказ 12211